Effect of Gamma Irradiation on Solid Polymer Electrolytes Using Deterministic Fractal Model

Thesis submitted for the degree of
Doctor of Philosophy (Science)
of Jadavpur University

By

Subhasish Ghosal
B. Sc.(Hons. in Physics), M. Sc. (Physics)
Ph. D. Registration no.: SOPHY1111416
Index Number: 114/16/Phys./24

Under the supervision of

Ex-Prof. Sujata Tarafdar
Department of Physics
Jadavpur University, Kolkata 700032, India

And

Ex-Prof. Tapas Ranjan Middya
Department of Physics
Jadavpur University, Kolkata 700032, India

– 2022 –

DEDICATED TO:

Parents:

Shree Sukumar Ghosal
Smt. Sarmila Ghosal

Grand Parents:

Late. Tarapada Ghosal
Late Kalyani Ghosal

Late. Ashutosh Goswami

Late Ila Goswami

.... And My Wife and Daughter....

CERTIFICATE FROM THE SUPERVISOR(S)

This is to certify that the thesis entitled **"Effect of Gamma Irradiation on Solid Polymer Electrolytes Using Deterministic Fractal Model"** is submitted by Sri **Subhasish Ghosal** who got his name registered on 30th **May, 2016** for the award of Ph. D (Science) degree of Jadavpur University, is absolutely based upon his own work under the supervision of **ex-Prof. Sujata Tarafder** and **Ex-Prof. Tapas Ranjan Middya** and that neither this thesis nor any part of it has been submitted for either any degree / diploma or any other academic award anywhere before.

S. Tarafder 20.01.2022

Condensed Matter Physics Research Centre
Department of Physics
Jadavpur University
Kolkata-700 032

Sujata Tarafdar
Ex-Professor
Department of Physics
Jadavpur University, Kolkata-700031, India

Tapas Ranjan Middya 20/01/2022

Tapas Ranjan Middya
Ex-Professor
Department of Physics
Jadavpur University, Kolkata-700031, India

Acknowledgement

The research work of this thesis entitled **"Effect of Gamma Irradiation on Solid Polymer Electrolytes Using Deterministic Fractal Model"** was initiated in January 2013 and has been carried out at the Condensed Matter Physics Research Centre (CMPRC), Department of Physics, Jadavpur University, Kolkata – 700032 Under the efficient guidance of Prof. Sujata Tarafdar and Prof. Tapas Ranjan Middya. I got my name registered on 30.05.2016 with Index No.: 114/16/Phys./24 and registration number: SOPHY1111416. As a sense of fulfillment at the completion of this phase of my academic career, I wish to express my gratitude to all those who made this thesis possible.

At first, I express my sincere gratitude to my supervisors Ex-Professor Sujata Tarafder and Ex-Professor Tapas Ranjan Middya, Condensed Matter Physics Research Centre (CMPRC), Jadavpur University. It has been my privilege to work under their guidance. From the beginning of my research work, Madam (Prof. Sujata Tarafder) provides me with an ambient environment to work effectively. Every single discussion with her enriches me with a new concept regarding my research work. I express my deep sense of gratitude to sir (Prof. Tapas Ranjan Middya) for his empathetic behaviour and all sorts of help. His insights into various problems and insistence on clarity have been most useful and inspiring. He has made himself available for me from his hectic schedule and gave me many valuable suggestions to modify my thesis properly. Madam has gone through the content regularly and sir cooperated with me whenever I have approached him with any kind of thesis-related problem. Also, I have received valuable advices and support from both of my guides in any kind of official activity.

I wish to express my sincere gratitude to Dr. Ruma Ray (Gurudas College) for spending her valuable time from her busy schedule on my research work. I express my deep sense of gratitude to her for her nice behavior, all sorts of help to learn the computer simulation procedure, and other research-related works throughout the time period. I wish

to acknowledge with sincere gratitude Prof. Tapas Kumar Ballabh (Jadavpur University) for his many important suggestions regarding the computer simulation process. I also deliver my sincere gratitude to Associate Professor Sanat Karmakar (Jadavpur University) for providing me with various important suggestions about writing my thesis.

I would like to express my sincere gratitude to Prof. Sukhen Das, former HOD,and Prof. Kalyan Kumar Chattopadhyay, present HOD of Department of Physics, Jadavpur University for their kind co-operation with me. In this regard, I would also like to thank all the teaching and non-teaching staff of the physics department, Jadavpur University for their cooperation in academic and research works. I also like to thank all the office staff of the Ph.D. cell, Arabinda Bhawan, Jadavpur University, and the Faculty Council of science Jadavpur University for their help regarding different office-related works at the time of submission of my thesis.

The environment of the working place plays an important role in your research works. In this regard, the working environment and cooperation that I have received from Condensed Matter Physics Research Center Lab (CMPRC Lab), Jadavpur University, is amazing. At first, I would like to give my sincere thanks to Prof. Brajadulal Chattopadhyay (Coordinator of CMPRC, Jadavpur University) for his kind help during my Ph.D. I would also like to express my sincere thanks to Dr. Tapati Dutta (St. Xavier's College Kolkata) for her kind co-operation. I would like to thank Dr. Subir Kumar Patla and Dr. Abhra Giri for their valuable suggestions as well as different technical supports at the different phases of my thesis writing. In addition to that, I am ever grateful to the entire CMPRC wings including all the senior as well as the junior research fellows. Their presence, cooperation, and hospitality made my entire journey in this lab memorable. I wish all of them a successful life ahead.

I would like to express my sincere thanks to the Commissionarate of School Education, Bikash Bhawan for giving me a NO OBJECTION certificate for continuing my research work without hampering my scheduled duties. In addition to that, I would like to thank the School Authority, Kalimpong Govt. High School for their kind co-operation regarding the continuation of my Ph.D. work.

I would like to express my gratitude to my friend Sayantan Dutta (Asstt. Teacher, Belgharia Texmaco High School) and my junior Sayantan Roy (Asstt. Professor of Mathematics, Jhargram Raj College) for their integral co-operation and valuable suggestions at

the different stages of my research work. I would like to thank Arindam Mitra for his technical support till the last end of the completion of my thesis. I would also like to express my gratitude to Dr. Bitan Ghoshal for his co-operation at the beginning of my research work. The beatification of the thesis was impossible without the integral cooperation of my beloved junior friend Udit Narayan Mesh. I am ever grateful to him. In addition to that, I would like to express my gratitude to my friend Sandip Roy for his assistance. I also express my heartfelt thanks to my junior fellow Arnab Kundu (St. Xavier's College) for his valuable suggestions regarding the overall modifications of my thesis.

My humble gratitude will go to Suchhanda Deb (kakima), Sujit Deb (Kaku), Sayan Deb, for providing me an excellent environment of thesis writing at Jadavpur and also encouraging me at the different phases of my journey.

I would like to express my gratitude to my wife Mrs. Kalpana Ghosal. She motivate me and provided her active participation at the different phases of my thesis writing. She undoubtedly stood beside me at the rough phase of my life and encouraged me to proceed in my research work just like a true life partner. The thesis will be incomplete if I do not give my love to my daughter Shreeparna Ghosal.

My humble and deepest gratitude will go to my grandparents Late. Tarapada Ghosal, Late. Ashutosh Goswami, Late, Kalyani Ghosal, and Late. Ila Goswami. Though they are not physically present with me, their guidance, love, encouragement, and blessings will remain with me throughout my life.

Finally, it's time to give my deepest and sincere gratitude to the cause of my existence: my parents Shri Sukumar Ghosal and Smt. Sarmila Ghosal. If there is anything good inside me, it's because of their guidance. The enormous co-operation, encouragement, and motivation that I have received from them, was unimaginable. They sacrifice everything for my education, Ph.D., and betterment of life. The thesis is dedicated to them.

Subhasish Ghosal
20.01.2022

Subhasish Ghosal
Condenced Matter Physics Research Centre (CMPRC)
Jadavpur University
Kolkata

Preface

The vast applicability of solid polymer electrolyte in field of different electrochemical devices attracts the attention of many researchers across the globe. There has been many resilient attempts in the field of experimental research studies by applying different techniques (e.g. ion beam irradiation, gamma irradiation, XRD studies, SEM and TEM studies etc.) to investigate the structural and transportational properties of solid polymer electrolytes (SPE) from the past few decades. This thesis is aimed at a constructive theoretical characterization to study the effect of gamma irradiation on the different structural properties as well as ionic conductivity of the SPE on the basis of computer simulation using deterministic fractal model. In spite of some artificiality, this happens to be a very promising approach where much attention can be invested for some reasonable positive outcomes regarding various unknown properties of SPE.

The unique structural pattern of different polymer molecules and the formation of large complex network of polymer chain segments happens to be the biggest challenge for researchers to construct the host polymer network mathematically. Fortunately, fractal like behavior of different types of polymer materials have been reported by many researchers till date. But these type of fractals are natural fractals where the fundamental self-similarity property has been maintained in a stochastic manner. Construction of these kind of natural fractals require rigorous mathematical techniques which eventually brings another level of complexity inside the simulation process. Considering all pros and cons we have decided to use a deterministic fractal as a tool to model a host solid polymer electrolyte sample mathematically and for this purpose, Vicsek fractal has been used as it is a deterministic, loop-less, finitely ramified fractal that provides substantial advantages in case of ionic transportation study inside the SPE sample. The desirable justification for the selection of Vicsek fractal for our present theoretical investigation, has been provided elaborately in chapter-3. The effect of gamma irradiation inside any arbitrary SPE can be observed in different forms. In the present study we are only focused to investigate the consequence of

radiation induced scission and intermolecular cross linking process inside the said sample. The entire thesis has been organized into five chapters.

Chapter-1 consists of a general introductory idea about polymers and their classifications. Post which, a brief idea regarding solid polymer electrolyte, its different characteristics, it's importance in solid state devices and applications has been delivered chronologically. In addition to that, the ion conduction mechanism inside the solid polymer electrolytes (SPE) have been discussed extensively. In this context, we have highlighted few theoretical models that provides a quantitative analysis regarding the bulk dc conductivity inside an arbitrary SPE. The temperature dependence of ionic conductivity and some relevant mathematical equations (e.g. Arrhenius theory, VTF, WLF equation) has also been discussed here. Finally, we have given a brief overview regarding different experimental techniques which are adopted for the enhancement in the performance of different SPE. The chapter ends with a short overview on the applicability of SPE in different wings of electrochemical devices.

Chapter-2 is basically segregated in two parts. The first part consists of a brief overview regarding the basic idea about fractals and their basic characteristics. The classifications of different fractals has also been discussed in this context. Application of different types of fractals to characterize various properties of disordered media has also been discussed here very briefly. The second part of this chapter deals with the detailed mathematical analysis regarding diffusion. Initially the theory of diffusion and its classifications has been discussed briefly. Later the nature of diffusion inside the fractal has been analyzed elaborately. The procedure of computer simulation to simulate the diffusion process inside the fractal object has also been included here. In this regard, two types of algorithm: "blind ant" and "myopic ant" has been discussed briefly.

Chapter-3 deals with the detailed theoretical investigation regarding the effect of gamma irradiation on the molecular distribution pattern of the SPE. Initially a host polymer sample has been constructed mathematically with the help of Vicsek fractal based on certain assumptions. The radiation induced scission and cross-linking process has been incorporated mathematically. Effect of gamma irradiation on molecular distribution has been extensively evaluated based on a Master equation. The variation of molecular distribution in both scission as well as cross-linking dominating region has been extensively studied in this chapter for both mono-disperse as well as poly-disperse samples.

Chapter-4 basically consists of the computer simulation study regarding the variation of different molecular weight averages of the solid polymer electrolyte sample due to the application of gamma irradiation. In present research work, four different types of molar mass averages have been considered for the investigation: number average molecular weight $\langle M_n \rangle$, weight average molecular weight $\langle M_w \rangle$, viscosity average molecular weight $\langle M_v \rangle$ and z-average molecular weight $\langle M_z \rangle$. Initially, quantitative discussion have been done regarding the four different molar mass averages. Post which the analysis of simulation procedure of those molar mass averages has been mentioned briefly. In this case we have used the molecular distribution of the sample that has been calculated from the master equation, mentioned in chapter-3. The simulated results have been extensively discussed for both mono-disperse and poly-disperse systems in four different cases: 1. pure scission and pure crosslinking cases, 2. Scission dominating region, 3. Cross-linking dominating region, 4. Intermediate case where scission and cross-linking occurs with equal probabilities.

Chapter-5 deals with the study of the variation in ionic conductivity inside the host SPE due to the application of external gamma irradiation. In this chapter, some basic assumptions have been taken initially to perform the computer simulation. The single ionic motion inside the host SPE is assumed to be controlled by two factors: 1. Intramolecular trapping of ions and 2. The segmental motion of the polymer chain segments. The implementation of these two effects inside the Vicsek fractal have been elaborately discussed here. We have taken a mathematical function $\tau_1(s) = (exp(-bs^c))$ empirically to incorporate the effect of segmental motion into the computer simulation process quantitatively and effect of trapping has been implemented with the help of the function:$\tau_2(s) = (3^s)^{d_w}$. We have also assumed unidirectional motion of ion to avoid any kind of computational complicacy.

Hence net time of travel as well as the total spatial distance traversed by the ionic species at a certain instant of time has been estimated with the help of computer simulation and from these data, ionic conductivity has been evaluated. The whole simulation has been performed for both mono-disperse and poly-disperse sample. The outcome of the simulation has been elaborately discussed in this chapter on the basis of radiation induced scission and cross-linking process in for different cases same as in chapter-4. Significant enhancement in ionic conductivity has been observed when scission process occurs with greater probability. Whereas the enhancement in ionic conductivity is reduced in the cross-linking dominating cases. Moreover, the enhancement is much more pronounced in case of mono-dispersed sample rather that the poly-disperse one. All these simulation results have been analyzed in details and compared with the experimentally observed fact in the discussion section of

each chapter.

Finally, a summary of the entire thesis work has been given in a separate section on the basis of the results obtained from the computer simulation, performed in each chapter. The overall summery is written on the basis of the effect of radiation induced scission and cross-linking process that occur simultaneously inside the host polymer sample and their impact on different structural as well as ion transporting parameters of the host SPE. At the end of this chapter we have discussed some future prospects regarding this topic.

Subhasish Ghosal
20.01.2022

Table of Contents

Dedication

Certificate from the Supervisor(s)

Acknowledgement i

Preface iv

1 Introduction 17

1.1 Alternative Energy Storage Device: A Short Overview 17

1.2 Polymer and Its Salient Features 18

1.3 Different Types of Polymers and their Characteristics 19

1.3.1 Rubbers, or elastomers: 20

1.3.2 Fibers 20

1.3.3 Thermoplastics: 20

1.3.4 Thermosets: 20

1.3.5 Linear polymers: 21

1.3.6 Branched Polymers: 22

1.3.7 Cross-linked or Network Polymers: 22

1.4 Ion Conducting Polymers 23

1.4.1 Polyelectrolyte 23

1.4.2 Polymer Electrolyte: 24
1.5 Polymer Electrolyte: Characteristics and Classification 24
1.5.1 Gel Polymer Electrolyte (GPE) 25
1.5.2 Composite Polymer Electrolyte (CPE) 25
1.5.3 Nanocomposite Polymer Electrolyte (NCPE) 26
1.5.4 Rubbery Polymer Electrolytes 27
1.5.5 Plasticized Polymer–Salt Complex: 27
1.5.6 Solid Polymer Electrolyte (SPE) 28
1.6 Solid Polymer Electrolyte and its Characterstics 28
1.7 Desirable Features of an Efficient SPE for Electrochemical Device Application. 31
1.7.1 Higher Mechanical Strength 31
1.7.2 High Ionic Conductivity 31
1.7.3 Excellent Processibility 32
1.7.4 Thermal Stability 32
1.7.5 Chemical and Electrochemical Stability. 32
1.7.6 Ionic Transference Number 33
1.8 Selection of Different Components of an Efficient SPE 33
1.8.1 Polymer 33
1.8.2 Salt 35
1.9 Different Methods to Enhance the Performance of SPE 37
1.9.1 Chemical Treatement 37
1.9.2 Physical Treatment 40
1.9.3 Application of External Irradiation on SPE 41
1.10 Mechanism of Ion Transportation Inside SPE 45
1.10.1 Temperature Dependence of DC Conductivity: A Short Overview . 48

1.10.2 Theoretical Models for The Characterisation of Bulk Conductivity . 50
1.11 Application of SPE 54
1.11.1 Solid State Batteries 55
1.11.2 Super Capacitor 57
1.11.3 Fuel Cell 58
1.11.4 Electro Chromic Display Devise (ECD) 59
1.11.5 Sensor 60

Bibliography **62**

2 Fractals and its Different Properties: A Short Review and Diffusion in Fractal Like Disordered Medium **84**

2.1 Introduction 85
2.2 Fractals and Their Intrinsic Characteristics 86
2.2.1 Self Similarity 86
2.2.2 Dialational Symmetry 88
2.2.3 Non Integer Dimension 88
2.2.4 Ramification 91
2.2.5 Fractals, with and without loop 93
2.3 Classification of Fractals 94
2.3.1 Deterministic Fractals 94
2.3.2 Random Fractal 100
2.4 Fractal Like Behavior of Host Polymer Sample: A Short Review 100
2.5 Theory of Diffusion 104
2.5.1 Fick's First and Second Law of Diffusion 105
2.6 Normal Diffusion 106
2.6.1 Theory of Random Walk 107

2.6.2 Random Walk in Continuous limit: Diffusion Equation and its Solution 110

2.6.3 Diffusion and Conductivity: Einstein's Relation 111

2.7 Anomalous diffusion 113

2.7.1 Continuous Time Random Walk 114

2.8 Nature of Diffusion inside Fractal 117

2.8.1 Random walk on fractal object 118

2.8.2 Conductivity and Einstein Relation inside Fractal Objects 121

2.9 Loopless Fractals and Their Role in Modelling Polymer Structures 122

2.9.1 Relation between the Structural and Transport Exponent in Loopless Fractal: 125

2.10 Computer Simulation of Random Walk Process 126

2.10.1 Computer Simulation Algorithm for Random Walk Process inside Fractals 127

2.10.2 Different types of Simulation Process: A Brief Overview 129

2.10.3 Different types of Discrete Random Walk Algorithm 130

2.10.4 Errors in Computer Simulation Process 131

2.10.5 Limitation of Computer Simulation Process in Fractal System 132

Bibliography **133**

3 Effect of Gamma Irradiation on the Molecular Weight Distribution of Solid Polymer Electrolyte: A Computer Simulation-based Theoretical Study on Deterministic Fractal Model. **141**

3.1 Introduction 142

3.2 Literature Review 142

3.3 Basic Assumptions for The Computer Simulation 147

3.4 Novelty of Using Vicsek Fractals as a Mathematical Tool for Modelling Polymer Sample 149

3.5 Method of Computer Simulation . . . 152
3.5.1 Modelling of the Host Polymer Sample . . . 152
3.5.2 Modelling of Mono-disperse SPE Sample . . . 152
3.5.3 Modeling of Poly-Disperse SPE Sample . . . 154
3.5.4 Implementation of Scission and Cross-linking Process Mathematically 157
3.5.5 Master Equation to Calculate the Molecular Weight Distribution . . 160
3.6 Detailed Analysis of the Results Obtained from Computer Simulation . . . 166
3.6.1 Effect of Gamma Irradiation on Molecular Distribution pattern of Mono-disperse SPE . . . 166
3.6.2 Effect of Gamma Irradiation on Molecular Distribution pattern of a Poly-disperse SPE Sample . . . 175
3.6.3 Discussion about the simulation results on the basis of Experimental outcomes . . . 185
3.7 Conclusion . . . 186

Bibliography **188**

4 Response of Different Molar Mass Averages of a Solid Polymer Electrolyte to Gamma Irradiation: A Theoretical Analysis Based on Computer Simulation on Deterministic Fractal Model **195**

4.1 Introduction . . . 196
4.2 Literature Review . . . 197
4.3 Classification of Molar Mass Averages . . . 200
4.3.1 Number Average Molecular Weight $\langle M_n \rangle$ . . . 202
4.3.2 Weight Average Molecular Weight $\langle M_w \rangle$ . . . 203
4.3.3 Viscosity Average Molecular Weight $\langle M_v \rangle$ . . . 205
4.3.4 Z-Average Molecular Weight $\langle M_z \rangle$ . . . 208

4.4 Computer Simulation Method to Study the Variation of Molar Mass Average due to Gamma Irradiation 208

4.4.1 Number average molecular weight $\langle M_n \rangle$ 211

4.4.2 Weight average molecular weight $\langle M_w \rangle$ 211

4.4.3 Viscosity Average Molecular Weight $\langle M_v(t) \rangle$ 212

4.4.4 Z-average molecular weight $\langle M_z(t) \rangle$ 214

4.5 Results of the computer simulation 214

4.5.1 Effect of Gamma Irradiation on Different Average Molecular Weights (Molar Mass Averages) for Mono-disperse SPE sample 215

4.5.2 Effect of Gamma Irradiation on Different Average Molecular Weights (Molar Mass Averages) for Poly-disperse SPE Sample 229

4.5.3 Discussion Regarding the Outcome of Simulation on the Basis of Various Experimentally Observed Facts 242

4.6 Conclusion 244

Bibliography **246**

5 Gamma Irradiation Induced Ionic Conductivity Variation on a Solid Polymer Electrolyte System: Theoretical Investigation Based on Deterministic Fractal Model. **251**

5.1 Introduction 252

5.2 Literature Review 252

5.3 Basic Assumptions for the Computer Simulation to Study the Radiation Induced Ion Conductivity Variation inside the SPE 258

5.4 Factors Affecting the Ionic Motion inside the Host Polymer Sample 260

5.4.1 Trapping of Ion inside the Host Polymer Molecules 260

5.4.2 Incorporation of the effect of Segmental Motion of the Polymer Chain Segments 264

5.5 Computer Simulation Framework to Study the Ionic Motion inside the Solid Polymer Electrolyte Sample 268

5.5.1 An Overall Analysis of the Variation in T(s) and $\frac{R(s)}{T(s)}$ for Different Fractal Stages 269

5.5.2 Simulation of Inter-molecular Ionic Motion inside the Solid Polymer Electrolyte Sample 271

5.6 Result of the computer Simulation Study 274

5.6.1 Variation in ionic conductivity in Case of Mono-disperse SPE Sample. 274

5.6.2 Conductivity Variation in Poly-disperse SPE Sample 285

5.6.3 Corroboration of Enhancement in Ionic Conductivity as an Effect of Radiation Induced Scission Process inside the SPE System. 296

5.7 Discussion Regarding the Outcome of the Simulation on the Basis of Different Experimentally Observed Facts 299

5.8 Conclusion 300

Bibliography **302**

Summary and Future Direction of Research Work **312**

Publications and Seminar Attended **315**

List of Figures

1.1 *Schematic diagram of three different types of polymers (a)Elastomer: Molecular arrangement of an arbitrary elastomer sample is shown where both the cross-linked and entangled arrangement of the polymer chain segments are presented(b)Thermoplastic: polymer branches are joined with the main carbon backbone with a weak secondary bond in a random direction. (c)Thermoset: A heavily cross-linked thick network-like structure is shown.* 19

1.2 *Different types of polymers in everyday life. 1. (a) water bottles and (b)baby toy representing the examples of thermoplastic. 2. (c)sportsware and (d)synthetic wool, are example of fibers. 3. (e) switch, electric charger and (g)casserole are example of thermoset. 4. (f) rubber band, example of elastomer or rubber.* 21

1.3 *Schematic diagram of three different types of polymers based on their structure (a)Linear Polymers: single polymer chains without any side branches(b)Branched polymers: Branches of different lengths are associated with the main polymer backbone. (c)Network Polymers: forms network like structure due to heavy cross-linking* 22

1.4 *Schematic diagram of three different types of Nanocomposite Polymer electrolytes. The arrangement of polymer chain segments and the nanocomposite materials are shown here* 26

1.5 *Schematic diagram of a Solid Polymer Electrolyte sample where the lithium(Li^+) ions are embedded inside the polymer chain segments* 29

1.6 *Semi-Crystalline behavior of the Polymer electrolyte sample. The embedded orderly arranged regions indicate the crystalline region whereas the randomly arranged polymer chains indicate the amorphous phase of the SPE.* 30

1.7 *Classification chart expressing different methods for the enhancement in performance of SPE* 36

1.8 *Pictorial representation of the filler particle addition to the host polymer matrix.* 38

1.9 *Schematic representation of the effect of chain scission due to irradiation on the SPE sample. (a) the unirradiated SPE sample. Both Crystalline (orderly arranged polymer chains) and amorphous regions are shown. (b) the same sample after irradiation. The chain scission regions are highlighted by red circles.* 43

1.10 *Schematic representation of the effect of chain cross-linking due to gamma irradiation on the SPE sample. (a) the unirradiated SPE sample. Simple molecular chain distribution is shown. (b) The same sample after gamma irradiation. Both the intermolecular and intramolecular cross-linking regions are labeled separately.* 44

1.11 *Schematic representation of the intrachain and interchain hopping of ionic species inside the host polymer matrix* 46

1.12 *Schematic representation of the ionic motion due to the segmental motion of the polymer chain segments* 47

1.13 *Schematic diagram of the displacement of molecule or chain segment A. Initially it was located at the position of B. Dislocation of A is occurred and its initial position is occupied by B. The arrow shows the next dislocation direction of A and B.* 50

1.14 *Schematic diagram of a solid state battery.* 56

1.15 *Classification chart of the supercapacitor.* 58

1.16 *Schematic diagram of a fuel cell.* 59

1.17 *Schematic diagram of a Electro Chromic Display Devise (ECD).* 60

2.1 *Self similarity behavior of vicsek fractal. Figure-(A),(B) and (C) represents the $1^{st}, 2^{nd}$ and 3rd stage of vicsek fractal respectively. It should be noted that the part WXYZ of 3rd stage Vicsek fractal is exactly similar with 2nd stage.* 87

2.2 *Fractal growth is schematically presented using Sierpinski Gasket (SG) fractal. In the first case, generation of higher stage fractals has been shown using subsequent division method. The second case shows the generation of higher stage SG fractal by subsequent growth method.* 90

2.3 *Schematic diagram of a 3rd stage Siesrpenski Gasket fractal which is showing the calculation of ramification in two different sites.* 92

2.4 *Schematic diagram of Sierpinski Carpet as an infinitely ramified fractal. The line segments AB, BD, DC, and CA are used to separate an arbitrary part ABDC of the fractal which indicates that Sierpinski Carpet is an infinitely ramified fractal .* 93

2.5 *Schematic diagram of (A)Sierpinski Gasket and (B)Sierpinski Tree. Interestingly both of them have the same fractal dimension but their patterns are different. The first one is a looped fractal whereas the second one is loop-less.* 94

2.6 *Schematic diagram of Cantor bar of $0^{th}, 1^{st}, 2^{nd}, 3^{rd}$ stages respectively* . . . 96

2.7 *Schematic diagram of Coch Curve of $1^{st}, 2^{nd}, 3^{rd}$ stages respectively* 97

2.8 *Schematic diagram of Sierpinski Gasket of $1^{st}, 2^{nd}, 3^{rd}$ stages respectively* . 98

2.9 *Different types of random fractals, found in nature. 1. (a) and (b) leaf of Curled Kale (**Brassica oleracea var.sabellica**) . Fractal like fragmented pattern can be seen at the edges of the leafs. 2. (c) and (d) veins of Papaya leaf (**Carica papaya**) and (e) Pak Choi veins (**Brassica rapa chinensis**) shows natural fractal like pattern. 3. (g) fractal like pattern of different branches of Broccoli (**Brassica oleracea var.italica**). 4. (f) and (h) fractal pattern of Cauliflower (**Brassica oleracea var.botrytis**) surface.* 99

2.10 *A schematic diagram of simple random walk. The net displacement of the walker from the initial point to final point is mentioned by the arrow mark.* 108

2.11 *A schematic diagram of random jump in 1-dimension. The walker start from the mth site and moves to the one of the either sites with equal probability.* . 110

2.12 *Waiting time distribution of the walker in case of continuous time random walk. The holes represent the waiting time of the walker. Bigger the size of the hole longer the waiting time of the walker at the respective site.* 115

2.13 *An example of Deterministic Loop less fractal.* 122

2.14 *A schematic diagram of Cayley tree.* 123

2.15 *A schematic diagram of a loopless fractal tree. It has same fractal dimension as of the Sierpinski Gasket but here loops are not present.* 125

3.1 *Schematic diagram of solid polymer electrolyte (SPE) sample. The un-irradiated sample has an arbitrary arrangement of polymer chain segments. The application of gamma irradiation introduces crystalline and amorphous phases inside the sample which can be seen clearly* 148

3.2 *Schematic representation of Vicsek fractal from* 1st *to* 5th *stage. It can be observed clearly that the number of monomers and the structural complexity is increased rapidly but the self-similarity behavior is maintained perfectly.* . 150

3.3 *Schematic representation of 1-dimensional mono-disperse polymer sample, modeled by* 7th *stage Vicsek fractals. Here Vicsek fractals are arranged linearly side by side and joined diagonally with each other along X-axis.* 7th *stage Vicsek fractal have a highly complicated structure that may not be observable easily in the present scaling, Therefore they are represented by the green squares in the picture.* 153

3.4 *Schematic representation of an un-irradiated poly-disperse sample, modeled by Vicsek fractals of different fractal stages. A random arrangement of* 2nd,3rd,4th,5th, *stages Vicsek fractals has been shown here. They are joined diagonally with each other along X-axis. It should be noted that the figure only shows the random alignment of the Vicsek fractals but they are not drawn as per their original scalling for better visualization.* 155

3.5 *Graphical representation of the molecular distribution among different fractal stages of an un-irradiated mono-disperse polymer sample, modeled by Vicsek fractals.(A) Symmetric distribution of weight fraction* $(W_f(s,t))$ *among* $5^{th}, 6^{th}, 7^{th}$ *stages. (B) Distribution of molecules N(s,t) among those stages. N(s,t) is plotted in log scale for better understanding.* 156

3.6 *Schematic representation of the radiation-induced intra-molecular scission process inside the SPE sample, modelled by Vicsek fractal. Here, scission process is presented in two consecutive time steps on 3rd and 2nd stage Vicsek fractal respectively.* 157

3.7 *Schematic representation of the radiation-induced inter-molecular Cross-linking process inside the SPE sample, modelled by Vicsek fractal. Here, scission process is presented in two consecutive time steps on 3rd and 2nd stage Vicsek fractal respectively.* 158

3.8 *Schematic representation of the computer simulation algorithm* 162

3.9 *Graphical presentation of the variation in molecular weight distribution in case of pure scission process. (A) $(W_f(s,t))$ vs fractal stage (s) curves for different irradiation time steps t. (B) N(s,t) vs s variation curve for different time step t. The continuous curves in (A) are for the "guide to the eye". Although, the respective data are in the form of discrete points.* 168

3.10 *Variation of weight fraction distribution and molecular number distribution in pure cross-linking (*100% *cross-linking)process inside a mono-disperse sample. (A) $(W_f(s,t))$ vs (s) curves for different time steps t. (B) N(s,t) vs s curves for different time step t. The continuous curves in (A) are for the "guide to the eye". Although, the respective data are in the form of discrete points.* . . 169

3.11 *Variation of $(W_f(s,t))$ distribution of a mono-disperse SPE sample for different time steps t in scission dominating region. (A) $(W_f(s,t))$ variation curve for different time steps t in case of 90% Scission process. (B) $(W_f(s,t))$ variation curve for different time steps t in case of 70% Scission process. The continuous curves in (A) and (B) are for the "guide to the eye". Though the respective data are in the form of discrete points.* 171

3.12 *Variation of $(W_f(s,t))$ distribution of a mono-disperse SPE sample for different time steps t in cross-linking dominating region. (A) $(W_f(s,t))$ variation curve for different time steps t in case of 90% Cross-linking process. (B) $(W_f(s,t))$ variation curve for different time steps t in case of 70% Cross-linking process.The continuous curves in (A) and (B) are for the "guide to the eye". Although, the respective data are in the form of discrete points.* . . 173

3.13 *Variation of molecular weight distribution curve for different irradiation time steps t when scission and cross-linking occurs in equal rates(50% scission). (A) ($W_f(s,t)$) vs s curves for different time steps t. (B) N(s,t) vs s curves for different time steps t. The continuous curves in (A) and (B) are for the "guide to the eye". Though, the respective data are in the form of discrete points.* 175

3.14 *Graphical presentation of the variation in molecular weight distribution in case of pure scission (100% scission) process for a poly-disperse SPE sample. (A) ($W_f(s,t)$) vs fractal stage (s) curves for different irradiation time steps t. (B) N(s,t) vs s variation curve for different time step t. The continuous curves in (A) and (B) are for the "guide to the eye". Although, the respective data are in the form of discrete points.* 176

3.15 *($W_f(s,t)$) and N(s,t) Variation curves in pure cross-linking (100% cross-linking) process inside a poly-disperse sample. (A) ($W_f(s,t)$) vs s curves for different time steps t. (B) N(s,t) vs t curves for different time steps t. The continuous curves in (A) and (B) are for the "guide to the eye". Though the respective data are in the form of discrete points.* 179

3.16 *Variation of weight fraction ($W_f(s,t)$) of a poly-disperse SPE sample in scission dominating region. (A) ($W_f(s,t)$) vs s curves for different time step t when the probability of scission is 90%. (B)The same ($W_f(s,t)$) vs s curves in case of 70% scission process. The continuous curves in (A)and (B) are for the "guide to the eye". Though, the respective data are in the form of discrete points* 181

3.17 *Variation of ($W_f(s,t)$) distribution of a poly-disperse SPE sample for different time steps t in cross-linking dominating region. (A) ($W_f(s,t)$) variation curve for different time steps t in case of 90% Cross-linking process. (B) ($W_f(s,t)$) variation curve for different time steps t in case of 70% Cross-linking process. The continuous curves in (A) and (B) are for the "guide to the eye".Although, the respective data are in the form of discrete points.* . . 182

3.18 *Variation of $(W_f(s,t))$ and N(s,t) distribution curves for a poly-disperse SPE sample when the probability of scission is 50%. (A) $(W_f(s,t))$ vs s curves for different time steps t. (B) N(s,t) vs s curves for different time steps t. The continuous curves in (A) and (B) are for the "guide to the eye". Though, the respective data are in the form of discrete points* 184

4.1 *Representation of the computer simulation process to study the radiation induced molar mass average variation with the help of a flow chart* 209

4.2 *Different types of molar mass averages and their mathematical expressions for computer simulation.* 213

4.3 *Variation of number average molecular weight $\langle M_n \rangle$ with the external gamma irradiation for pure scission and pure cross-linking process. (A) Rapidly decreasing $\langle M_n \rangle$ variation curve in case of pure scission process. (B) $\langle M_n \rangle$ variation curve increases sharply in the case of pure cross-linking process. The variation of molecular distribution in the case of pure scission and cross-linking process are respectively shown in the inset of both figures.* 216

4.4 *$\langle M_n \rangle$ vs t variation curves for radiation induced intermediate cases.(A) Rapidly decreasing $\langle M_n \rangle$ vs time step t curves in the case of intermediate scission dominating region (50% to 90% scission process). (B) $\langle M_n \rangle$ vs time step t curves in the case of intermediate cross-linking dominating process (10% to 40% scission process).* 217

4.5 *Variation of weight average molecular weight $\langle M_w \rangle$ with the exposure time to irradiation (time steps (t)). (A) $\langle M_w \rangle$ decreases sharply with time steps (t) in case of pure scission (100% scission) process. (B) The fast increasing behavior of $\langle M_w \rangle$ variation curve for the pure cross-linking (100% cross-linking) process is shown here.* 219

4.6 *Variation of weight average molecular weight $\langle M_w \rangle$ with the exposure time to irradiation or time steps (t) for intermediate cases where scission and cross-linking processes occur simultaneously. (A) $\langle M_w \rangle$ variation curves for different scission percentages (60% to 90% scission probability) in case of intermediate scission process dominating region. The peaks of the individual curves can be noted. (B) $\langle M_w \rangle$ variation curves in the case of the intermediate cross-linking process dominating process (20% to 50% scission probability) are presented here. The individual curves attain saturation stage very fast.* . 220

4.7 *Variation of viscosity average molecular weight $\langle M_v \rangle$ with the exposure time to irradiation or time steps (t). (A) $\langle M_v \rangle$ vs t graphs in case of pure scission process (100% scission). Value of the exponent α =0.5. The graph will be identical for α =0.7 too. (B) $\langle M_v \rangle$ variation curve for pure cross-linking (100% cross-linking) process. Two graphs (for α =0.5 and 0.7) differ from each other at the saturation region when the system becomes poly-disperse* . 223

4.8 *Variation of viscosity average molecular weight $\langle M_v \rangle$ with the exposure time to irradiation or time steps (t) in case of intermediate scission dominating region (50% to 90% scission probability) for two different values of the exponent α.(A) $\langle M_v \rangle$ vs t variation curves for α = 0.5. (B) $\langle M_v \rangle$ vs t variation curves for α = 0.7.* 224

4.9 *Viscosity average molecular weight $\langle M_v \rangle$ variation with the exposure time to irradiation or time steps (t) in case of cross-linking process dominating region (10% to 40% scission) for two different values of α. (A)$\langle M_v \rangle$ vs t curves for α =0.5 (B) $\langle M_v \rangle$ vs t curves for α =0.7* 225

4.10 *Variation of Z- average molecular weight $\langle M_z \rangle$ with the exposure time to irradiation or time steps (t) in two extreme cases. (A) Rapid decrease in the behaviour of $\langle M_z \rangle$ vs t curve for pure scission (100% scission) process. (B) $\langle M_z \rangle$ increases sharply with time steps (t) in case of the pure cross-linking (100% cross-linking) process.* 227

4.11 *Variation of Z-average molecular weight $\langle M_z \rangle$ with irradiation time steps (t) for intermediate cases where scission and cross-linking processes occur simultaneously. (A) $\langle M_z \rangle$ variation curves in the scission process dominating region (50% to 90% scission probabilities). (B) $\langle M_z \rangle$ variation curves in case of the intermediate cross-linking dominating region (10% to 40% scission probabilities).* 228

4.12 *Variation of number average molecular weight $\langle M_n \rangle$ with respect to the irradiation time step (t). (A) A spontaneous sharp nonlinear decrease of $\langle M_n \rangle$ is noticed in the pure scission (100% scission) process. (B) Gradual enhancement of $\langle M_n \rangle$ is observed followed by a saturation region of $\langle M_n \rangle$ in case of pure cross-linking (100% cross-linking) process.* 230

4.13 *Variation of Number Average Molecular Weight $\langle M_n \rangle$ for intermediate cases where scission and cross-linking occurs simultaneously. (A) A sharp nonlinear decrease of $\langle M_n \rangle$ in case of intermediate scission process dominating region (60% to 90% scission). (B) Variation of $\langle M_n \rangle$ in case of cross-linking process dominating region (i.e. 10% to 50% scission probability). The trend of gradual decrease in behavior is changed here in the case of 10% scission probability.* 232

4.14 *Variation of weight average molecular weight $\langle M_w \rangle$ due to the application of external gamma irradiation in two extreme cases. (A) $\langle M_w \rangle$ decreases very fast in the case of the pure scission (100% scission) process. Later the curve attains its saturation value. (B) An abrupt step-like jump is observed in the $\langle M_w \rangle$ variation curve at t=7 for the pure cross-linking process.* 233

4.15 *Variation of weight average molecular weight $\langle M_w \rangle$ due to the application of external gamma irradiation in the intermediate cases where scision and cross-linking process occur simultaneously. (A) Gradual reduction of $\langle M_w \rangle$ vs t curves in case of intermediate scission (50% to 90% scission) process dominating region. (B) A gradual step-like enhancement is observed in ($\langle M_w \rangle$) vs t variation curve for the cross-linking process dominating(10% to 40% scission) region.* 235

4.16 *Variation of viscosity average molecular weight ($\langle M_v \rangle$) with time steps (t) for a poly-disperse sample in case of pure scission and pure cross-linking process. (A) $\langle M_v \rangle$ vs t curve for $\alpha = 0.5$ and $\alpha = 0.7$ incase of pure scission process. (B) Variation of $\langle M_v \rangle$ in case of pure cross-linking (i.e. 100% cross-linking) process. The red curve is for $\alpha = 0.7$ and the blue one is for $\alpha = 0.5$.* . . . 236

4.17 *Viscosity average molecular weight $\langle M_v \rangle$ variation curves for intermediate scission dominating region. (A) Variation of viscosity average molecular weight $\langle M_v \rangle$ in case of intermediate scission dominating region (60% to 90% scission probabilities) where the value of the exponent $\alpha = 0.5$. (B) $\langle M_v \rangle$ vs t variation curves for the same scission dominating region (50% to 90% scission probabilities) where the value of the exponent $\alpha = 0.7$.* 237

4.18 *Variation of $\langle M_v \rangle$ with respect to the irradiation time steps (t) in case of the cross-linking dominating region. (A) Four $\langle M_v \rangle$ vs t curves ranging from 10% to 40% scission process where $\alpha = 0.5$. (B) The same $\langle M_v \rangle$ vs t curves are plotted taking $\alpha = 0.7$* 238

4.19 *Variation of Z-average molecular weight $\langle M_z \rangle$ with external gamma irradiation in two extreme cases. (A) $\langle M_z \rangle$ vs time step (t) curve for pure scission process. (B) $\langle M_z \rangle$ vs t variation curve in case of pure cross-linking process.* 240

4.20 *Variation of z-average molecular weight $\langle M_z \rangle$ due to the application of external gamma irradiation in two intermediate cases where scission and cross-linkig processes occur simultaneously. (A) $\langle M_z \rangle$ vs t curves in scission process dominating region (50% to 90% scission).(B) Variation of $\langle M_z \rangle$ in case of intermediate cross-linking process dominating region (10% to 40% scission).* 241

5.1 *Unidirectional ionic motion inside a SPE sample which is modelled by a 1-dimensional array of Vicsek fractals having different fractal stages. The single ion (indicated by the blue ball) moves along the positive X-axis as per our assumption.* 259

5.2 *Random hopping of ion inside a polymer chain segment. The entrance, as well as exit of the ion, is symbolized by the prominent green balls. Whereas, the faded green balls indicate the intermediate positions of the ion inside the polymer chain segment.* 260

5.3 *Random walk motion of ion inside the Vicsek fractal. Ion enters from one end of diagonal (A) and exits from the opposite end (B). In the meantime, the ion moves randomly through different accessible sites inside the Vicsek fractal. The red arrows show the trajectory of the ion inside the fractal lattice. This is a schematic diagram. The trajectory can be different from that is shown in the figure* 261

5.4 *(A) Variation of trapping time $\tau_1(s)$ of an ion with the fractal stage (s) of molecules. $\tau_1(s)$ is plotted along Y-axis in log scale as it increases very rapidly with the increase in fractal stage (s). (B) Variation of the total number of monomer M(s) in an arbitrary fractal molecule with its fractal stage (s).* . . 263

5.5 *A schematic diagram representing the segmental motion of polymer chain segments and enhancement in ionic motion associated with the respective chains. 3 consecutive stages have been used. In stage-1, chain-a and chain-b are at their initial arbitrary positions and the ion (green ball) is associated with chain-a by making a chemical bond. The arrangement of chain-b is changed in stage-2 due to its segmental motion and it eventually comes closer to the ion. As a result, the ion moved from chain-a to chain-b by making a new chemical bond with the respective atom of chain-b. The chain-b in association with that ion moves apart from chain-a in stage-3 due to its segmental motion resulting in a fast ionic transport from one position to another.* . . . 265

5.6 *Implementation of the concept of segmental motion on Vicsek fractal. 3rd stage Vicsek fractal has been taken into account and the segmental motion of the polymer chain segments are represented by the motion of four arms-(1), (2), (3), and (4) of the Vicsek fractal. Initially, the four arms are placed at their respective position at time=t as shown in stage-1. The ion (indicated by the blue ball), under consideration, is associated with the arm-(1). The arm-1 changes its position at the time=(t+1) due to the segmental motion and comes closer to the arm-2. The ion which is associated with arm-1 is eventually moved to arm-2 as shown in the stage-2. The arm-4 also changes its position in this stage. In stage-3, arm-1 and arm-4 return to their previous location whereas arm-2 comes closer to arm-3. As a result, the ion moves from arm-2 to arm-3.* 267

5.7 *(A)Variation $\tau_2(s)$ of the individual molecules with their respective fractal stages. $\tau_2(s)$ is plotted along Y-axis in log scale. As the size of the molecule i.e. its fractal stage (s) increases, the magnitude of $\tau_2(s)$ decreases very rapidly. The values of the fitting parameters b and c are taken as 9.0 and 0.4 respectively. (B) Variation in the number of monomers M(s) of the Vicsek fractals with their fractal stages.* 268

5.8 *Variation of the total traveling time T(s) of an ion inside an arbitrary fractal molecule with a fractal stage (s). The magnitude of T(s) is plotted along Y-axis and it is taken in log scale as its value increases very rapidly with the increase in fractal stage (s).* 270

5.9 *Variation in [K(s)] i.e. the ratio of the diagonal distances R(s) of a fractal molecule to the total traveling time T(s) ($\frac{R(s)}{T(s)}$) of an ion inside that polymer molecule, with its fractal stages (s). The curve shows a peak at s=4 indicating that the highest value of K(s) comes for the molecules with fractal stage s=4.* 271

5.10 *(a) Unidirectional ionic motion through the linear array of polymer molecules modeled with Vicsek fractals of different stages. The fractals are arranged diagonally side by side in a random manner in the XY plane. (b) Unidirectional ion hopping from one molecule to another one from a macroscopic point of view. (c) Random motion of the ion inside the individual fractal molecule with arbitrary fractal stage.* 273

5.11 *(A) Variation in ionic conductivity $\sigma(t)$ with respect to the exposure time to irradiation or time step (t) in case of pure scission process (100% scission or 0% cross-linking). $\sigma(t)$ is plotted along Y-axis and time step (t) is along X-axis. The $\sigma(t)$ vs t curve has a peak at the 3rd time step. (B) Molecular distribution among different fractal stages (s) in different time steps (t). The system remains mono-disperse throughout the irradiation process.* 276

5.12 *(A) Variation in ionic conductivity ($\sigma(t)$) with the exposure time to irradiation or time step (t) in case of radiation-induced pure cross-linking (100% cross-linking or 0% scission) process. The $\sigma(t)$ vs t curve shows a gradual decrease in the rate of reduction and $\sigma(t)$ remains unchanged after time step t=4. (B) Molecular distribution in the polymer sample among different fractal stages (s) in different time steps (t).* 277

5.13 *Variation of ionic conductivity ($\sigma(t)$) with respect to the time step (t) in case of radiation-induced scission process domination region (ranging from 90% to 60% scission process). $\sigma(t)$ is plotted along Y-axis and time step (t) is along X-axis. All the $\sigma(t)$ vs t variation curves have definite peaks which indicate a significant enhancement in $\sigma(t)$. The height and sharpness of the peak in $\sigma(t)$ vs t curves reduces with the reduction in scission percentage.* 280

5.14 *Variation in ionic conductivity $\sigma(t)$ with the exposure time to irradiation or time step (t) in case of radiation-induced cross-linking process domination region. Total six $\sigma(t)$ vs t curves are shown indicating 30%,35%,37%,40%,42% and 45% scission probabilities respectively. $\sigma(t)$ vs t variation graphs have been plotted over a long duration of irradiation time steps (ranging from 0 to 250 units). Enhancement in $\sigma(t)$ is reduced significantly with the decrease in scission probability. An initial reduction in $\sigma(t)$ is observed in most of the curves.* 281

5.15 *Variation in ionic conductivity ($\sigma(t)$) to the exposure time to irradiation or time step (t) in the case of radiation-induced cross-linking process domination region. The rate of cross-linking is very high and a total of three $\sigma(t)$ vs t curves are shown here indicating 10%, 15%, and 20% scission probabilities respectively. Each $\sigma(t)$ vs t curve shows gradual decrease in behaviour and each of them achieves a steady-state value after t=20.* 282

5.16 *(A) Variation of ionic conductivity $\sigma(t)$ with respect to the exposure time to irradiation or time step (t) in the case where scission and cross-linking processes occur with equal probabilities (50% scission and 50% cross-linking). $\sigma(t)$ is plotted along Y-axis and time step (t) is along X-axis. A peak curve is observed in this case and $\sigma(t)$ attains its minimum value after t= 150 units. (B) Distribution of the total number of molecules N(s,t) having fractal stage (s) at different irradiation time steps (t). The gradually diminishing peaks of the distribution curves shift towards the left side in the higher fractal stage region as the irradiation time steps increase gradually.* 284

5.17 *(A) Variation of ionic conductivity ($\sigma(t)$) with respect to the exposure time to irradiation or time step (t) in case of radiation-induced pure scission process (100% scission or 0% cross-linking) for poly-disperse sample. The $\sigma(t)$ vs t curve has a peak at 4th time step. (B) Molecular distribution pattern of the polymer sample in different time steps. The number of molecules (N(s,t)) are plotted along Y-axis in log scale as N(s,t) increases very rapidly with the increase in (t).* 287

5.18 *(A) Variation of ionic conductivity ($\sigma(t)$) with respect to the exposure time to irradiation or time step (t) in case of radiation-induced pure cross-linking (100% cross-linking or 0% scission) process for poly-disperse sample. No conductivity enhancement is observed in this case. The rate of fall of $\sigma(t)$ with time step (t) is not so fast as in the case of the mono-disperse system. (B) Molecular distribution of the polymer sample in different time steps. The number of molecules (N(s,t)) are plotted along Y-axis in log scale and the fractal stages are taken along the X-axis. As the time step increases, the value of N(s,t) is reduced and the size of the molecules increases though the peak of the distribution curve remains at the same position.* 288

5.19 *Variation of ionic conductivity ($\sigma(t)$) with respect to the exposure time to irradiation or time step (t) in case of radiation-induced scission process dominating region ranging from 60% to 90% scission process for the poly-disperse SPE system. All the $\sigma(t)$ vs t variation curves have definite peaks showing definite enhancement in ionic conductivity $\sigma(t)$.* 290

5.20 *Variation of ionic conductivity ($\sigma(t)$) with respect to the exposure time to irradiation or time step (t) in case of radiation-induced cross-linking process dominating region for the poly-disperse SPE system. Six $\sigma(t)$ vs t curves are shown here indicating 30%, 35%, 37%, 40%, 42% and 45% scission probabilities respectively. Enhancement in $\sigma(t)$ is reduced gradually with the decrease in scission percentage. The initial reduction in $\sigma(t)$ is not so intense as observed in the case of mono-disperse samples.* 292

5.21 *Variation in ionic conductivity ($\sigma(t)$) with respect to the exposure time to irradiation or time step (t) for radiation-induced cross-linking process dominating region in case of a poly-disperse sample. A total of three $\sigma(t)$ vs t curves are shown indicating 10%, 15%, and 20% scission probabilities respectively. $\sigma(t)$ variation shows gradually decreasing curves and therefore no conductivity enhancement has been observed.* 294

5.22 *Ionic conductivity ($\sigma(t)$) variation with irradiation time step (t) for the poly-disperse system in case where scission and the cross-linking processes occur with equal probabilities (50% scission and 50% cross-linking). $\sigma(t)$ vs t curve attains the peak at t=12 and this curve attains a steady-state value after t= 50 units which is much earlier than as compared to mono-disperse system. (B) The variation of the total number of molecules N(s,t) having different fractal stages with the irradiation time steps (t). The peak of the distribution curve shifts towards the left side in the higher fractal stage region as the irradiation time steps increase gradually.* 295

5.23 *Variation in maximum ionic conductivity $\sigma_{max}(G)$ as a function of scission probabilities (i.e. G) for the mono-disperse system. Maximum ionic conductivity $\sigma_{max}(G)$ is reduced with the reduction in scission probabilities and attains a steady-state value after the 30% scission process.* 297

5.24 *Variation in maximum ionic conductivity i.e. $\sigma_{max}(G)$ as a function of scission probabilities for the poly-disperse system. Here also maximum ionic conductivity $\sigma_{max}(G)$ is reduced with the reduction in scission probabilities and attains a steady-state value after the 35% scission probability.* 298

Chapter-1

Introduction

Chapter 1

Introduction

1.1. Alternative Energy Storage Device: A Short Overview

One of the most important challenges in the 21st century is to provide a constant and uninterrupted supply of energy for modern civilization. Conventional energy sources like fossil fuels have inadequate storage and result in many significant adverse impacts on nature. In this scenario, an extensive search for alternative energy sources happens to be an inevitable consequence. Alternative energies such as solar, tidal, hydro, wind energy, etc. are proved as very efficient and environment-friendly sources. However, portability, budget, durability, miniaturization etc. are also happened to be serious concerns for scientists. In short, the invention of a user-friendly, portable energy storage device happens to be the prime objective of research activities across the globe for the past few decades. In this regard, the application of different electrochemical devices is considered an elegant and smart approach in the field of energy storage research as they provide high conversion efficiency without delivering a huge amount of harmful gases[1,2].

Electrochemical devices and their significant contribution towards humankind happens to be an overwhelmingly acknowledged fact by us and hardly need any separate discussion[3]. They appear as the lifeline of modern civilization. The fundamental part of these devices is the batteries or cells, which comprise an anode, cathode, and electrolyte. Different types of electrolytes have been used so far in batteries and liquid electrolytes are proved to be very effective. Faster ion transportation can be observed in liquid electrolytes and therefore, desirable ionic conductivity can be achieved easily. But some major disadvantages are the harmful chemical reaction of the electrolyte materials with metal electrodes, leakage of

poisonous chemicals, difficulties in portability, etc. have also been reported[4]. The use of solid electrolytes has been proved to be very useful to overcome these drawbacks[5]. Solid electrolytes provide a rigid structure, which eventually gives a strong thermal as well as mechanical stability compared to liquid electrolytes. As a result, electrochemical devices, made from solid electrolytes, happen to be more compact and portable. Despite such advantages, ionic conductivity inside solid electrolytes happens to be very low at ambient temperature due to their rigid structure[6,7] which eventually makes them unsuitable for the large-scale application in electrochemical devices. Under such circumstances, researchers have performed an extensive investigation to find materials that can fulfill the requirements. In this regard, some polymers under certain conditions have been reported as efficient materials to be used in electrochemical devices.

1.2. Polymer and Its Salient Features

The use of polymeric substances has a profound history from the dawn of civilization. Their versatile applicability, lightweight, compact form, less chemically reactive nature, well accessibility, portability, etc. enhance the possibility of their practical application in a different realm of industries and research. Thus starting from the toothbrush that we use after waking up to the mattress made of synthetic cotton which we use at the time of sleep, almost every necessary item that we use in our everyday life, is made of polymer materials.

Polymer happens to be an organic compound with a large molecular weight. The word polymer was originated from the composition of two words: poly, which means many, and meres means parts. Each polymer molecule has a repeating structural unit called a monomer. These monomers are joined chemically with the help of a suitable polymerization process and generate a polymer molecule. Polymer materials depict different types of physical as well as chemical properties depending on the flexibility of the molecular chains, presence of different functional groups, regularity, etc. Primarily, polymers can be classified into two categories based on their source: biopolymers and synthetic polymers. Biopolymers are originated from living organic systems and are generally used without any significant modification. Textile fibers like silk, wool, cotton, wood, or rubber are examples of biopolymers. A large portion of materials that are used in our everyday life belongs to this category. On the other hand, synthetic polymers are produced artificially.

The structure of a polymer sample is highly complicated and cannot be described perfectly with the help of any mathematical simulation. One of the significant structural

features of polymer materials is their semi-crystalline nature. Generally, the crystallinity level inside a polymer sample is characterized by the degree of crystallinity and is expressed in the form of percentage[8–12]. A perfectly crystalline or amorphous polymer is very hard to prepare. Different types of experimental techniques like X-ray diffraction (XRD), Differential Scanning Calorimetry (DSC)[13,14], Small Angle X-ray Scattering (SAXS)[15], Infrared Spectroscopy[16,17] are used to measure the crystallinity level inside a polymer sample.

1.3. Different Types of Polymers and their Characteristics

Polymers are available in nature with their huge varieties. They can be classified into different categories based on different types of intrinsic and extrinsic properties. Therefore detailed discussion regarding all types of polymers is hardly possible in this present thesis. Hence, we will focus our attention on few types of polymer. It is well known that inter-molecular force (van-der Waal forces, hydrogen bonding, etc.) has a significant influence on mechanical properties of a polymer sample, such as tensile strength, toughness, elasticity, etc.[18]. Based on the inter-molecular force and the structure of the carbon backbone, polymers can be classified into the following categories:

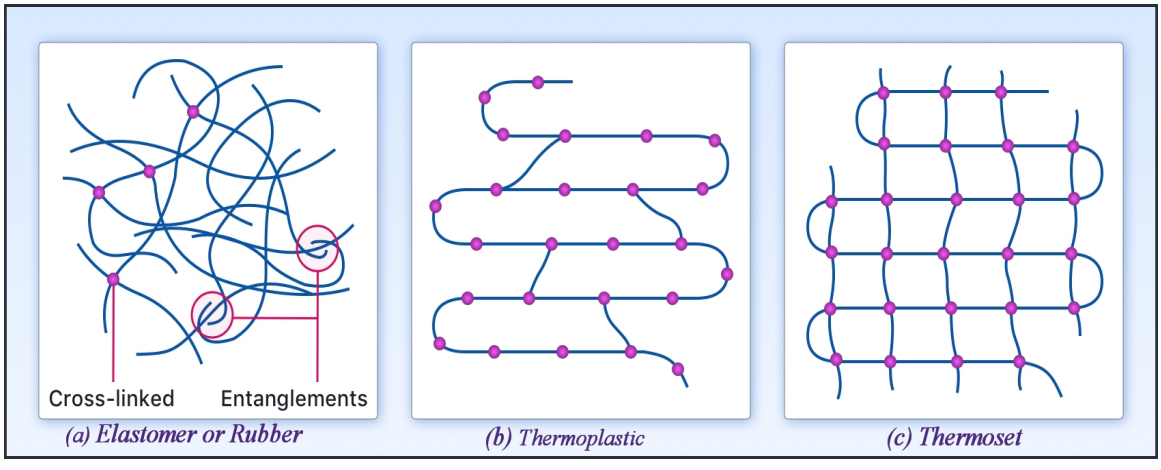

Figure 1.1: *Schematic diagram of three different types of polymers (a)Elastomer: Molecular arrangement of an arbitrary elastomer sample is shown where both the cross-linked and entangled arrangement of the polymer chain segments are presented(b)Thermoplastic: polymer branches are joined with the main carbon backbone with a weak secondary bond in a random direction. (c)Thermoset: A heavily cross-linked thick network-like structure is shown.*

1.3.1. Rubbers, or elastomers:

These types of polymers can form cross-linked networks. They constitute polymer chains that can be tangled. A schematic diagram of elastomers has been shown in figure-1.1. They are stretchable and their cross-linked structure sometimes helps them to restore their initial shape. Elastomers have the weakest intermolecular attractive force[18] and a very low degree of crystallinity. They are workable above their glass transition temperature (T_g). The uses of these polymers are observed mostly in tire industries.

1.3.2. Fibers

The inter-molecular attractive force is very high. They are configured with long chains of carbon that have a few branches (sometimes no branches). The inter-molecular force produces a crystalline arrangement. High tensile strength is seen inside them. They are used in textile industries in most cases. $Nylon-6, Nylon-66$, Terylene[18].etc. are very commonly used fibers.

1.3.3. Thermoplastics:

Inter-molecular attractive forces of this type of polymers are intermediate between elastomers and fibers[18]. Thermoplastics are more often called plastics and they are made of linear or branched polymer chains which have been depicted in figure-1.1(b). These branches are joined with the main carbon backbone of the polymer molecule with a weak secondary bond in a random direction. The flexibility of the thermoplastics is enhanced significantly at higher temperatures and they often melt when heated sufficiently. Most of the thermoplastics are generated by suitable chain polymerization reactions. The addition of plasticizers modifies the shape of the thermoplastic material and reduces the value of their glass transition temperature (Tg). Thermoplastics are mostly used in insulating materials, food packaging, automobile bumpers, etc[19].

1.3.4. Thermosets:

They are heavily cross-linked polymers that eventually generate a thick 3-dimensional network. A schematic diagram of the molecular structure of the thermoset has been presented



Figure 1.2: *Different types of polymers in everyday life. 1. (a) water bottles and (b)baby toy representing the examples of thermoplastic. 2. (c)sportsware and (d)synthetic wool, are example of fibers. 3. (e) switch, electric charger and (g)casserole are example of thermoset. 4. (f) rubber band, example of elastomer or rubber.*

in figure-1.1(c). They are hard and do not soften or meltdown on heating rather they decompose at high temperatures. Epoxy resins and some poly-carbonates are some examples of thermosets. Few types of thermoplastics, fibers, thermosets and elastomers which are used in our everyday life, are shown in figure-1.2.

Polymer materials can also be categorized into different types based on their structural properties. Some of those polymers are mentioned below:

1.3.5. Linear polymers:

In this case, the monomer units are closely packed with each other and generate long carbon chains where the side branches are absent. Linear polymers have high density, tensile strength, and melting point. Some examples of linear polymers are PVC which is used for pipes, electric cables, etc. Figure-1.3 shows a schematic diagram of a linear polymer molecule.

1.3.6. Branched Polymers:

This type of polymer molecule has different side branches of different lengths and they are joined with the main polymer backbone as shown in figure-1.3. Polypropylene, amylopectin, glycogen are some examples of this type of polymer. The monomer units are not closely packed and the density, melting point, tensile strength happens to be lower than that of the linear polymers.

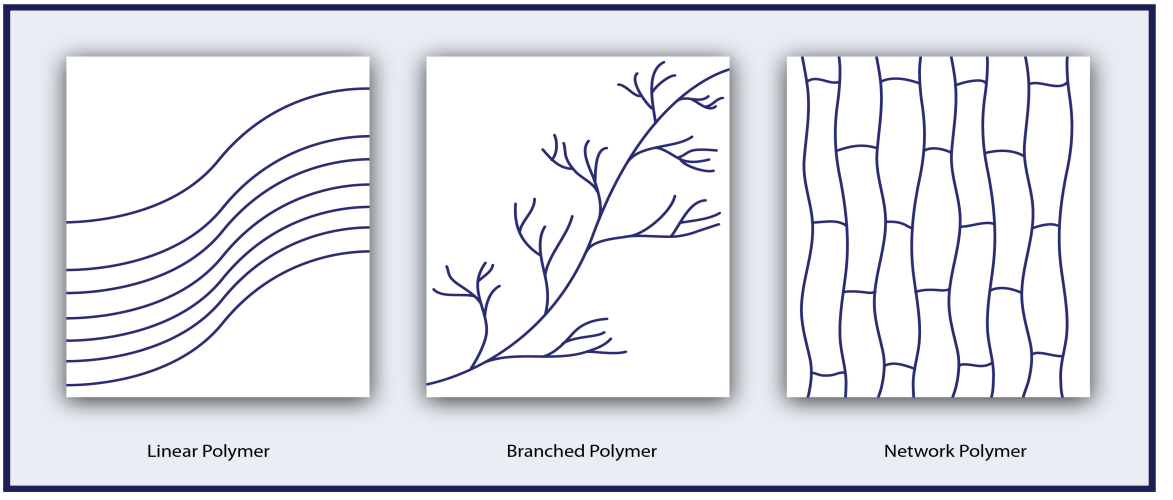

Figure 1.3: *Schematic diagram of three different types of polymers based on their structure (a)Linear Polymers: single polymer chains without any side branches(b)Branched polymers: Branches of different lengths are associated with the main polymer backbone. (c)Network Polymers: forms network like structure due to heavy cross-linking*

1.3.7. Cross-linked or Network Polymers:

They are generated due to the joining of the macromolecular polymer chain segments with the help of covalent bonds. The strength of the bond is stronger than that of linear polymers. Therefore, temperature stability, elasticity is increased as well as, solvent resistance, rates of creep, etc. are decreased. They are rigid, brittle, and hard by nature because of their network structure. Network polymers have a wide range of applications such as cross-linked polyolefin which is used in making tires, chemically cross-linked networks that are used in biomaterials industries, etc. Figure-1.3 represents a schematic diagram of network polymer. Besides these categories, polymers can be classified on the basis of other properties such as:

♣ 1. Addition polymers and 2. Condensation polymers (based on the polymerization

process)

♣ 1. natural polymers, 2. semisynthetic polymers, 3. Synthetic polymers. (based on the source of origin)

♣ 1. Homopolymers and 2. Copolymers (based on homogeneity of polymers)

♣ 1. Chain growth polymerization and 2. Step growth polymerization (based on growth polymerization techniques)[18].

1.4. Ion Conducting Polymers

Ionic transportation happens to be one of the primary desirable features of a host polymer sample. A polymer sample that can conduct ionic species through itself is known as an ion-conducting polymer (ICP). These materials have a bright prospectus in different electrochemical industries because of their significant properties like flexibility, easily fabricable nature, highly moldable behavior, etc. Ion conducting polymers are classified into two types: 1. Polyelectrolyte and 2. Polymer electrolyte.

1.4.1. Polyelectrolyte

These are special kind of polymer that contains multiple numbers of ionizable groups, which are joined with the main polymer chain[20]. The dissociating groups can be segregated into polycations, polyanions, and polysalt. Polyelectrolytes contain both the properties of polymer and electrolytes. Polyelectrolytes contain both cationic as well as anionic groups to make themselves electrostatically neutral. Among them, primary, secondary and quaternary ammonium ($–NH_3^+, = NH_2^- and - PO_3^{2-}$) groups are very common cationic groups, and carboxylate (–COO-), phosphonate ($-PO_3H^-, PO_3^{2-}$) and sulfonate ($-SO_3^-$) is the most common anionic groups[21]. Incorporation of appropriate crosslinking agents into the polyelectrolyte initiates the chemical crosslinking process inside it and forms a 3-dimensional large network which is known as hydrogel or superabsorbent polymers (SAP's) because they can absorb water a maximum of 500 times of their weight.

The behavior of the polyelectrolyte in its solution depends on the nature of the electrostatic interaction of the charged group associated with the polymer backbone and the light molecular weight ion in the solution. Researchers have reported the vast applicability of polyelectrolyte materials so far. They can be used as thickeners, dispersant agents,

conditioners, emulsifiers, ion-exchanger, and clarifying agents. They can also be used to enhance the stability of aqueous colloids and gels. Polyelectrolytes can also be used in many cosmetics, shampoo, soap, etc., and also be used as food coatings[21].

1.4.2. Polymer Electrolyte:

Polymer electrolytes, in their different forms, have made a distinguished mark in different areas of the scientific and industrial sectors of electronic devices like rechargeable batteries, sensors, fuel cells, displays, and so on[22]. Especially, the outstanding applicability of Polymer Electrolytes in the field of rechargeable lithium-ion batteries brings it under the limelight. Different types of polymer electrolytes have been prepared so far by researchers across the globe. The nature and classification of them are discussed elaborately in the preceding section.

1.5. Polymer Electrolyte: Characteristics and Classification

Polymer electrolytes appear as a conducting membrane produced by dissolving different types of alkali salts into any appropriate host polymer with high molecular weight. They exhibit a special structural property where crystalline and amorphous phases co-exist inside the sample. In 1973[23], Fenton and his co-workers have shown that polyethylene oxide (PEO) and alkali metal ($Li^{+}ion$) salt complex can exhibit higher ionic conductivity at ambient temperature. Armand et al[24] also suggested these polymer salt complexes for a practical application in all-solid-state lithium-ion batteries. Berthier et al[25] have shown that polymer electrolytes exhibit a significant amount of ionic conductivity in their amorphous phase. Detailed experimental research involving the generation, transportation properties, structural characterization, morphology, etc. of PEO+salt complexes were also reported by different researchers[26,27].

Owing to their vast applicability in the field of electrochemical devices, polymer materials have been used as host elements for different types of conducting ions like H^{+}, Li^{+}, Na^{+}, K^{+}, Ag^{+}, Mg^{2+} etc.[28]. On the other hand, various types of theoretical approaches have been adopted by the researchers to investigate the ion transport mechanism and the chemical as well as physical processes occurring in the electrolyte and electrode interface[29,31,33–36] Different types of research articles have been published throwing some light on the material, structural, thermal, and ion transport characterization studies of the

host polymer electrolyte system. Based on different preparation techniques of film casting and their physical conditions, polymer electrolytes can be classified into the following categories[37,38]:

1.5.1. Gel Polymer Electrolyte (GPE)

Gel polymer electrolytes are prepared by adding a sufficient amount of organic liquid solvent or liquid plasticizer into the polymer matrix which produces a stable gel with the host polymer substrate[30,31]. GPE exhibits both the cohesive properties of the polymer matrix and the diffusive behavior of liquid electrolytes[39]. The addition of a plasticizer increases the polymer chain flexibility that helps ions to move faster. As a result, enhancement in the ionic conductivity can be observed at ambient temperature which happens to be greater than the dry polymer electrolytes. Moreover, thermal and electrochemical properties are also improved in GPE. However, the excessive amount of plasticizer, present in this sample reduces the mechanical stability.

Polymer gel electrolytes containing lithium salts are used in lithium-ion battery applications[40]. Proton conducting gel electrolytes are used in fuel cells and other devices. Though GPE can produce a considerably high amount of conductivity, but they also have some disadvantages such as the mechanical integrity of the polymer film decreases considerably, it is also involved in a corrosive reaction at the metal electrode. Moreover, they have a strong tendency to evaporate and syneresis after a certain period which results in the loss of organic solvent[41].

1.5.2. Composite Polymer Electrolyte (CPE)

These types of polymer electrolytes are prepared by dispersing a little amount of micro or nano-sized organic, inorganic, or ceramic particles as filler in a host solid polymer electrolyte (SPE) matrix having high molecular weight[28,42,43]. They are sometimes called wonder materials because of their interesting nature. The addition of fillers prevents the ion-ion association and restricts the production of ion-pairs and ion triplets which in turn enhance the single ionic motion inside the host polymer matrix[44].

CPE is very similar to the normal two-phased composite solid electrolyte system. Here the SPE behaves as the phase-I material whereas dispersed filler material acts as phase-II. Many researchers[45–48] have reported that the size, as well as the surface area of

the dispersed filler particles, plays a significant role in enhancing the physical properties like ionic conductivity, mechanical stability, and the interfacial activity of SPE in a considerable amount. The primary objective of the preparation of CPE is to increase or modify one or more than one characteristic of the material, inclusive reduction in cost and develop and control the processing properties, etc.[49].

1.5.3. Nanocomposite Polymer Electrolyte (NCPE)

Sometimes dispersal of organo-modified nano-sized fillers into the host polymer matrix improves its electrical, mechanical, and physical properties significantly[28,50,51]. These types of newly formed compounds are known as nanocomposite polymer electrolyte (NCPE)[52,53]. Different types of clays are used to construct those NCPE. Montmorillonite (MMT) from the smectite family is used extensively. Insertion or dispersion of organo-modified ceramic fillers

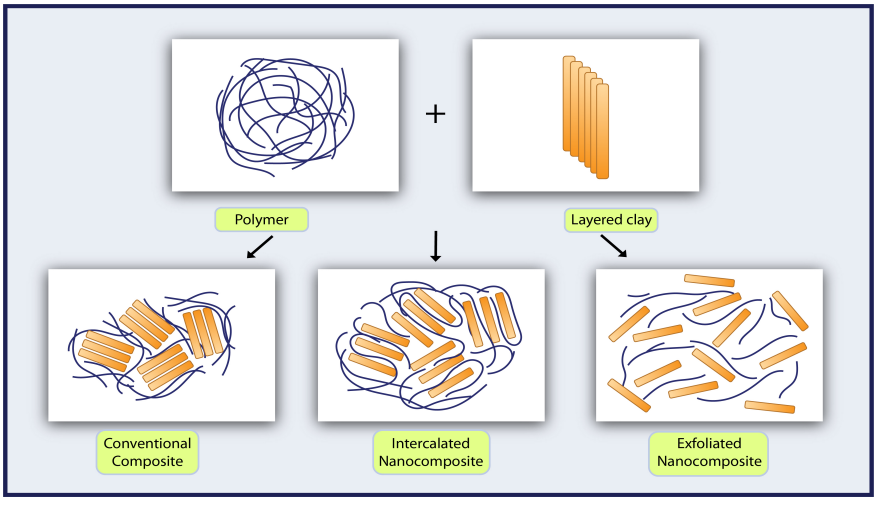

Figure 1.4: *Schematic diagram of three different types of Nanocomposite Polymer electrolytes. The arrangement of polymer chain segments and the nanocomposite materials are shown here*

into the polymer-salt complex results in two significant effects. i. reduction of ion-pairing effect due to the segregation of cations and the anions from the clay channels. ii. they can enclose the cations coordinated polymer chains inside the nanoscopic clay gallery. These significant effects increase the cationic conductivity inside the sample. On the other hand, the insertion of desired nanometric substances having a high aspect ratio as well as high stiffness into the host polymer matrix enhances the performance of the polymer significantly[54]. The shape and size as well as the volume fraction of the filler nanoparticles influence the

electrical performance of the NCPE[55]. Many researchers have used different types of inorganic nanoparticles with various types of polymer matrices. Metal nanoparticles[56], carbon nanotubes[57,58], silica[59], calcium carbonate[60], and zinc oxide[61] are significant among them. Researchers have reported different types of NCPE such as intercalated NCPE (where the clay sheets are merely arranged regularly), exfoliated NCPE (where the organo-modified clay has been homogeneously dispersed), dispersed phase NCPE (here nanomaterials or clay are dispersed homogeneously all over the polymer salt system). A schematic diagram of these three types of NCPE has been shown in figure-1.4.

1.5.4. Rubbery Polymer Electrolytes

This type of polymer electrolytes is also known as the 'polymer-in-salt' system. It has an exceptional processing technique. Unlike the other types of polymer electrolytes, rubbery electrolytes are prepared by adding a small quantity of polymer having higher molecular weight like PEO, PPO, etc. into a large amount of salts[62,63]. The sample eventually turns into a "polymer-in-salt" system rather than "salt-in polymer"[28]. The rubbery nature is maintained as the glass transition temperature (T_g) of the material is low and this phenomenon effectively results in the higher value of ionic conductivity. The main disadvantage of these types of materials is that the excessive amount of salts, which is complexed or dissolved in the sample, tends to crystallize gradually resulting in the inability of the practical application of these samples in electrochemical devices.

1.5.5. Plasticized Polymer–Salt Complex:

Plasticized polymer–salt complexes are prepared by the addition of low molecular weight plasticizers like polyethylene glycol (PEG), propylene carbonate ethylene carbonate, etc.[64] into the host polymer substrate. The resultant material poses an intermediate state between SPE and liquid electrolytes. The addition of plasticizer weakens the intermolecular and intramolecular forces between the polymer chains[65]. This eventually decreases the rigidity and the mechanical as well as thermomechanical features of the three-dimensional structure of the film[65,66].

The addition of a plasticizer also reduces the glass transition temperature (Tg) which eventually reduces the crystallinity and increases the salt dissociation capability of the sample. As a consequence, enhancement in the charge carrier transport can be observed.

At the same time, the mechanical strength of the sample is reduced[67]. There are some drawbacks in using the plasticized polymer electrolyte samples such as corrosive reaction of the polar solvent with a metal electrode, reduction of mechanical features at a greater level of plasticization, solvent volatility, etc.[64,68]

1.5.6. Solid Polymer Electrolyte (SPE)

This class of polymer electrolytes refers to the group of macromolecular substances where alkali metal salts are dissolved or complexed into a host coordinating polar polymer substrate. The addition of salts increases the ionic conductivity in a considerable amount. Detailed discussion regarding SPE is done in the preceding section.

1.6. Solid Polymer Electrolyte and its Characterstics

Solid polymer electrolytes (SPEs) are special kinds of polymer+salt complex where the solvent is not present. Generally, both the alkali metal salts and host polymer compound are suspended or dissolved into a common solvent and then the solvent is removed producing the desired solvent-free polymer electrolyte. A convenient technique to prepare the SPE film or membrane is either by the solution casting or hot-press method[28]. Though SPE doesn't have ionic conductivity as much high as gel polymer electrolytes, they can provide some additional advantages like enhanced mechanical stability, improved interface capability, solvent-free nature, etc. These distinguishing characteristics of SPE enable us to use them widely in fields like electrochemical devices, electronics, solar cells, electronic vehicles, medical implant devices, etc. A schematic diagram of a host solid polymer matrix in association with the lithium-ion (Li^+) is shown in the figure-1.5.

Detailed structural analysis of solid polymer electrolyte confirms the fact that SPEs are bi-phasic by nature i.e. crystalline and amorphous phase co-exists inside the SPE[69,70]. Generally, the long chains of polymer molecules are arranged in a highly disordered fashion in the solution or molten condition and maintain the amorphous nature of the sample. On the other hand, long polymer chain segments, sometimes, arrange themselves in an orderly fashion and form crystalline parts, embedded inside the amorphous region as shown in the figure-1.6.

The long chains are generally arranged orderly at the time of crystallization and form three-dimensional sheet-like areas having different fibril or lamellae-like structures. They are

known as spherulites and they form polycrystalline regions embedded inside the amorphous part of the materials[71]. Spherulites show circular symmetry initially but they tend to join with the other at the time of growth which results in a polygonal structure at the final stage. Besides this, fractal-like structures are also observed inside the SPE in the form of diffusion-limited aggregates (DLA)[72]. The final structure of the SPE significantly depends on the

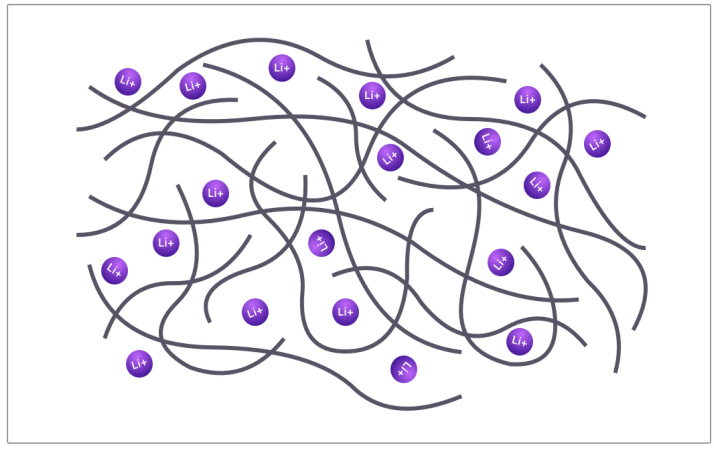

Figure 1.5: *Schematic diagram of a Solid Polymer Electrolyte sample where the lithium*(Li^+) *ions are embedded inside the polymer chain segments*

nature of the solvent, used at the time of preparation of the film, and its removal techniques on the thermal history[73]. The crystalline phase of the SPEs can be measured with the help of DSC and XRD[74]. Plenty of research studies have reported that the crystalline part of the polymer complex exhibits a negligible amount of conductivity whereas the amorphous regions inside the sample helps in the ionic conduction inside the SPE sample[75,76]. Owing to this fact, different methods have been adopted by the researchers so far to increase the amorphous nature and reduce the crystallinity part of the sample which will be discussed in the later section

Most of the SPEs, reported so far, are mainly made of definite polar polymeric substances with high molecular weight e.g. poly(ethylene oxide) (PEO), poly(propylene oxide) (PPO), (polyethylene glycol) (PEG), Poly(methyl methacrylate) (PMMA) etc.[32,33]. On the other side, alkali metal salts with large size anion like $LiClO_4$, LiSCN, NaI, NaSCN, NHPE, $AgNO_3$, NaCOOH, $NaPF_3$, $NaCF_3SO_3$, KNO_3, $Cu(ClO_4)_2$, $Zn(ClO_4)_2$, $Mg(CF_3SO_3)_2$, etc. are used for the preparation of solid polymer electrolyte. Polymeric substances like PEO, PPO, PEG, etc. exhibit some salient features like they can form stable dry complexes which result in comparatively higher ionic conductivity rather than other solvating

polymers. Polar groups like: $-O-$, $-H-$, $-C-H-$, which are placed in polymer chains and sequential oxyethylene groups like $-CH_2-CH_2-O-$ play a significant role to complex or dissolve ionic salts inside them[28,29,33].

The generation and consistency of the resultant SPE also depend on the lattice as well as the solvation energy of the alkali salt and the polymer[77]. The lower the lattice energy of the inorganic salt and the polymers, the more stable will be the resultant SPE. In the majority of research activities, poly (ethylene oxide) (PEO) is used as the host polymer material to prepare a desirable SPE sample. PEO has an intrinsic characteristic to dissolve a variety of salts in a considerably high proportion and form a stable polymer-salt complex that can show higher ionic conductivity at room temperature. Since the materials are solvent-free, the structural characteristics and ion transport mechanisms happen to be an interesting topic of research from the last three decades. Many researchers around the globe

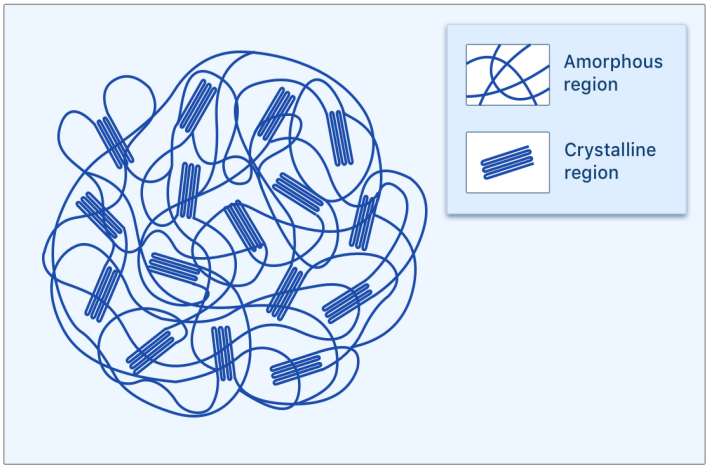

Figure 1.6: *Semi-Crystalline behavior of the Polymer electrolyte sample. The embedded orderly arranged regions indicate the crystalline region whereas the randomly arranged polymer chains indicate the amorphous phase of the SPE.*

have worked with various polymer + salt complexes[78–81] and many others have delivered their remarkable contributions in this field. These research activities reveal many important properties of SPEs. Presently we will discuss some important desirable properties of SPE.

1.7. Desirable Features of an Efficient SPE for Electrochemical Device Application.

The successful application of an efficient SPE to any all-solid-state electrochemical device is possible if it can inherently have the following properties[29,31]

1.7.1. Higher Mechanical Strength

The mechanical properties of SPEs significantly depend on different factors such as the motion of the polymer chains, morphology, crystallinity, the orientation of the molecules, molecular weight, etc. In addition to that, some external parameters like temperature, pressure, moisture content, time scale, types of deformation, etc. also play a significant role to determine the mechanical properties of SPEs. Thus, its detailed theoretical and experimental analysis is much more difficult and changes frequently with the change of the above-mentioned factors[82]. Unlike the other types of polymer electrolytes, SPEs happen to be more mechanically stable. They are Viscoelastic by nature in the intermediate range of frequencies and temperature i.e. they have the characteristics of both elastic solids and viscous liquid[83]. They act like solids but their structural characteristics and conductivity are familiar to the liquid state.

This special feature enables SPEs to perform more efficiently and they can be handled easily. As a result, any kind of physical damage can be minimized and large-scale production of these materials can be achieved. The mechanical strength of an SPE system can be analyzed from the static measurement of the stress-strain curve at a constant temperature. The said curve depicts significant nonlinear nature which concludes that the second-order elastic constant shows a strong dependence on the strain. Moreover, the value of young modulus (estimated by depth-sensitive indentation (DSI)) varies from point to point. Despite these difficulties, an approximate estimation of mechanical strength is very much needed to study its applicability in different electrochemical devices.

1.7.2. High Ionic Conductivity

To minimize the self-discharging process and enhance the ion transportation, an SPE sample must behave as a good ionic conductor as well as a good electronic insulator[84]. The electrochemical behavior and the internal impedance is determined by the ionic conductivity of the host SPE for different charging and discharging rate. An arbitrary SPE should

have ionic conductivity more than $10^{-4}Scm^{-1}$ to attain a fast charging-discharging rate[85].

1.7.3. Excellent Processibility

The use of SPE in an electrochemical device becomes easier if the material under concern is easily processed. An efficient SPE must maintain some salient features that make them more mechanically stable and also rigid by nature. Thus fabrication of thin film becomes much easier. Moreover, these materials show more consistency and flexibility which helps one to use them in different areas of electrochemical devices.

1.7.4. Thermal Stability

Different types of electrochemical reactions between the electrolyte and the electrode materials generate a considerable amount of heat, which may reduce the performance of the SPE sample used in any electrochemical device. Hence, it is desirable to make the SPE thermally stable that can be operated under a wide range of temperature variations. Good thermal stability also refers to secure use of the SPE sample in different electrical and thermal abuses like shorting, overcharge, flame, etc.

1.7.5. Chemical and Electrochemical Stability.

Different types of SPEs are used as electrolyte materials in different electrochemical devices. In that case, SPE membranes are fabricated by various techniques and are sandwiched between appropriate electrodes. Generally, there is a high chance of undesirable chemical reactions at the interface of electrolyte and electrode materials. Therefore the SPE material should have a sufficient level of chemical stability to refrain from this kind of undesirable chemical reaction. On the other hand, the electrochemical stability window indicates the electrode electric potential range where the material does not participate in any oxidation and reduction reaction. This happens to be one of the most important properties of an SPE sample. In this case, the said SPE sample has to be inert to both electrodes. It has been observed that SPEs should have a greater level of electrochemical stability ranging from 0V to 4/5 V for an efficient electrochemical device application[28].

1.7.6. Ionic Transference Number

The value of the ionic transference number should be close to unity (i.e. $t_{ion} \sim 1$) and this happens to be the most essential criteria for a polymer electrolyte sample to be used in electrochemical device application[28]. In association with that, the SPE sample is desirable to act perfectly as an ion(single ion and mostly cation)conducting system and as an electronic separator. The electronic conductivity inside SPEs happens to be negligible i.e. around 10^{-9} S/cm for the ideal case. In most of the cases, the cationic transference number has been reported ≤ 0.5[28] which clearly suggests that a maximum 50% of the actual transporting ions move inside the polymer electrolyte sample[88,89]. A higher value of the cationic transference number eventually reduces the concentration polarization of the SPE at the time of the charging and discharging process and generates greater power density[90].

1.8. Selection of Different Components of an Efficient SPE

Solid polymer electrolyte (SPE) can be manifested as a membrane that is capable of transporting ions, that is comparable to any lithium salt dissociation in an arbitrary liquid electrolyte[92]. Various types of desirable properties like nonflammability, absence of electrolyte leakage, less possibility of an internal short circuit, etc.[93] ensure the extensive application of SPE in different electrochemical devices. Extensive research activities were performed across the globe to find the optimal conditions for the preparation of efficient SPE for practical application. It is very much clear that the prime constituent elements of SPE are polymer, which acts as a host, and salt. Hence, these two components must fulfill some conditions to obtain an efficient SPE

1.8.1. Polymer

The selection of polymer electrolytes for different electrochemical devices is based on their morphological, structural, and electrical characteristics[94,95]. A desirable SPE must be capable of easy formation of the thin film with the required shape, should be able to form good electrode-electrolyte contact, and must have desirable mechanical strength[94,96,97]. Moreover, it is an experimentally verified fact that host polymer material, in most of the cases is semi-crystalline by nature[70,98]. In many cases, SPE displays high crystallinity as well as low ionic conductivity[52]. The host polymer sample used to have high molecular weight and it acts as a solid solvent[90]. Considering all pros and cons, we can say an efficient

SPE must contain a host polymer material that has the following properties:

i. The primary step for the formation of SPE is the mixing of inorganic salt having low lattice energy with host polar polymer matrix. Hence, a host polymer must have donor atoms, which have a strong ability to coordinate with the cation part of the added salt. The motion of cations in the long-range takes place by dissociative steps. In this case, cations hop to either inter or intramolecular neighboring coordinating sites of the host polymer molecule[100]. Hence, the interaction of the cation with the neighboring coordinating sites should have to be optimum so that both the dissolution and mobility are feasible. This could be possible when the host polymer must satisfy some important conditions, i.e. the host polymer sample must contain polar (functional) group of atoms that can act as the adequate electron donor to generate a coordination bond with the cation[99]. In addition to this, there should be less obstacle in case of bond rotation to maintain the flexibility of the polymer chains[99]. Moreover, the respective coordination centers must be situated at an optimum distance from each other to generate intramolecular bonds.

ii. Amorphicity happens to be another essential factor to determine the efficiency of the host polymer. We have discussed earlier that SPE is generally semi-crystalline in nature. Nevertheless, it has been experimentally well-proved fact that ionic transport takes place mainly in the amorphous region of the host polymer matrix. Thus, a host polymer material must retain a considerably greater level of amorphicity.

iii. Besides the high ionic conductivity, electrochemical stability is another essential criterion to be maintained by an efficient SPE. In association with that, the host polymer material must possess a sufficiently high level of thermal and mechanical stability. The addition of nano-sized fillers[44] can be useful to increase the electrochemical stability of the polymer.

iv. The glass transition temperature (T_g) of the host SPE sample happens to be another parameter to justify the efficiency of an SPE. T_g is basically a threshold value of temperature above which the polymer chain segments have greater mobility and the host polymer system can have a greater amount of amorphous state which eventually facilitates the ionic motion significantly. Below T_g, the system forms a large network of polymer chain segments and turns itself into a stiff glassy state. The significance and effect of T_g on ionic motion inside the host polymer sample have been extensively studied by different

researchers and it has been reported that the magnitude of T_g close to the room temperature happens to be another essential criterion for the SPE sample to achieve an efficient SPE.

v. When salt is mixed with the host polymer material, it undergoes the ionic dissociation process. The dielectric constant of the host polymer sample helps in this salt dissociation. Hence greater the value of the dielectric constant larger will be the probability of the presence of a large amount of dissociated ions inside the host SPE. As a result, ionic conductivity is enhanced significantly. Therefore, an efficient SPE must require a desirable polymer host whose dielectric constant is considerably high.

Considering the above-mentioned requirements, scientists across the globe have invented different types of host polymer samples for the generation of efficient SPE. Some of the most recognized samples are polypropylene Oxide (PPO), Poly (acrylonitrile) (PAN), poly (vinyl chloride) (PVC), etc. Recently scientists are using Poly Vinyl pyrrolidone (PVP) and Polyvinyl alcohol (PVA) as host polymer materials because of their low cost and environment-friendly nature.

1.8.2. Salt

The concentration of the added salt to the host polymer matrix plays a crucial role in determining the ionic conductivity[111] and also modifies the morphological behavior of the host polymer sample. A set of polymer electrolyte samples with different percentages of salt content has been prepared following different types of techniques to study different structural and transportational changes. One such technique is solvent casting method[163]. The addition of salt in the host polymer sample decreases the porous nature and thus improves mechanical properties, modifying the surface morphology by the formation of a homogeneous surface and the system becomes more homogeneous[167].

The FTIR study has reported the shifting of C-O-C stretching peaks with the increase of salt concentration which eventually indicates robust interaction among the PS films. It also influences the association or dissociation of ions inside the host polymer sample. We know that a lower value of lattice energy enhances the probability of the formation of a stable polymer-salt complex and ion dissociation in SPE. The ability of the polymer chain segments to coordinate with the cations of the salts happens to be another essential criterion. The polymer chains generally wrap around the cation with less amount of

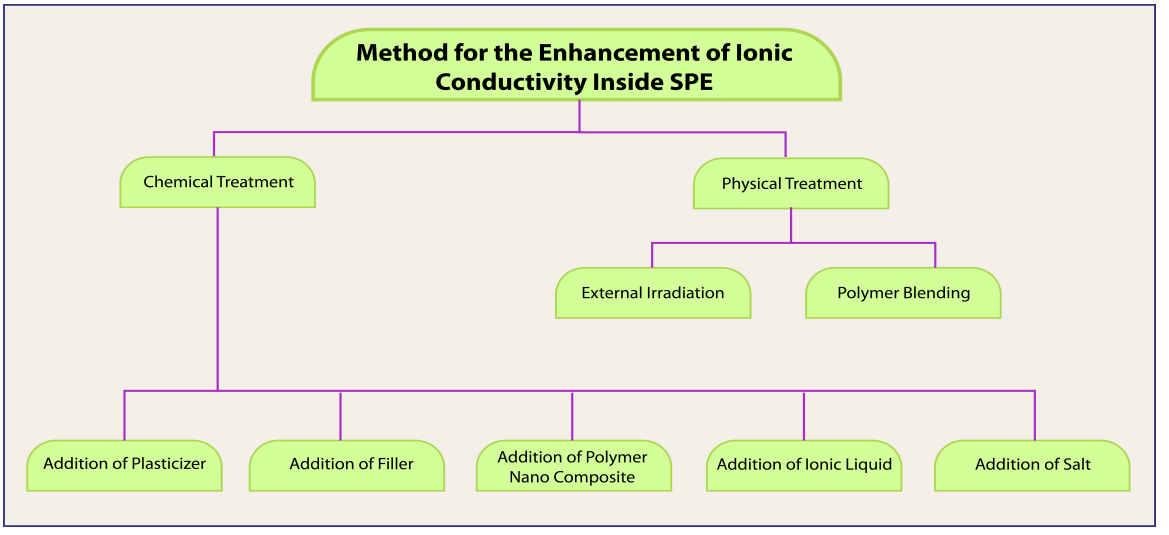

Figure 1.7: *Classification chart expressing different methods for the enhancement in performance of SPE*

strain. Experimental research studies have reported that salt having anions, bigger in size (e.g. SO_2CF_3, PF_6, TFSI, TFSM) facilitate the dissolution process and enhancement of the ionic conductivity. Thus I^- and Br^- happen to be more soluble than Cl^- and F^-. Bigger size anions also produce the plasticizing effect in the host polymer matrix which eventually enhances the ionic conductivity. The amount of charge and the heaviness of the anion obstruct its mobility.

The addition of salt introduces a highly disturbing effect on the arrangement of the polymer chain segments, which enhances the ionic conductivity in effect[163]. At the initial stage, enhancement in cationic concentration eventually reduces the crystallinity of the polymer sample. As a result, the overall conductivity is enhanced with the increase in the concentration of the charge carrier[164,165]. Further increase in salt fraction introduces transient intermolecular or intramolecular cross-linking between the polymer chains. This reduces the segmental motion of the polymer chain segments and hinders the ionic motion inside the host polymer matrix leading to the reduction in conductivity and the ionic transference number[112,166]. It has also been reported that the presence of an excess amount of salt results in (a) formation of ion pairs, which reduces the number of free ions for conduction inside the polymer host and (b) interruption of ionic motion due to the polymer chain segments[113] which eventually reduces the ionic conductivity. Also, the generation of positively and negatively charged ion triplets have been reported at higher salt concentration and temperature[114,128]. Excessive charge delocalization of salt is also proved to be an

effective way for the enhancement of ionic conduction inside the host polymer sample.

1.9. Different Methods to Enhance the Performance of SPE

It has been experimentally observed that different microstructural properties of SPE such as high level of crystallinity, low level of mechanical stability, etc. happen to be the main drawbacks for using them in any electrochemical devices. Several strategies have been applied by different researchers to enhance the performance of SPE. These methods are briefly discussed below. Also, a classification chart has been present in figure-1.7 for a clear understanding of these methods.

1.9.1. Chemical Treatement

The addition of chemical compounds to the host polymer matrix for the enhancement in the functionality of the polymer sample happens to be an effective method. The added compounds interact with the host polymer molecules chemically. Different types of chemical compounds are added to the host polymer matrix which has been discussed below:

1.9.1.1. Addition of Plasticizer

The addition of a plasticizer is considered an effective technique to enhance the ionic conductivity of the polymer electrolyte at room temperature. Plasticizers are basically organic solvents that produce plasticized or gel polymer electrolyte when it is added into the host polymer matrix[129]. Various types of organic compounds are used as plasticizers but the frequently used plasticizers like ethylene carbonate (EC), dimethyl carbonate (DMC), propylene carbonate (PC), diethyl carbonate (DEC) are low molecular weight organic solvents[129].

When a plasticizer is added to the polymer matrix, it infiltrates between the polymer chains because of their small molecular size. The cohesive force between the polymer chain segments is disrupted which results in the rearrangement of polymer chain segments. As a result, new free volumes are generated and the overall free volume of the host polymer matrix is enhanced. This phenomenon results in a significant enhancement in ionic conductivity inside the polymer material[86].

It has been experimentally observed that the incorporation of plasticizer enhances

the amorphous phase inside the host polymer matrix and promotes the segmental motion of the polymer branches[130,131]. The low viscosity and high dielectric constant of the plasticizer stimulate the ion-pair dissociation and increase the carrier concentration of the transportable charge carriers.[128,132,133] Dissociation of ion pairs due to the addition of plasticizer eventually increases the carrier concentration for charge transport and this phenomenon is considered as one of the principal reasons for the enhancement in ionic conductivity[134]. The addition of a plasticizer also reduces the glass transition temperature (T_g) of an arbitrary host polymer. As a result, the segmental motion of the polymer backbones is increased and the charge carriers can move easily resulting in a significant enhancement in ionic conductivity[44]. Experimental studies have also reported that the addition of plasticizer into the PEs results in a sufficient amount of thermal and mechanical stabilities[135,136]. However, plasticizers have some drawbacks also, for example, narrow range of working voltage, low flash point, high vapor pressure, reaction with lithium electrode, narrow electrochemical potential window, etc.[137,138].

1.9.1.2. Addition of Fillers

Fillers are basically rigid, immiscible with the host polymer matrix in either solid or molten state, and contain a fibrous or plate-like structure that introduces a different kinds of structural characteristics into the host polymer sample. They are electrochemically inert materials and are smaller in size which introduces a significant improvement in the performance of SPE[139]. A schematic diagram of a composite polymer, doped with a filler

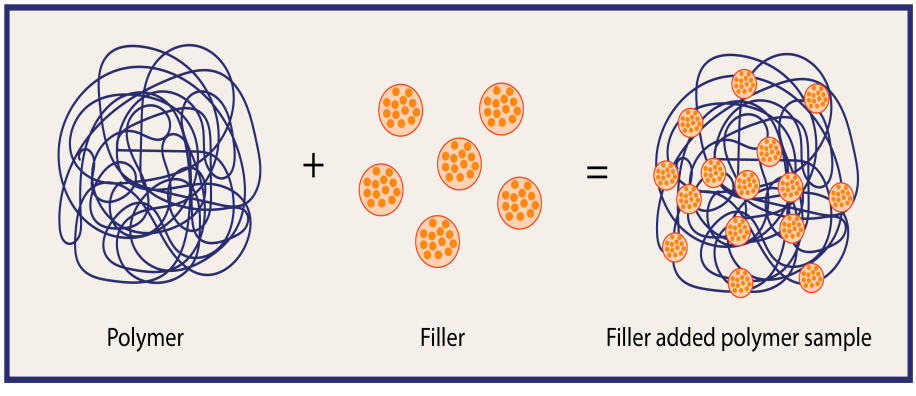

Figure 1.8: *Pictorial representation of the filler particle addition to the host polymer matrix.*

element is shown in the figure-1.8. Incorporation of filler particles into the host polymer matrix not only enhance ionic transportation[141,154] but also introduce significant amount

of mechanical stability, electrolyte-electrode stability[142,143] thermal stability, reduction of crystallinity[144]. Addition of filler enhances the dielectric constant of the sample, which eventually reduces the glass transition temperature (T_g)[86]. It also stabilizes the amorphous phase of the host polymer matrix and introduces better interfacial stability in contact with different types of electrode elements[145–147]. The crystalline phase of the host polymer sample is greatly reduced due to the addition of fillers. This process eventually reduces the recrystallization process and increases the amorphous phase inside the polymer sample and helps to achieve a greater degree of ionic conductivity inside the polymer sample[148]. Some fillers have a Lewis acid surface group which is used to interact with both the polymer and the conducting ion, thereby prohibiting the coupling of ion.[86].

An inorganic compound such as an aluminum oxide (Al_2O_3), titanium oxide (TiO_2), zirconium oxide (ZrO_2), and hydrophobic-fumed silica are reported to be used as fillers in most of the cases because of their high surface area[145,149,150]. Blending the polymer electrolyte with filler happens to be a convenient way to prepare the composite polymer electrolyte[151]. Inorganic metallic oxides such as zeolites, MgO, $Al2O_3$, SiO_2, or TiO_2 can also be used as fillers that are added with the host polymer matrix[152–154].

1.9.1.3. Addition of Nanofillers

In many cases, nanomaterials can be used as filler substances to enhance the performance of the polymer host and they are known as nanofillers. It is a multiphase compound where one of the phases (at least one dimension of the added filler) is in the order of the nanometer scale. The interaction between nanomaterials and polymer host inhibits the crystallization of the host polymer sample and improves its ionic conductivity as well as the mechanical strength[155]. Nanosized silica SiO_2 was used as nanofiller for the first time into the $PEO - LiClO_4$ sample[156]. It was also reported that the addition of nanosized aluminum oxide (Al_2O_3) into the PE sample leads to a significant enhancement in ionic conductivity[157] of the PE sample whereas hydrotalcite-doped nanocomposite PEs shows greater mechanical strength[158]. The added nanoparticles contain large surface areas which eventually introduces a substantial amount of interface in the composite sample. Moreover, the addition of nanoparticles into the host polymer matrix introduces some changes in the intermolecular interaction inside the polymer host and helps to reveal many important features of polymer nanocomposites[49]. Different types of morphological properties, workability, flexibility, conductivity significantly depend on the shape, size as well as concentration of the

nanoparticles[159].

1.9.1.4. Addition of Ionic Liquid

The addition of ionic liquid is another technique to enhance the performance of SPEs. Ionic liquids are basically molten salts that contain inorganic anions highly delocalized charges and asymmetric organic cations, bigger in size which eventually helps in salt dissociation in the polymer matrix. Incorporation of ionic liquid provides high thermal, mechanical chemical, and electrochemical stability, high ionic conductivity, wide electrochemical window, etc.[168–170]. Three types of ionic liquids can be found based on their composition: aprotic, protic, and zwitter which are used in different electrochemical devices[91,171]. Room-temperature ionic liquids can be used as excellent electrolyte solvents for lithium-ion batteries as well as some other solid-state electrochemical devices like a supercapacitor, fuel cell, etc.[172–176],. The application of an ionic liquid in the polymer salt system also increases the interfacial contact between the electrolyte and electrode.

1.9.2. Physical Treatment

The second kind of method is called the physical method which does not involve any type of chemical reaction of any added compound with the host polymer molecules. Polymer blending happens to be under this category. It is a popular method among researchers and very effective for the enhancement of the performance of the host SPE.

1.9.2.1. Polymer Blending

The blending of two polymers is considered as an effective technique to enhance the performance of the polymer sample, which cannot be achieved with a single polymer[177]. The polymer blending process is done by the physical mixing of two or more than two homogeneous homopolymers or copolymers which have different structural properties. The physical mixing of these polymer substances does not involve any generation of a covalent bond between intermolecular atoms rather, the interaction takes place through secondary forces. The blending of polymers generates a resultant substance that contains the desirable properties of both polymers. As a result, one can get various types of advantages like improved processability, enhanced quality in some specific properties like impact strength, fast alteration in the formulation, etc.[177].

1.9.3. Application of External Irradiation on SPE

The application of high-energy irradiation is also considered as another effective treatment to improve the performance of the host polymer matrix. The speciality of this approach lies in its temperature-independent, clean, and controlled process which generates products without any chemical residue[178–180]. Sometimes it results in the breaking of long polymer chains and generates numbers of fragments having lower molecular weight. Similarly, sometimes inter/intramolecular cross-linking process takes place between the polymer chain segments and generates polymer molecules with a higher molecular weight.

The application of external irradiation generally introduces ion impinging on the host polymer matrix, which eventually initiates a chain of chemical reactions and alters the chemical structure of the polymer matrix. Besides that, a certain amount of energy is being transferred by the irradiated ion or electron to the host polymer matrix. These atomic-level events result in some additional consequences like the generation of free radicals and low mass fragments, oxidation, etc. In addition to that, some significant irreversible morphological changes can also be noticed[181]due to some chemical alterations such as movements of hydrogen and atomic displacement inside SPE system, carbonization, etc.[182]. Therefore, the structure and properties of the basic polymers are changed due to the transfer of energy from particle to the polymer matrix[183]. As a result, different macroscopic properties like mechanical strength, electrical conductivity, color, etc. are modified significantly[184,185].

Different types of external radiation have been used by researchers so far such as x-rays, accelerated electron beams, UV radiation, gamma-ray, swift heavy ion (SHI) and low energy ion (LEI) beams, nuclear reactor radiation, etc. They are classified into two categories based on their particle and wave nature[186,187]. Different properties of the SPE are changed depending on the types of radiation used, its dose, and the nature of the polymer[188]. The gamma-ray or the electron beam radiation that is used by different researchers, does not have a sufficient amount of energy to start a nuclear reaction. Therefore, these radiation-induced samples don't retain any radioactivity[199].

Many researchers have reported the importance of ion beam and electron beam irradiation as they introduce significant alteration in molecular structure. The radiation-induced structural changes occur due to the rearrangements of molecular bonds, scission and/or cross-linking of polymer chain segments, generation of new functional groups etc.[189–193]. Some researchers have also reported some selective modification of optical, mechanical, electrical, and chemical properties of SPE due to ion beam irradiation[194,195].

Moreover, the effectiveness of irradiation is influenced by many other factors such as the mobility and flexibility of the polymer chains, chemical properties of the main chain, the existence of side groups, etc.

However, different types of irradiation produce different impact on the host SPE sample. The resultant product generated due to the high energy release from SHI irradiation happens to be different from those obtained from conventional irradiation e.g. electron beam and gamma irradiation[196]. The high-energy irradiation interacts with the respective atoms inside the SPE molecule by virtue of elastic or inelastic collision. The elastic collision, known as nuclear stopping results in atomic displacement and promotes chain scission inside SPE. Whereas, inelastic collision is called electronic stopping which is estimated from the velocity and the charge state of the ion[197] In our thesis, we have considered gamma-ray as external irradiation on the mathematically configured host polymer matrix. The effect of gamma irradiation on SPE has been discussed in the preceding section.

1.9.3.1. Application of Gamma Irradiation

Application of gamma irradiation is considered as one of the efficient techniques to improve different structural as well as transportational characteristics of the SPE. Gamma-ray is a highly energized electromagnetic radiation that originates due to the de-excitation of the nucleus. Two types of gamma-ray sources are considered as convenient options for nuclear spectroscopy[198]. Gamma-ray originates as a continuous spectrum by an electron that is used as a target in betatrons, linear accelerators, X-ray tubes, etc. It is also emitted from an excited nucleus as a prompt or delayed radiation due to the isomeric transition. Similarly, it can appear as prompt radiation after the beta and alpha decay from a nucleus of a comparatively long half-life.[198].

Gamma-ray is considered as one of the most energetic EM radiation that is used by different researchers. The frequencies and wavelengths of gamma-ray are more than 10^{18} hertz (Hz) and (4×10^{-9}) inches or 100 picometers. Generally, Cobalt (Co^{60}) and Cesium (Cs^{137}) are used as a source of gamma-ray. The energy of gamma-ray is transferred to the molecules of the medium due to the Compton Scattering and emitting secondary electrons with high velocity[199]. These electrons further hit the bound electrons inside the irradiated sample and take them out resulting in ionization and excitation of the sample molecules. Gamma-ray coming from Co^{60} source shows very high penetrating power. Its intensity is decreased up to 1/10 of its initial unirradiated value.

The application of gamma irradiation has a significant impact on the structural features of SPE. Interaction of gamma-ray with the polymer chain fragments is based on three different ways named: Compton effect, photoelectric effect, and pair production[200,201]. It introduces some noticeable changes in the structural properties through the crosslinking, generation of free radicles, splitting of macromolecular chains, etc.[202,203]. Gamma irradiation also initiates radiation-induced polymerization (graft polymerization and curing), cross-linking, and degradation to modify the polymer structure[206]. On the other hand, the radiation-induced chemical reaction introduces some alteration in molecular structure inside the host polymer[207,208]. In some cases, some short-lived radicals are produced due to the radiation-induced processes like ionization, scattering, excitation, etc., and some stable products are formed by different combinations[209]. Among all the outcomes, mentioned above, the primary governing consequence noticed in the semicrystalline polymer sample are: scission and cross-linking which are discussed below:

1.9.3.2. Chain Scission

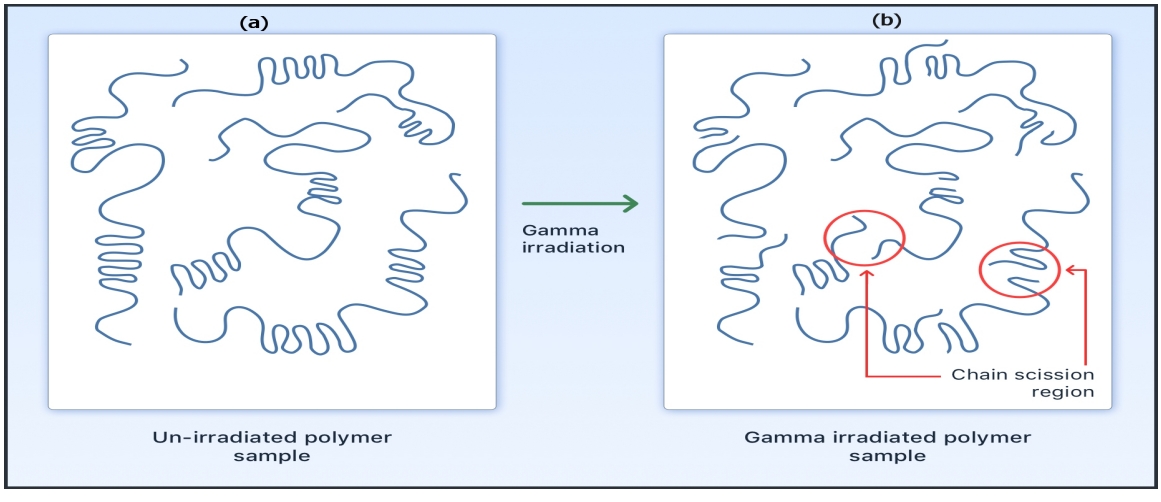

Figure 1.9: *Schematic representation of the effect of chain scission due to irradiation on the SPE sample. (a) the unirradiated SPE sample. Both Crystalline (orderly arranged polymer chains) and amorphous regions are shown. (b) the same sample after irradiation. The chain scission regions are highlighted by red circles.*

External irradiation causes the breakage of the intermolecular bond between two atoms of an arbitrary three-dimensional polymer chain and they undergo degradation, which eventually reduces their molecular weight. The chain scission process changes the molecular distribution pattern of the host polymer sample.This phenomenon affects its mechanical

strength. The chain scission also hardens the polymer chains which brings embrittlement nature to the host polymer sample and also releases gas. Gaseous products are sometimes trapped inside the polymer matrix and originate some local stress which eventually leads to the subsequent crazing and cracking inside the sample. There are other features like color change, softening, development of crack that can also be observed. Chain scission inside the host polymer sample also results in a significant reduction of chain hardness, elasticity, and enhancement in elongation as well as a decrease in the yield stress for the plastic flow. The reduction of young modulus can also be observed. The fragmentation of polymer chains hinders the process of formation of a large polymer network which eventually reduces the crystalline nature as well as increases the amorphous behavior of the host sample. A schematic diagram of the radiation-induced scission process has been presented in figure-1.9.

1.9.3.3. Chain Cross-linking

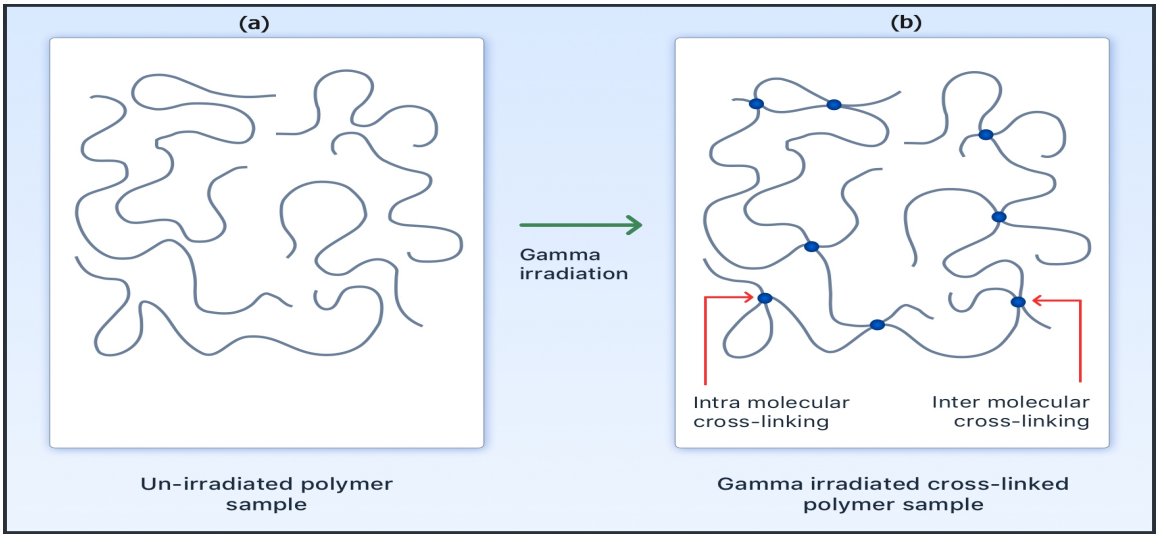

Figure 1.10: *Schematic representation of the effect of chain cross-linking due to gamma irradiation on the SPE sample. (a) the unirradiated SPE sample. Simple molecular chain distribution is shown. (b) The same sample after gamma irradiation. Both the intermolecular and intramolecular cross-linking regions are labeled separately.*

Application of external irradiation also causes radiation-induced cross-linking and generates inter or intramolecular chemical bonds between the neighboring atoms of the three-dimensional polymer chains. The radiation-induced chain crosslinking process increases the polymer chain length and therefore the molecular weight is increased with a substantial change in the molecular distribution pattern of the host polymer sample. The

enhancement of chain length eventually generates a large network of the polymer chains and as a result, the crystallinity inside the sample is enhanced remarkably. At the same time, the amorphous part of the sample is reduced which decreases the ionic conductivity of the sample. The mechanical strength of the sample is enhanced in this case.

The effect of ionizing radiation introduces a series of structural modification which include the generation of volatile fragments, carbonaceous clusters, ions, and free radicals that helps in rearrangement or construction of new bond[210,211]. Similarly, different types of functional groups like carbonyls, esters, carboxyls, hydroxyls, etc. are generated due to the oxidative degradation and damage caused by the external irradiation[212].

1.10. Mechanism of Ion Transportation Inside SPE

Pure polymer materials are nonconductors of charge-carrying ions. Hence a specific amount of alkali salts are added with the host polymer material to get a considerable amount of ionic conductivity. Cation concentration inside the polymer matrix plays an important role in this case. We know that the mobility of the conducting charge particle and the electrical conductivity (σ) can be related by the equation[160]:

$$\sigma = N.q.\mu \tag{1.1}$$

Where, N stands for the number of carriers, q and μ are the amount of charge and the mobility of the charge carrier respectively. On the other hand, the mobility of the charge carrier and the coefficient of diffusion are related by the Nernst-Einstein equation[160]:

$$\frac{\mu}{D} = \frac{q}{K.T} \tag{1.2}$$

Here, D is the coefficient of diffusion, K represents the Boltzman constant and T is the absolute temperature. It is very evident from the equation-(1.1) and (1.2), the mobility (μ) of the conducting ion is directly proportional to their coefficient of diffusion (D) at a definite temperature. Considering the conducting charge particles are identical, the mobility (μ) of the charge carriers will be constant for a definite value of diffusion coefficient (D). Under this situation, the conductivity (σ) inside the host polymer matrix is directly proportional to the cationic concentration of the added salt inside the SPE. Thus increasing the cationic concentration may lead to the gradual enhancement of ionic conductivity. It has been observed that the cationic (Li^+) conductivity inside the polymer sample with high molecular

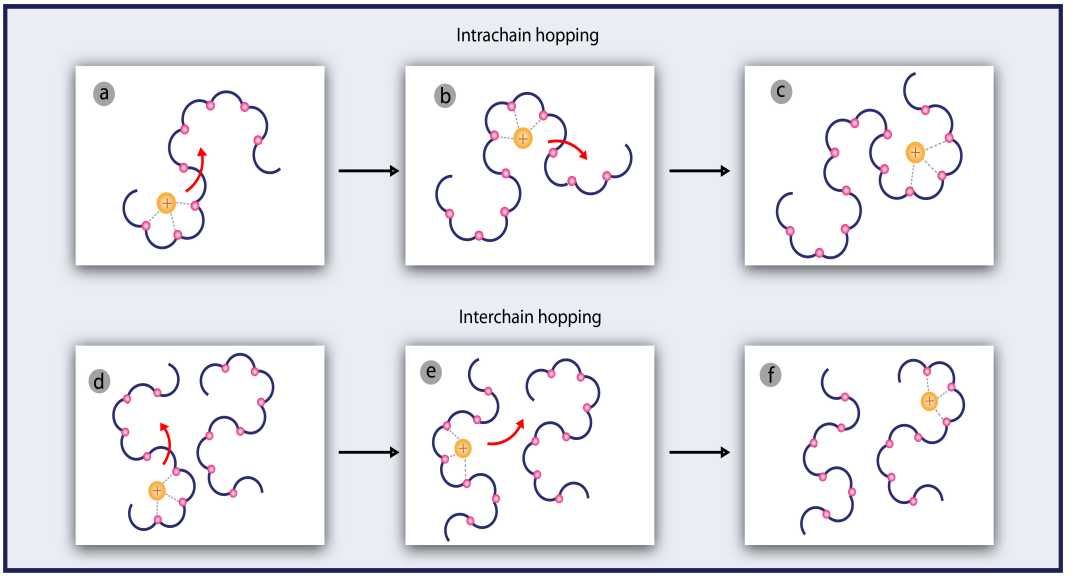

Figure 1.11: *Schematic representation of the intrachain and interchain hopping of ionic species inside the host polymer matrix*

weight is controlled by the segmental dynamics[161,162]. The detailed investigation on the ion transport mechanism in solid polymer electrolytes happens to be well-discussed but yet to be a complicated topic of research. We have seen from our previous discussion that SPEs are bi-phasic by nature i.e. both crystalline and amorphous phases co-exist inside SPE[69,70] at room temperature. A detailed NMR study reveals the fact that the amorphous phase of the sample is mainly responsible for ionic motion.[101,102]. Because of the complicated structural phenomenon, it is difficult to understand the detailed ion transport mechanism inside the host polymer matrix. Many researchers have proposed different types of theories as well as models so far but none of them is acceptable universally.

However, the prime objective of every research activity is to achieve a considerably high amount of ionic conductivity inside SPE by adopting different techniques as per requirement. In this regard, the host polymer is chosen such a way that it exhibits high solvating characteristics, which stimulates the inorganic salt to interact with some coordination sites of the host polymer matrix. Considering the fact that the hopping motion of cations of the dissociating salt is responsible for the high ionic conductivity inside the host polymer matrix, different types of inorganic salts containing various kinds of cations are complexed with the host solid polymer matrix. On the other hand, the anions are chosen heavier and larger in size. The propelling motion, generated by the polymer chains in the amorphous phase region helps the local segments to regenerate new coordination

sites continuously and as a result, the dissociated ions coordinate from one site to another and generate a hopping motion. Both the interchain and intra-chain hopping motion can be seen in the case of the dissociated ions which has been represented with the help of a schematic diagram in figure-1.11. The application of the external electric field results in a directional ionic motion inside the polymer matrix[103,104].

Besides the ionic hopping through the polymer chain segments, the segmental relaxation of the polymer chain segments also plays an important role in case of the ion transportation inside the polymer sample. As per the classical theory, the ionic conductivity inside the polymer sample and the segmental relaxation time τ_x at the temperature T are related with the following mathematical equation[105]:

$$\sigma.\tau_x.T = K_x(constant) \tag{1.3}$$

Equation-(1.3) suggests a coupling of polymer segmental dynamics with the ionic diffusion. This eventually reveals the fact that a large amplitude rearrangement of the polymer chain segments must be required to achieve a sustained ionic motion. Researchers have also reported that structural relaxation of the host polymer chains also provides a time-varying path or opportunities for the charge carriers to move to the sites with lower energy levels. The bulk ionic conductivity cannot be possible without the intra molecular ionic exchange. However, the crystalline region act as an obstacle for ion transportation. The polymer chains

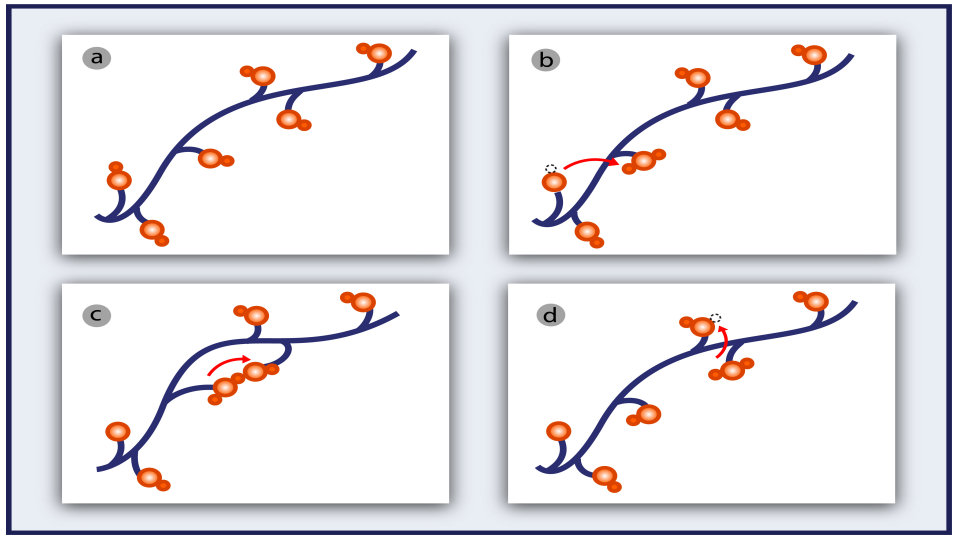

Figure 1.12: *Schematic representation of the ionic motion due to the segmental motion of the polymer chain segments*

in the crystalline region arrange themselves to form the interlocked cylindrical tunnel-like

channels inside an ordered framework. The cation (e.g. Li^+) resides in the channels and coordinated with the help of the functional group[106,107]. Whereas, the anion is situated outside and does not co-ordinate with the cation[108,109]. The chain entanglement of the host polymer matrix results in a solid-like behavior of the sample. But the continuous process of breaking and re-generating the cation-Oxygen bonds (Li-O bond) between the adjacent chain segments, generates the inter-chain and/or intra-chain hopping of cation inside PEO based electrolyte which is shown in the figure-1.11. In association with that, the continuous segmental rearrangement gives rise to the long-range displacement of lithium-ion and they exhibit a liquid-like behavior where the iron conduction takes place due to the local segmental motion of the polymer chain. It has been observed that this segmental motion becomes significantly slow near the glass transition temperature of PEO[110]. The cationic movement due to the segmental motion of the polymer chain segments above T_g has been presented schematically in figure-1.12. SPE, in all cases, exhibits a significant amount of ionic conductivity above T_g. Below this temperature, the magnitude of the ionic conductivity drops down significantly. The bulk ionic conductivity happens to be the fundamental measurable electrical parameter for SPE and it is, in fact, the ionic conductivity at the very low frequency ($\omega \longrightarrow 0$) region. It depends on the room temperature and the composition of the SPE. Detailed theory regarding the bulk (dc) ionic conductivity inside SPE has been discussed in the proceeding section.

1.10.1. Temperature Dependence of DC Conductivity: A Short Overview

The temperature dependence of bulk ionic conductivity can be considered as a phenomenological model. The quantitative analysis is characterized by three fundamental laws. They are discussed below:

♣ Arrhenius studied the temperature dependence of ionic conductivity inside SPE. This law suggests that ionic conductivity depends on the temperature and conductivity increases with the increase in temperature. The Arrhenius law can be mathematically expressed as:

$$\sigma = \sigma_0 . Exp. \left[\frac{E_a}{K_B . T}\right] \tag{1.4}$$

Here σ in equation-(1.4) represents the ionic conductivity inside the polymer system at the temperature T, E_a is the activation energy, K_B Boltzman constant. In this equation, E_a happens to be the most important phenomenological parameter which represents the energy that must be required for an arbitrary ion to hop from one site to another site

by overcoming the crystallization as well as re-arrangement of polymer chain segments. The activation energy of a system can be evaluated from the slope of $log(\sigma/\sigma_0)$ vs $1/T$ graph[123,124], which eventually gives a straight line. Arrhenius behavior in a system is basically indicative of a liquid-like behavior.

♣ In many cases, it has been experimentally observed that the linear relationship between the conductivity and temperature in some SPE samples cannot be maintained properly. This kind of nonlinear behavior can be fitted with the Vogel-Tamman-Fulcher (VTF)[125,126] equation. This equation can be mathematically expressed as:

$$\sigma = \sigma_0 . T^{-\frac{1}{2}} Exp. \left[\frac{-C}{K_B.(T - T_0)}\right] \tag{1.5}$$

Here, σ_0 in equation-(1.5) is the pre-exponential factor, which is proportional to the net amount of carrier ions and also depends on the transport coefficient. C is also a constant parameter having the dimension of energy. (T_0) represents the equilibrium glass-transition temperature at a thermodynamic equilibrium[122]. The VTF nature of any SPE material can be studied from the $log(\sigma)$ vs $1/(T - T_0)$ graph which shows a non-linear behavior. This non-linear behavior is assumed to be the notion of conductivity mechanism based on the hopping of ion in association with the relaxation of polymeric chain motion[125,126]. The bent (VTF) conductivity can also be explained most simply by considering the ions moves from one free volume space to another inside the host polymer matrix. The availability of free volume space is represented by the factor $(T - T_0)$[122]. VTF equation holds good in polymeric conductors as well as in glasses and it clearly explains the dependence of ionic conductivity on glass transition temperature and segmental motion at higher concentration when the polymer chain segments become rigid due to ionic cross-linking[122].

♣ An extension of the VTF equation has been proposed by Williams, Landel, and Ferry to study the temperature-dependent conductivity variation in amorphous and glass-forming systems. This relation is known as Williams-Landel-Ferry or WLF equation. As per this equation, we can write:

$$log a_T = \frac{C_1(T - T_r)}{C_2 + (T - T_r)} \tag{1.6}$$

Where, $\sigma(T)$ and $\sigma(T_r)$ in equation-(1.6)are the conductivity at the temperature T and reference temperature T_r respectively. C_1 and C_2 are two constants and a_T happens to be a shift factor which can be evaluated experimentally.

1.10.2. Theoretical Models for The Characterisation of Bulk Conductivity

Characterisation of ionic motion inside the Polymer matrix happens to be a complicated phenomenon. Being a weak electrolyte, ion association inside the polymer sample results in the generation of ion pairs, triplets, and multiplets which makes the analysis more difficult. Several models have been proposed so far for the sake of a clear understanding of the ion transportation mechanism inside the polymer host but none of them are applicable for all types of polymer electrolytes. Nevertheless, they provide an overall idea regarding the transport process. Some of those models have been discussed below:

1.10.2.1. Free Volume Model

Cohen and Turnbull suggested this model[116] to investigate the ion transport mechanism inside a pure polymer electrolyte system and this model supports the VTF and WLF characteristics satisfactorily. According to this model, molecules inside the host polymer matrix experience anharmonic vibrations and create interstitial space or localized vacant spaces called "free volume". The mobile ions or molecules need not retain any definite amount of

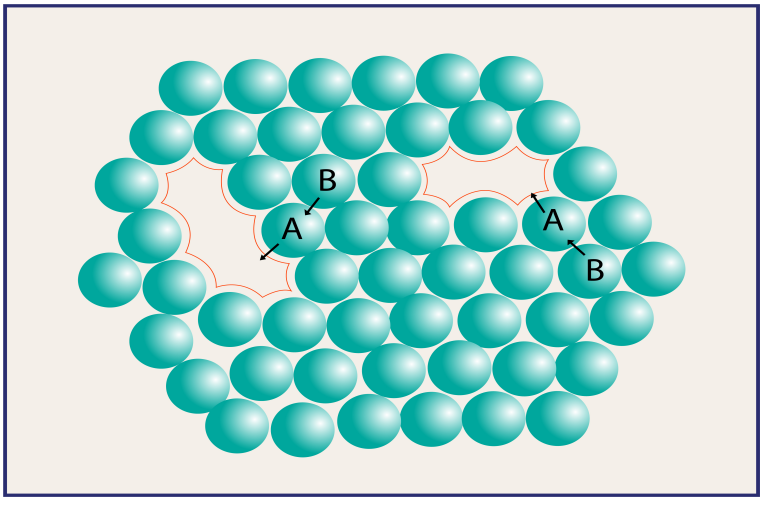

Figure 1.13: *Schematic diagram of the displacement of molecule or chain segment A. Initially it was located at the position of B. Dislocation of A is occurred and its initial position is occupied by B. The arrow shows the next dislocation direction of A and B.*

energy to overcome the activation energy barrier. They just experience a translational motion by jumping into the free volume, generated inside the host polymer matrix. According to Cohen and Turnbull, local empty spaces i.e the interstitial free volumes are originated

due to finite expansivity as the temperature of the host polymer increases. The mobile ions associated with the polymer chain segments can move easily through the free volume and the ion transportation happens through the polymer sample due to the redistribution of the free volume inside the host polymer matrix. Free volume V_f, molar volume V_m, and the glass transition temperature T_g can be related through the following equation:

$$V_f = V_m \left[-0.025 + \alpha \left(T - T_g\right)\right] \tag{1.7}$$

Here, T in equation-(1.7) is the experimental temperature range and α is the thermal expansivity. This model describes the enhancement in ionic conductivity with the temperature inside SPE as the result of the thermal expansion of the free volume which eventually promotes the motion of solvated molecules, ions, and polymer chains[117]. There are some limitations regarding the applicability of the free volume model e.g. formation of ion aggregates and ion pairs, the poly-crystalline structure of the host polymer sample, etc.

1.10.2.2. Configurational Entropy Model

This model was proposed by Gibbs and his co-workers[118,119] and is based on the free volume model where the VTF and WLF nature of the host polymer has been taken into account. Configurational entropy model is basically the modification of the free volume model where the different types of additional parameters like fluctuation of entropy, number of lattice sites and distorted bonds, semi-crystalline nature of the polymer matrix, tendency to form ion pairs, degree of order in the system and glass transition temperature due to the introduction of cations, etc. has been taken into account[119]. The fundamental idea of this model is based on the assumption that ion transportation inside the host polymer matrix takes place due to the rearrangement of the polymer chain segments instead of hopping off the charge carriers. The probability of this rearrangement can be expressed as:

$$W = C_{con}.Exp\left[\frac{-\Delta.\mu.S_c^*}{K_B.T.S_c}\right] \tag{1.8}$$

Here, S_c in equation-(1.8) represents the configuration entropy at the temperature T and S_c^* stands for the minimum configurational entropy for rearrangement; $(\Delta.\mu)$ is the free energy barrier per mole and K_B Boltzman constant. Ion transportation inside the host polymer material can be explained with the help of this model but the conductivity of ion cannot be explained properly[120].

In addition to that, many other factors like the microscopic behavior of transport properties as a function of molecular weight; dielectric relaxation, etc. cannot be explained fully with the help of this model.

1.10.2.3. Static Bond Percolation Model

Ratner and his fellow workers[120] proposed this model. The static bond percolation model deals with the motion of ions in a rigid polymer framework where the ion transportation is characterized by the percolation process. The percolation process is characterized by the hopping rate of ions between two sites. The hopping of ion takes place between two sites when they are mutually accessible i.e. the link between them is open (open bond) and hopping is not possible if the sites are linked already (closed bond). Here the sites in the host polymer matrix represent those arbitrary positions where the mobile ions or electrons reside. Thus the probability of finding a mobile charge carrier at an arbitrary i^{th} site can be expressed as:

$$P_i = \Sigma.\,[P_j.W_{ji} - P_i.W_{ij}] \tag{1.9}$$

P_i in equation-(1.9) represents the fraction of bonds that a mobile charge can be found at the ith site and W_{ij} and W_{ji} stand for the hopping rate of charged particles from i^{th} to j^{th} site and j^{th} to i^{th} site respectively. Generally, it is considered that $W_{ij} = W_{ji}$, and this hopping rate to the neighboring sites are determined by the equation as follows:

$$\begin{aligned} W_{ij} &= W \qquad for\ \ the\ \ probability\ \ P_r \\ &= 0 \qquad for\ \ the\ \ probability\ \ (1 - P_r) \end{aligned} \tag{1.10}$$

Where, P_r in equation-(1.10) represents the probability of getting an open bond between two localized sites and $(1-P_r)$ be the probability when the bond is occupied or unavailable. Many experimental outcomes have been explained successfully by this model. It is also used successfully to explain the contribution of the amorphous part of the polymer matrix in the ion transportation process. But this model does not include the effect of dynamic aspect i.e. the simultaneous effect of ion hopping and the segmental motion of the polymer chains on the ion transportation property above T_g.

1.10.2.4. Dynamic Bond Percolation Model

Ionic conductivity inside SPE can be characterized qualitatively by using the free volume and the configurational entropy models, which are eventually quasi thermodynamic models. However, the analysis from the microscopic point of view is not possible by these models. In that case, the dynamic bond percolation model serves the purpose. Durger and his coworkers[121] proposed this model where the actual scenario of ion transportation inside the polymer material has been taken into account. According to this model, the resultant motion of ion is considered as the combined effect of two simultaneous factors:

- ♣ The translational motion or hopping of ion
- ♣ The random motion of the polymer chain segments above T_g.

The polymer chain segments are assumed to be dynamic and perform continuous orientational rearrangement inside the host polymer matrix. Hence different stable sites containing mobile charged species move with respect to one another resulting in a spontaneous change in the position of the sites. In that case, the hoping probability of the charge carriers is modified by modifying their values on a time scale related to the motion of the polymer chains. Ratner and his coworkers[122] reviewed this model focusing on the limitations in case of application to the polymer electrolyte sample.

1.10.2.5. Effective Medium Theory

This theory is introduced to provide a quantitative analysis of the ion transport mechanism inside a multiphase host electrolyte system such as composite polymer electrolytes (CPE) consisting of different fillers or clays, polymer salt complexes, etc. It was basically originated from Landauer's (1952) effective medium approach and later Nan and Smith (1991) used this theory to analyze the ion conductivity enhancement inside CPEs. It was previously believed that the amorphous phase region is responsible for the ionic conduction inside the polymer substrate. On the other hand, experimental studies conclude that a mixed-phase host polymer substrate consists of three different phases: a. the polymer matrix phase responsible for the cationic conduction. B. fillers phase. C. The polymer–filler interface layer phase. As per the effective medium theory, the above mentioned three phases contribute simultaneously to the overall ionic conduction inside the host polymer matrix. Therefore, if σ_{oc} represents the overall ionic conductivity inside the polymer substrate, then it can be

expressed as follows:

$$\sigma_{oc} = \sigma_{pf}.\frac{2.\sigma_{pf} + \sigma_g + 2.\chi(\sigma_{pf} - \sigma_g)}{2.\sigma_{pf} + \sigma_g - \chi(\sigma_{pf} - \sigma_g)} \tag{1.11}$$

Where, σ_{pf} in equation-(1.11) represents the ionic conductivity inside the polymer-filler interface layer phase and σ_g stands for the conductivity of the grains and χ represents the volume fraction of the fillers. Equation-(1.8) stands for the quantitative evaluation of the ionic conductivity of a composite. Whereas the net conductivity of a mixed phased composite polymer sample containing polymer, salt, and filler, can be evaluated from the equation given below:

$$\frac{\chi_{ad}}{\chi}.\frac{\sigma_{oc} - \sigma_T}{\sigma_{oc} + (\frac{1}{\Gamma_T} - 1).\sigma_T} + (1 - \frac{\chi_{ad}}{\chi}).\frac{\sigma_{oc} - \sigma_T}{\sigma_{oc} + (\frac{1}{\Gamma_T} - 1).\sigma_T} = 0 \tag{1.12}$$

Here, σ_T in equation-(1.12)stands for the ionic conductivity of the composite electrolyte. σ_{oc} stands for the conductivity of the composite unit. Γ_T represents the percolation threshold and χ_{ad} happens to be an adjustable parameter. The different electrical properties of various heterogeneous systems such as polymer composites can be explained satisfactorily with the help of effective medium theory. As per this theory, the enhancement in ionic conductivity in CPEs depends on the size and distribution pattern of the dispersed particles and interface layer conductivity. A greater level of conductivity enhancement is achieved for the smaller size of the dispersed particles and relatively smaller volume fraction.

There exist many other models like the Dielectric model, Almond west model, Amorphous phase model, and Space charge model, etc. for both qualitative and quantitative analysis of ion transportation inside the host polymer matrix.

1.11. Application of SPE

The use of solid polymer electrolytes (SPE) in their different forms as mentioned earlier, is considered as one of the most significant inventions in the field of electrochemical device applications. The application of SPE in electrochemical devices overcomes many shortcomings that are faced in the case of liquid electrolytes. Extensive experimental research studies have reported some basic requirements that an arbitrary polymer electrolyte should maintain such as longevity, good performance, and low costing. Moreover, they poses some intrinsic characteristics that provides wide acceptability in fabrication of different electrochemical devices and these salient features are mentioned below:

i. SPE materials are more durable as they function for a long duration of time under various operating conditions and in a wide range of temperature variation.

ii Costing happens to be the most important factor for the practical application of any polymer electrolyte. In the case of SPE, this requirement is fulfilled successfully as their preparation on a large scale can be done at a considerable low cost.

iii. The performance of an arbitrary electrochemical material is determined by the conductivity that it exhibits under the optimum conditions. An arbitrary SPE can provide the maximum amount of ionic conductivity at some optimum physical conditions without changing its solid-state nature. Experimental research studies show that an SPE can provide ionic conduction of the order of 10^{-4} S/cm at room temperature. This high ionic conduction eventually delivers power in the output terminal at a considerably high rate. This feature is very much applicable in some electrochemical devices like supercapacitors, sensors, etc.

The performances of any arbitrary electrochemical device solely depend on the nature of different structural components of the materials. In the case of SPE, different types of ions such as H^+, Li^+, Na^+, K^+, Ag^+, Mg^+, etc. are used as transporting ion inside the host solid polymer sample as per their requirements. Therefore, one can conclude that the use of SPE is solely based on three purposes: 1.To provide fast ionic transportation of the selected ionic species. 2. Separating two electrodes. 3. To use as better insulating material.

Considering all these advantages of using SPE, it is successfully recommended for different electrochemical devices like solid-state batteries, supercapacitor, fuel cell, photoelectrochemical cell, solid-state reference electrode, sensors, electrochemical display services, high vacuum electrochemistry, electrochemical switching, electrochemical transistor action, thermoelectric generators, etc. In this present section, we are going to review the operational as well as the applicational perspectives of SPE briefly in case of some devices.

1.11.1. Solid State Batteries

Solid-state batteries are electrical device that stores chemical energy and converts it into electrical energy when connected with an external circuit. Generally, it consists of two

components: a. electrolyte material and b. two active electrodes i.e. anode and cathode. Depending on the mode of use, batteries are generally classified into two categories: a. primary batteries which are commercially used for a single time, and after use they are thrown away, b. secondary batteries which can be used several times by charging and discharging many times. The use of gelled polymer electrolyte (GPE) in the solid-state battery is considered as a very lucrative option as the ionic conductivity inside these elements is of the order of 10^{-3} S/cm under suitable conditions[213–215]. But lack of mechanical stability happens to be the main point of concern. In this regard, some other types of polymer electrolytes e.g. SPE, NCPE in the form of both thin as well as a flexible film can be considered as a convenient option for using in all types of lightweight, leak-proof, solid-state batteries having various types of shapes and sizes[94,96,216–219]. The use of Li^+ ion-based

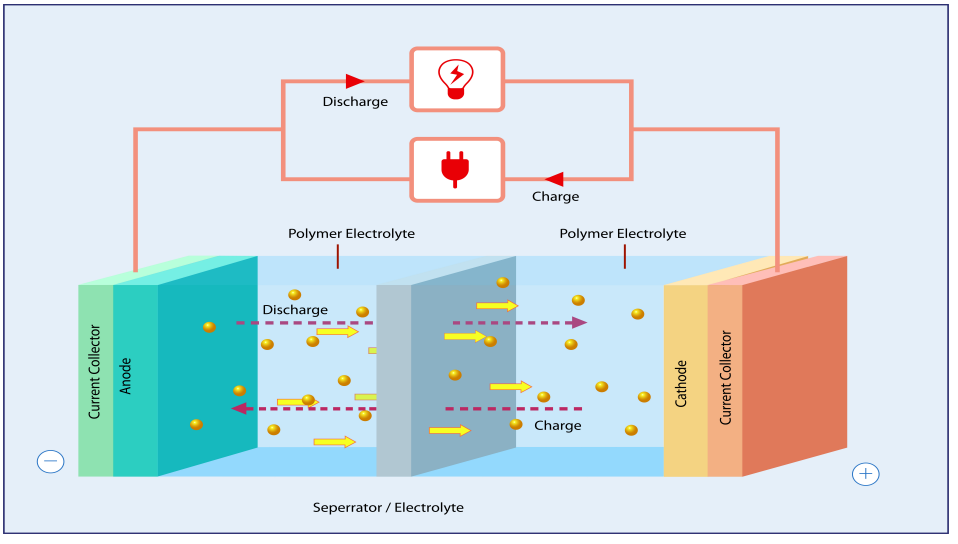

Figure 1.14: *Schematic diagram of a solid state battery.*

salt to construct solid-state batteries is considered as a very well acceptable approach. It is observed that Lithium Polymer Batteries (LBP) provide desirable ambient electrochemical characteristics as compared to the other battery systems. The structure and different components of an arbitrary solid-state battery have been shown in the figure-1.14. Besides the remarkable advantages, Li^+ batteries have some disadvantages like safety issues. Sometimes these batteries have faced explosion or inflammation as lithium-based compounds are highly reactive, toxic, environmentally unfriendly, and are difficult to handle in the open environment. To overcome these problems, researchers have worked with different types of non-lithium salts having H^+, Na^+, K^+, Ag^+, Mg^+, Li^+, Zn^+ as cation[28,35,220].

Researchers have reported that chemicals having Cu^+ as a transporting ion are

comparatively less reactive, less toxic, easy to handle, safe to use, and cheaper also. Hence they can be used in all-solid-state polymer electrolyte batteries. Presently use of SPE inside the solid-state batteries as a battery device becomes a very demanding trend and in most cases, polyethylene oxide (PEO) is used as a host polymer material with different types of inorganic salts dissolved inside it. Despite the several advantages, SPE has some drawbacks also. The ionic conductivity inside the SPE sample is less than that of liquid and gel electrolytes. Hence, intense research studies (both theoretical as well as experimental) are still going on across the globe for the further improvement of the performance of SPE to use in solid-state batteries as a conducting polymer host.

1.11.2. Super Capacitor

Supercapacitors are one of the important electrochemical devices where two electrodes having wide specific surface area and high electrochemical stability restore electrostatic charge with the help of the reversible adsorption process of ions. Supercapacitors differ from batteries in the case of their electrode. Two different types of electrodes (cathode and anode) are used in the case of batteries whereas supercapacitors consist of identical electrode materials (active or blocking) Electrolytic supercapacitor is classified into two categories: Redox capacitor and Electrical Double Layer Capacitors (EDLCs). In a redox capacitor, an electron-conducting polymer such as polypyrrole (PPy), polyaniline (PANI), etc. are used as pseudocapacitive active materials for the storage of charge with the help of quick and reversible surface reaction[221,222]. The different types of classification of super capacitors are shown in the adjoining classification chart in figure-1.15. The value of capacitance in the case of a supercapacitor is nearly 10^3 to 10^5 times higher than the regular capacitors with the range from mF to F and their charge storage capability along with the charging/discharging rate are much higher than the batteries. The operating range of specific power is also significantly higher than the batteries[223–225] and they poses a long cycle of life.

Ion conducting SPE happens to be a promising element to be used in supercapacitors due to their flexibility, chemical stability, malleability. In this regard, Gel polymer electrolytes can also be considered as a well-fitted candidate because of their higher level of ionic conductivity ($10^{-3} S/cm$)[204,205]. The use of SPEs reduces the manufacturing cost significantly. These materials (SPE and gel polymer electrolytes) are experimentally well-preferred due to their large field potential window, leakage-free components, reliability,

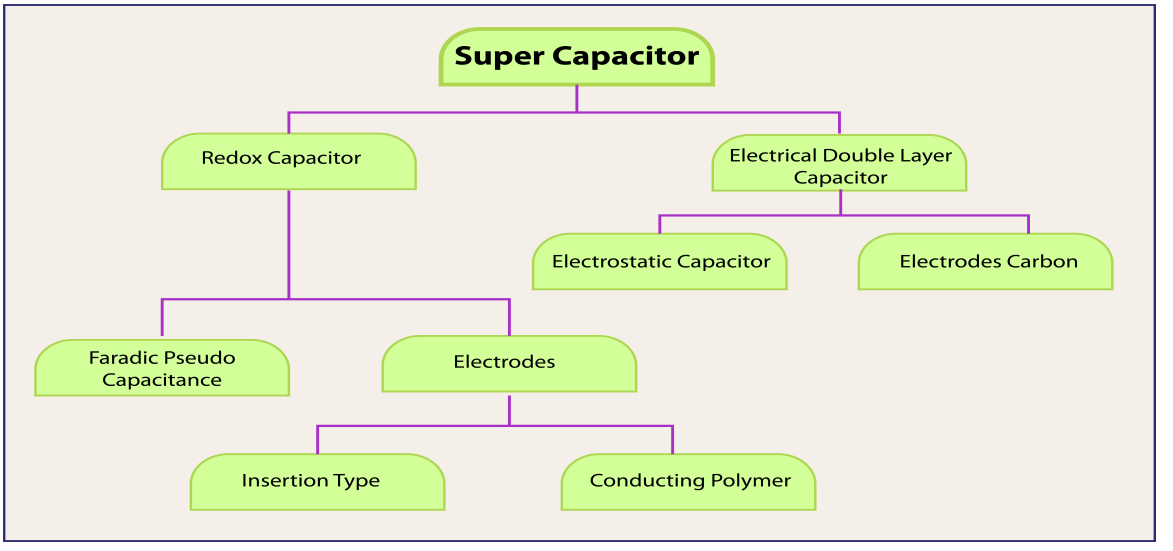

Figure 1.15: *Classification chart of the supercapacitor.*

and compactness. They can be used in portable electronic equipment, computer memory backups, load leveling, memory applications, etc.[223–225]

1.11.3. Fuel Cell

It is another kind of electrochemical device where the chemical energy is converted to electrical energy because of the redox reaction that takes place in the electrolyte membrane between the fuel and oxidant. Generally, O_2, air, H_2O_2, halogens, etc are used as oxidant whereas H_2, CH_4, NH_3, N_2H_4, CH_3OH are used as fuel most often. Depending on the mechanism, the fuel cell can be classified following categories:

♣ i.Direct fuel cell$\Longrightarrow$ where fuels can be supplied directly to the fuel cell and also a direct reaction takes place with the electrolytes.

♣ ii.Indirect fuel cell$\Longrightarrow$In this case fuel is extracted from another source, here fuel is initially be converted

♣ iii.Regenerative fuel cells $\Longrightarrow$ Where fuels are reused for a number of times.[226,227]

Different types of fuel cells are available in the market e.g. solid oxide fuel cell, solid polymer electrolyte fuel cell, proton exchange membrane fuel cell, molten carbonate fuel

cell, phosphoric acid fuel cell, and alkaline fuel cell. However, proton exchanging fuel cells are considered a more promising one for practical application. High proton conductivity, good thermal and mechanical stability, etc. are considered as the main requirements for fuel cell membrane[228,229]. The use of SPE in fuel cells happens to be a productive idea as

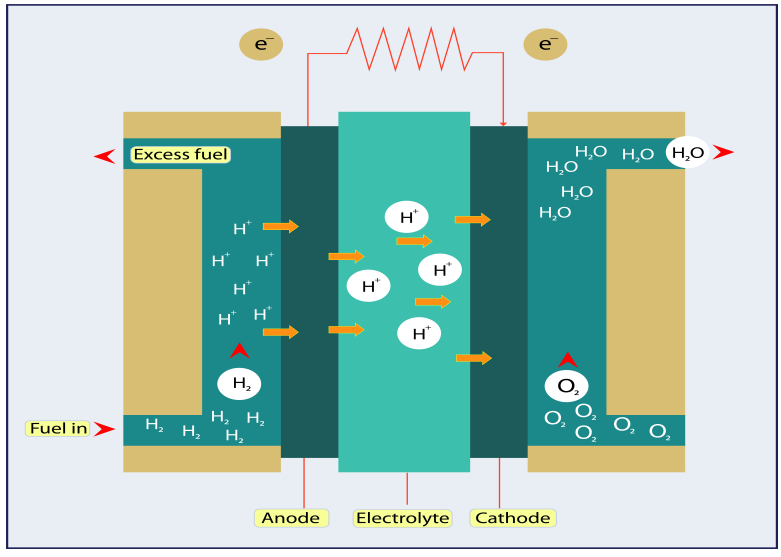

Figure 1.16: *Schematic diagram of a fuel cell.*

reported by the researchers. Recent studies have reported that polyelectrolyte membrane can also be used in a fuel cell as a carrier of OH^- ion from cathode to anode. A schematic representation of the SPE-based fuel cell has been given in the figure-1.16. SPE fuel cells can deliver high power densities at a comparatively low working temperature which can be considered as a very lucrative option for its practical application. The researchers have also reported a vast range of applicability of fuel cells in different fields like stationary and portable power generation, transportation, space program to produce electricity, drinking water for astronauts, etc.

1.11.4. Electro Chromic Display Devise (ECD)

These types of electrochemical devices are made of a special kind of material called electrochromic materials[230,231]. They have a unique feature called electrochromism under which they can change their color under the application of an external electric field or electric current. Electrochromic devices can adjust the absorption and reflectance of light continuously. Moreover, they can retain their present optical state without consuming any power. The use of SPE in ECD is becoming a very promising trend because of their easy

processibility of making very thin films and small ohmic losses. In addition to that SPE can provide a sufficiently high value of ionic conductivity of the order of 10^{-4} S/cm. Application of SPE on ECD can eliminate some limitations like photo-corrosion, side reaction, etc. On the other hand, electrolyte leakage of polymeric electrolytes can be eliminated by making laminated electrochromic devices. In these cases, SPE performs a double role i.e.

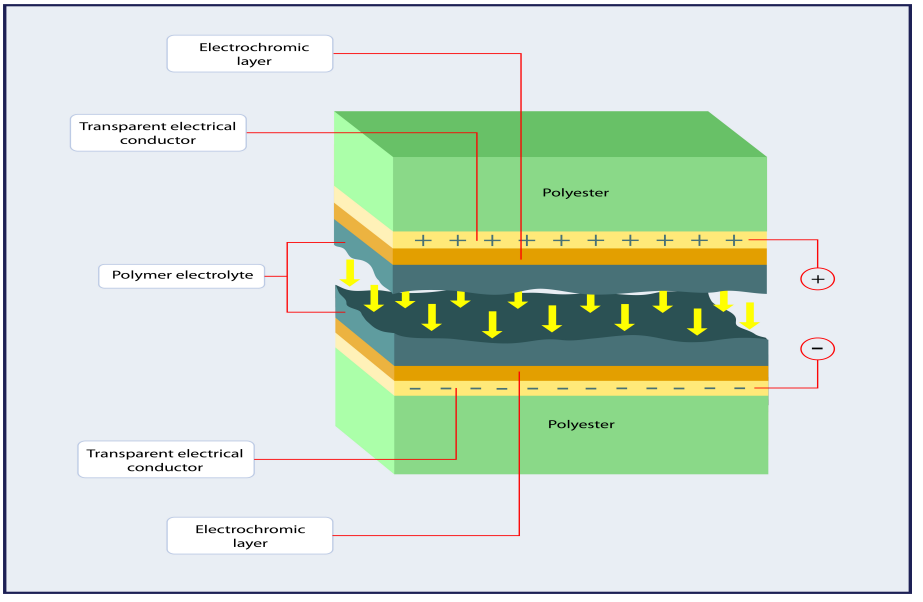

Figure 1.17: *Schematic diagram of a Electro Chromic Display Devise (ECD).*

mechanical adhesive and ion-conducting electrolyte. Many researchers have reported that ionomers like polystyrene sulfonic acid, poly AMPS, etc. can be used in ECD. They provide protonic acid $-SO_3H$ group on the polymer chain.[232,233]. A schematic diagram of an arbitrary ECD has been shown in the adjoining figure-1.17. ECD is used in different kinds of electrochemical devices like a light-emitting diode (LED), liquid crystal display (LCD), etc.

1.11.5. Sensor

Liquid electrochemical sensors happen to be heavy and suffer from various types of difficulties like drying and leakage of electrolyte material. These problems eventually reduce the lifetime of the sensors as well as hinder them from doing the proper function. The use of solid polymer electrolytes (SPE) can be considered as a noble alternative as they eliminate the above mentioned limitations successfully. SPE-based sensors are two types: a. Impedance type sensor, where variation in electrical impedance in response to an external

signal happens to be the working principle of the sensor. B. electrochemical type sensor: where the working feature solely depends on the electrochemical reaction at the electrode-electrolyte interface. Various kinds of solid polymer electrolyte based sensing devices are available, $K^2CO_3 - PEG$ and porous ceramic-based CO_2 sensor, NAFION based O_2 sensor, $PVA - H_2PO_4$ based H_2 sensor, porous hydrophobic poly (ethylene) based sensor etc.[234,235].

Bibliography

[1] Tarascon, J.M., 2010. Key challenges in future Li-battery research. Philosophical Transactions of the Royal Society A: Mathematical, Physical and Engineering Sciences, 368(1923), pp.3227-3241.

[2] Bhatt M.D. and O'Dwyer, C., 2015. Recent progress in theoretical and computational investigations of Li-ion battery materials and electrolytes. Physical Chemistry Chemical Physics, 17(7), pp.4799-4844.

[3] E.P. Chavez, R. Oviedo-Roa, G. Contreras P erez, J.M. Martínez-Magadan F.L. Castillo-Alvaradob, Theoretical studies of ionic conductivity of crosslinked chitosan membranes, Int. J. Hydrogen Energy 35 (2010),12141e12146.

[4] Balbuena, P.B., 2014, June. Electrolyte materials-Issues and challenges. In AIP Conference Proceedings (Vol. 1597, No. 1, pp. 82-97). American Institute of Physics.

[5] Kato, Y., Hori, S., Saito, T., Suzuki, K., Hirayama, M., Mitsui, A., Yonemura, M., Iba, H. and Kanno, R., 2016. High-power all-solid-state batteries using sulfide superionic conductors. Nature Energy, 1(4), pp.1-7.

[6] L. Cheng, C. H. Wu, A. Jarry, W. Chen, Y. Ye, J. Zhu, R. Kostecki, K. Persson, J. Guo, M. Salmeron, G. Chen and M. Doeff, 2015, ACS Appl. Mater. Interfaces, 7, 17649–17655

[7] J. G. Kim, B. Son, S. Mukherjee, N. Schuppert, A. Bates, O.Kwon, M. J. Choi, H. Y. Chung and S. Park, 2015, A review of lithium and non-lithium based solid state batteries J. Power Sources, 299–322..

[8] Pandey, K., Dwivedi, M.M. and Tripathi, M., 2009. Structure, interaction and thermal study in electrolyte of polyethylene oxide/silica/ammonium thiocynate nanocomposites. Polymer composites, 30(4), pp.503-509.

[9] Charlesby, A., 1953. Effect of high-energy radiation on long-chain polymers. Nature, 171(4343), pp.167-167.

[10] Basu, T. and Tarafdar, S., 2016. Influence of gamma irradiation on the electrical properties of LiClO4-gelatin solid polymer electrolytes: Modelling anomalous diffusion through generalized calculus. Radiation Physics and Chemistry, 125, pp.180-198.

[11] Rajendran, S., Bama, V.S. and Prabhu, M.R., 2010. Preparation and characterization of PVAc–PMMA-based solid polymer blend electrolytes. Ionics, 16(3), pp.283-287.

[12] K. Sownthari, S. A. Suthanthiraraj, 2013, Synthesis and characterization of an electrolyte system based on a biodegradable polymer,eXPRESS Polymer Letters,7(6), 495-504.

[13] Ulaganathan, M., Nithya, R. and Rajendran, S., 2012. Surface analysis studies on polymer electrolyte membranes using scanning electron microscope and atomic force microscope. In Scanning Electron Microscopy. Intechopen.

[14] Wong, C.S., Badri, K.H., Ataollahi, N., Law, K.P., Su'ait, M.S. and Hassan, N.I., 2014. Synthesis of New Bio-Based Solid Polymer Electrolyte Polyurethane-LiClO4 via Prepolymerization Method: Effect of NCO/OH Ratio on Their Chemical, Thermal Properties and Ionic Conductivity. International Journal Of Chemical Molecular, Nuclear, Materials, And Metallurgical Engineering, 8(11), pp.1216-1223.

[15] Zhang, A.L., Cao, F.Y., Na, G.Z., Wang, S., Li, S.X. and Liu, J.C., 2016. A novel PEO-based blends solid polymer electrolytes doping liquid crystalline ionomers. Ionics, 22(11), pp.2103-2112.

[16] Polu, A.R. and Rhee, H.W., 2017. Ionic liquid doped PEO-based solid polymer electrolytes for lithium-ion polymer batteries. international journal of hydrogen energy, 42(10), pp.7212-7219.

[17] Porcarelli, L., Gerbaldi, C., Bella, F. and Nair, J.R., 2016. Super soft all-ethylene oxide polymer electrolyte for safe all-solid Lithium batteries. Sci Rep 6: 19892.

[18] Mustafa, N.S., Omer, M.A.A., Garlnabi, M.E. and Ismail, H.A., Reviewing of General Polymer Types, Properties and Application in Medical Field.

[19] Basu, T., Middya, T.R. and Tarafdar, S., 2013. Ion-conductivity study and anomalous diffusion analysis of plasticized gelatin films. Journal of Applied Polymer Science, $130(4), pp.3018 - 3024$

[20] Hara, M. ed., 1992. Polyelectrolytes: science and technology. CRC Press.

[21] *https//polymerdatabase.com/polymer%20classes/Polyelectrolyte%20type.html*

[22] Scrosati, B. ed., 1993. Applications of electroactive polymers (Vol. 75). London: Chapman and Hall.

[23] Fenton, D.E., 1973. Complexes of alkali metal ions with poly (ethylene oxide). polymer, 14, p.589.

[24] Armand, B, Chabagno J.M., Duclot M., in: Vahista P., Mundy J.N., Shenoy G.K. (Eds.), 1979, Fast Ion Transport in Solids, Elsevier, North Holland, New York, p. 131.

[25] Berthier, C., Gorecki, W., Minier, M., Armand, M.B., Chabagno, J.M. and Rigaud, P., 1983. Microscopic investigation of ionic conductivity in alkali metal salts-poly (ethylene oxide) adducts. Solid State Ionics, 11(1), pp.91-95.

[26] Ratner A., in: Maccallum J.R. , Vincent C.A (Eds.),1987. Polymer Electrolyte Reviews-I, Elsevier, New York, 1987, p. 173.

[27] Vincent, C.A.,1990, In Electrochemical Science and Technology of Polymers 2. (Ed. R.G. Linford), Elsevier Applied Science, London, p. 47.

[28] Agrawal, R.C. and Pandey, G.P., 2008. Solid polymer electrolytes: materials designing and all-solid-state battery applications: an overview. Journal of Physics D: Applied Physics, 41(22), p.223001.

[29] Gray, F.M. and Gray, F.M., 1991. Solid polymer electrolytes: fundamentals and technological applications (pp. 83-93). New York: VCH.

[30] Tarascon, J.M., Gozdz, A.S., Schmutz, C., Shokoohi, F. and Warren, P.C., 1996. Performance of Bellcore's plastic rechargeable Li-ion batteries. Solid State Ionics, 86, pp.49-54.

[31] Alamgir M, Abraham K. M., Pistoia. G.(ed), 1994, Lithium Batteries: New Materials, Developments and Perspectives,Amsterdam: Elsevier, p 93 Ref1.2.23

[32] Armand, M., 1990. Polymers with ionic conductivity. Advanced Materials, 2(6-7), pp.278-286.

[33] MacCallum, J.R. and Vincent, C.A., 1987. and 1989 Polymer electrolyte reviews.

[34] Bruce P G (ed) 1995 Solid State Electrochemistry(Cambridge: Cambridge University Press)

[35] Scrosati, B. ed., 1993. Applications of electroactive polymers (Vol. 75). London, Chapman and Hall.

[36] Meyer, W.H., 1998. Polymer electrolytes for lithium-ion batteries. Advanced materials, 10(6), pp.439-448.

[37] Scrosati, B. and Vincent, C.A., 2000. Polymer electrolytes: the key to lithium polymer batteries. Mrs Bulletin, 25(3), pp.28-30.

[38] Jacob, M.M.E., Hackett, E. and Giannelis, E.P., 2003. From nanocomposite to nanogel polymer electrolytes. Journal of Materials Chemistry, 13(1), pp.1-5

[39] Stephan, A.M., 2006. Review on gel polymer electrolytes for lithium batteries. European polymer journal, 42(1), pp.21-42.

[40] Feuillade, G. and Perche, P., 1975. Ion-conductive macromolecular gels and membranes for solid lithium cells. Journal of Applied Electrochemistry, 5(1), pp.63-69.

[41] Jeon, J.D., Kwak, S.Y. and Cho, B.W., 2005. Solvent-Free Polymer Electrolytes: I. Preparation and Characterization of Polymer Electrolytes Having Pores Filled with Viscous. Journal of the Electrochemical Society, 152(8), p.A1583.

[42] Wieczorek, W., Such, K., Przyłuski, J. and Floriańczyk, Z., 1991. Blend-based and composite polymer solid electrolytes. Synthetic metals, 45(3), pp.373-383.

[43] Weston, J.E. and Steele, B.C.H., 1982. Effects of inert fillers on the mechanical and electrochemical properties of lithium salt-poly (ethylene oxide) polymer electrolytes. Solid State Ionics, 7(1), pp.75-79.

[44] Aziz, S.B., Woo, T.J., Kadir, M.F.Z. and Ahmed, H.M., 2018. A conceptual review on polymer electrolytes and ion transport models. Journal of Science: Advanced Materials and Devices, 3(1), pp.1-17.

[45] Croce, F., Appetecchi, G.B., Persi, L. and Scrosati, B., 1998. Nanocomposite polymer electrolytes for lithium batteries. Nature, 394(6692), pp.456-458.

[46] Croce, F., Persi, L., Ronci, F. and Scrosati, B., 2000. Nanocomposite polymer electrolytes and their impact on the lithium battery technology. Solid State Ionics, 135(1-4), pp.47-52.

[47] Appetecchi, G.B., Croce, F., Persi, L., Ronci, F. and Scrosati, B., 2000. Transport and interfacial properties of composite polymer electrolytes. Electrochimica Acta, 45(8-9), pp.1481-1490.

[48] Golodnitsky, D., Ardel, G. and Peled, E., 2002. Ion-transport phenomena in concentrated PEO-based composite polymer electrolytes. Solid State Ionics, 147(1-2), pp.141-155.

[49] Xanthos . M. Ed., 2005, Functional Fillers for Plastics, John Wiley and Sons, ISBN 3-527-31054-1

[50] Croce, F., Appetecchi, G.B., Persi, L. and Scrosati, B., 1998. Nanocomposite polymer electrolytes for lithium batteries. Nature, 394(6692), pp.456-458.

[51] Mohapatra, A., Rautray, T.R., Patra, A.K., Vijayan, V. and Mohanty, R.K., 2009. Trace element-based food value evaluation in soft and hard shelled mud crabs. Food and Chemical toxicology, 47(11), pp.2730-2734.

[52] Borgohain, M.M., Joykumar, T. and Bhat, S.V., 2010. Studies on a nanocomposite solid polymer electrolyte with hydrotalcite as a filler. Solid State Ionics, 181(21-22), pp.964-970.

[53] Mulmi, S., Park, C.H., Kim, H.K., Lee, C.H., Park, H.B. and Lee, Y.M., 2009. Surfactant-assisted polymer electrolyte nanocomposite membranes for fuel cells. Journal of Membrane Science, 344(1-2), pp.288-296.

[54] Passador, F.R., Ruvolo-Filho, A. and Pessan, L.A., 2017. Nanocomposites of polymer matrices and lamellar clays. In Nanostructures (pp. 187-207). William Andrew Publishing.

[55] Kontos, G.A., Soulintzis, A.L., Karahaliou, P.K., Psarras, G.C., Georga, S.N., Krontiras, C.A. and Pisanias, M.N., 2007. Electrical relaxation dynamics in TiO2-polymer matrix composites. Express Polym Lett, 1(12), pp.781-9.

[56] Jurczyk, M.U., Kumar, A., Srinivasan, S. and Stefanakos, E., 2007. Polyaniline-based nanocomposite materials for hydrogen storage. International Journal of Hydrogen Energy, 32(8), pp.1010-1015.

[57] Terife, G. and Narh, K.A., 2011. Properties of carbon nanotube reinforced linear low density polyethylene nanocomposites fabricated by cryogenic ball-milling. Polymer composites, 32(12), pp.2101-2109.

[58] Chang, C.M., Hsu, K.Y. and Liu, Y.L., 2012. Matrix-polymer-functionalized multi-walled carbon nanotubes as a highly efficient toughening agent for matrix polymers. Journal of Polymer Science Part B: Polymer Physics, 50(16), pp.1151-1155.

[59] Rahimi, M., Iriarte-Carretero, I., Ghanbari, A., Böhm, M.C. and Müller-Plathe, F., 2012. Mechanical behavior and interphase structure in a silica–polystyrene nanocomposite under uniaxial deformation. Nanotechnology, 23(30), p.305702.

[60] Eiras, D. and Pessan, L.A., 2009. Mechanical properties of polypropylene/calcium carbonate nanocomposites. Materials Research, 12(4), pp.517-522.

[61] Olad, A. and Nosrati, R., 2012. Preparation, characterization, and photocatalytic activity of polyaniline/ZnO nanocomposite. Research on Chemical Intermediates, 38(2), pp.323-336.

[62] Angell, C.A., Liu, C. and Sanchez, E., 1993. Rubbery solid electrolytes with dominant cationic transport and high ambient conductivity. Nature, 362(6416), pp.137-139.

[63] Angell, C.A., Xu, K., Zhang, S.S. and Videa, M., 1996. Variations on the salt-polymer electrolyte theme for flexible solid electrolytes. Solid State Ionics, 86, pp.17-28.

[64] Stephan, A.M., Kumar, T.P., Kulandainathan, M.A. and Lakshmi, N.A., 2009. Chitin-incorporated poly (ethylene oxide)-based nanocomposite electrolytes for lithium batteries. The Journal of Physical Chemistry B, 113(7), pp.1963-1971.

[65] Honary, S. and Orafai, H., 2002. The effect of different plasticizer molecular weights and concentrations on mechanical and thermomechanical properties of free films. Drug development and industrial pharmacy, 28(6), pp.711-715.

[66] HONARI, S. and GOLKAR, M., 2003. Effect of polymer grade and plasticizer molecular weights on viscoelastic behavior of coating solutions.

[67] Samir, M.A.S.A., Mateos, A.M., Alloin, F., Sanchez, J.Y. and Dufresne, A., 2004. Plasticized nanocomposite polymer electrolytes based on poly (oxyethylene) and cellulose whiskers. Electrochimica Acta, 49(26), pp.4667-4677.

[68] D. Saikia, H.-Y. Wu, Y.-C. Pan, C.-P. Lin, K.-P. Huang, K.-N. Chen, G.T.K. Fey, H.-M. Kao, 2011. Highly conductive and electrochemically stable plasticized blend polymer electrolytes based on PVdF-HFP and triblock copolymer PPG-PEGPPG diamine for Li-ion batteries, J. Power Sources 196, 2826-2834.

[69] Nicolau, A., Nucci, A.M., Martini, E.M. and Samios, D., 2007. Electrical impedance spectroscopy of epoxy systems II: Molar fraction variation, resistivity, capacitance and relaxation processes of 1, 4-butanediol diglycidyl ether/succinic anhydride and triethylamine as initiator. European polymer journal, 43(6), pp.2708-2717.

[70] Aziz, S.B. and Abidin, Z.H.Z., 2015. Ion-transport study in nanocomposite solid polymer electrolytes based on chitosan: electrical and dielectric analysis. Journal of Applied Polymer Science, 132(15).

[71] Maitra M., 2008, Correlating electrical, mechanical, thermal and structural properties of a solid polymer electrolyte and studying the effect of irradiation on these properties, thesis submitted for the degree of doctor of philosophy (science), Jadavpur University

[72] Vicsek, T., 1992. Fractal growth phenomena. World scientific.

[73] Vincent, C.A., 1987. Polymer electrolytes. Progress in solid state chemistry, 17(3), pp.145-261.

[74] Saroj, A.L. and Singh, R.K., 2011. Studies on ionic liquid 1-ethyl-3-methyl imidazolium ethylsulphate complexed with PVA. Phase Transitions, 84(3), pp.231-242.

[75] Berthier, C., Gorecki, W., Minier, M., Armand, M.B., Chabagno, J.M. and Rigaud, P., 1983. Microscopic investigation of ionic conductivity in alkali metal salts-poly (ethylene oxide) adducts. Solid State Ionics, 11(1), pp.91-95.

[76] Quartarone, E., Mustarelli, P. and Magistris, A., 1998. PEO-based composite polymer electrolytes. Solid State Ionics, 110(1-2), pp.1-14.

[77] .Armand, W. Gorecki and R. Andreani , Crosati B., ed ,1990, Proc. 2nd Int.Meeting on Polymer Electrolytes (New York), Amsterdam: Elsevier, p 91

[78] Wright, P.V., 1975. Electrical conductivity in ionic complexes of poly (ethylene oxide). British polymer journal, 7(5), pp.319-327.

[79] Armand, M.B., 1986. Polymer electrolytes. Annual Review of Materials Science, 16(1), pp.245-261.

[80] Ratner, M.A. and Shriver, D.F., 1988. Ion transport in solvent-free polymers. Chemical Reviews, 88(1), pp.109-124.

[81] Giles, J.R.M., Gray, F.M., MacCallum, J.R. and Vincent, C.A., 1987. Synthesis and characterization of ABA block copolymer-based polymer electrolytes. Polymer, 28(11), pp.1977-1981.

[82] Landel, R.F. and Nielsen, L.E., 1993. Mechanical properties of polymers and composites. CRC press.

[83] Bower D.I., 2002, An Introduction to Polymer Physics, Cambridge University press, New York

[84] Kulkarni A. R, Solid State Ionics, Proc. Asian Conf., 8th, 2002, 273–282.

[85] Long, L., Wang, S., Xiao, M. and Meng, Y., 2016. Polymer electrolytes for lithium polymer batteries. Journal of Materials Chemistry A, 4(26), pp.10038-10069.

[86] Arya, A. and Sharma, A.L., 2017. Insights into the use of polyethylene oxide in energy storage/conversion devices: a critical review. Journal of Physics D: Applied Physics, 50(44), p.443002 .

[87] Song, J.Y., Wang, Y.Y. and Wan, C.C., 1999. Review of gel-type polymer electrolytes for lithium-ion batteries. Journal of power sources, 77(2), pp.183-197.

[88] Bruce, P.G., Hardgrave, M.T. and Vincent, C.A., 1992. The determination of transference numbers in solid polymer electrolytes using the Hittorf method. Solid state ionics, 53, pp.1087-1094.

[89] Doyle, M. and Newman, J., 1995. Analysis of transference number measurements based on the potentiostatic polarization of solid polymer electrolytes. Journal of the Electrochemical Society, 142(10), p.3465.

[90] Song, J.Y., Wang, Y.Y. and Wan, C.C., 1999. Review of gel-type polymer electrolytes for lithium-ion batteries. Journal of power sources, 77(2), pp.183-197.

[91] Armand, M., Endres, F., MacFarlane, D.R., Ohno, H. and Scrosati, B., 2011. Ionic-liquid materials for the electrochemical challenges of the future. In Materials For Sustainable Energy: A Collection of Peer-Reviewed Research and Review Articles from Nature Publishing Group (pp. 129-137).

[92] Stephan, A.M., 2006. Review on gel polymer electrolytes for lithium batteries. European polymer journal, 42(1), pp.21-42.

[93] N.H. Idris, M.M. Rahman, J.Z. Wang, H.K. Liu, Microporous gel polimer electrolytes for lithium rechargeable battery application, J. Power Sources 201 (2012),294–300,

[94] Aziz, S.B., Abidin, Z.H.Z. and Kadir, M.F.Z., 2015. Innovative method to avoid the reduction of silver ions to silver nanoparticles in silver ion conducting based polymer electrolytes. Physica Scripta, 90(3), p.035808.

[95] Zang, L., Luo, J., Guo, J., Liu, H. and Ru, J., 2010. Preparation and characterization of poly (ethylene glycol)/organo-vermiculite nanocomposite polymer electrolytes. Polymer bulletin, 65(7), pp.669-680.

[96] Aziz, S.B., Abidin, Z.H.Z. and Arof, A.K., 2010. Effect of silver nanoparticles on the DC conductivity in chitosan–silver triflate polymer electrolyte. Physica B: Condensed Matter, 405(21), pp.4429-4433.

[97] Hema, M., Selvasekerapandian, S., Hirankumar, G., Sakunthala, A., Arunkumar, D. and Nithya, H., 2009. Structural and thermal studies of PVA: NH4I. Journal of Physics and Chemistry of Solids, 70(7), pp.1098-1103.

[98] Aziz, S.B. and Abidin, Z.H.Z., 2013. Electrical conduction mechanism in solid polymer electrolytes: new concepts to arrhenius equation. Journal of soft matter, 2013.

[99] Aziz, S.B., 2013. Li+ ion conduction mechanism in poly (ϵ-caprolactone)-based polymer electrolyte. Iranian Polymer Journal, 22(12), pp.877-883.

[100] Vincent, C.A., 1995. Ion transport in polymer electrolytes. Electrochimica Acta, 40(13-14), pp.2035-2040.

[101] Stainer, M., Hardy, L.C., Whitmore, D.H. and Shriver, D.F., 1984. Stoichiometry of formation and conductivity response of amorphous and crystalline complexes formed between poly (ethylene oxide) and ammonium salts: PEO x· NH 4 SCN and PEO x· NH 4 SO 3 CF 3. Journal of The Electrochemical Society, 131(4), p.784.

[102] MacGlashan, G.S., Andreev, Y.G. and Bruce, P.G., 1999. Structure of the polymer electrolyte poly (ethylene oxide) 6: LiAsF 6. Nature, 398(6730), pp.792-794.

[103] Chen, R., Qu, W., Guo, X., Li, L. and Wu, F., 2016. The pursuit of solid-state electrolytes for lithium batteries: from comprehensive insight to emerging horizons. Materials Horizons, 3(6), pp.487-516.

[104] Meyer, W.H., 1998. Polymer electrolytes for lithium-ion batteries. Advanced materials, 10(6), pp.439-448.

[105] Wang, Y., Agapov, A.L., Fan, F., Hong, K., Yu, X., Mays, J. and Sokolov, A.P., 2012. Decoupling of ionic transport from segmental relaxation in polymer electrolytes. Physical review letters, 108(8), p.088303.

[106] Golodnitsky, D., Strauss, E., Peled, E. and Greenbaum, S., 2015. On order and disorder in polymer electrolytes. Journal of The Electrochemical Society, 162(14), p.A2551.

[107] Long, L., Wang, S., Xiao, M. and Meng, Y., 2016. Polymer electrolytes for lithium polymer batteries. Journal of Materials Chemistry A, 4(26), pp.10038-10069.

[108] Gadjourova, Z., Andreev, Y.G., Tunstall, D.P. and Bruce, P.G., 2001. Ionic conductivity in crystalline polymer electrolytes. Nature, 412(6846), pp.520-523.

[109] Stoeva, Z., Imrie, C.T. and Ingram, M.D., 2003. Effect of pressure on ion transport in amorphous and semi-crystalline polymer electrolytes. Physical Chemistry Chemical Physics, 5(2), pp.395-399.

[110] Xue, Z., He, D. and Xie, X., 2015. Poly (ethylene oxide)-based electrolytes for lithium-ion batteries. Journal of Materials Chemistry A, 3(38), pp.19218-19253.

[111] Ren, T., Huang, X., Zhao, X. and Tang, X., 2003. The effects of salt concentration on ion state and conductivity in comb cross-linked polymer electrolytes. Journal of materials science, 38(14), pp.3007-3011.

[112] Olsen, I., Koksbang, R., and Skou, E. 1995. Transference number measurements on a hybrid polymer electrolyte. Electrochimica Acta, 40(11), 1701–1706

[113] Petersen, G., Jacobsson, P. and Torell, L.M., 1992. A Raman study of ion—polymer and ion—ion interactions in low molecular weight polyether—LiCF3SO3 complexes. Electrochimica acta, 37(9), pp.1495-1497.

[114] Gray, F.M. and Gray, F.M., 1991. Solid polymer electrolytes: fundamentals and technological applications (pp. 83-93). New York: VCH.

[115] Gray, FM and Connor, JA (ed.) 1997, polymer electrolytes. rsc Materials Monographs, Royal Society of Chemistry, Cambridge, UK

[116] Turnbull, D. and Cohen, M.H., 1961. Free-volume model of the amorphous phase: glass transition. The Journal of chemical physics, 34(1), pp.120-125.

[117] Miyamoto, T. and Shibayama, K., 1973. Free-volume model for ionic conductivity in polymers. Journal of Applied Physics, 44(12), pp.5372-5376.

[118] Gibbs, J.H. and DiMarzio, E.A., 1958. Nature of the glass transition and the glassy state. The Journal of Chemical Physics, 28(3), pp.373-383.

[119] Adam, G. and Gibbs, J.H., 1965. On the temperature dependence of cooperative relaxation properties in glass-forming liquids. The journal of chemical physics, 43(1), pp.139-146

[120] Ratner, M.A. and Shriver, D.F., 1988. Ion transport in solvent-free polymers. Chemical Reviews, 88(1), pp.109-124.

[121] Druger, S.D., Ratner, M.A. and Nitzan, A., 1983. Polymeric solid electrolytes: Dynamic bond percolation and free volume models for diffusion. Solid State Ionics, 9, pp.1115-1120.

[122] Ratner, M.A., Johansson, P. and Shriver, D.F., 2000. Polymer electrolytes: ionic transport mechanisms and relaxation coupling. Mrs Bulletin, 25(3), pp.31-37.

[123] Meyer, W.H., 1998. Polymer electrolytes for lithium-ion batteries. Advanced materials, 10(6), pp.439-448.

[124] Maier, J., 2009. Fundamentals, applications, and perspectives of solid-state electrochemistry: a synopsis. Solid State Electrochemistry I: Fundamentals, Materials and their Applications, pp.1-13.

[125] Vogel, H., 1925. Phys. Z, 22, 645 (1921); GS Fulcher. J. Am. Chem. Soc, 8, p.339.

[126] Fulcher, G. S. (1925). Analysis of Recent Measurements of The Viscosity of Glasses. Journal of the American Ceramic Society, 8(6), 339–355.

[127] W. and Tammann, G., 1926. Dependence of viscosity on the temperature of supercooled liquids. Anorg. Allgem. Chem., 156, pp.245-257.

[128] Gray, F.M., 1997. Polymer electrolytes. Royal Society of Chemistry.

[129] Qian, X., Gu, N., Cheng, Z., Yang, X., Wang, E. and Dong, S., 2002. Plasticizer effect on the ionic conductivity of PEO-based polymer electrolyte. Materials Chemistry and Physics, 74(1), pp.98-103.

[130] Klongkan, S. and Pumchusak, J., 2015. Effects of nano alumina and plasticizers on morphology, ionic conductivity, thermal and mechanical properties of PEO-LiCF3SO3 solid polymer electrolyte. Electrochimica Acta, 161, pp.171-176.

[131] Chaurasia, S.K., Gupta, A.K., Verma, Y.L., Singh, V.K., Tripathi, A.K., Saroj, A.L. and Singh, R.K., 2015. Role of ionic liquid [BMIMPF 6] in modifying the crystallization kinetics behavior of the polymer electrolyte PEO-LiClO 4. RSC advances, 5(11), pp.8263-8277.

[132] Su'ait, M.S., Ahmad, A. and Rahman, M.Y.A., 2009. Ionic conductivity studies of 49 percent poly (methyl methacrylate)-grafted natural rubber-based solid polymer electrolytes. Ionics, 15(4), pp.497-500.

[133] Othman, L., Chew, K.W. and Osman, Z., 2007. Impedance spectroscopy studies of poly (methyl methacrylate)-lithium salts polymer electrolyte systems. Ionics, 13(5), pp.337-342.

[134] Kim, Y.T. and Smotkin, E.S., 2002. The effect of plasticizers on transport and electrochemical properties of PEO-based electrolytes for lithium rechargeable batteries. Solid State Ionics, 149(1-2), pp.29-37.

[135] MacCallum, J.R. and Vincent, C.A., 1987. Polymer electrolytes reviews Elsevier

[136] Ramesh, S., Yin, T.S. and Liew, C.W., 2011. Effect of dibutyl phthalate as plasticizer on high-molecular weight poly (vinyl chloride)–lithium tetraborate-based solid polymer electrolytes. Ionics, 17(8), p.705.

[137] Ramesh, S. and Bing, K.N., 2012. Conductivity, mechanical and thermal studies on poly (methyl methacrylate)-based polymer electrolytes complexed with lithium tetraborate and propylene carbonate. Journal of materials engineering and performance, 21(1), pp.89-94.

[138] Raghavan, P., Zhao, X., Manuel, J., Chauhan, G.S., Ahn, J.H., Ryu, H.S., Ahn, H.J., Kim, K.W. and Nah, C., 2010. Electrochemical performance of electrospun poly (vinylidene fluoride-co-hexafluoropropylene)-based nanocomposite polymer electrolytes incorporating ceramic fillers and room temperature ionic liquid. Electrochimica Acta, 55(4), pp.1347-1354.

[139] Quartarone, E., Mustarelli, P. and Magistris, A., 1998. PEO-based composite polymer electrolytes. Solid State Ionics, 110(1-2), pp.1-14.

[140] Chung, S.H., Wang, Y., Persi, L., Croce, F., Greenbaum, S.G., Scrosati, B. and Plichta, E., 2001. Enhancement of ion transport in polymer electrolytes by addition of nanoscale inorganic oxides. Journal of power sources, 97, pp.644-648.

[141] Croce, F., Appetecchi, G.B., Persi, L. and Scrosati, B., 1998. Nanocomposite polymer electrolytes for lithium batteries. Nature, 394(6692), pp.456-458.

[142] Nan, C.W., Fan, L., Lin, Y. and Cai, Q., 2003. Enhanced Ionic Conductivity of Polymer Electrolytes Containing Nanocomposite S i O 2 Particles. Physical review letters, 91(26), p.266104.

[143] Stephan, A.M. and Nahm, K.S., 2006. Review on composite polymer electrolytes for lithium batteries. Polymer, 47(16), pp.5952-5964.

[144] Ngai, K.S., Ramesh, S., Ramesh, K. and Juan, J.C., 2016. A review of polymer electrolytes: fundamental, approaches and applications. Ionics, 22(8), pp.1259-1279.

[145] Kim, H.S., Kum, K.S., Cho, W.I., Cho, B.W. and Rhee, H.W., 2003. Electrochemical and physical properties of composite polymer electrolyte of poly (methyl methacrylate) and poly (ethylene glycol diacrylate). Journal of Power Sources, 124(1), pp.221-224.

[146] Walls, H.J., Zhou, J., Yerian, J.A., Fedkiw, P.S., Khan, S.A., Stowe, M.K. and Baker, G.L., 2000. Fumed silica-based composite polymer electrolytes: synthesis, rheology, and electrochemistry. Journal of Power Sources, 89(2), pp.156-162.

[147] Rajendran, S., Mahendran, O. and Kannan, R., 2002. Ionic conductivity studies in composite solid polymer electrolytes based on methylmethacrylate. Journal of Physics and Chemistry of Solids, 63(2), pp.303-307.

[148] Croce, F., Scrosati, B. and Mariotto, G., 1992. Electrochemical and spectroscopic study of the transport properties of composite polymer electrolytes. Chemistry of materials, 4(6), pp.1134-1136.

[149] Ramesh, S. and Wen, L.C., 2010. Investigation on the effects of addition of SiO 2 nanoparticles on ionic conductivity, FTIR, and thermal properties of nanocomposite PMMA–LiCF 3 SO 3–SiO 2. Ionics, 16(3), pp.255-262.

[150] Raghavan, S.R., Riley, M.W., Fedkiw, P.S. and Khan, S.A., 1998. Composite polymer electrolytes based on poly (ethylene glycol) and hydrophobic fumed silica: dynamic rheology and microstructure. Chemistry of materials, 10(1), pp.244-251.

[151] Itoh, T., Ichikawa, Y., Uno, T., Kubo, M. and Yamamoto, O., 2003. Composite polymer electrolytes based on poly (ethylene oxide), hyperbranched polymer, BaTiO3 and LiN (CF3SO2) 2. Solid State Ionics, 156(3-4), pp.393-399.

[152] Dai, Y., Wang, Y., Greenbaum, S.G., Bajue, S.A., Golodnitsky, D., Ardel, G., Strauss, E. and Peled, E., 1998. Electrical, thermal and NMR investigation of composite solid electrolytes based on PEO, LiI and high surface area inorganic oxides. Electrochimica acta, 43(10-11), pp.1557-1561.

[153] Golodnitsky, D., Ardel, G., Strauss, E., Peled, E., Lareah, Y. and Rosenberg, Y., 1997. Conduction Mechanisms in Concentrated LiI-Polyethylene Oxide-Al2 O 3-Based Solid Electrolytes. Journal of The Electrochemical Society, 144(10), p.3484.

[154] Chung, S.H., Wang, Y., Persi, L., Croce, F., Greenbaum, S.G., Scrosati, B. and Plichta, E., 2001. Enhancement of ion transport in polymer electrolytes by addition of nanoscale inorganic oxides. Journal of power sources, 97, pp.644-648.

[155] Zhang, P., Yang, L.C., Li, L.L., Ding, M.L., Wu, Y.P. and Holze, R., 2011. Enhanced electrochemical and mechanical properties of P (VDF-HFP)-based composite polymer electrolytes with SiO2 nanowires. Journal of membrane science, 379(1-2), pp.80-85.

[156] Capiglia, C., Mustarelli, P., Quartarone, E., Tomasi, C. and Magistris, A., 1999. Effects of nanoscale SiO2 on the thermal and transport properties of solvent-free, poly (ethylene oxide)(PEO)-based polymer electrolytes. Solid state ionics, 118(1-2), pp.73-79.

[157] Golodnitsky, D., Ardel, G. and Peled, E., 2002. Ion-transport phenomena in concentrated PEO-based composite polymer electrolytes. Solid State Ionics, 147(1-2), pp.141-155.

[158] Borgohain, M.M., Joykumar, T. and Bhat, S.V., 2010. Studies on a nanocomposite solid polymer electrolyte with hydrotalcite as a filler. Solid State Ionics, 181(21-22), pp.964-970.

[159] Ahn, J.H., Wang, G.X., Liu, H.K. and Dou, S.X., 2003. Nanoparticle-dispersed PEO polymer electrolytes for Li batteries. Journal of power sources, 119, pp.422-426.

[160] McKee, R.A., 1981. A generalization of the nernst-Einstein equation for self-diffusion in high defect concentration solids. Solid State Ionics, 5, pp.133-136.

[161] Mongcopa, K.I.S., Tyagi, M., Mailoa, J.P., Samsonidze, G., Kozinsky, B., Mullin, S.A., Gribble, D.A., Watanabe, H. and Balsara, N.P., 2018. Relationship between segmental dynamics measured by quasi-elastic neutron scattering and conductivity in polymer electrolytes. ACS Macro Letters, 7(4), pp.504-508.

[162] Bruce, P.G. and Vincent, C.A., 1993. Polymer electrolytes. Journal of the Chemical Society, Faraday Transactions, 89(17), pp.3187-3203.

[163] Rajendran, S., Sivakumar, P. and Babu, R.S., 2007. Studies on the salt concentration of a PVdF–PVC based polymer blend electrolyte. Journal of power sources, 164(2), pp.815-821.

[164] Seanor, D.A. ed., 2013. Electrical properties of polymers. Elsevier.

[165] Miller H., 1966, Structure of Polymers,Reinhold,New York

[166] Yang L.L. Huq R, Farmington G.C. Chiodelli G., 1986, Solid State Ionics, 18/19,291

[167] Ahmad, A., Rahman, M.Y.A., Low, S.P. and Hamzah, H., 2011. Effect of LiBF4 salt concentration on the properties of plasticized MG49-TiO2 based nanocomposite polymer electrolyte. ISRN Materials Science, 2011.

[168] Ramesh S, Liew CW(2012) Rheological characterizations of ionic liquid-based gel polymer electrolytes and fumed silica-based composite polymer electrolytes. Ceram Int 38:3411–3417

[169] Vioux A, Viau L, Volland S, Bideau JL (2009) Use of ionic liquids in sol-gel; ionogels and applications. C R Chim 13:242–255

[170] Lu J, Yan F, Texter J (2009) Advanced applications of ionic liquids in polymer science. Prog Polym Sci 34:431–448

[171] Lu, J., Yan, F. and Texter, J., 2009. Advanced applications of ionic liquids in polymer science. Progress in Polymer Science, 34(5), pp.431-448.

[172] Sato, T., Masuda, G. and Takagi, K., 2004. Electrochemical properties of novel ionic liquids for electric double layer capacitor applications. Electrochimica Acta, 49(21), pp.3603-3611.

[173] Sekhon, S.S., Lalia, B.S., Park, J.S., Kim, C.S. and Yamada, K., 2006. Physicochemical properties of proton conducting membranes based on ionic liquid impregnated polymer for fuel cells. Journal of Materials Chemistry, 16(23), pp.2256-2265.

[174] Seki, S., Mita, Y., Tokuda, H., Ohno, Y., Kobayashi, Y., Usami, A., Watanabe, M., Terada, N. and Miyashiro, H., 2007. Effects of alkyl chain in imidazolium-type room-temperature ionic liquids as lithium secondary battery electrolytes. Electrochemical and Solid State Letters, 10(10), p.A237.

[175] Sutto, T.E., 2007. Hydrophobic and hydrophilic interactions of ionic liquids and polymers in solid polymer gel electrolytes. Journal of the Electrochemical Society, 154(10), p.P101.

[176] Ye, H., Huang, J., Xu, J.J., Khalfan, A. and Greenbaum, S.G., 2007. Li ion conducting polymer gel electrolytes based on ionic liquid/PVDF-HFP blends. Journal of the Electrochemical Society, 154(11), p.A1048.

[177] Utracki, L.A. and Wilkie, C.A. eds., 2002. Polymer blends handbook (Vol. 1, p. 2). Dordrecht: Kluwer academic publishers.

[178] Nanda, P., De, S.K., Manna, S., De, U. and Tarafdar, S., 2010. Effect of gamma irradiation on a polymer electrolyte: variation in crystallinity, viscosity and ion-conductivity with dose. Nuclear Instruments and Methods in Physics Research Section B: beam Interactions with Materials and Atoms, 268(1), pp.73-78.

[179] Pucić, I. and Turković, A., 2005. Radiation modification of (PEO) 8ZnCl2 polyelectrolyte and nanocomposite. Solid State Ionics, 176(19-22), pp.1797-1800.

[180] Furusawa, K., Dobashi, T., Morishita, S., Oyama, M., Hashimoto, T., Shinyashiki, N., Yagihara, S. and Nagasawa, N., 2005. Structural and kinetic modification of aqueous hydroxypropylmethylcellulose (HPMC) induced by electron beam irradiation. Physica A: Statistical Mechanics and its Applications, 353, pp.9-20.

[181] Raghu, S., Archana, K., Sharanappa, C., Ganesh, S. and Devendrappa, H., 2016. Electron beam and gamma ray irradiated polymer electrolyte films: Dielectric properties. Journal of Radiation Research and Applied Sciences, 9(2), pp.117-124.

[182] Raghu, S., Archana, K., Sharanappa, C., Ganesh, S. and Devendrappa, H., 2015. The physical and chemical properties of gamma ray irradiated polymer electrolyte films. Journal of Non-Crystalline Solids, 426, pp.55-62.

[183] Gray, F.M., 1991. Solid Polymer Electrolytes: Fundamental and Technological Application, VCH, Publishers. Inc., New York.

[184] Guang-hou, W., Guo-qiang, P., Lie, D., Rui-xin, Y., Teng, Z., Shan-gen, J. and Qing-lai, D., 1987. Proton beam modification of isotactic polypropylene. Nuclear Instruments and Methods in Physics Research Section B: Beam Interactions with Materials and Atoms, 27(3), pp.410-416.

[185] Švorčík, V., Rybka, V., Hnatowicz, V., Bačáková, L., Lisá, V. and Kocourek, F., 1995. Surface properties and biocompatibility of ion-implanted polymers. Journal of Materials Chemistry, 5(1), pp.27-30.

[186] Phillips, M.H., Frankel, K.A., Lyman, J.T., Fabrikant, J.I. and Levy, R.P., 1990. Comparison of different radiation types and irradiation geometries in stereotactic radiosurgery. International Journal of Radiation Oncology* Biology* Physics, 18(1), pp.211-220.

[187] Gerling, R., Schimansky, F.P. and Wagner, R., 1987. Restoration of the ductility of thermally embrittled amorphous alloys under neutron-irradiation. Acta Metallurgica, 35(5), pp.1001-1006.

[188] Nanda P., 2010, Effect of Gamma Irradiation on Properties of Polymer Electrolytes,thesis,Jadavpur University,Kolkata,India

[189] Laxmayyaguddi, Y., Mydur, N., Shankar Pawar, A., Hebri, V., Vandana, M., Sanjeev, G. and Hundekal, D., 2018. Modified Thermal, Dielectric, and Electrical Conductivity of PVDF-HFP/LiClO4 Polymer Electrolyte Films by 8 MeV Electron Beam Irradiation. ACS omega, 3(10), pp.14188-14200.

[190] Manjunatha, H., Damle, R., Pravin, K. and Kumaraswamy, G.N., 2018. Modification in the transport and morphological properties of solid polymer electrolyte system by low-energy ion irradiation. Ionics, 24(10), pp.3027-3037.

[191] Raghu, S., Archana, K., Sharanappa, C., Ganesh, S. and Devendrappa, H., 2016. Electron beam and gamma ray irradiated polymer electrolyte films: Dielectric properties. Journal of Radiation Research and Applied Sciences, 9(2), pp.117-124.

[192] Manjunatha, H., Damle, R. and Kumaraswamy, G.N., 2016, May. Ion beam irradiation as a tool to improve the ionic conductivity in solid polymer electrolyte systems. In AIP Conference Proceedings (Vol. 1728, No. 1, p. 020404). AIP Publishing LLC.

[193] Demappa, T., Ganesha, S., Divakara, S., Pattabi, M. and Somashekar, R., 2008. Physical and thermal properties of 8 MeV electron beam irradiated HPMC polymer films.

Nuclear Instruments and Methods in Physics Research Section B: Beam Interactions with Materials and Atoms, 266(18), pp.3975-3980.

[194] Sofield, C.J., Sugden, S., Ing, J., Bridwell, L.B. and Wang, Y.Q., 1993. Ion beam modification of polymers. Vacuum, 44(3-4), pp.285-290.

[195] Vacik, J., Cervena, J., Fink, D., Klett, R., Hnatowicz, V., Popok, V. and Odzhaev, V., 1997. High fluence boron implantation into polymers. Radiation effects and defects in solids, 143(2), pp.139-156.

[196] Banerjee, S., Deka, M., Kumar, A. and De, U., 2013. Ion Irradiation Effects in some Electro-Active and Engineering Polymers Studies by Conventional and Novel Techniques. In Defect and Diffusion Forum (Vol. 341, pp. 1-49). Trans Tech Publications Ltd.

[197] Deka, M. and Kumar, A., 2013. Dielectric and conductivity studies of 90 MeV O 7+ ion irradiated poly (ethylene oxide)/montmorillonite based ion conductor. Journal of Solid State Electrochemistry, 17(4), pp.977-986.

[198] Tayal D.C., 2009, Nuclear Physics, Himalaya Publishing House

[199] Chapiro. A.,2004,Radiation Effect in Polymers, Encyclopedia of Materials: Science and Technology, doi: 10.1016/B0-08-043152-6/01918-5

[200] Grosswendt, B. and Waibel, E., 1975. Determination of detector efficiencies for gamma ray energies up to 12 MeV II. Monte Carlo calculation. Nuclear Instruments and Methods, 131(1), pp.143-156.

[201] Fornalski, K. W.,2018, Simple Empirical Correction Functions to Cross Sections of the Photoelectric Effect, Compton Scattering, Pair and Triplet Production for Carbon Radiation Shields for Intermediate and High Photon Energies. Journal of Physics Communications , 2, 035038

[202] Guang-hou, W., Guo-qiang, P., Lie, D., Rui-xin, Y., Teng, Z., Shan-gen, J. and Qinglai, D., 1987. Proton beam modification of isotactic polypropylene. Nuclear Instruments and Methods in Physics Research Section B: Beam Interactions with Materials and Atoms, 27(3), pp.410-416.

[203] Švorčík, V., Rybka, V., Hnatowicz, V., Bačáková, L., Lisá, V. and Kocourek, F., 1995. Surface properties and biocompatibility of ion-implanted polymers. Journal of Materials Chemistry, 5(1), pp.27-30.

[204] Choudhury, N.A., Sampath, S. and Shukla, A.K., 2009. Hydrogel-polymer electrolytes for electrochemical capacitors: an overview. Energy and Environmental Science, 2(1), pp.55-67.

[205] Rodríguez, J., Navarrete, E., Dalchiele, E.A., Sánchez, L., Ramos-Barrado, J.R. and Martín, F., 2013. Polyvinylpyrrolidone–LiClO4 solid polymer electrolyte and its application in transparent thin film supercapacitors. Journal of Power Sources, 237, pp.270-276.

[206] Charlesby A., 1967,Radiation Mechanisms in Polymers, Adv in Chem, American Chemical Soc, Washington, DC,

[207] Reichmanis, E., Frank, C.W., O'Donnell, J.H. and Hill, D.J., 1993. Radiation effects on polymeric materials: a brief overview.

[208] Charlesby A., 1960, Atomic radiation and polymers, Pergamon Press, New York, 556 pp.DOI: 10.1002/pol 1960.1204514637.

[209] Dannoux, A., Esnouf, S., Amekraz, B., Dauvois, V. and Moulin, C., 2008. Degradation mechanism of poly (ether-urethane) Estane® induced by high-energy radiation. II. Oxidation effects. Journal of Polymer Science Part B: Polymer Physics, 46(9), pp.861-878.

[210] Saito, O., 1972. The radiation chemistry of macromolecules, Ed. M. Dole.

[211] Fink, D., Klett, R., Chadderton, L.T., Cardoso, J., Montiel, R., Vazquez, H. and Karanovich, A.A., 1996. Carbonaceous clusters in irradiated polymers as revealed by small angle X-ray scattering and ESR. Nuclear Instruments and Methods in Physics Research Section B: Beam Interactions with Materials and Atoms, 111(3-4), pp.303-314.

[212] Kiran E, Rodriguez F, 23 international congress of pure Applied. Chemistry, 1971, Butterworths, London, Vol.8, P. 175

[213] Liu, R., Wu, Z., He, P., Fan, H., Huang, Z., Zhang, L., Chang, X., Liu, H., Wang, C.A. and Li, Y., 2019. A self-standing, UV-cured semi-interpenetrating polymer network reinforced composite gel electrolytes for dendrite-suppressing lithium ion batteries. Journal of Materiomics, 5(2), pp.185-194.] J. C. Wang, N. J. Dudney, Solid State Ionics 1986, 18–19, 112

[214] Stephan, A.M., 2006. Review on gel polymer electrolytes for lithium batteries. European polymer journal, 42(1), pp.21-42.

[215] Song, J.Y., Wang, Y.Y. and Wan, C.C., 1999. Review of gel-type polymer electrolytes for lithium-ion batteries. Journal of power sources, 77(2), pp.183-197.

[216] Croce, F., Settimi, L. and Scrosati, B., 2006. Superacid ZrO2-added, composite polymer electrolytes with improved transport properties. Electrochemistry communications, 8(2), pp.364-368.

[217] Croce, F., Curini, R., Martinelli, A., Persi, L., Ronci, F., Scrosati, B. and Caminiti, R., 1999. Physical and chemical properties of nanocomposite polymer electrolytes. The Journal of Physical Chemistry B, 103(48), pp.10632-10638.

[218] Kim, S., Hwang, E.J., Jung, Y., Han, M. and Park, S.J., 2008. Ionic conductivity of polymeric nanocomposite electrolytes based on poly (ethylene oxide) and organo-clay materials. Colloids and Surfaces A: Physicochemical and Engineering Aspects, 313, pp.216-219.

[219] Chen, H.W., Chiu, C.Y., Wu, H.D., Shen, I.W. and Chang, F.C., 2002. Solid-state electrolyte nanocomposites based on poly (ethylene oxide), poly (oxypropylene) diamine, mineral clay and lithium perchlorate. Polymer, 43(18), pp.5011-5016.

[220] Chandra, S., 1981. Superionic solids: principles and applications (p. 56). Amsterdam: North-Holland.

[221] Gupta, V. and Miura, N., 2005. Electrochemically deposited polyaniline nanowire's network: a high-performance electrode material for redox supercapacitor. Electrochemical and Solid State Letters, 8(12), p.A630.

[222] Simon, P. and Gogotsi, Y., 2010. Materials for electrochemical capacitors. In Nanoscience and technology: a collection of reviews from Nature journals (pp. 320-329).

[223] Birss, V.I., Conway, B.E. and Wojtowicz, J., 1997. The role and utilization of pseudocapacitance for energy storage by supercapacitors.

[224] Conway, B.E., 1991. Transition from "supercapacitor" to "battery" behavior in electrochemical energy storage. Journal of the Electrochemical Society, 138(6), p.1539.

[225] Hashmi, S.A., Kumar, A. and Tripathi, S.K., 2005. Investigations on electrochemical supercapacitors using polypyrrole redox electrodes and PMMA based gel electrolytes. European Polymer Journal, 41(6), pp.1373-1379.

[226] Krumpelt, M., Kumar, R. and Myles, K.M., 1994. Fundamentals of fuel cell system in integration. Journal of power sources, 49(1-3), pp.37-51.

[227] Shukla, A.K., Manoharan, R. and Ramesh, K.V., 1983. Electrochemical ways of tapping solar energy: an appraisal. Bulletin of Materials Science, 5(3-4), pp.267-276.

[228] Vaghari, H., Jafarizadeh-Malmiri, H., Berenjian, A. and Anarjan, N., 2013. Recent advances in application of chitosan in fuel cells. Sustainable Chemical Processes, 1(1), p.16..

[229] Sequeira, C. and Santos, D. eds., 2010. Polymer electrolytes: fundamentals and applications. Woodhead Publishing Limited, Cambridge, UK, Elsevier.

[230] Chang I.F.,Gilbert B.C. and Sun T.,I. ,i. Electrochem. Soc. 122 (1975) 955.

[231] Green, M., 1974. A solid state electrochromic cell—the RbAg4I5/WO3 system. TSF, 24(2), pp.S45-S46.

[232] Bozkurt, A., 2002. Application of proton conducting polymer electrolytes to electrochromic devices. Turkish Journal of Chemistry, 26(5), pp.663-668.

[233] Singh, K.P., Singh, R.P. and Gupta, P.N., 1995. Polymer based solid state electrochromic display device using PVA complex electrolytes. Solid state ionics, 78(3-4), pp.223-229.

[234] Sadaoka, Y., Sakai, Y. and Akiyama, H., 1986. A humidity sensor using alkali salt—poly (ethylene oxdide) hybrid films. Journal of materials science, 21(1), pp.235-240.

[235] Kuwata, S., Miura, N. and Yamazoe, N., 1988. A solid-state amperometric oxygen sensor using NAFION membrane operative at room temperature. Chemistry Letters, 17(7), pp.1197-1200.

Chapter-2

Fractals and its Different Properties: A Short Review and Diffusion in Fractal Like Disordered Medium.

Chapter 2

Fractals and its Different Properties: A Short Review and Diffusion in Fractal Like Disordered Medium

2.1. Introduction

The sole purpose of the present thesis is to investigate the effect of external gamma irradiation on the different structural and transportational properties of a solid polymer electrolyte (SPE) theoretically. It is obvious that we have to use a convenient mathematical model for this purpose and construction of the said mathematical model appears to be one of the biggest challenges for us. As we come to know from the theoretical discussion in the previous chapter (chapter-1), an arbitrary polymer sample does not have any definite structural pattern similar to the crystallized systems. They contain complex microstructural behaviour with high molecular weight[1], semi-crystalline nature where crystalline and amorphous phase co-exists[2,3]. Glass transition temperature (T_g) plays significant impact on the performance of the SPEs[4]. There are many experimental outcomes where the polymer electrolyte material shows fractal-like behaviour[5], in fact, many polymer systems show diffusion limited aggregates (DLA)[5] structure which is basically a stochastic fractal. A short review regarding the experimentally observed fractal-like nature of different polymer samples has been given later in this chapter.

Considering this fact, we have taken the initiative to construct the host polymer matrix mathematically using a fractal model. There exist different types of fractals and they have their respective characteristics. Therefore, it is unquestionably important for us to have a clear idea regarding the fractal concept, its classification, and its respective characteristics before we process our main investigation. The present thesis also aimed at the detailed theoretical study regarding the gamma irradiation-induced ionic conductivity behaviour inside the SPE sample. Hence, it is obvious to acquire a clear understanding of the diffusion phenomena inside a disordered medium like a fractal.

The present chapter consists of an initial discussion regarding the fundamental features of fractals, their classifications, availibility among natural objects, etc. Different distinguishable features like non-integer dimension, self-similarity, diatiolational symmetry, etc have been discussed in detail. A quantitative study regarding the theory of diffusion, its classifications, and its nature inside fractal objects has also been discussed here. The end part of this chapter consists of the computer simulation process inside fractal. Therefore the entire quantitative analysis of the present chapter has been aimed for a detailed understanding of the basic treaties of the fractal objects and the nature of diffusion inside a disordered medium that possesses fractal-like behaviour.

2.2. Fractals and Their Intrinsic Characteristics

Nature is crowded with an enormous number of objects which are irregular and fragmented by nature. The shapes and boundaries of the clouds, coastlines of different countries, snowflakes of different sizes, mountains, branches of trees are a few examples of such kinds of irregular systems that cannot be characterized by the conventional Euclidian geometry. The idea of the fractal was introduced to characterize these types of complex structures in nature which shows a lack of isotropy and homogeneity. The word Fractal comes from the Latin word "fractus" which means broken. The rough and fractured nature at every single point with non-integer dimension makes the pioneer mathematician Benoit Mandelbrot use the word "fractal".

A convenient and universally accepted explicit definition of fractal has not been made yet. But the characterization of fractals requires detailed knowledge regarding some fundamental properties. Dimension happens to be one of them. The idea of fractal dimension is different from the conventional Euclidean dimension and it will be discussed in the preceding section. All disordered materials cannot be characterized by fractals. An object that exhibits self-similarity behavior, can be considered fractal. Fractal objects possess scale-invariant structure and this phenomenon is maintained by them either perfectly or in a statistical sense. The conventional physical laws, applicable in Euclidean space, are not valid completely for the fractal system. Unlike the crystalline materials, fractals don't have translational symmetry rather, a new symmetry has been observed here which is known as dilatational symmetry. The importance of fractal concept and its application in different fields are extensively studied by Mandelbrot,[6], and then carried out by other renowned scientists and mathematicians like Feder[7], Vicsek[8] etc. All disordered and complex medium in nature does not essentially show fractal-like behaviour. An object that shows fractal-like nature, must possess some important characteristics that are discussed below.

2.2.1. Self Similarity

Self similarity[6–8] is one of the most fundamental properties of the fractals. It suggests that a certain part of the system happens to be similar to the whole pattern itself. Mandelbrot used the word "contracting similarity"[6] which is basically the linear geometric contraction of the whole figure with an isotropic contraction ratio. For better understanding, let us consider the structural characteristic of Vicsek fractal. A Vicsek fractal of $1^{st}, 2^{nd}$ and 3rd stages

are shown in figure-2.1. If a portion, say WXYZ of the 3rd stage fractal is separated and is magnified by three times then it resembles with the 3rd stages fractal itself and moreover the pattern of the magnified portion will be exactly similar the 2nd Vicsek fractal. Therefore if we focus on the minute structures of a certain part of the fractal, it will represent a small replica of the whole fractal itself i.e. the magnification brings out the finer structure on each length scale which are still invisible. Hence the previous configuration is considered as the seed of the subsequent higher stage. Self-similarity behavior of a fractal objects makes it infinitesimally fragmented and disordered in nature. Exact self-similar fractals are ideal mathematical concept and they are constructed through infinite numbers of iterations. Most of the natural substances like polymers, percolation clusters, different kind of aggregates etc. are finite in size and eventually they have a lower and upper cutoff of the length scale between which the self-similarity behavior is maintained in a stochastical manner. These types of self-similarity are known as stochastic self-similarity[8] The concept of self-similarity

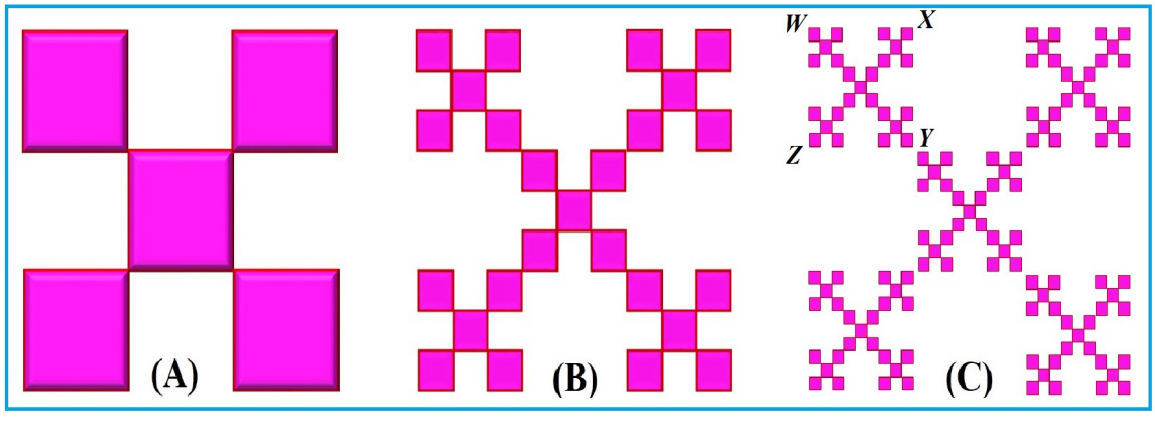

Figure 2.1: *Self similarity behavior of vicsek fractal. Figure-(A),(B) and (C) represents the* $1^{st}, 2^{nd}$ *and* 3rd *stage of vicsek fractal respectively. It should be noted that the part WXYZ of* 3rd *stage Vicsek fractal is exactly similar with* 2nd *stage.*

can be represented alternatively based on the scale-invariant nature of the said patterns. Generally, the construction of an arbitrary pattern starts from a generator of infinitesimally small length scale and it continues to generate the same pattern up to an indefinitely large scale. Therefore, details of the smaller structures are invisible when the pattern is observed from a definite length scale. As we continue to reduce the length scale of observation by an appropriate reduction ratio, finer structures become more visible but the structural pattern appears identical as it is observed on large scale. This phenomenon eventually results in the unique scale invariance nature of fractals. Let us consider the Vicsek Fractal of stage 3 as shown in the figure-2.1(C). In this case, the appropriate reduction factor is 3 ($n = 3$).

If we reduce the present length scale by the reduction factor 3, we get the same Vicsek fractal of stage 2 as shown in the figure-2.1(B). Thus on reducing the length scale by proper reduction ratio (in this case it is 3), we can observe the finer structure of Vicsek fractals but the structural pattern remains exactly the same. Scale invariance nature of fractals can also be explained with the help of the growth process where we can increase the length scale with a proper growth factor and get the same pattern, larger in size.

2.2.2. Dialational Symmetry

An arbitrary crystal lattice shows translational symmetry where the entire lattice can be configured by the simple translation of the lattice vector. Therefore a crystal lattice is said to be translationally invariant. After the careful observation of the construction procedure of Vicsek fractal in figure-2.1, it is very evident that the said fractal is not translationally invariant. Rather if someone dilates an appropriate portion of the said fractal it becomes similar to the whole fractal object. As we have already seen that the dilation of a portion WXYZ of the 3rd stage Vicsek fractal in figure-2.1(c) will produce the exact pattern of 2nd stage Vicsek fractal as shown in figure-2.1(b). Therefore a new kind of symmetry can be seen in the case of fractal objects which is obtained by suitable dilation of an appropriate portion of the entire pattern. This symmetry is known as dilational symmetry which happens to be one of the intrinsic characteristics of a fractal object.

2.2.3. Non Integer Dimension

The dimension of any object can be defined in different ways. The most common and most used one is known as the Euclidian dimension and is denoted by (D_E). It must take integer values such as 1,2,3 etc. The second kind of dimension is known as topological dimension and it is denoted by (D_T). It can be understood as follows: If a cut having the dimension = k is required to divide the system under consideration into two parts, then the topological dimension of the system will be (k+1). Therefore topological dimension ((D_T)) of a line is 1 as the cut which is required to divide the line into two-part happens to be a point that has a dimension k=0. Similarly, the cut which is required to divide an arbitrary surface into two parts must be in the form of a line having dimension k=1. Therefore the topological dimension ((D_T)) of a surface is 2. The segregation of a solid into two parts must require a cut in the form of a surface having dimension k=2 which makes any arbitrary solid a three-dimensional object. The topological dimension of any object must be an integer number

and its estimation for any regular object is not so complicated.

Calculation of dimension is not so straightforward in the case of any fractal object as they are highly disordered and fragmented by nature. Sometimes fractal dimensions are used as a tool to measure the complexity of the pattern or the roughness of the surface[8]. An important phenomenon of an fractal object is that their fractal dimension is always greater than their topological dimension ($D_f > D_T$)[6]. Dimension of any fractal object that is embedded into a d-dimensional Euclidean space can be evaluated in different methods and all these methods lead to a general conclusion that fractal objects have non-integer dimensions. The concept of fractal dimension was first successfully proposed by Felix Hausdorff (1868-1942) and Abram Besicovitch(1891-1970)[8] Let us consider a fractal object is embedded in space and the measurable quantity (e.g. volume, surface area, length, etc.) of the fractal object is considered as mass M. If M(X) is the measured value of mass on a certain length scale X and $M(\frac{X}{k})$ be the value of the same mass, measured in a new length scale $(\frac{X}{k})$ then we must say that:

$$\begin{aligned} M\left(\frac{X}{k}\right) &= k^{d_f}.M(X) \\ d_f &= \left[\frac{log\left[\frac{M(\frac{X}{k})}{M(X)}\right]}{log(k)}\right] \end{aligned} \tag{2.1}$$

Equation-(2.1) is known as the mathematical form of the Hausdorff- Besicovitch dimension. It can be shown from equation-(2.1) that the values of d_f for the length, area, and volume, in classical geometry, are 1,2, and 3 respectively. Whereas d_f takes fractional value in most of the cases for fractal objects. We can verify following the Hausdorff- Besicovitch dimension rule, mentioned above.

Let us consider the 2nd stage Sierpinski gasket as shown in the figure-2.2. If we measure the length of the 2nd stage SG with a yardstick of length X which is the same as the length of the SG then the mass of the fractal will be M(X) = 1. Because in this case, detailed smaller structures can not be seen. Now if we reduced our scale to X/4 the inner structures can be seen and in this case M(X/4) = 9 and M(X/4)/ M(X) = 9. Hence the Hausdorff- Besicovitch dimension will be:

$$d_f = \frac{log(9/1)}{log(4)} = \frac{log(3)}{log(2)} = 1.583 \tag{2.2}$$

which is different from the dimension of embedding Euclidian space. A different approach[8]

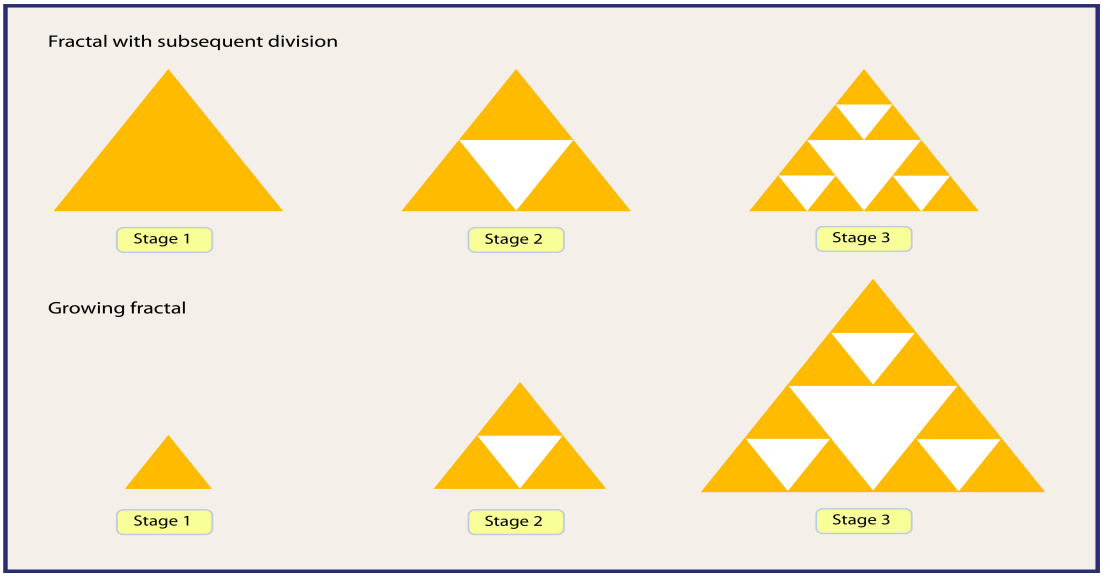

Figure 2.2: *Fractal growth is schematically presented using Sierpinski Gasket (SG) fractal. In the first case, generation of higher stage fractals has been shown using subsequent division method. The second case shows the generation of higher stage SG fractal by subsequent growth method.*

can be made to define the fractal dimension d_f. Let us cut a d-dimensional region from the fractal pattern having linear size R. The volume of the cut is V(R) which happens to be a function of the linear size (R) of the said pattern. Now, V(R) can be estimated by covering the entire pattern with balls having linear size r. Let us consider N(R) will be the number of such types of balls and the volume V(R) of the pattern is, therefore, = N(R). In the case of the evaluation of fractal dimension, the linear size of the balls i.e. the value of r is kept fixed while the linear size of the selected pattern i.e. R is increasing. Therefore as the linear size R increases, the value of N(R) increases such a way that we can write:

$$N(R) \sim R^{d_f} \tag{2.3}$$

$$d_f = lim_{R\to\infty}\left[\frac{lnN(R)}{ln(R)}\right] \tag{2.4}$$

It is very evident from the concept of growing fractal that the N(R) diverges as $R \to 0$. On the other hand, the value of R is kept constant and r is reducing in the case of fractals which are generated by subsequent divisions. Therefore those fractals having a finite size

and infinitely small ramifications, one can say:

$$N(R) \sim r^{-d_f} \tag{2.5}$$

$$d_f = lim_{r\to\infty}\left[\frac{lnN(r)}{ln(\frac{1}{r})}\right] \tag{2.6}$$

The physical fractals having finite size enables to represent physically admissible systems by using a dimensionless quantity: x= r/R. Therefore the expression of N(R) and N(r) can be written in the same form as:

$$N(x) \sim x^{-d_f} \tag{2.7}$$

Here $x \ll 1$ and N(x) stands for the total number of d-dimensional balls having a radius (xL) which is required to cover the entire fractal pattern under consideration. It should be noted that the definition of fractal dimension given by Hausdorff and Besicovitch happens to be more general than the above expression. In that case, it has been assumed that the measuring ball that has been used to evaluate the entire volume of the fractal structure has the volume x^{d_f}. The mathematical form of the Hausdorff-Besicovitch dimension has been given in the beginning part of this subsection. There are some special situations where the fractal dimension can have an integer value. There exists many other ways to define fractal dimension which have been discussed in different works of literature.

2.2.4. Ramification

Hausdorff- Besicovitch dimension can give a rough estimation of the structural characteristics of a fractal object. But fractals with identical d_f can have a different structural pattern. Hence it is necessary to introduce another parameter that can be able to distinguish between fractals with the same dimension. In this case, ramification provides some extra information regarding the structural properties of a fractal. Ramification characterizes the branching as well as the connectivity between different parts inside the fractal structure. Order of ramification at a certain point O is defined as the minimum number of points or bonds or significant interactions[6] that must be cut to isolate a certain small part of an arbitrary fractal. Fractal objects, whose internal neighbouring gaps meet at certain points, are finitely ramified and their order of ramification varies from a fixed maximum (T_{max}) to a minimum (T_{min}) value[6]. This is explained in figure-2.3 using the Sierpinski gasket. In this case, two circles **ABC** and **ABCD** are drawn in two different parts of the 3rd stage

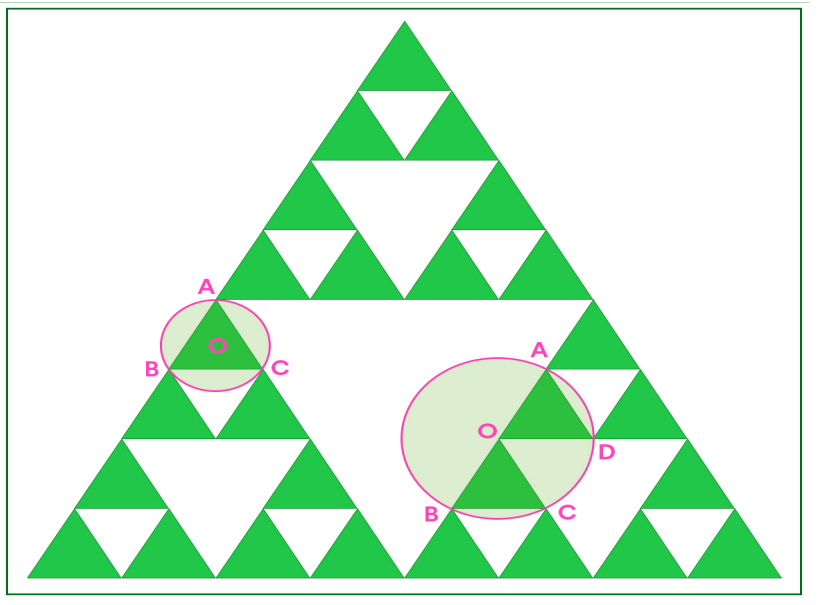

Figure 2.3: *Schematic diagram of a* 3rd *stage Siesrpenski Gasket fractal which is showing the calculation of ramification in two different sites.*

SG fractal taking O as their centre (not common). In the first case, minimum 3 (T_{min}) points[6] i.e. A, B, and C points are required to separate the said portion (ABC) of the SG covered by the smaller circle with centre O and maximum 4 (T_{max}) points i.e. A, B, C, D are needed to isolate a certain portion from SG surrounded by the bigger circle with centre at O as shown in the figure-2.3. These two values remain invariant with the increase of the fractal stage. Hence, the Sierpinski gasket is known as a finitely ramified fractal.

On the other hand Sierpinski carpet (SC), shown in figure-2.4, have a very different structure. Here the neighboring gaps don't meet at any arbitrary point. Therefore, if someone need to cut an arbitrary portion of the said fractal, he or she has to cut at a line segment instead of points. This can be clearly understood in figure-2.3 we have considered a certain portion **ABCD** of SC. In this case i.e. in figure-2.4, we need a line segment to cut this portion **ABCD** of SC. This line segment gets interrupted and the number of cuts increases with the increase of the fractal stage. Therefore, an infinite number of cuts will be required mathematically after infinite numbers of iteration. Thus Sierpinski carpet is infinitely ramified fractal. Urysohn proves that the relation between the maximum (T_{max}) and the minimum (T_{min}) value of the order of ramification of a finitely ramified fractal will be $(T_{max}) \geq [2(T_{min}) - 2]$. For a homogeneous system, the condition is $(T_{max}) = (T_{min})$. According to Mandelbrot[6] a system will be said to be quasi-homogeneous if the inequality sign will be removed and the equation becomes $(T_{max}) = [2.Tmin - 2]$. The ramification is

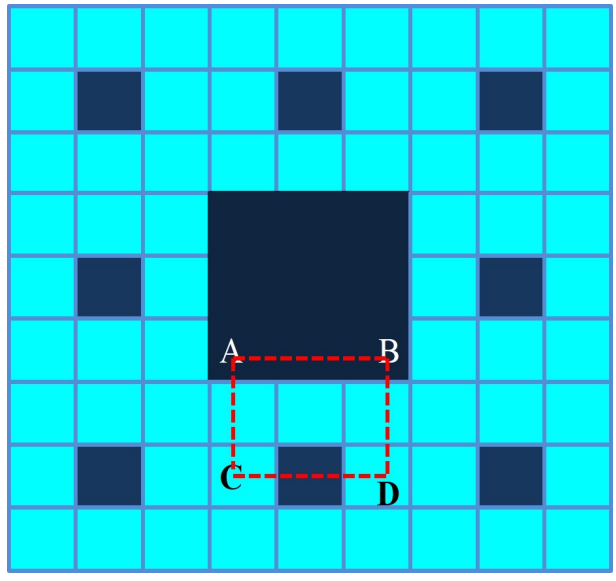

Figure 2.4: *Schematic diagram of Sierpinski Carpet as an infinitely ramified fractal. The line segments AB, BD, DC, and CA are used to separate an arbitrary part ABDC of the fractal which indicates that Sierpinski Carpet is an infinitely ramified fractal .*

an important parameter which helps us to study the anomalous diffusion as well as some mechanical properties of fractal objects.

2.2.5. Fractals, with and without loop

The characterization of fractals can also be accomplished based on the existence or absence of loops inside the pattern. A large class of fractals can be found that are characterized by the absence of loops whose end parts are either open or closed. If any two arbitrary points inside a fractal can be joined with a unique path without any alternative connectivity, it will be called loop less fractal. It can be observed frequently that fractals having the same fractal dimension may pose very different structural patterns due to the presence or absence of loops. figure-2.5 is very relevant in this context where a Sierpinski gasket and a Sierpinski tree have been shown. Both of them have the same fractal dimension but the second one is a loopless fractal unlike the first. Study of different transportational properties happens to be much easier in the case of loop-less fractals as diffusion and chemical exponents of these types of fractals are related with some exact relation[10]. Study of different structural properties also becomes easier in case of loopless fractals[10]. Many physical systems can be modeled by neglecting the loops due to their structural simplicity. Linear polymer chains configured by self-avoiding walk are the simplest kind among them[11]. Other systems like

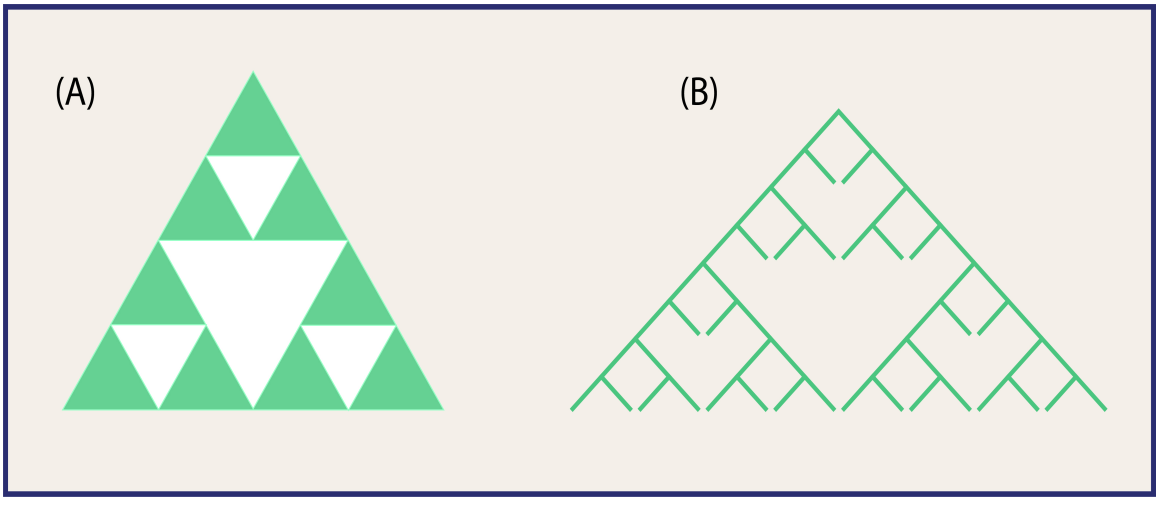

Figure 2.5: *Schematic diagram of (A)Sierpinski Gasket and (B)Sierpinski Tree. Interestingly both of them have the same fractal dimension but their patterns are different. The first one is a looped fractal whereas the second one is loop-less.*

percolation on the Cayley tree[10], branched polymers configured by lattice animals[12,13], different aggregates that are modeled by DLA[14,15] are very relevant examples of loopless structures. All of these systems must possess a backbone-like structure which is specified uniquely to study different transport properties[10] Vicsek fractal which is finitely ramified is also a loopless fractal, unlike the Sierpinski Gasket.

2.3. Classification of Fractals

As discussed before, the foundation of the fractal concept lies in some fundamental properties. Self-similarity and scale invariance are significant among them. In the real world, disordered systems most often show fractal-like behavior where the concept of self-similarity and scale invariance behavior is maintained in a statistical sense.[8]. Fractals can be classified into different categories based on their different properties. Here we are going to discuss two important types of fractals.

2.3.1. Deterministic Fractals

Deterministic fractals are an idealized mathematical concept where all the fundamental properties like self-similarity, scale invariance, dilatational symmetry, etc. are maintained

perfectly. Generation of the deterministic fractal is accomplished by some rigorous mathematical processes. It generally starts with a genus (unit cell) of definite size say (m) which is called initiator[9]. A set of operations are performed recursively in such a way that this process is continued till $n \to \infty$ number of iteration to achieve the required pattern. This set of operations is known as generator[9]. Deterministic fractals can be obtained by two different types of iterative operations.

In the case of growing mathematical fractals, one can start with an initiator which has a finite linear size m. Therefore the 1st stage (k=1) fractal pattern has been constructed by arranging n number of initiators in a definite pattern such that the resulting configuration has the linear size r= x.m where $x > 1$. In the next stage i.e. second stage, the arrangement of the initiators remains the same, only each initiator of the first stage is replaced by the entire 1st stage configuration itself. Therefore, total number of initiators in 2nd stage will be n^2 with linear size $x^2.m$. The same iterative process is followed to construct the higher-stage fractal pattern. Thus, k^{th} stage fractal pattern is achieved by replacing each particle of the first stage pattern with the entire $(k-1)^{th}$ stage fractal itself. Therefore , the linear size of the fractal pattern in it's k^{th} stage will be $r = x^k.m$ and the number of seeds (particle) will be $N(r) = n^k$[8]. This process will continue in a limit of infinite iteration ($i \longrightarrow \infty$) and generate a perfect deterministic mathematical fractal. The final fractal pattern has a lower cut-off length but doesn't have any upper limit in size. The fractal dimension can be written as[8]:

$$d_f = \frac{ln(N(r))}{ln(r)} = \frac{ln(n)}{ln(x)} \tag{2.8}$$

An alternative approach for the construction of a deterministic fractal can be performed by the subsequent division method which has been mentioned earlier. In this process, the resulting fractal pattern has a definite upper cutoff length. But the size of the unit cell (seed) or the initiator keeps changing with the change in the fractal stage. Initially, n numbers of unit cells arrange themselves in a definite pattern to form the 1st stage of the said fractal. Let us consider the linear size of the 1st stage fractal is L and the size of the unit cell is (1/x) times of the original fractal length L. The nature of the said fractal pattern remains the same in the 2nd stage. But every particle of the 2nd stage has been replaced by the $(1/x)$ times reduced version of the 1st stage pattern. Therefore, the linear size of the seed or initiator in 2nd stage is reduced by a factor of $(1/x)^2$ of its initial length L, and the number of seeds, in this case, becomes n^2[8]. The infinite iteration of this process yields the perfect deterministic fractal generated by the subsequent division method. The determination of the fractal

dimension yields the same mathematical expression as mentioned before. The generation of deterministic fractal in both the growing method as well as in the subsequent division method has been shown in figure-2.2. Here both of these two methods have been applied to Sierpinski Gasket (SG). Some well known deterministic fractals and their characteristics have been discussed below:

2.3.1.1. Cantor Set

In 1883 German mathematician Georg Cantor introduced the concept of Cantor set. It is probably the simplest example of a perfectly self-similar, loopless deterministic fractal which consists of disconnected line segments embedded in 1-D space. Figure-2.6 represents a schematic diagram of a Cantor set. The construction of the Cantor set starts with a line

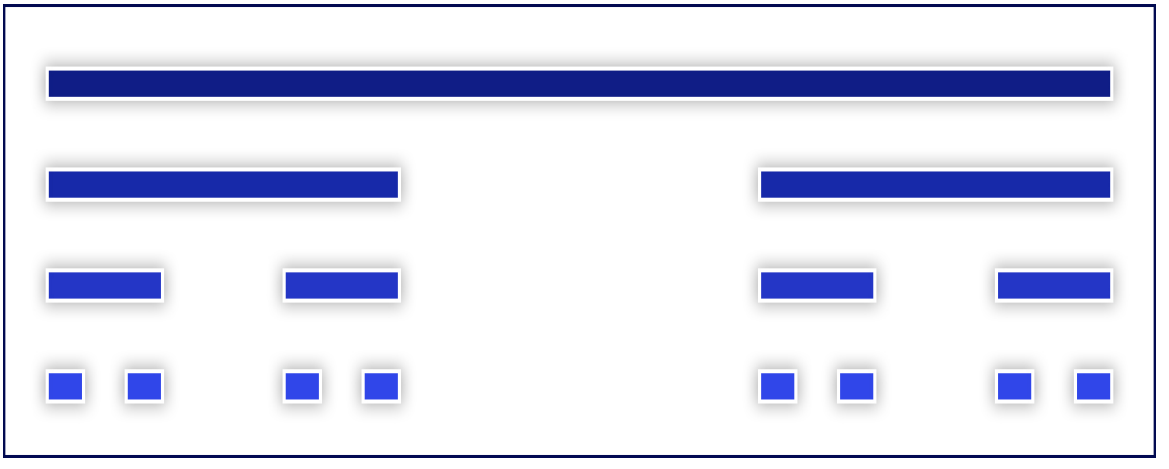

Figure 2.6: *Schematic diagram of Cantor bar of* $0^{th}, 1^{st}, 2^{nd}, 3^{rd}$ *stages respectively*

segment of unit length with the interval [0,1]. In the 1st stage, the line segment is subdivided into three equal parts each of which has length 1/3, and the middle part is removed. The same process is applied on each existing line segment of the 1st stage to get the 2nd stage of Cantor set as shown in figure-2.6. This procedure is applied iteratively to construct the higher stages and the final pattern is achieved after infinite iteration of this generator. The fractal dimension of the cantor set considering the 1st stage pattern, is:

$$d_f = \frac{ln(n)}{ln(x)} = \frac{ln(2)}{ln(3)} = 0.6309 \tag{2.9}$$

It is noteworthy that the fractal dimension of the Cantor set is a non-integer number and less than 1. Cantor set is very much useful to simulate the signal pulse and other physical properties.

2.3.1.2. Koch Curve

Helge von Koch, a Swedish mathematician gave the idea of the Koch curve in 1904. It is a non-linear, perfectly self-similar, and finitely ramified[6] curve that is continuous at every point but differentiable nowhere. Figure-2.7 represents some initial stages of the Koch curve. Initially one can start with a unit line segment of an interval [0,1] same as Cantor Set in stage 0. In the 1st stage, the line segment is divided into three equal parts of length 1/3 and the middle part is replaced with an equilateral triangle and its base is removed. The triangle is headed upward and the length of its two sides are 1/3 as shown in figure-2.7. In the next stage, each line segment (initiator) of the 1st stage pattern is replaced by the (1/3) times reduced version of the 1st stage fractal itself as shown in figure-2.7. This process is carried out indefinitely in a recursive manner so that we get the final form of this fractal. The

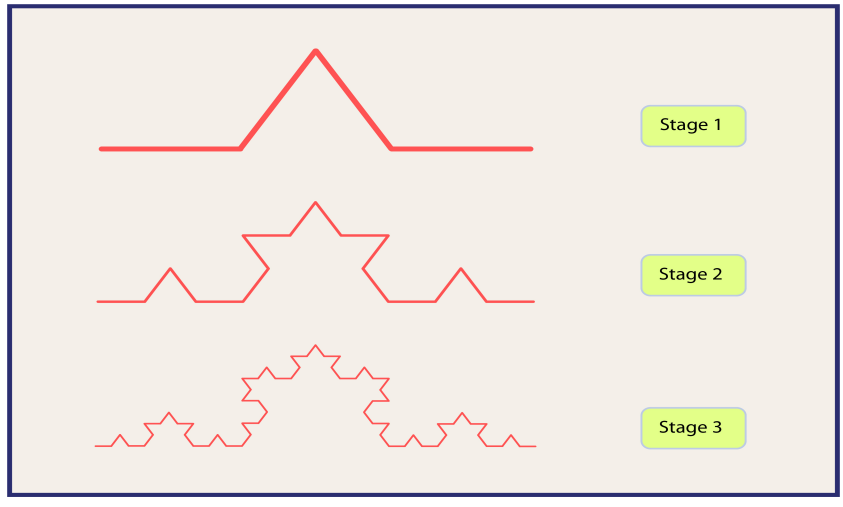

Figure 2.7: *Schematic diagram of Coch Curve of* $1^{st}, 2^{nd}, 3^{rd}$ *stages respectively*

limiting structure is infinitely fragmented with infinite length but limited in a finite region. Its dimension can be calculated easily in similar fashion of cantor set. Let us consider the 1st stage Koch curve. The number of line segments, used to construct the 1st stage is n= 4 and the length of the fractal in the unit of seed length is x= 3. Hence the fractal dimension, according to the equation-(2.8) is :

$$d_f = \frac{ln[N(x)]}{ln(x)} = \frac{ln(n)}{ln(x)} = \frac{ln(4)}{ln(3)} = 1.262 \tag{2.10}$$

2.3.1.3. Sierpinski Gasket

Polish mathematician Waclaw Sierpinski introduced this fractal in 1916. It is another well-known deterministic fractal which is finitely ramified[6] with loops. Its construction begins with a solid equilateral triangle which is considered as the initiator of the fractal. The generation of the first three consecutive stages of Sierpinski Gasket (SG) by subsequent division method has been shown in the figure-2.8. Initially, this triangle is subdivided into four equilateral triangles of the same size and the middle one is removed which results in the 1st stage fractal pattern. In the case of the 2nd stage, each unit cell (solid triangle) of the 1st stage is replaced by the 1st stage SG fractal pattern itself whose length scale is reduced by a factor of 1/2. The same process has been followed to generate the 3rd stage SG pattern as shown in the figure-2.8. Therefore the final SG fractal pattern can be achieved after the infinite iterations. The fractal dimension can be evaluated readily with the help of equation-(2.8). The dimension of the Sierpinski gasket can be calculated as follows: We

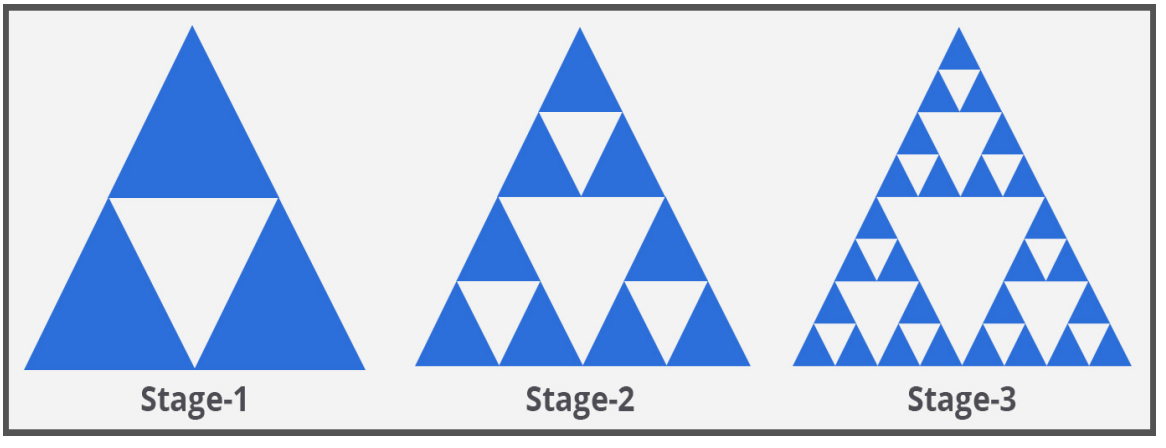

Figure 2.8: *Schematic diagram of Sierpinski Gasket of* $1^{st}, 2^{nd}, 3^{rd}$ *stages respectively*

consider the 2nd stage fractal pattern. Total number of unit cells (solid triangles) are N(r) = 9. The length of the 2nd stage fractal in the unit cell length scale is r = 4.

$$d_f = \frac{ln(N(r)}{ln(r)} = \frac{ln(9)}{ln(4)} = \frac{ln(3)}{ln(2)} = 1.585 \tag{2.11}$$

2.3.1.4. Vicsek Frractal

Thomas Vicsek gave the idea of this deterministic fractal. It is a perfectly self-similar fractal whose initiator may be square, circle, or any other type of geometrical shape. figure-2.1 represents a schematic diagram of the Vicsek fractal of the first three steps. The initiator

is taken as a square in the present case. Let us consider the length of each initiator of 1st stage is unity. Thus the 1st stage of Vicsek fractal is constructed by five unit cells i.e. N(r) = 5 and its length is r = 3 in the unit cell length scale. Therefore the fractal dimension of Vicsek fractal is:

$$d_f = \frac{ln[N(r)]}{ln(r)} = \frac{ln(n)}{ln(x)} = \frac{ln(5)}{ln(3)} = 1.465 \tag{2.12}$$

Vicsek fractal is perfectly deterministic and finitely ramified in nature but unlike the SG, it is loop-less. Hence there exists an exact relationship between the diffusion exponent (d_w) and fractal dimension (d_f) as: $d_w = 1 + d_f$. In case of Vicsek fractal d_f is calculated exactly as 1.465. Hence the value of d_w can be estimated as: $d_w = 1 + d_f = 2.465$. In our whole simulation study, we have used Vicsek Fractal as a mathematical tool to construct host solid polymer sample.

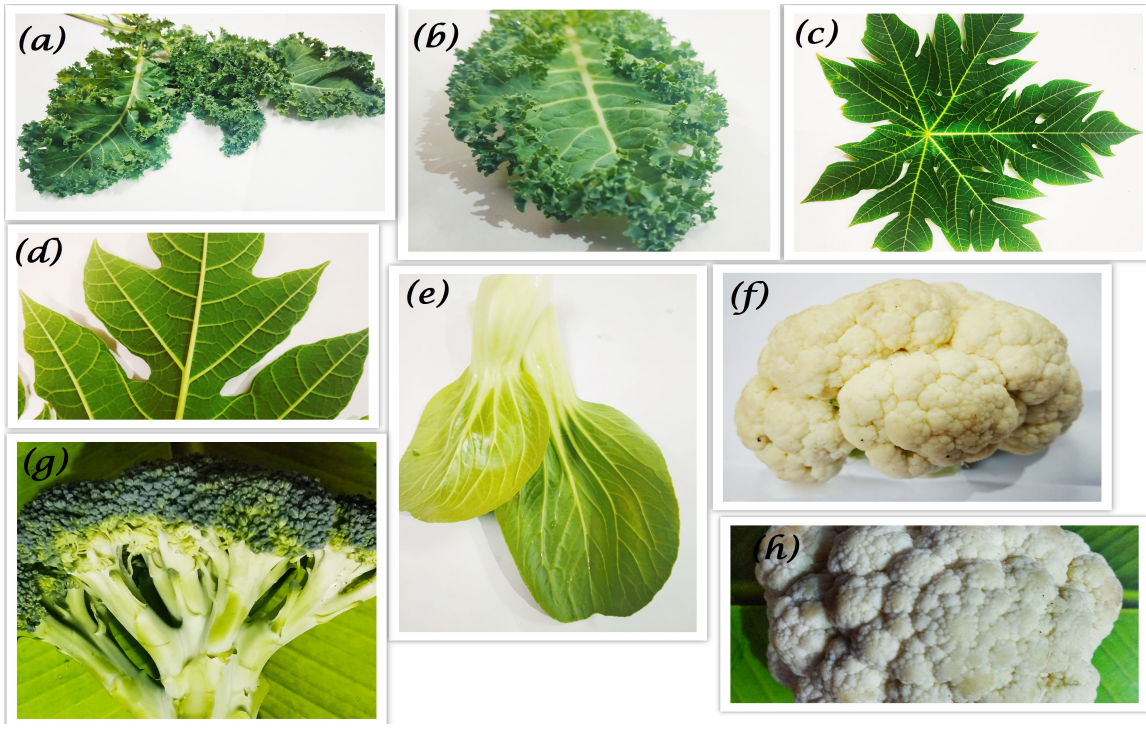

Figure 2.9: *Different types of random fractals, found in nature. 1. (a) and (b) leaf of Curled Kale (**Brassica oleracea var.sabellica**) . Fractal like fragmented pattern can be seen at the edges of the leafs. 2. (c) and (d) veins of Papaya leaf (**Carica papaya**) and (e) Pak Choi veins (**Brassica rapa chinensis**) shows natural fractal like pattern. 3. (g) fractal like pattern of different branches of Broccoli (**Brassica oleracea var.italica**). 4. (f) and (h) fractal pattern of Cauliflower (**Brassica oleracea var.botrytis**) surface.*

2.3.2. Random Fractal

Many natural objects show fractal-like behavior but hardly follow the strict deterministic rule as observed in deterministic fractals. The structural analysis of these types of objects can be done with the help of random fractals. Random fractals are such kinds of fractal objects where the self-similarity property can be applied in a statistical sense. Unlike the deterministic fractals, the magnified view of an arbitrary portion of the entire fractal pattern resembles the whole pattern not exactly but in an average manner. Hence the distribution of "holes" and embedding mass of the said fractals is very different from that of deterministic fractals. Random fractals can be homogeneous or heterogeneous depending on the distribution of mass on every hierarchical level[16]. Due to their statistical self-similarity, the dimension of a random fractal can not be measured directly from equation-(2.8) rather different theoretical techniques[10] are applied. structure of many natural objects like sedimentary rocks, colloidal aggregates, aerogels, the trail of random walk, etc. are examples of random fractal as their structural phenomenon are very much analogus to the natural objects. Some natural objects showing fractal like behaviour has been presented in figure-2.9.

2.4. Fractal Like Behavior of Host Polymer Sample: A Short Review

The different structural properties of long flexible chains of polymer samples were extensively studied by de Gennes 1979, Flory 1971. They mentioned the use of different techniques like neutron diffraction, inelastic scattering of laser light, for a more detailed structural study of the polymer sample. In addition, to that, some theoretical methods like exact summation on short chains, Monte Carlo simulations are used to analyze the statistical properties of polymer chains.[17]. S Havlin and D Ben-Avraham[18] performed a numerical study about the fractal dimensionality of long single polymer chains that are traced out by the self-avoiding walk method on a plane lattice and found that the local fractal dimension (LFD) represents the winding of polymer chains under any length scale. for a system with a large size the fractal dimension (FD) remains unchanged irrespective of any length scale and represents the self-similarity property nature of the polymer chain.

M. E. Cates[19] deal with a class of flexible polymers like gelation clusters, branched polymers, or any flexible types of fractal aggregates with fractal connectivity at a short length scale. They have characterized some preliminary dynamical results such as the

viscoelasticity of a solution of that polymeric fractal. and discuss their statics and dynamics in a single framework. The use of anomalous spectral or fracton dimension proved to be very useful to describe the static partition function and dynamical properties of a fractal. The excluded-volume problem is discussed at the Flory level.

M. Muthukumar and H. Henning Winter[20,24] studied the fractal dimension of cross-linking polymer at gel point and proposed a theory on the basis of frequency dependence of the complex viscosity where the fractal dimension of any molecular cluster has been considered as the main parameter. They also compare the theory with the experimental observation which shows a good agreement.

B.W'asserman[21] have delivered some experimental results with different techniques that provide knowledge regarding the mechanism of electrical conductivity and spin diffusion in ion-implanted polymers with the help of fractal formalism. He measures critical exponent for electrical conductivity versus fluence range from 4 to 5. Similarly, the fractal exponent of dielectric relaxation has been measured ranging from 0.22 to 0.85. Also, a rapid increase of the real part of the dielectric constant has been seen at the low-frequency range.

The structural characterization of different random and complex system like condensation polymer[22] , cross-linked poly(dimethylsiloxane)[23,24], diffusion-limited polymerization of the conducting polymer polypyrrole[25] has been done previously with the concept of fractal objects. Benjamin Chu,Chi Wu, and Dan-qing Wu[26] use the small-angle X-ray scattering (SAXS) method to determine the fractal dimension and study the epoxy polymer structure. It was also turned out to be very useful to investigate the change in epoxy structure beyond the gelation threshold.

The segmental motion of the polymer chains in their glassy state can be described with the concept of a hole or free volume which don't have fractal or Hausdorff dimension. T. S. Chow[27] studied the spatial as well as the temporal dependent hole density-density correlation function and produce a fractal dimension that does not depend on any spatial structure. The self-similar connectivity of hole motion and the hole density of state spectra has been analyzed with this intrinsic parameter.

Sapoval et. al.[28–30] have studied the diffusion at the interface of two same or different types of polymer materials. He addressed the borderline between the connected and the non-connected regions of the diffusion field as "diffusion front" and showed that it has a fractal-like behavior. They had also developed a convenient method to characterize

the roughness of the interface. Richard P.Wool et. al.[31] have studied the fractal structure of the polymer-polymer interface following the method proposed by Sapoval et. al. In that case they have used gradient percolation concept to characterize the ramified as well as the fractal-like nature of that interface. A diffuse interface has been produced by metallization of polymer substrate and welding of amorphous polymer interface where the silver-polyimide interface has been used. They found that the random nature of diffusion at higher dimensions produces a complex fractal-like structure and they also investigate different properties and structures of the interface.

Amita Chandra et.al.[5] did some experiments and observed the formation of large size fractals in ion conduction polymer electrolyte films. They have chosen $PEO : NH_4I$ film of different compositions which were prepared under the solution casting method. It was observed that diffusion-limited fractal aggregates of large size (2-3cm) have been formed due to the random motion of the ions in the PEO salt complex.

Mohammed Dahmani and his fellows[33] prepared a homogeneous solution of PVC aggregates at $150°C$ and quenched at room temperature. The viscometry and static light scattering measurements from a laser source have been carried out and the modulus concentration relation was determined. They have used the theory developed by Jones and Marques[32]. A longitudinal fractal dimension ($D_f = 1.5 \pm 0.1$) of the PVC fibers has been determined from the light scattering which happens to be independent of the solvent type.

Deepak Dhar has performed[34] a theoretical study regarding the number of the different possible structures of an n-bond branched polymer. He used the Mandelbrot family of fractal whose different members has been characterized by an integer b where $2 \leqslant b \leqslant \infty$ and follow the exact real-space renormalization group technique. The fractal dimension changes from $log_2 3$ to 2 as b is varied from 2 to ∞. The no. of a possible configuration of branched polymer of n-bonds was expressed by a parameter $< A_n >$. He established that $< A_n >$ varies as $\lambda^n exp(bn^{\psi})$ for all values of $b \geq 3$. Where λ and b are constants and $0 < \psi < 1$. The numerical value of ψ and size exponent γ has been calculated exactly.

Shahizat Amir et. al.[35] investigate the fractal natures of the polymer electrolyte membranes. They used a mathematical model for simulation of growth patterns and the stages of the fractals which is based on Brownian motion theory. This simulation investigates the fractal growth pattern successfully and evaluates the fractal dimension which is in agreement with the dimension of the real polymer electrolyte membranes.

Nan Li et.al.[36] worked with amphiphilic random azo copolymer (PPAPE). Initially,

they prepared colloidal spheres with hydrophobic cores due to the hydrophobic aggregation of PPAPE in H_2O/THF medium. After that, an aqueous solution of NaOH (0.2 M) has been added into the weakly acidic dispersion of the colloidal spheres. The fractal structure of the aggregates was thoroughly analyzed by TEM, SEM, SLS, and DLS. The results show that the morphology, as well as the fractal dimension (D_f) of the colloidal fractal aggregates, can be changed by adjusting the pH level of the dispersion from 8.2 to 11.7. The respective fractal dimension varies from 1.68 ± 0.03 up to 2.24 ± 0.02 . The experimental observation confirms a well-arranged fractal structure achieved at high pH dispersion and they are generated by the aggregation of partially dissociated colloidal spheres.

Jinhua Sun and his fellow workers[37] found a technique to prepare the fractal-like structure of thermocleavable polythiophene (TCPT). Initially dry and solid thermocleavable polythiophene films were taken and the solvent vapour annealing (SVA) method was used to prepare the fractal-like structure of insoluble polythiophene under the influence of high humidity and thermal curing. The morphological changes of the sample were investigated through the Atomic force microscope and transmission electron microscope. It was observed that the generation of fractal-like structures was highly influenced by the humidity of the surroundings. The holes are formed at the initial stage of SVA method, after that fractal-like structures of the order of micron scale were seen. The nature of crystallinity can also be improved following this technique. The fractal-like structure can be preserved by the application of proper thermal curing.

Trystan Domenech et. al[38] performed a detailed study regarding the structural properties of organoclay dispersion in polypropylene/OMMT nanocomposites with the help of shear rheology. They focused on the fractal-like structure generated by the partially flaked platelets within the nanocomposites. They also studied how the long-time aging nature of the nanocomposite influences the development of a fractal network formed by the clay particles within the matrix. The fractal dimension Df of the network was calculated on the basis of linear viscoelastic properties based on apparent yield stress and critical strain measurements. Generation kinetics of the fractal-like network structure at rest has been analyzed with the help of linear and nonlinear rheological investigations.

Xiang Li and his co-workers[39] mixed two different types of tetra armed polyethylene glycol (PEG) containing complementary end groups and produce a series of critical polymer clusters. The structural properties were investigated by small-angle neutron scattering at different dilution levels. The nature of the scattering has been studied on the basis of scattering vector (q), volume fraction (ϕ), correlation length (ξ). For $q < \xi - 1$, the scaling

laws were observed for semi dilute polymer clusters and the cluster size distribution gave a significant impact on the scattering intensity in the range $q < \xi - 1$. The scaling law between (ξ) vs (ϕ) and A vs (ϕ) helped to estimate the fractal dimension (D_s) of the dilute polymer chains as (D_s) = 2.0 $\pm$0.1 and it was found that the value of Ds is unique and does not depends on the preparation condition of the polymer cluster.

Suyong Shin et. al.[40] was successful in one shot preparation of polymer fractal nanostructure in solution from PTD-b-PPV BCPs. They apply polymerization and self-assembly kinetics and invent a simple one-shot ring-opening metathesis polymerization (ROMP) technique to produce polymer fractal nanostructure. Some external parameters like reaction concentration, presence of an additive, etc. influence the structural properties of the sample significantly. The generation of fractal structures in solution was confirmed by different imaging techniques like atomic force microscopy, transmission electron microscopy (TEM), and cryogenic TEM. They also concluded that the uncontrolled polymerization kinetics was the main reason for the formation of fractal branches.

2.5. Theory of Diffusion

Diffusion is a process of mass transport due to the motion of a particle under the influence of concentration gradient or thermal energy. It is a very common phenomenon inside liquid or gas but sometimes it can be observed inside solid also. It originates due to the random motion of the atoms or molecules inside the medium. A drop of ink spreads all over the liquid or a wisp of smoke diffuses uniformly all around the room happens to be a very common example of diffusion. Examples of diffusion inside solids are also abundant in nature e.g. annealing of metals and alloys, absorption of gases inside a solid, etc. Besides this, there is a special case where particles diffuse among the same species. This phenomenon is known as self-diffusion which can be studied by labeling both stable and radioactive isotopes with the diffusing particles or using the NMR techniques[41] Different types of diffusion can be observed in nature. Sometimes the diffusion process can be characterized by the microscopic point of view considering the random motion of the diffusing particles inside the medium. This is known as tracer diffusion. Diffusion that takes place in the presence of concentration or any chemical potential gradient as mentioned before is known as mass diffusion and it can be explained quantitatively with the help of Fick's law. The two types of diffusion theories are associated with two different diffusion coefficients.

2.5.1. Fick's First and Second Law of Diffusion

The quantitative analysis of collective mass diffusion from the macroscopic point of view was done by Adolf Fick in 1855. He proposed that the mass density flux (J) is directly proportional to the negative concentration gradient of the medium. The relation for the isotropic medium can be expressed mathematically in one dimension as:[42,43].

$$J_z = -D\frac{\delta C(z,t)}{\delta z} \tag{2.13}$$

Where C(z,t) is the concentration of the diffusing particles at the point z at time t. J_z represents the diffusion flux along Z-direction. The negative sign indicates that the particles diffuse along a direction opposite to the concentration gradient. In the case of a d-dimensional system, this equation can be written as:

$$J = -D\nabla_d C \tag{2.14}$$

In both cases, D represents a constant of proportionality which is known as diffusivity of the medium and considered as a scalar quantity. It is an intrinsic property of the medium and is generally assumed to be independent of position and time. Equation (2.13) and (2.14) are known as Fick's first law for 1-dimension and d-dimension respectively and applicable when the system is in a steady state. Fick proposed another mathematical relation by combining the 1st law and the equation of continuity which is known as Fick's second law and can be expressed in one dimension as:

$$\frac{\delta C}{\delta t} = \frac{\delta}{\delta z}\left(D\frac{\delta C}{\delta z}\right) \tag{2.15}$$

Fick's second law in d-dimensional system can be expressed as :

$$\frac{\delta C}{\delta t} = \nabla_d \left(D\nabla_d C\right) \tag{2.16}$$

In the case of a homogeneous medium, the parameter D becomes constant. In that case, Fick's second law turns out to be the well-known diffusion equation:

$$\frac{\delta C}{\delta t} = D.\nabla_d^2 \left(C\right) \tag{2.17}$$

Equation (2.15) and (2.16) both are second order linear partial differential equation.Assuming the initial condition as $C(z,0) = N\delta(z)$ and $C(r,0) = N\delta(r)$, the solution of these equations

will be:

$$C(z,t) = \frac{N}{\sqrt{4\pi Dt}} \exp -\frac{z^2}{4Dt} \qquad for \;\; 1-dimension \tag{2.18}$$

$$C(r,t) = \frac{N}{(4\pi Dt)^{d/2}} \exp -\frac{r^2}{4Dt} \quad for \;\; d-dimension, \;\; here \;\; N = \int C(r,t)dr \tag{2.19}$$

This equation represents the concentration of the diffusing particles C(z,t) or C(r,t) that can be found at the position z or r at time t when N number of particles initially participate in the diffusion process.

However, there are many cases where the diffusivity will not be constant with time. These cases will be discussed in later sections.

2.6. Normal Diffusion

An extensive study of diffusion from the microscopic point of view can be done with the help of a random walk theory. In that case, prime importance is given to evaluate the probability distribution function (PDF) $P(r,t)$ of the final position of the random walker concerned. If the d-dimensional step length (A) of the random walker is considered as an independent identically distributed random variable and the random displacement vector R has finite first and second moment i.e. the average values of the variables R and R^2 are finite ($i.e. \langle R \rangle \neq \infty$ and $\langle R^2 \rangle \neq \infty$), then the PDF P(R,t) shows a Gaussian-like behaviour[9] provided the number of such random steps are very large ($N \to \infty$). This phenomenon is familiar to the solution of the diffusion equation mentioned in the previous section. It can be mathematically verified that the probability distribution function (PDF) $P(r,t)$ of the position of the random walker can be considered as the generalization of the d-dimensional central limit theorem and the mean square displacement $\langle R^2 \rangle$ varies linearly with time t i.e. $\langle R^2 \rangle \sim t$. This behavior confirms that diffusion is normal. The trajectories of tracer particles that experience normal diffusion are irregular and can be represented by small discrete steps. If we study the square root scaling of the width of the PDF P(R,t),we found it grows as[44] $R \sim (\langle R^2 \rangle N)^{1/2}$. Normal diffusion plays significant role on many physical systems like dusty plasma[46] nuclear physics[47], different natural systems with various phases[45] etc.

2.6.1. Theory of Random Walk

Let us consider the simplest case where a walker is performing a simple random walk in a d-dimensional lattice with lattice spacing (A). At every consecutive step, the walker moves to one of its accessible nearest neighboring sites with equal probability. Every step of the walker is independent of its previous step and thus the process is Markovian by nature. The total displacement of the walker after N such consecutive steps are:

$$R(N) = \sum_{j=1}^{N} A_j \tag{2.20}$$

Where A_j indicates the unit translational vector at j^{th} step in d-dimensional lattice which satisfy the condition $\langle A_i.A_j\rangle = \delta_{ij}$. Since the process is completely random, we can write: $\langle R(N)\rangle = 0$. Under this condition the mean square displacement can be expressed as:

$$\begin{aligned} \langle R^2(N)\rangle &= \langle (\sum_j A_j)^2\rangle = N.A^2 + \sum_{j\neq i}\langle A_i.A_j\rangle \\ &= N.A^2 \\ \Rightarrow \langle R^2(N)\rangle &\sim N \end{aligned} \tag{2.21}$$

In the case of a simple random walk, the step time (τ) is assumed to be uniform. Hence The total time of the walk will be $t = N.\tau$. Therefore we can write:

$$\langle R^2(N)\rangle = \langle R^2(t)\rangle = (2d).Dt \tag{2.22}$$

Where $D = A^2/2d.\tau$ is known as diffusion constant. A convenient way to study the simple random walk is to estimate the probability of the walker to find at a distance r at a time t after N consecutive steps so that we can study different physical parameters stochastically[9, 48, 49]. Let us consider that the random walk process is performed in R^d dimension in continuous space and $p(r')_{q,s}$ is the probability of the walker to move from q^{th} site(at a distance r' from origin) to s^{th} site(at a distance r from origin). The essential conditions to be satisfied by the walker will be:

$i\rangle$. $p(r')_{q,s} = \frac{1}{2d}$ when q and s are nearest neighbour and
$= 0$ otherwise

$ii\rangle$. $\int_s p(r')_{q,s} d^d r' = 1$

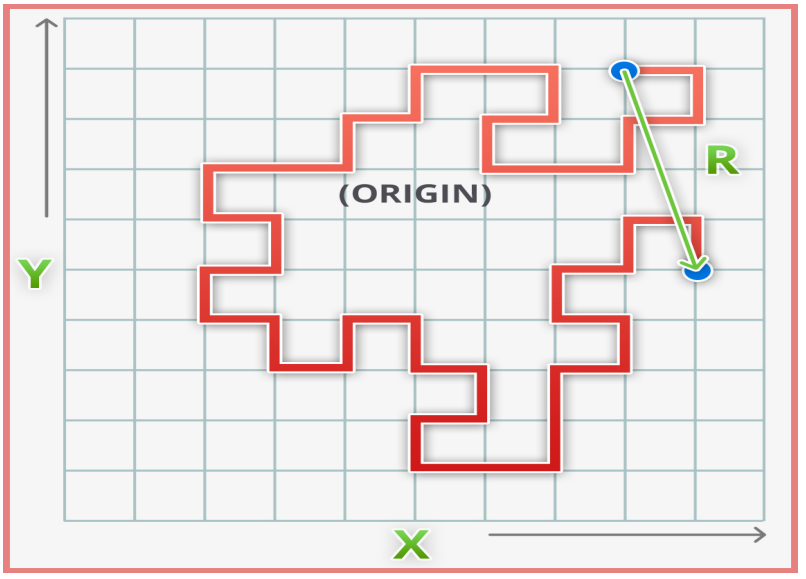

Figure 2.10: *A schematic diagram of simple random walk. The net displacement of the walker from the initial point to final point is mentioned by the arrow mark.*

Taking the Fourier transformation of $p(r^{'})_{q,s}$ we obtain the structure function in k space as:

$$\Lambda(k) = \int p(r^{'})_{q,s} \exp(ik.r^{'}) d^d r^{'} \tag{2.23}$$

We assume that each step of the walker is independent of its previous step. Hence the probability of finding the walker at a distance (R) after (N) consecutive steps is:

$$P_N(R) = \int P_{N-1}(r^{'}) p(R - r^{'})_{q,s} d^d r^{'} \tag{2.24}$$

The characteristic function of $P_N\,(r)$ will be:

$$\begin{aligned} \Gamma_N(k) &= \int P_N(R) \exp(ik.R) d^d R \\ &= \int (\int P_{(N-1)}(r^{'}).p(R - r^{'})_{q,s} d^d r^{'}) \exp(ik.R) d^d R \\ \Gamma_N(k) &= \Gamma_{N-1}(k).\Lambda(k) \end{aligned} \tag{2.25}$$

This recursive relation holds for any value of N. Hence we can write:

$$\Gamma_N(k) = [\Lambda(k)]^N \tag{2.26}$$

Taking the inverse Fourier transformation we can write the probability distribution function $P_N(R)$ as:

$$P_N(R) = \frac{1}{(2\pi)^d}\int \Gamma_N(k).\exp(-ik.R)d^dk = \frac{1}{(2\pi)^d}\int [\Lambda(k)]^N \exp(-ik.R)d^dk \tag{2.27}$$

Let us consider a 1D system where the step probability function $p\left(x^{'}\right)_{q,s}$ gives finite variance and zero mean i.e.

$$\int x^{'}.p\left(x^{'}\right)_{q,s}.dx^{'} = 0 \tag{2.28}$$

$$\int (x^{'})^2.p(r).dx^{'} = \sigma^2 < \infty \tag{2.29}$$

Therefore the structure function $\Lambda(k)$ can be simplified in 1-D as:

$$\Lambda(k) = \int p_{q,s}(x^{'})\exp(ik.x^{'})dx^{'} = 1 - \frac{k^2.\sigma^2}{2!} + O(k^2) \tag{2.30}$$

Thus the characteristic function for a large value of N can be written as[9]:

$$\Gamma_N(k) = \exp\left[-\frac{Nk^2.\sigma^2}{2!} + N.O(k^2)\right]$$

When the walk is executed for a very long time i.e. the walk steps are very large ($N \ggg 1$) we can neglect the higher-order terms i.e. the terms $N.O(k^2)$ can be neglected[9]. Therefore $\Gamma_N(k)$ can can be approximated to:

$$\Gamma_N(k) = \exp\left[-\frac{Nk^2.\sigma^2}{2!}\right] \tag{2.31}$$

Taking the inverse Fourier transformation we get the PDF as:

$$P_N(x) = \frac{1}{2\pi}\int \exp\left[-\frac{Nk^2.\sigma^2}{2!}\right].\exp(-ik.x)dk = \frac{1}{\sqrt{2\pi\sigma^2 N}}\exp\left[-\frac{x^2}{2\sigma^2 N}\right] \tag{2.32}$$

Including the temporal part, the $P_N(x)$ can be written as:

$$P_N(x,t) = \frac{1}{\sqrt{(4\pi Dt)}}\exp\left[-\frac{x^2}{4Dt}\right] \tag{2.33}$$

Where we have used the value of D mentioned earlier. In the case of d dimensional system the PDF $P_N(R,t)$ can be written as:

$$P_N(R,t) = \frac{1}{\sqrt{(4\pi Dt)^d}}\exp\left[-\frac{R^2}{4Dt}\right] \tag{2.34}$$

This analysis suggests, the probability distribution function shows a Gaussian-like behavior and can be considered as a generalization of the central limit theorem(CLT) under a long time asymptotic limit.

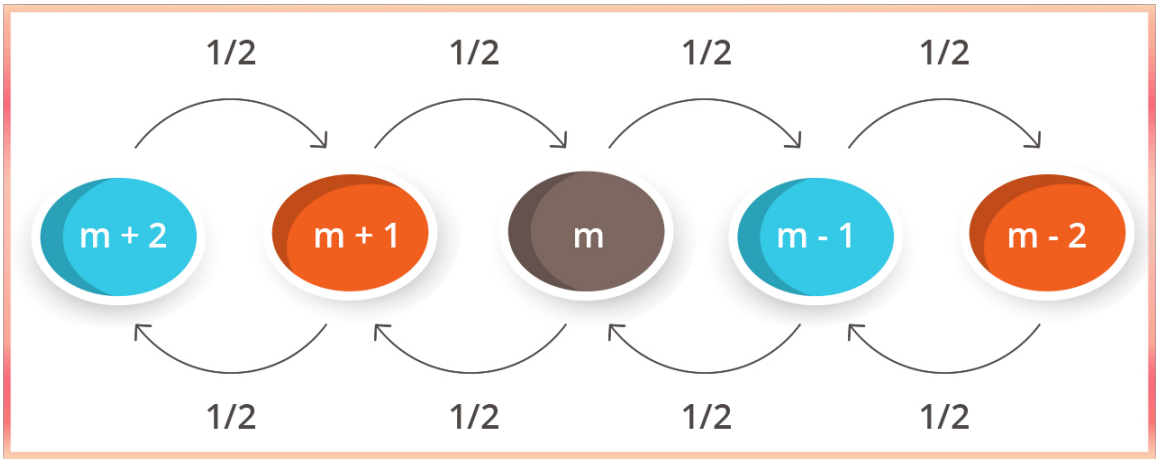

Figure 2.11: *A schematic diagram of random jump in 1-dimension. The walker start from the mth site and moves to the one of the either sites with equal probability.*

2.6.2. Random Walk in Continuous limit: Diffusion Equation and its Solution

The nature of random walk in discrete-time limits was discussed in the previous section. In this section, we will discuss the nature of the random walk in continuous space and time limits. Initially, we consider the one-dimensional random walk in discrete spatial and temporal cases. Here the walker hops on either side of its present position with equal probability $\frac{1}{2}$. Hence the probability that the walker will remain on the ith site after $(j+1)^{th}$ step will be:

$$\begin{aligned} P_{j+1}(i) &= \frac{1}{2}P_j(i-1) + \frac{1}{2}P_j(i+1) \\ or \quad P_{j+1}(i) - P_j(i) &= \frac{1}{2}P_j(i-1) - P_j(i) + \frac{1}{2}P_j(i+1) \end{aligned} \tag{2.35}$$

If the lattice spacing is (a) and step time is considered as τ then the total distance covered by the walker after i^{th} step can be expressed as (x=i.a) and total walk time t will be $(j.\tau)$. In the limit $a \to 0$ and $\tau \to 0$, we replace the term $P_j(i)$ by P(x,t) which eventually represents

the probability density function. Under this limit,equation (2.35) takes the form as:[50]:

$$P(x,t+\delta t) = \frac{1}{2}P(x-a,t) + \frac{1}{2}P(x+a,t)$$

$$\Rightarrow P(x,t+\delta t) = \frac{1}{2}\left[P(x,t) + (x-a-x)\frac{\delta P}{\delta x} + \frac{(x-a-x)^2}{2!}.\frac{\delta^2 P}{\delta x^2} + ...\right]$$

$$+ \frac{1}{2}\left[P(x,t) + (x+a-x)\frac{\delta P}{\delta x} + \frac{(x+a-x)^2}{2!}.\frac{\delta^2 P}{\delta x^2} + ...\right]$$

$$\Rightarrow P(x,t+\delta t) = \frac{1}{2}\left[P(x,t) - a\frac{\delta P}{\delta x} + \frac{a^2}{2}\frac{\delta^2 P}{\delta x^2} + ...\right]$$

$$+ \frac{1}{2}\left[P(x,t) + a\frac{\delta P}{\delta x} + \frac{a^2}{2}\frac{\delta^2 P}{\delta x^2} + ...\right] = P(x,t) + \frac{a^2}{2}.\frac{\delta^2 P}{\delta x^2}$$

$$\Rightarrow \frac{P(x,t+\delta t) - P(x,t)}{\delta t} = \frac{a^2}{2.\delta t}.\frac{\delta^2 P}{\delta x^2}$$

$$\Rightarrow \frac{\delta P}{\delta t} = D.\frac{\delta^2 P}{\delta x^2} \tag{2.36}$$

Equation- (2.36) is known as diffusion equation in 1-D. Where $D = \lim_{a,\delta t\to 0}\frac{a^2}{2.\delta t}$ is the diffusion coefficient of the medium. In this case, we have consider the term $(a^2/\tau) = 2D$ is constant. The initial conditions of 1-D diffusion equation-(2.36) is $:P(x,0) = \delta(x - x_0), P(x\to\infty,t) = 0, \frac{\delta P}{\delta t}\mid_{x\to\infty}= 0$. Different method can be applied to solve this equation though the final solution will be same. Applying the boundary conditions for one dimension system, one can get the resultant solution as:

$$P(x,t) = \frac{1}{\sqrt{4\pi Dt}}\exp\left[-\frac{(x-x_0)^2}{4Dt}\right] \tag{2.37}$$

The solution is the same as that we get in the case of the normal random walk approach. the probability distribution function (PDF), derived here is Gaussian in nature and hence the diffusion is normal.

2.6.3. Diffusion and Conductivity: Einstein's Relation

Simple random walk theory suggests that each step of the walker is completely random. Hence the walker can move in all directions with equal probability. As a result, the diffusion equation does not contain any term arising from the drift motion of the walker. Let us

consider a more generalized situation in a 1-D system, where the walker has an overall motion towards a particular direction say, along the right side. We assume the probability of the walker to step towards our right side is $(\frac{1}{2} + \Delta\phi)$ and towards our left is $(\frac{1}{2} - \Delta\phi)$. Where $\Delta\phi$ happens to be a positive number. The master equation for the evolution of occupation probability will be:

$$P(x, t + \Delta t) = (\frac{1}{2} + \Delta\phi)P(x - \Delta x, t) + (\frac{1}{2} - \Delta\phi)P(x + \Delta x, t) \tag{2.38}$$

Following the same procedure as we have adopted in the case of equation-(2.36), the final solution of the equation-(2.38) takes the form as[9]:

$$\frac{\delta P(x,t)}{\delta t} + V.\frac{\delta P(x,t)}{\delta x} - D.\frac{\delta^2 P}{\delta x^2} = 0 \tag{2.39}$$

This equation is known as convection diffusion equation[52] where $v = 2.\Delta\phi.\frac{(\Delta x)}{\Delta t}$. is the biased velocity of the walker and $D = \frac{(\Delta x)^2}{2.\Delta t}$ is the diffusivity. In the limit $(\Delta x \to 0)$,the ratio $\frac{v}{D} = \frac{2}{\Delta x}$ diverges and as a result the convective or drifting term $(\frac{\delta P(x,t)}{\delta x})$ dominates over the diffusive term $(\frac{\delta^2 P}{\delta x^2})$. The final solution of the equation-(2.39) is:

$$P(x,t) = \frac{1}{\sqrt{4\pi Dt}} exp\left[-\frac{(x - vt)^2}{4Dt}\right] \tag{2.40}$$

The diffusion equation-(2.39) can be written in the form of the equation of continuity as:

$$\frac{\delta P(x,t)}{\delta t} + \frac{\delta J}{\delta x} = 0 \quad Where \quad J = vP - D.\frac{\delta P(x,t)}{\delta x} \tag{2.41}$$

Here J is defined as the probability current density. The equation of continuity, mentioned above, gives the idea about the conservation of probability and also confirms the fact that walkers cannot be created or destroyed. It also holds good for conducting materials.

Let us consider the charged particles as walkers and they diffuse inside an arbitrary metallic system with a diffusion constant D. If an electric field E is applied externally, the charged particles move with a terminal velocity v that follows Ohm's law $nev = \sigma E$. Here (n) stands for the volume charge density and σ represents the dc conductivity of the medium. In a state of thermal equilibrium at temperature T, the charged particles follow Boltzman's distribution law. Hence the probability distribution function in the state of equilibrium can be expressed as[9]:

$$P_{eq}(x) = P(0) \times \exp\left[-\frac{\epsilon e}{K_B T}\right] = P(0) \times \exp\left[-\frac{eEx}{K_B T}\right] \tag{2.42}$$

Here ϵ represents the electric potential and K_B stands for Boltzmas's constants. In a state of thermal equilibrium, there is no net flow of charge inside the medium. Hence, using this expression we can determine the probability current density at thermal equilibrium as:

$$\begin{aligned} J &= vP - D.\frac{\delta P(x,t)}{\delta x} = 0 \\ \Rightarrow &\left[v - \frac{D.e.E}{K_B.T}\right].P(0)\exp\left[-\frac{eEx}{K_BT}\right] = 0 \\ \Rightarrow &\left[v - \frac{D.e.E}{K_B.T}\right] = 0 \\ \Rightarrow &\ v = \frac{D.e.E}{K_B.T} \end{aligned} \tag{2.43}$$

Using the value of v in above expression in ohm's law ,we get:

$$\sigma = \frac{ne^2}{K_BT}.D \tag{2.44}$$

This equation is known as Einstein's relation which relates conductivity σ and diffusion coefficient D. The expression indicates a linear relationship between conductivity and diffusivity of a medium when the temperature of the system is constant. In the case of disordered medium, this relation may take a different form which will be discussed later.

2.7. Anomalous diffusion

Normal diffusion exhibits a linear dependence of time with a mean square displacement of the diffusing particle i.e. $\langle R^2\rangle \sim t$. There exist many cases where particle diffuses at either a faster or slower rate than the normal diffusion process. This phenomenon results in a non-linear scaling of the mean square displacements $\langle R^2\rangle$ and time t and the relation is expressed as $\langle R^2\rangle \simeq D.t^{\beta}$[9,10,49,53]. Diffusion that can be mathematically characterized by this equation, is known as anomalous diffusion. Here β represents the scaling index and the nature of diffusion depends on the values of β. If $\beta = 1$, the linear relationship between $\langle R^2\rangle$ and t is restored perfectly resulting in a normal diffusion behaviour of the particle inside the sample. Anomalous diffusion occurs for all other values of β except 1. When $\beta > 1$, one can observe super diffusion and in case of $\beta < 1$, subdiffusive behavior can be observed.

Researchers have reported many factors that are responsible for the diffusion being anomalous by nature. One such important factor is the trapping of the diffusing particle[54–56] inside the substrate molecules. In this case, the particle is trapped inside some molecules or clusters for a long period of time and as a result, the diffusion process is slowed down. This phenomenon introduces subdiffusive behavior among the diffusing particles. In the case of continuous-time random walk theory, the trapping effect is characterized by a parameter called 'waiting time' and it is expressed by the waiting time distribution function $\psi(t)$[57] which we will discuss in the next section.

Diffusing particles sometimes takes a 'long flight' where the step length is exceptionally larger than its previous steps. In this case, the particle covers a long special distance and linear relation of $\langle R^2 \rangle$ with time is violated and $\langle R^2 \rangle$ varies more rapidly. This phenomenon is considered as another major factor for the diffusion process being anomalous by nature. This kind of enhanced diffusion can be explained with the help of the Levy flight model and Levy walks[58]. In this case, the jump length variable does not follow the normal Gaussian distribution law. Theoretical analysis has been performed by researchers[59] through computer simulation where only step length and trapping time probability distribution function has been taken into account. The result is in good agreement with the conventional theoretical outcomes.

2.7.1. Continuous Time Random Walk

We have discussed in the previous section about the random walk process where the step time (τ) is considered as an invariant quantity. Let us now consider a more general situation where the walker pauses for some time between two consecutive steps. We call it waiting time which is stochastically independent for the different jumps. We introduce a function $\psi(t)$ that represents the probability density of a walker to remain on a site for a time t (waiting time) before it takes its next step.[9,49] $\psi(t)$ must be normalized which means $\int \psi(t_1)dt_1 = 1$. Hence the probability that the walker pauses at the same site for a time greater than t is:

$$\Psi(t) \quad = \quad \int_t^\infty \psi(t_1)dt_1 \tag{2.45}$$

We now introduce a function $\psi_m(t)$ which represents the probability density that the walker performs its mth jump at the time t. Thus we can write $\psi_1(t) = \psi(t)$ for the initial step of the walker. Since the waiting time between the consecutive steps is independent with each

other, it will satisfy the following recursion relation:

$$\psi_m(t) = \int_0^t \psi_{m-1}(t^{'}).\psi(t-t^{'})dt^{'} \tag{2.46}$$

The Laplaces transformation of $\psi(t)$ is given by[9]:

$$\psi(\omega) = \int_0^\infty \psi(t^{'}).\exp(-\omega t^{'})dt^{'} \tag{2.47}$$

Similarly the Laplace's transformation of $\Psi(t)$ is given by:

$$\Psi(\omega) = \int_0^\infty \Psi(t^{'}).\exp(-\omega t^{'})dt^{'} = \frac{1-\psi(\omega)}{\omega} \tag{2.48}$$

If we apply the convolution theorem of Laplace's transformation on $\psi_m(t)$, it gives the value of $\psi_m(\omega)$ as[9,60] :

$$\psi_m(\omega) = \psi(\omega).\psi_{m-1}(\omega) = [\psi(\omega)]^m \tag{2.49}$$

Let us consider $P_m(r)$ be the probability of the walker to arrive at a distance r from the

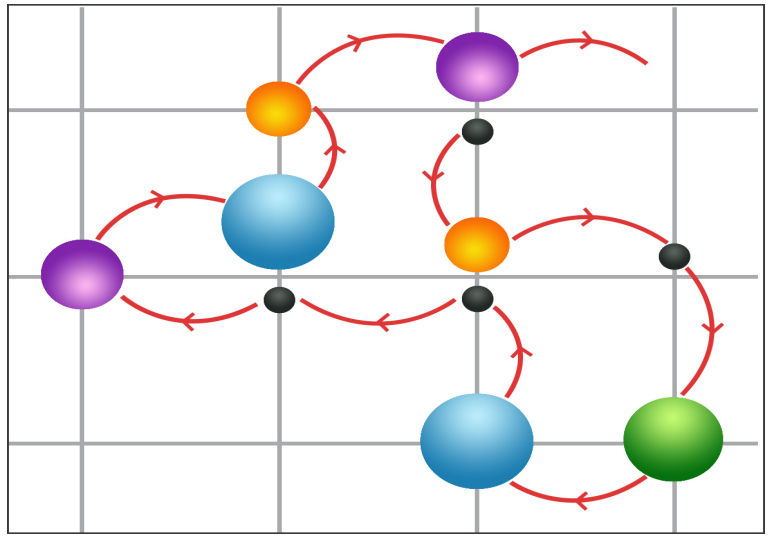

Figure 2.12: *Waiting time distribution of the walker in case of continuous time random walk. The holes represent the waiting time of the walker. Bigger the size of the hole longer the waiting time of the walker at the respective site.*

origin at the mth step of the walk and $\psi_m(t)$ happens to be the probability that the mth step occurs at the time t. The spatial ($P_m(r)$) and temporal ($\psi_m(t)$) transitions of the walker are assumed to be independent of each other. We now introduce a new variable Q(r,t) such

a way that Q(r,t)dt represents the probability that the walker may arrive at r within the time interval t and (t+dt). Therefore Q(r,t)can be mathematically expressed as:

$$Q(r,t) = \Sigma_{m=0}^{\infty} P_m(r).\psi_m(t) \tag{2.50}$$

Let us consider the walker has arrived at r at the time $t^{'}$ right after the walker performed a step. If the walker may stay at r for a time interval (t-$t^{'}$) then the probability of finding the walker at the position r within the time interval (0,t) will be:

$$X_1(t) = 1 - \int_0^{t^{'}} \psi(t_1)dt_1 = \int_t^{\infty} \psi(t_1)dt_1 = \Psi(t) \tag{2.51}$$

If we consider the probability of finding the walker at the position r till the time t is p(r,t), then the relation between p(r,t) and Q(r,t) can be expressed as:

$$p(r,t) = \int_0^t Q(r,t^{'})\Psi(t-t^{'})dt^{'} \tag{2.52}$$

Using the value of Q(r,t) from equation-(2.50) on equation-(2.52), we can find the expression of p(r,t) as:

$$\begin{aligned} p(r,t) &= \int_0^t Q(r,t^{'})\Psi(t-t^{'})dt^{'} \\ &= \int_0^t \Sigma_{m=0}^{\infty} P_m(r).\psi_m(t)\Psi(t-t^{'})dt^{'} \\ &= \Sigma_{m=0}^{\infty}.P_m(r).\int_0^t \psi_m(t)\Psi(t-t^{'})dt^{'} \end{aligned} \tag{2.53}$$

The integral in equation-(2.53) represent the probability that the walker once had arrived at r at time $t^{'}$, it would stay until time t. Taking the Laplace transformation of p(r,t) we get:

$$\begin{aligned} T(r,\omega) &= L.p(r,t) = \Sigma_{m=0}^{\infty}.P_m(r).L.\int_0^t \psi_m(t)\Psi(t-t^{'})dt^{'} \\ &= \Sigma_{m=0}^{\infty}.P_m(r).\psi_m(\omega)\Psi(\omega)d\omega \end{aligned} \tag{2.54}$$

Using the values of $\Psi(\omega)$ and $\psi_m(\omega)$ from equation- (2.48) and equation-(2.49) in equation-(2.54), we get the value of $T(r,\omega)$ as:

$$\begin{aligned} T(r,\omega) &= L.p(r,t) = \Sigma_{m=0}^{\infty}.P_m(r).L.\int_0^t \psi_m(t)\Psi(t-t^{'})dt^{'} \\ &= \Sigma_{m=0}^{\infty}P_m(r)\psi^m(\omega).\frac{1-\psi(\omega)}{\omega} \end{aligned} \tag{2.55}$$

We now take the Furier transformation of $T(r,\omega)$ and get:

$$\begin{aligned} X(k,\omega) &= F.T(r,\omega) = \Sigma_{m=0}^{\infty} F.P_m(r)\psi^m(\omega).\frac{1-\psi(\omega)}{\omega} \\ &= \Sigma_{m=0}^{\infty}\Gamma_m(k).\psi^m(\omega).\frac{1-\psi(\omega)}{\omega} \end{aligned} \tag{2.56}$$

Using the value of $\Gamma_m(k)$ from equation-(2.26) we can write:

$$\begin{aligned} X(k,\omega) &= \Sigma_{m=0}^{\infty}\Lambda^m(k).\psi^m(\omega).\frac{1-\psi(\omega)}{\omega} \\ &= \frac{1-\psi(\omega)}{\omega}.\Sigma_{m=0}^{\infty}\left[\Lambda(k).\psi(\omega)\right]^m \\ &= \frac{1-\psi(\omega)}{\omega}.\frac{1}{1-\Lambda(k).\psi(\omega)} \\ &= \frac{\left[1-\psi(\omega)\right]}{\omega\left[1-\Lambda(k).\psi(\omega)\right]} \end{aligned} \tag{2.57}$$

This equation is known as Montroll-Weiss equation[54]. From the above expression,we can calculate $\langle R(\omega)\rangle$ and $\langle R^2(\omega)\rangle$[9]:

$$\langle R(\omega)\rangle = \frac{V_1\psi(\omega)}{\omega\left[1-\psi(\omega)\right]} \tag{2.58}$$

$$\langle R^2(\omega)\rangle = \frac{V_2\psi(\omega)}{\omega\left[1-\psi(\omega)\right]} + \frac{2.\left[V_1\psi(\omega)\right]^2}{\omega\left[1-\psi(\omega)\right]^2} \tag{2.59}$$

Where $V_n = \int R^n.P(R)dR$.The nature of the diffusion depends on the selection of waiting time distribution $\psi(t)$. If we choose $\psi(t) = \delta(t-\tau)$ or any other form of it where it falls very rapidly, the result will be the same as the simple random walk. But if $\psi(t)$ is chosen in such a way that it does not have any characteristic time scale then the result leads to anomalous diffusion.

2.8. Nature of Diffusion inside Fractal

Diffusion phenomena in disordered medium (e.g. fractal objects) is a well-known topic of research[61]. The analysis of dynamical processes like diffusion inside fractal by statistical approach is aimed for two reasons: firstly to perform some convenient numerical as well as analytical methods to calculate different parameters like mean square displacement, dynamical quantities, reaction velocities, etc[62]. Secondly: to investigate the diffusion process inside the fractal more deeply. The problem of diffusion inside fractal has some similarities

to the other problems inside fractal objects, like electrical conductivity, mechanical vibration[63], Schrödinger equation[64] etc. The probability distribution function (PDF) P(N, t) of the walker plays a significant role to study the diffusion process inside fractal objects stochastically. Several analytical techniques[48,61,65] have been adopted so far to investigate the nature of diffusion inside fractals. Two fundamental approaches among them have already been discussed in our previous section which is as follows:

a Simple random walk approach where the diffusing particle experience Markovian nature of walk with constant step time to the neighbouring sites.

b. A non-Markovian process of the random walk where the diffusing particle has a waiting time distribution on different sites.

In this present section, we will study the nature of the diffusion process inside fractals.

2.8.1. Random walk on fractal object

The random walk process inside an arbitrary fractal system is not the same as that regular object. Intrinsic characteristics such as self-similarity, non-integer dimension, dilatational symmetry, etc. make the system unique and more challenging to analyze different properties through the conventional ways. We initially introduced the Markovian Master equation of random walk in d-dimension discrete space and discrete time as[68]:

$$P(R,n) = P(R,n-1) + \sum_{R'}^{Z} T(R' \rightarrow R)P(R',n-1) - \sum_{R}^{Z} T(R \rightarrow R')P(R,n-1) \quad (2.60)$$

Where P(R,n) is the probability of the walker reaching a distance R, after n consecutive steps. $T(R' \rightarrow R)$ is the probability of jump from the position R' to R where $T(R \rightarrow R) = 0$. z is the total number of accessible nearest neighbour sites around the walker at position R. The continuous-time version of Equation-(2.60) is:

$$\frac{\delta P(R,t)}{\delta t} = \sum_{R'}^{Z} T(R' \rightarrow R)P(R',t) - \sum_{R}^{Z} T(R \rightarrow R')P(R,t) \quad (2.61)$$

Here P(R,t) is the probability of finding the walker at the position R at the instant of time t, and $T(R' \rightarrow R)$ is the transition probability per unit time of the walker from R' to R. Now we write $\{P(R,t)\}(R \in s)$ in the form of a column vector as P(t). Therefore equation-(2.61) can be written as $\delta_t P = VP(t)$ where V represent an operator. Taking the laplaces transformation of P(t) one get: $P(s) = (s - V)^{-1}P(0)$. Therefore one has to find the spectrum and resolvant of V. In most of the cases, an arbitrary site r couple with its

nearest neighbour sites s. In the spatial continuum limit, if V poses some isotropic nature, then V becomes the second-order differential operator ∇_d^2. In that case, equation-(2.61) becomes the well-known diffusion equation of probability P(R,t).

$$\frac{\delta P(R,t)}{\delta t} = k_1.\nabla^2 P(R,t) \tag{2.62}$$

Where the spherically symmetric initial condition is $P(R,0) = \delta^d(R)$. Where d stands for the Eucledian dimension. The angular integration results[68]:

$$\frac{\delta P(R,t)}{\delta t} = \frac{k_1}{R^{d-1}} \frac{\delta P(R,t)}{\delta r} \tag{2.63}$$

under the most general condition of jump probability $T(R^{'} \rightarrow R)$ (prime condition is to have finite mean and variance i.e. $\Sigma_R (R - r^{'})^j . T(R^{'} \rightarrow R) < \infty \ \ where \ \ j = 1, 2 \ \ and \ \ \bigvee r^{'} \in s)$), the PDF $P(R,t)$ follows normal distribution nature at the asymptotic limit and the solution of the equation will be:

$$P(R,t) \sim t^{\frac{-d}{2}} . Exp(\frac{-R^2}{t}) \tag{2.64}$$

Here the constant factors are not mentioned explicitly. They can be estimated with respevt to the appropreate physical dimension. The mean square displacement $< R^2 >$can be estimated from the (2.64) as:

$$< R^2 > \sim K_z . t \tag{2.65}$$

It should be noted that equation-(2.65) shows the linear dependence of $< R^2 >$ with walk time t and it is independent of the dimension of the system. This behaviour is very unlikely to be followed by the hierarchical structures such as fractal objects. IN that case, evaluation of P(R,t) requires different approach which is explained as follows:
Let us consider $P(0,t)$ represents the return probability of the walker to its initial position inside the d-dimentional medium. In case of regular lattice, one can write[68]:

$$P(0,t) \sim t^{\frac{-d}{2}} \Longrightarrow P(0,t) \sim t^{\frac{-d}{d_w}} \quad where \quad d_w = 2 \tag{2.66}$$

In case of fractal system the return probability can be calculated differently. Here we assume a fractal object with fractal dimension d_f embedded in a d-dimensional hyper sphere. The number of fractal sites embedded inside the hypersphere with radius R will be :$M(R) \sim R^{d_f}$.

On the other hand, the value of d_w deviates from the value=2. The return probability of a walker to its initial position in case of fractal lattice can be written as:[9,68] :

$$P(0,t) \sim t^{\frac{d_f}{d_w}} \Rightarrow P(0,t) \sim t^{\frac{1}{\frac{d_s}{2}}} \tag{2.67}$$

Where d_s is the spectral dimension. It is found that[68] $\frac{d_f}{d_w} < \frac{d}{2}$ in case of fractal objects. Hence the return probability P(0,t), in case of fractal system is always greater than that of a regular lattice. Study of random walk as well as the diffusion phenomena inside a fractal system requires a smart estimation of PDF P(R,t) that will satisfy a diffusion equation in spatial continuum limit. In this regard, one may follow the coarse-graining or smoothing procedure to define P(r,t). The equation will be the counterpart of the equation-(2.63) in case of fractal object. In that case the diffusion equation can be modified such a fashion that the diffusion cofficient $k_1(R)$ is no longer constant but depends on scale such a way that the anomolous diffusion can be incorporated inside the fractal system. In case of fractal system, we have $\langle R^2 \rangle \sim t^{\frac{2}{d_w}}$[9,10,68]. Hence the diffusion coefficient inside the fractal can be scales like[68]:

$$K_1(R) \sim K/R^{(d_w-2)}. \tag{2.68}$$

We introduce a new parameter $g = d_w - 2$. The differential equation in case of fractal object is transformed into:[68,69]

$$\frac{\delta P(R,t)}{\delta t} = \frac{K}{R^{d_f-1}} \frac{\delta}{\delta r} \left[R^{(d_f-g-1)} \frac{\delta P}{\delta r} \right] \tag{2.69}$$

Here g in an important exponent which depends on the nature of the fractal concerned.If the initial condition of the above equation is symmetric by nature then its solution will be given by :

$$P(R,t) \sim \frac{1}{t^{\frac{d_f}{d_w}}}.Exp\left(\frac{-R^{d_w}}{t}\right) \tag{2.70}$$

The solution is not Gaussian by nature and it can be written as:

$$P(R,t) \sim \frac{1}{t^{\frac{d_s}{2}}}.Exp\left(\frac{-R^{d_w}}{t}\right) \tag{2.71}$$

A more accurate estimation of the solution of equation-(2.69) would be:

$$P(R,t) \sim \frac{1}{t^{\frac{d_s}{2}}}.Exp\left(\frac{-R^{d_w}}{t}\right)^{k_2} \tag{2.72}$$

Where K_2 is an exponent. It controls the shape of the curve and is bounded as[68]:

$$\frac{k_3^{'}}{(d_w - k_3^{'})} \geq k_2 \geq \frac{1}{(d_w - 1)} \tag{2.73}$$

$K_3^{'}$ is known as the chemical distance exponent inside the fractal system. in the case of 3-d system value of K_3 lies between 0.37 and 0.58[68]

2.8.2. Conductivity and Einstein Relation inside Fractal Objects

In the present section, we will study the relation between diffusivity and conductivity (Einstein relation) inside the fractal system. As we know, diffusion inside fractal is anomalous in nature[9,10,68] . In this case, we can write:

$$D \equiv \frac{(\langle R^2(t) \rangle)}{t} \sim \frac{L^2}{t} \tag{2.74}$$

Where L is the average distance traveled by the walker in time t.Einstein's relation to conductivity has already been discussed previously. For a d dimensional system, we can write $V \sim L^d$. In case of fractal $M = L^{d_f}$ where d_f is the fractal dimension. Thus carrier density n can be written as:

$$n = \frac{M}{V} \sim \frac{L^{d_f}}{L^d} = L^(d_f - d) \tag{2.75}$$

Let us assume μ is the conductivity exponent of the fractal object. Hence the conductivity inside a fractal object can be expressed as a power of its linear size L as $\sigma \sim L^{-\mu}$. We insert these values in Einstein relation and get:

$$\begin{aligned} \sigma &= \frac{ne^2.D}{k_B T} \\ \Rightarrow L^{-\mu} &\sim \frac{e^2.L^{2+d_f-d}}{k_B T.t} \\ \Rightarrow t &\sim \frac{e^2.L^{2+d_f+\mu-d}}{k_B T} \\ \Rightarrow t &\sim L^{2+d_f+\mu-d} \end{aligned} \tag{2.76}$$

On the other hand, the trace subtended by a random walker is a stochastic fractal and hence we can write: $t \sim L^{d_w}$.[9,10] Comparing these two relations, we can write:

$$d_w = 2 + d_f + \mu - d \tag{2.77}$$

Let us define α as resistivity exponent. Hence the resistance Z can be scaled as $Z = L^{\alpha}$. Ohm's law can be written as: $V = I.Z$. Again we know that $V \sim E.L$. Thus Ohm's law can alternatively be written as:

$$E = I.L^{(\alpha-1)} \tag{2.78}$$

Similarly, another form of Ohm's law is given by $J = \sigma E$. If total current is I for a d-dimensional system, then we can write:$J = \frac{I}{L^{d-1}}$. Hence:

$$E = I.L^{(\mu-d+1)} \tag{2.79}$$

Comparing these two equations we can write $\alpha = 2 - d + \mu$ which is the desired relation between the exponents inside fractals like objects.

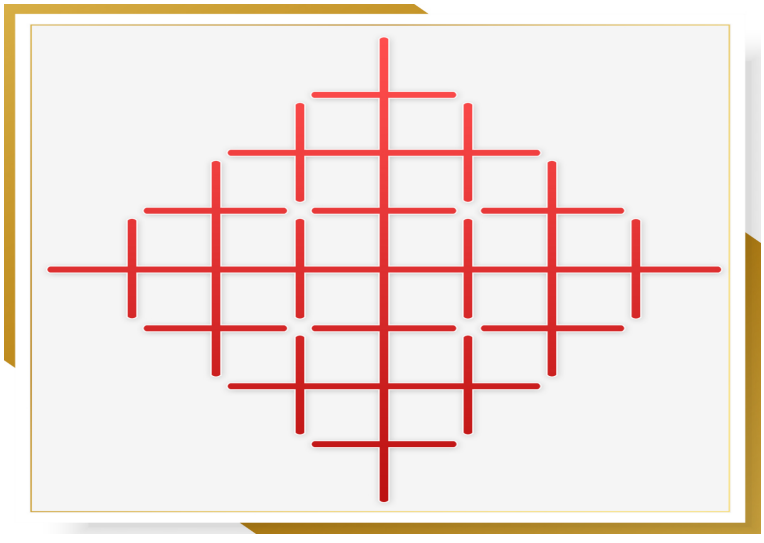

Figure 2.13: *An example of Deterministic Loop less fractal.*

2.9. Loopless Fractals and Their Role in Modelling Polymer Structures

There exist many objects in nature where loops are either absent or can be neglected. The simplest kind of loopless structure is the 1-D linear polymer chain, constructed by

Self Avoiding Walk (SAW). Many other objects such as DLA, cluster-cluster aggregates[14], branched polymers modelled by lattice animals[71], complicated disordered substances like percolation clusters constructed by infinitely long or varying teeth length, etc. are examples where loops are either absent or can be neglected. These types of disordered objects can be modelled by loopless fractals. Here we discuss some basic features of loop-less fractals. One

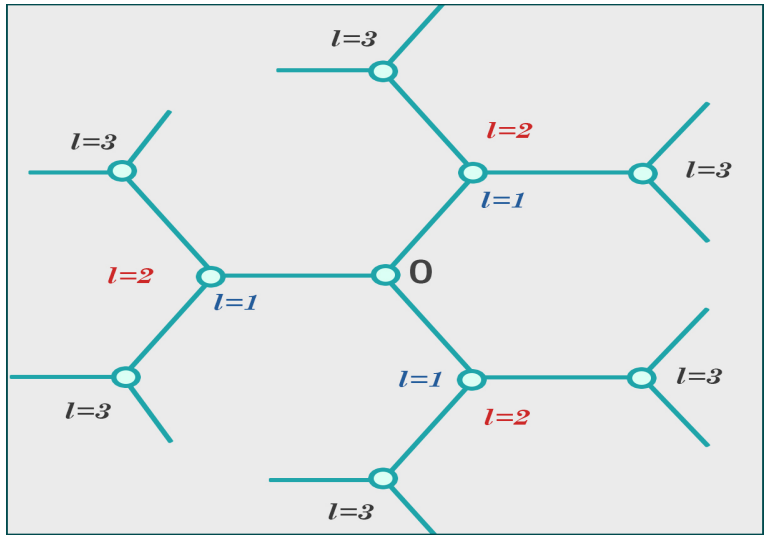

Figure 2.14: *A schematic diagram of Cayley tree.*

of the simplest models that are used to construct loopless aggregates mathematically is the Cayley tree model. The generation of the Cayley tree starts from an arbitrary central site called origin or root. The origin generates G numbers of branches whose endpoints are also considered as individual sites. These G sites altogether form the first shell of the Cayley tree. Each site of the first shell generates (G-1) individual branches. Hence G(G-1) number of sites generates the second shell. In this manner, (G-1) new branches will emerge from each site of the lth shell. The endpoints of all these branches will be included in $(l+1)^{th}$ shell. Hence the lth shell will contain $G(G-1)^{l-1}$ sites[9]. Thus the number of sites in each shell grows very rapidly so we can construct a lattice of infinite dimension with the help of it. Cayley tree is considered as a convenient model to construct percolation clusters for dimension $(D) \geq 6$[9,10].

The study of different transport properties in the disordered medium becomes more simple when they are modelled mathematically with the help of loopless fractals. Loopless fractals can be characterized by their backbones. The backbone of a loopless fractal structure is the collection of the smallest chemical paths joining the origin to the arbitrary peripheral

site we are concerned about. If $N_B(R)$ is the number of backbone sites, then we can write $N_B(R) \sim R^{d_f^B}$ where d_f^B is the fractal dimension of the backbone. On the other hand $N(R) \sim R^{d_f}$ is well known for random walk theory. If l is the chemical distance between two sites of a fractal object, then one can write:

$$N(l) \sim l^{d_l} \tag{2.80}$$

$$N_B(l) \sim l^{d_l^B} \tag{2.81}$$

Where N(l) is the mass of the loopless fractal object d_l is the chemical length exponent. Likewise $N_B(l)$ is the total number of backbone sites in chemical length scale and d_l^B is the fractal dimension of the backbone in chemical space. The relation between the spatial distance and the chemical length exponent can be expressed as follows:

$$R(l) \sim l^{\theta_l} \tag{2.82}$$

Here θ_l represents the chemical length exponent and d_f is the fractal dimension of the backbone path. From these two relations we can conclude:

$$d_l = \theta_l . d_f \tag{2.83}$$

$$d_l^B = \theta_l . d_f^B \tag{2.84}$$

Another well-known example of a deterministic loopless fractal is a polynomial tree which is characterized by its growth rate. It is a special kind of loopless fractal which poses the values $d_l^B = 1$ and $\theta_l = 1$. The nodes in a polynomial tree are generated in a completely random fashion. The total number of nodes that are generated in the lth chemical shell can be evaluated from the relation:

$$N(l) = N_0 l^{d_l - 1} \tag{2.85}$$

Where N(l) is the number of nodes in its lth chemical shell. The generation of these N(l) nodes occurs with equal probabilities from any of the nodes in $(l-1)^{th}$ shell. An exact recursion relation can be established to evaluate the number of nodes ($N_B(l)$) in the lth shell of the backbone as the growth of the fractal tree happens to be Markovian in nature. Hence a quantitative relation between the total mass and the backbone mass of the polynomial tree can be estimated from the relation below:

$$d_l^B = 1 \qquad for \quad d_l < 2 \tag{2.86}$$

$$d_l^B = d_l - 1 \qquad for \quad d_l \geq 2 \tag{2.87}$$

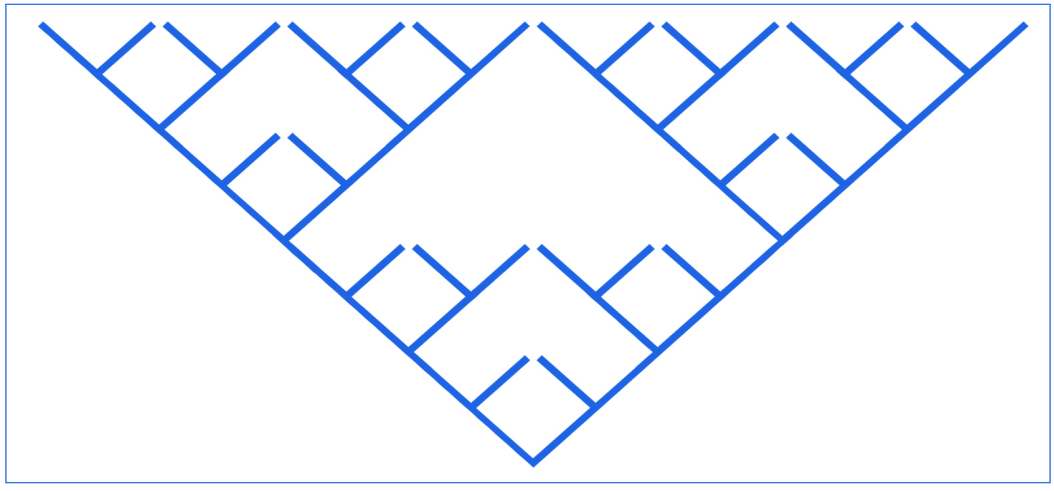

Figure 2.15: *A schematic diagram of a loopless fractal tree. It has same fractal dimension as of the Sierpinski Gasket but here loops are not present.*

A definite conclusion can be drawn from the above discussion which states that there exists an exact relation between the structural exponents (e.g. fractal dimension and chemical length exponent) to the dynamical exponent (like spectral dimension and walk dimension). Hence evaluation of different physical parameters inside loopless fractals becomes easier than the structures with loops.

2.9.1. Relation between the Structural and Transport Exponent in Loopless Fractal:

Transport properties like diffusion, conductivity, etc. can easily be evaluated from the structural properties of loopless fractals[72]. As we know that the resistance between two lattice sites inside a fractal can be expressed as $Z \sim R^{\alpha}$. where R is the distance between two lattice sites. In the case of a loopless fractal, the shortest distance between two lattice sites is unique and it is known as the chemical length of a fractal. Hence, the resistance will be proportional to the chemical length (l) i.e.,

$$Z \sim l \tag{2.88}$$

$$\Rightarrow Z \sim R^{\frac{d_f}{d_l}} \Rightarrow \alpha = \frac{d_f}{d_l} \tag{2.89}$$

We recall the Einstein's relation

$$d_w = \alpha + d_f = d_f \left(1 + \frac{1}{d_l}\right) \tag{2.90}$$

This equation suggests that the transport exponents α and d_w can be estimated from the structural exponent d_f and d_l. The mathematical relation, derived above, can also be established in chemical space. If d_w^l be the diffusion exponent in chemical space, then we can say: $l \sim t^{\frac{1}{d_w^l}}$. Since $R \sim l^{\theta_1}$, we can write:

$$d_w^l = \theta_1 . d_w \tag{2.91}$$

$$\Rightarrow d_w^l = \frac{d_l}{d_f} . d_w \tag{2.92}$$

$$\Rightarrow d_w^l = 1 + d_l. \tag{2.93}$$

The spectral dimension can be evaluated in a similar fashion as:

$$\frac{2d_f}{d_w} = \frac{2d_l}{1 + d_l} \tag{2.94}$$

This expression suggests that the transport exponent in chemical space depends only on d_l not on d_f, generally $d_l > 1$ in case the loopless tree. This indicates the delay of the walker due to trapping inside the branches. As a result, one can observe anomalous diffusion inside the fractal trees in chemical space. The diffusing sites can be imagined as a part propagating surface known as diffusion front. The time rate of increase of the growing sites on the diffusion front X(l) can be calculated from the Rammal-Toulouse equation:[9,67]

$$\frac{ds}{dt} = \frac{X}{S} \tag{2.95}$$

Where S is the number of distinct sites and can be expressed as: $D \sim l^{d_l}$.Hence X(l) can be expressed as: $X(l) \sim l^{d_l - 1}$

This suggests that the diffusion front can be considered as a spherical cut of the tree in chemical space. This fact makes chemical distance a natural length parameter to investigate the diffusion behaviour in loopless aggregates.

2.10. Computer Simulation of Random Walk Process

The computer simulation process of random walk study in a crystalline substrate in Euclidean space happens to be easier than any other type of system. The unbiased random walk algorithm is done with the help of the following steps:

A large number of periodically arranged lattice sites has been taken to configure the substrate in Euclidean space where an arbitrary lattice point has been chosen as the origin.

The walker starts its walk from the defined origin and hops to any one of the nearest neighbouring sites with equal probability. The number of nearest neighbour sites around the walker depends on the dimension of the substrate. Therefore the walker avails the various number of nearest neighbour sites in the case of 1D, 2D, and 3D substrates respectively. A computer-generated random number is used to estimate the probability of jump of the walker into its neighbourng sites. This process is carried on for every step of the walker.

The total distance R traversed by the walker from the origin after N such consecutive steps are evaluated after completion of the entire random walk process. Since the process is completely random therefore we can write: $\langle R\rangle = 0$. The random walk process is executed in a substrate embedded in Euclidean space where the latest sites are arranged periodically. Therefore we must say:

$$\langle R^2\rangle \sim N \tag{2.96}$$

The averaging is evaluated over a large number of walk steps to get a stable saturated value. But if the randomness persists, the averaging is performed over several configurations.

In the case of biased random walk, we follow the same algorithm mentioned above except for a slight modification in the walking algorithm. Here the jumping probability of the walker along the biased direction is chosen to be greater than the other nearest neighbour sites. Since the random walk is biased, therefore, the value ($\langle R\rangle$ is not zero. Hence the parameter ($\langle R^2\rangle - \langle R\rangle^2$) is evaluated for a large number of walk steps. The ($\langle R^2\rangle - \langle R\rangle^2$) vs t graph will be a straight line in this case and the diffusion coefficient is evaluated from the slope of that straight line plot.

2.10.1. Computer Simulation Algorithm for Random Walk Process inside Fractals

Fractals are considered to be disordered media and random walk process inside a fractal object happens to be more complicated than it is in case of regular lattice. The mean square displacement $\langle R_N^2\rangle$ shows a power law variation with time step (t) in this case which can be expressed as: $\langle R_N^2\rangle \sim t^{2/d_w}$. Therefore Diffusion exponent d_w plays a significant role to study the nature of diffusion inside fractal objects. The computer simulation algorithm to perform the random walk process inside an arbitrary fractal object is executed following some basic steps which are mention below:

1. Initially, a host system is configured mathematically inside an embedding Euclidean lattice using a fractal model and following a convenient algorithm. Several algorithms have been applied by the researchers. Some of those will be discussed later. Fractal lattices are not regular like the normal crystal lattice. The sites that belong to the fractal lattice, are accessible for the random walker and the rest of the sites are blocked. The walker initially starts from an arbitrary site which is considered as the origin and jumps to any of its nearest neighbouring accessible sites. The probability of jumping on an arbitrary nearest neighbour site is chosen by a computer-generated random number. If the site is accessible, the walker will jump immediately and if the site is blocked, it will remain on the same site and performs a next attempt of jump following the same procedure. Two methods are applied to simulate the discrete random walk inside fractal lattice: 'Blind ant' and 'Myopic ant' which will be discussed later in this section.

2. Evaluation of $\langle R_N^2 \rangle$ requires a successful execution of random walk process inside the fractal for a large number of time steps. Since it is a complete stochastic process, a single set of the walk may not give a non-fluctuating saturated value of $\langle R_N^2 \rangle$. Therefore we have to repeat this entire process on a large number of identical systems. In that case, we consider an ensemble consisting of a set of identical systems. Each system consists of B number of identical accessible fractal sites. A walker accomplishes a random walk with N number of steps in each system for a duration of time t. The distance R travelled by the walker for the same value of time step t will be different in different systems. The value of R_N^2 as well as the required time t to cover the distance R_N is calculated after the completion of the total walk process inside a system. Since the process is completely random, R_N is different for every system. Hence we calculate $\langle R_N^2 \rangle$ by averaging over all possible values of R_N in the defined ensemble.

3. If R_N represents total distance of the walker from origin after N-number of walk steps and t_N is the total time taken for the walk then we get: $\langle R_N^2 \rangle \sim N$ in the limit $N \to \infty$ We know that the trace of random walk can be considered as a stochastic fractal with walk dimension d_w[9] . Hence we can write $R^{d_w} \sim N$ or $R^{d_w} \sim t$ which gives the concluding final relation $\langle R_N^2 \rangle \sim t^{\frac{2}{d_w}}$[9,10]. The value of d_w is evaluated from the slope of $\ln\langle R_N^2 \rangle$ vs ln(t) plot. To draw the graph, we prepare a set of $\langle R_N^2 \rangle$ values for different walk times ranging from 0 to t with a definite interval of time τ_i. This set of data is used to draw the $\ln\langle R_N^2 \rangle$ vs ln(t) plot.

Natural fractal objects are not so simple as the deterministic, loopless, finitely ramified fractals mentioned before. Rather they are stochastic by nature. Therefore simple

algorithm, mentioned above, may not be adequate. In this case, we generally adopt some mathematical techniques which consist of two steps:
a. Initially, a suitable technique is adopted to construct the structure of the system on the computer. Different types of techniques are used as per the requirement.
b. As mentioned before, the fractal medium is disordered by nature. therefore all the nearest neighbouring sites may not be accessible to them. Therefore a convenient algorithm is used to study the diffusion process inside the substrate.

2.10.2. Different types of Simulation Process: A Brief Overview

Researchers have reported about different types of simulation processes to study the random walk process inside the regular as well as disordered systems. A few of them have been discussed below.

2.10.2.1. Monte Carlo Simulation Method

It is a straightforward method to study the diffusion phenomena in complex mediums. In that case, one must need a double Monte Carlo (MC) approach where the first approach is for simulating the substrate and the second method is meant for characterizing the diffusion process. The cluster growth method[73,74] and the Hosen-Kopelman algorithm[75] is used to simulate the substrate for percolation clusters. This method can also be used for simulating DLA clusters[10,76]. The main drawback of MC simulation is that the cluster simulated by MC simulation can be used for one random walk process only and all possible random walks, initiating from an arbitrary point on this substrate are averaged. The error bar in a plot of d_w vs N is considerably high for a complex system.

2.10.2.2. Exact Enumeration Method

This is considered another useful technique to simulate the diffusion phenomenon inside the fractal substrate. According to the exact enumeration method, the probability of finding a particle at any arbitrary site (j) at any instant τ, solely depends on the probability of the existence of the walker on its neighbouring sites at its previous instant of time $(\tau - 1)$[9]. Initially we define two matrices $X_1\{j\}_{\tau'}$ and $X_2\{j\}_{\tau'}$ that contain all information regarding the probability of existence of that walker on the site j, at any two discrete times τ and $\tau^{'}$ i.e. $P(r, \tau)$ and $P(r, \tau^{'})$. The set of all accessible sites in the substrate is represented here

by $\{j\}$. Hence , if we know the distribution function $X_1\{j\}_{\tau-1}$ at an instant of time $(\tau-1)$ then the new distribution function $X_2\{j\}_\tau$ at a time τ will be:

$$X_2\{j\}_\tau = \sum_{n\{j\}} X_1\left[n\{j\}\right]_{\tau-1} U\left[n\{j\} \to j\right] \tag{2.97}$$

Here $n\{j\}$ represents a set of all possible nearest neighbours of j. We define a new matrix $U[n\{j\} \to j]$ that represents the transition probability of a walker from an arbitrary nearest neighbour site from the set $n\{j\}$ to the site j. It should be noted that $U[n\{j\} \to j]$ depends on the nature of the walker we use. The role of the matrices, defined previously is reversed in the next step $(\tau+1)$. The input value at an instant τ is taken from the matrix $X_2[n\{j\}]_\tau$ and the output data are stored in the matrix $X_1[n\{j\}]_{\tau+1}$[9] which is evaluated from the new transformation equation as:

$$X_1\{j\}_{\tau+1} = \sum_{n\{j\}} X_1\left[n\{j\}\right]_{\tau} U\left[n\{j\} \to j\right] \tag{2.98}$$

Temporal variation of the probability distribution is evaluated by the successive iteration. Once the probability distribution is known, we can evaluate different quantities like mean square displacement $\langle R_N^2 \rangle$, number of the distinct site visited, etc. One notable advantage of this process is that it reduces the error bar in comparison with the Monte Carlo simulation. The exact enumeration process depends on the walk algorithm and it has been successfully applied to study the diffusion process in different fields of research like determination of moments as well as scaling the PDF in exact fractal[78], diffusion through the backbone of the percolation clusters[79], diffusion on DLA. Etc.

2.10.3. Different types of Discrete Random Walk Algorithm

The transition probability $U[n\{j\} \to j]$, mentioned in the previous section solely depends on the nature of the walker. Initially, de Gennes introduced the concept of 'Ant in the labyrinth method. Later two different types of ants are introduced depending on their jumping probabilities to characterize diffusion behaviour inside the fractal lattice. The two types of ants are i. Blind and. ii. Myopic ant.

2.10.3.1. Blind Ant Algorithm

This type of ant blindly attempts to step into all nearest neighbour sites whether it might be open or blocked. If the site is open, the attempt is successful and the walker moves to a

different site. But if the site is blocked, the walker waits at its initial position[9]. Thus the transition probability will be:

$$\tilde{U}[n\{j\} \to j] = \begin{cases} \frac{1}{Z\{j\}} & \text{for the transition to every open nearest neighbour sites} \\ \frac{(z\{j\}-k_j)}{z\{j\}} & \text{for the rest of the blocked sites.} \end{cases}$$

Here $z\{j\}$ is the coordination number of the lattice and k_i represents the total number of open nearest neighbour sites around the jth site. It should be noted that the parameter $n\{j\}$ also includes the site j itself in addition to the other nearest neighbour sites.

2.10.3.2. Myopic Ant Algorithm

These types of walkers only attempt the accessible nearest neighbouring sites and avoid stepping into the blocked sites. Therefore the myopic ant poses zero probability for resting in the respective site. As a result, it moves to any one of its accessible sites with the same probability. Therefore, the transition probability for a Myopic walker to its nearest neighbour sites will be:

$$\tilde{U}[n\{j\} \to j] = \begin{cases} \frac{1}{k_j} & \text{for the transition to every open nearest neighbour sites} \\ 0 & \text{for the rest of the blocked sites.} \end{cases}$$

Though the basic approach of these two algorithms are different by nature but in the asymptotic region both of them gives the same result[77] but the only difference is that the simulation results performed by the blind ant algorithm converge more quickly than as the case of Myopic ant[77,80].

2.10.4. Errors in Computer Simulation Process

The computer simulation procedure involves two different types of errors which are discussed below:

1. **Statistical Error:** It is one of the most significant errors that occurs at the time of the simulation. A statistical error can be made small by increasing the identical simple at the time of performing the configurational average. It has been found that statistical error

is proportional to $1/(N_v)^{1/2}$. Here $(N_v)^{1/2}$ stands for the total number of configurations over which the averaging is done to evaluate the desired macroscopic property.

2. **Controllable systemic error:** This happens to be another type of error that occurs at the time of computer simulation. It has been reported that this error originates from the finite size effect.

2.10.5. Limitation of Computer Simulation Process in Fractal System

The analytical study, done in the previous section helps us to conclude that transport phenomena in the fractal system can be characterized efficiently by computer simulation techniques. But it also has some limitations. Here we will discuss some major difficulties one can face to simulate diffusion phenomena in fractals.

The diffusion behaviour through random walk in a disordered medium is analyzed by the linear fit of $\ln\langle R_N^2\rangle$ vs ln(t). If the walk performed by the walker, is not sufficiently long, the resultant step length distribution may not be Gaussian in nature and as a result the $\ln\langle R_N^2\rangle$ vs ln(t) graph does not give correct values. To construct a typical disordered system mathematically, one must include at least five to six different stages of the respective fractal. The total no. of sites or mass M of a fractal of nth stage is $(M \sim (L^{d_f})^n$. Where L and d_f are the lengths of the 1st stage fractal and fractal dimension respectively. The number of sites increases very rapidly as the stage (n) of the fractal increases. Thus, random walk on a complete fractal structure requires a large number of the walk which results in a large computational time.

The dilational symmetry of fractal objects introduces a new type of difficulty. In this case, periodic boundary conditions cannot be used. Therefore the system must be large enough so that the walker never reaches the boundary of the system. In the case of a single random walk, it has been found that a particular step with a definite step length is chosen in maximum number. Hence the value of $\langle R_N^2\rangle$ for a single run can never give a correct result. This brings in another kind of complication which is, in this case, the value of $\langle R_N^2\rangle$ is different for the different run. To overcome this problem one has to take self averaging random walk for a large number of steps which is extremely difficult to simulate. So we can use separate random walks with different random number sequences and different starting points.

Bibliography

[1] Kuleznev, V.N. and Shershnev, V.A., 1990. The chemistry and physics of polymers. MIR publishers.

[2] Berthier, C., Gorecki, W., Minier, M., Armand, M.B., Chabagno, J.M. and Rigaud, P., 1983. Microscopic investigation of ionic conductivity in alkali metal salts-poly (ethylene oxide) adducts. Solid State Ionics, 11(1), pp.91-95.

[3] Song Y, Wu S, Jing X, Sun J,Chen D (1997) Thermal, mechanical and ionic conductive behaviour of gamma–radiation induced PEO-PVDF(SIN)–LiClO4 polymer electrolyte system. Radiat Phys Chem 49:541–546

[4] Imbrogno, J., Maruyama, K., Rivers, F., Baltzegar, J.R., Zhang, Z., Meyer, P.W., Ganesan, V., Aoshima, S. and Lynd, N.A., 2021. Relationship between Ionic Conductivity, Glass Transition Temperature, and Dielectric Constant in Poly (vinyl ether) Lithium Electrolytes. ACS Macro Letters, 10(8), pp.1002-1007.

[5] Chandra, A. and Chandra, S., 1994. Experimental observation of large-size fractals in ion-conducting polymer electrolyte films. Physical Review B, 49(1), p.633.

[6] Mandelbrot, B.B., 1983. The fractal geometry of nature (Vol. 173, p. 51). New York: WH freeman.

[7] Feder, J., 2013. Fractals. Springer Science and Business Media.

[8] s Vicsek, T., 1992. Fractal growth phenomena. World scientific.

[9] Ben-Avraham, D. and Havlin, S., 2000. Diffusion and reactions in fractals and disordered systems. Cambridge university press.

[10] S. Havlin and D. Ben-Avraham, Diffusion in disordered medium (1987). Adv. Phys., 36, p.695.

[11] Orr, W.J.C., 1947. Statistical treatment of polymer solutions at infinite dilution. Transactions of the Faraday Society, 43, pp.12-27.

[12] Zimm, B.H. and Stockmayer, W.H., 1949. The dimensions of chain molecules containing branches and rings. The Journal of Chemical Physics, 17(12), pp.1301-1314.

[13] Lubensky, T. C., and Isaacson, J., 1981, Phys. Rev. Lett., 46, 871.

[14] Witten Jr, T.A. and Sander, L.M., 1981. Diffusion-limited aggregation, a kinetic critical phenomenon. Physical review letters, 47(19), p.1400.

[15] Meakin, P. and Stanley, H.E., 1983. Spectral dimension for the diffusion-limited aggregation model of colloid growth. Physical review letters, 51(16), p.1457.

[16] www.jfgouyet.fr/fractal/fractauk/chapter1.pdf

[17] De Gennes, P.G. and Gennes, P.G., 1979. Scaling concepts in polymer physics. Cornell university press.

[18] Havlin, S. and Ben-Avraham, D., 1982. Fractal dimensionality of polymer chains. Journal of Physics A: Mathematical and General, 15(6), p.L311.

[19] Cates, M.E., 1984. Statics and dynamics of polymeric fractals. Physical review letters, 53(9), p.926.

[20] Muthukumar, M., 1985. Dynamics of polymeric fractals. The Journal of chemical physics, 83(6), pp.3161-3168.

[21] Wasserman, B., 1986. Fractal nature of electrical conductivity in ion-implanted polymers. Physical Review B, 34(3), p.1926.

[22] Pfeifer, P., Avnir, D. and Farin, D., 1984. Scaling behavior of surface irregularity in the molecular domain: from adsorption studies to fractal catalysts. Journal of Statistical Physics,36(5-6), pp.699-716.

[23] Chambon, F. and Winter, H.H., 1985. Stopping of crosslinking reaction in a PDMS polymer at the gel point. Polymer Bulletin,13(6), pp.499-503.

[24] Muthukumar, M. and Winter, H.H., 1986. Fractal dimension of a crosslinking polymer at the gel point. Macromolecules,19(4), pp.1284-1285.

[25] Kaufman, J. H.; Baker, C. K.; qazzal, A. I.; Flickner, M. Melroy, 0. R. Phys. Rev. Lett. 1986, 56, 1932.

[26] Chu, B., Wu, C., Wu, D.Q. and Phillips, J.C., 1987. Fractal geometry in branched epoxy polymer kinetics.Macromolecules, 20(10), pp.2642-2644.

[27] Chow, T.S., 1991. Fractal dynamics in polymeric glasses.Physical Review A, 44(10), p.6916.

[28] Sapoval, B., Rosso, M. and Gouyet, J.F., 1985. The fractal nature of a diffusion front and the relation to percolation.Journal de Physique Lettres, 46(4), pp.149-156.

[29] Ziff, R.M. and Sapoval, B., 1986. The efficient determination of the percolation threshold by a frontier-generating walk in a gradient. Journal of Physics A: Mathematical and General,19(18), p.L1169.

[30] Sapoval, B., Rosso, M. and Gouyet, J.F., 1989. Fractal interfaces in diffusion, invasion and corrosion (pp. 227-245). New York: Wiley.

[31] Wool, R.P. and Long, J.M., 1993. Fractal structure of polymer interfaces. Macromolecules, 26(19), pp.5227-5239.

[32] Jones, J.L. and Marques, C.M., 1990. Rigid polymer network models. Journal de Physique, 51(11), pp.1113-1127.

[33] Dahmani, M., Fazel, N., Munch, J.P. and Guenet, J.M., 1997. Poly (vinyl chloride) thermoreversible gels: A fractal approach to the relation between structure and mechanical properties.Macromolecules, 30(5), pp.1463-1468.

[34] Dhar, D., 2005. Branched polymers on the Given-Mandelbrot family of fractals. Physical Review E, 71(3), p.031801.

[35] Amir, S., Mohamed, N.S. and Ali, S.A.H., 2010. Simulation model of the fractal patterns in ionic conducting polymer films.Central European Journal of Physics, 8(1), pp.150-156.

[36] Li, N., Li, Y. and Wang, X., 2011. Fractal structures from amphiphilic random azo copolymer. Macromolecules, 44(21), pp.8598-8606.

[37] Sun, J., Wu, G. and Geng, J., 2013. Preparation of fractal-like structures of insoluble polythiophene via solvent vapor annealing of solid thermocleavable polythiophene films and subsequent thermal curing. Polymer journal, 45(8), p.813.

[38] Domenech, T., Zouari, R., Vergnes, B. and Peuvrel-Disdier, E., 2014. Formation of fractal-like structure in organoclay-based polypropylene nanocomposites. Macromolecules,47(10), pp.3417-3427.

[39] Li, X., Hirosawa, K., Sakai, T., Gilbert, E.P. and Shibayama, M., 2017. SANS study on critical polymer clusters of tetra-functional polymers. Macromolecules, 50(9), pp.3655-3661.

[40] Shin, S., Gu, M.L., Yu, C.Y., Jeon, J., Lee, E. and Choi, T.L., 2017. Polymer self-assembly into unique fractal nanostructures in solution by a one-shot synthetic procedure.Journal of the American Chemical Society, 140(1), pp.475-482.

[41] Kónya, J. and Nagy, N.M., 2018. Nuclear and radiochemistry. Elsevier, P249

[42] Mehrer, H., 2007. Diffusion in solids: fundamentals, methods, materials, diffusion-controlled processes (Vol. 155). Springer Science and Business Media, 27-28

[43] Evangelista L.R, Lenzi E.K, From Normal to Anomalous Diffusion, Cambridge University Press,P 74-75

[44] Rycroft, C.H. and Bazant, M.Z., 2005. Lecture 1: Introduction to Random Walks and Diffusion. Thecnical Report, Department of Mathematics-MIT, 2.

[45] Lecture Notes in Physics 2002 Stochastic Processes in Physics, Chemistry and Biology, LNP 557 (Edited by Freund J A and Poschel T, Berlin: Springer Publishing)

[46] Shukla, P.K. and Mamun, A.A., 2002. Introduction to Dusty Plasma Physics (Bristol: IOP).

[47] Stacey W H 2001 Nuclear reactor physics (New York: Wiley Publishing)

[48] Haus, J.W. and Kehr, K.W., 1987. Diffusion in regular and disordered lattices. Physics Reports, 150(5-6), pp.263-406.

[49] Bouchaud, J.P. and Georges, A., 1990. Anomalous diffusion in disordered media: statistical mechanisms, models and physical applications. Physics reports, 195(4-5), pp.127-293

[50] Sabhapandit. S., 2010,Lecture notes on Stochastic process, RRI school on Stastical Physics

[51] rw Chapter 2 Random Walk. https://ocw.mit.edu/courses/mathematics/18-366 random walks and diffusion fall 2006/lecture-notes/lec01.pdf

[52] http://physics.bu.edu/ redner/542/book/rw.pdf

[53] Hughes B.D., Random Walks and Random Environments, Vol. 1: Random Walks, OxfordUniversity Press, Oxford, 1995.

[54] Montroll, E.W. and Weiss, G.H., 1965. Random walks on lattices. II. Journal of Mathematical Physics, 6(2), pp.167-181.

[55] H. Scher and EW Montroll, Phys. Anomalous transit-time dispersion in amorphous solids (1975). Phys. Rev. B, 12, p.2455.

[56] Metzler, R. and Klafter, J., 2000. From a generalized chapman - kolmogorov equation to the fractional klein - kramers equation. The Journal of Physical Chemistry B, 104(16), pp.3851-3857.

[57] Chechkin, A.V., Gonchar, V.Y., Klafter, J. and Metzler, R., 2006. FUNDAMENTALS OF LE "VY FLIGHT PROCESSES.

[58] Shlesinger, M.F., West, B.J. and Klafter, J., 1987. Lévy dynamics of enhanced diffusion: Application to turbulence. Physical Review Letters, 58(11), p.1100.

[59] Alves, S.B., de Oliveira Jr, G.F., de Oliveira, L.C., de Silans, T.P., Chevrollier, M., Oriá, M. and Cavalcante, H.L.D.S., 2016. Characterization of diffusion processes: Normal and anomalous regimes. Physica A: Statistical Mechanics and its Applications, 447, pp.392-401

[60] http://physics.gu.se/ frtbm/joomla/media/mydocs/LennartSjogren/kap2.pdf

[61] Bunde, A. and Havlin, S., 1996. Percolation I. In Fractals and disordered systems (pp. 59-114). Springer, Berlin, Heidelberg.

[62] Renner, U., Schütz, G.M. and Vojta, G., 2005. Diffusion on fractals. In Diffusion in Condensed Matter (pp. 793-811). Springer, Berlin, Heidelberg.

[63] Gefen, Y., Aharony, A., Mandelbrot, B.B. and Kirkpatrick, S., 1981. Solvable fractal family, and its possible relation to the backbone at percolation. Physical Review Letters, 47(25), p.1771.

[64] Domany, E., Alexander, S., Bensimon, D. and Kadanoff, L.P., 1983. Solutions to the Schrödinger equation on some fractal lattices. Physical Review B, 28(6), p.3110.

[65] Renner, U., 1993. Stochastische Theorie von Transportprozessen in ungeordneten und fraktalen Systemen(Doctoral dissertation, Verlag nicht ermittelbar)

[66] Srivasatava, J.P., 2014. Elements of solid state physics. PHI Learning Pvt. Ltd.

[67] Rammal, R. and Toulouse, G., 1983. Random walks on fractal structures and percolation clusters. Journal de Physique Lettres, 44(1), pp.13-22.

[68] Balakrishnan, V., 1995. Random walks on fractals. Materials Science and Engineering: B, 32(3), pp.201-210.

[69] O Shaughnessy, B. and Procaccia, I, 1985. Diffusion on fractals. Physical Review A, 32(5), p.3073.

[70] Acedo, L. and Yuste, S.B., 1998. Short-time regime propagator in fractals. Physical Review E, 57(5), p.5160.

[71] Day, A.R. and Lubensky, T.C., 1982. E expansion for directed animals. Journal of Physics A: Mathematical and General, 15(6), p.L285.

[72] Havlin, S., 1984. Comment on the Aharony-Stauffer conjecture. Physical Review Letters, 53(17), p.1705.

[73] Alexandrowicz, Z., 1980. Critically branched chains and percolation clusters. Physics Letters A, 80(4), pp.284-286.

[74] Leath, P.L., 1976. Cluster size and boundary distribution near percolation threshold. Physical Review B, 14(11), p.5046.

[75] Hoshen, J. and Kopelman, R., 1976. Percolation and cluster distribution. I. Cluster multiple labeling technique and critical concentration algorithm. Physical Review B, 14(8), p.3438.

[76] Meakin, P., 1983. Formation of fractal clusters and networks by irreversible diffusion limited aggregation. Physical Review Letters, 51(13), p.1119.

[77] Majid, I., Ben-Avraham, D., Havlin, S. and Stanley, H.E., 1984. Exact-enumeration approach to random walks on percolation clusters in two dimensions. Physical Review B,30(3), p.1626.

[78] Havlin, S., Weiss, G.H., Ben-Avraham, D. and Movshovitz, D., 1984. Structure of clusters generated by random walks. Journal of Physics A: Mathematical and General, 17(15),p.L849.

[79] Hong, D.C., Havlin, S., Herrmann, H.J. and Stanley, H.E., 1984. Breakdown of Alexander-Orbach conjecture for percolation: Exact enumeration of random walks on percolation backbones. Physical Review B, 30(7), p.4083.

[80] Mitescu, C. D., 1983, Percolation Structures Processes, edited by G. Deutscher, R. Zallen and J. Adler, Ann. Isr. phys. Soc., Vol. 5 (Bristol, UK: Adam Hilger).

Chapter-3

Effect of Gamma Irradiation on the Molecular Weight Distribution of Solid Polymer Electrolyte: A Computer Simulation-based Theoretical Study on Deterministic Fractal Model.

Chapter 3

Effect of Gamma Irradiation on the Molecular Weight Distribution of Solid Polymer Electrolyte: A Computer Simulation-based Theoretical Study on Deterministic Fractal Model.

3.1. Introduction

As we have discussed in chapter-1, the application of gamma irradiation has significant impacts on different structural and transportational properties of the solid polymer electrolyte (SPE). Radiation-induced polymer molecules are involved in the chain scission process where the bigger size molecules are fragmented into the smaller ones. In association with that, they can also involve in radiation-induced chain cross-linking process where the formation of a new bond between two neighboring atoms eventually produces bigger size molecules[1,2]. Chain scission and chain crosslinking occur simultaneously resulting in a considerable amount of structural as well as morphological changes inside the host polymer sample[1,3]. Plenty of experimental research works have been performed across the globe to investigate the response of the host polymer sample to the external gamma irradiation[6–9]. But theoretical analysis of the experimentally observed results is yet to be done with more attention. Moreover, the theoretical configuration of the host polymer molecules happens to be a highly complicated topic of research because of their complicated and multipatterned structures. Researchers have followed various methods to find more convenient ways for the analysis of the host polymer structure theoretically.

In the present chapter, we have performed a theoretical investigation regarding the effect of gamma irradiation on the molecular distribution pattern of the host SPE through computer simulation. Here we have configured the host polymer matrix mathematically with the help of a fractal model and studied the impact of radiation-induced scission and cross-linking process on it. Theoretical modeling of polymer macromolecules having different branches and entanglements with the help of fractals has been reported earlier by some researchers[4,5]. A comparatively simpler approach has been adopted here by considering deterministic, loopless Vicsek fractal as a mathematical tool to configure both the mono-disperse and the poly-disperse polymer host. The result of the computer simulation is analyzed in detail and the variation of the molecular distribution pattern of the mathematically modeled host polymer matrix is studied with respect to the exposure time of the polymer sample to gamma irradiation (time step (t)).

3.2. Literature Review

Ferloni et al.[2] worked with pure polyethylene oxide (PEO) both in water solution and film as well as dry powder form. In addition to that, they have also used film and an aqueous

solution of composition $PEO_{20}LiCIO_4$. All of these samples were exposed to gamma irradiation at room temperature to study the variation in thermal as well as electrical behavior due to the cross-linking process. Moreover, an ESR study was performed to investigate the radiolytic degradation and cross-linking process in both solid and in an aqueous solution of PEO. The experimental study concludes that irradiation gives more impact on PEO and $PEO_n - LiClO_4$ in water solution rather than in solid polymer. Moreover, the mechanical strength and amorphous nature can be observed in a higher amount in the case of cross-linked polymer film melted at low temperature than the other samples, prepared in general casting method on the anhydrous state.

Moad et al.[10] have performed a survey of literature based on the quantitative analysis of radiation-induced degradation of the polymer in terms of two parameters: scission G(s) and cross-linking G(X). They have followed gel permeation chromatography (GPC), sedimentation velocity, and dynamic light scattering measurement to quantify the irradiation effect on the molecular size distribution and from this study, the value of G(s) and G(G) was estimated. The overall study confirms the fact that though the radiation-induced scission and cross-linking are random and cannot be useful to quantify the chemical change inside the polymer sample (based on the value of G(s) and G(X)) they give an authentic index of change of molecular size distribution and average molecular weight.

Suarez et al.[11] have worked with virgin low-density polyethylene (LDPE) and it was exposed to gamma irradiation up to 2000kGy with a dose rate of 2.5kGy/h at room temperature. Rockwell hardness measurements were done according to ASTM standard D785 using a Model RBS Pantec hardness tester follow the R scale (60kg and 0.5 in steel ball) before and after irradiation. The effect of gamma irradiation on the physical, chemical, mechanical properties of the material as well as the performance of the sample was characterized by various methods like Fourier transform infrared spectroscopy (FTIR), size exclusion chromatography (SEC), scanning electron microscopy (SEM), differential scanning calorimetry (DSC), optical absorption in the infrared range (near IR). They have observed that the respective properties e.g. gel content, hardness, yellowing, etc enhance with the increase of gamma irradiation dose. On the other hand cross-linking process predominates at the lower dose of irradiation whereas chain scission is processed at the higher dose.

Singh et al.[12] worked with $(PEG)_xLiClO_4$, made of poly(ethylene)glycol of molecular weight 2000 and $LiClO_4$. Analysis with DSC results in an enhancement in glass transition temperature and a reduction in the crystallinity with the increase in salt concentration. They have also performed ^1H and ^7Li NMR studies for the said sample and

observed that the ^1H linewidth as well as crystallinity fraction reduced with the enhancement in salt concentration. They have also reported the nature of the variation of ionic conductivity at room temperature.

Jurjiu et al.[13] used the bead and spring model which happens to be the generalization of the Rouse model for chains, to configure the polymer network. Generalized Gaussian Structure (GGS) has been discussed and investigated the method in which their connectivity matrix provides a good understanding regarding their relaxation pattern. Moreover, an Eigenvalue spectra for an entire series of regular fractal Sierpinski gasket has been presented. They have also mentioned the procedure to embed GGS inside the Euclidian spaces of low dimensions and suggested that the said GGS may show up naturally in cross-linked polymers. Mechanical moduli $G(\omega) and G^{"}(\omega)$ were calculated for a huge class of fractal structure and the results were compared with the respective measurement of long-chain branched polypropylene. In their next work[14], Jurjiu et al. have used Vicsek fractal as a mathematical tool as they resemble the tree-like hyperbranched structure and investigate their dynamics following the Zimm and Rouse condition. The necessary calculations were performed following GGS. Large size Vicsek fractal has been taken specifically in Rouse case and evaluate the Eigenvalues with the help of a very efficient method.

Pucic et al.[15] worked with PEO and studied the effect of gamma irradiation on the crystallization of the sample. They have applied gamma irradiation from ^{60}Co source in air and nitrogen environment and study the sensitivity in DSC that predict the change in crystallinity of PEO. The crystallization thermogram shows an additional peak due to the gamma irradiation in the air above the dose of 50 kGy which is caused by a polymorphic transition that results in additional macro conformation originated due to the degradation as well as cross-linking. After the irradiation in a higher dose, the change is more prominent. In the nitrogen environment, the width of the peak increased and the crystallization temperature decreased with dose due to the less perfect crystallization.

Amir et al.[16] have performed a simulation study to know about the growth of complex geometric patterns as well as the fractal-like behavior of $PEO - NH_4I$ polymer membrane. They prepared a polymer electrolyte membrane of Polyethylene Oxide-Ammonium Iodide ($PEO - NH_4I$) films by taking a different amount of PEO(mol. wt $\sim 6X10^5$) and NH_4I with different ratios $(80:20, 70:30 and 60:40)$. The structural characterization has been done based on the Wiener process which is a continuous-time stochastic process based on Brownian motion theory. The string production method of the L-system was used to simulate the program. The fractal dimension of the DLA structure is eventually matched

with the experimentally obtained fractal dimension.

Sharma et al.[17] have worked with CR-39 polymer and analyze the UV-Visible absorption spectra due to the virgin and gamma irradiation (20-800 kGy) on the said polymer. In this regard, they have used the Shimadzu Double beam Double Monochromator UV-Visible Spectrophotometer (UV-2550). The bandgap of CR-39 polymer was measured quantitatively by increasing the gamma irradiation up to 800kGy. More importantly, the existence of direct and indirect bandgap in CR-39 polymer has been reported for the first time to the best of the author's knowledge.

Sinha et al.[18] worked with $PEO - NH_4ClO_4$ to investigate the effect of gamma irradiation on this sample with doses of 2 and 10 kGy and the observable parameters were compared with the unirradiated sample. Impedance spectroscopy was used to measure the conductivity at 50^oC. Moreover, activation energy and the variation of admittance (real part) with frequency were also measured which provides a direct estimation of fractal dimension, as well as the microstructure of the sample. It was observed that though conductivity decreases at room temperature due to the application of irradiation it increases at a higher temperature. They also reported that the interface fractal dimension between conducting and insulating regions enhanced from 2.43 to 2.55 which eventually suggested greater irregular structure in 3-dimensional space.

Khafagy et al.[19] prepared a solid polymer electrolyte sample by blending different concentrations of $LiOH.H_2O$ salt with poly (vinyl alcohol) (PVA) with the help of gamma irradiation and casting techniques. Fourier transform, Raman spectroscopy, and XRD study were done for its structural characterization. On the other hand, DSC and TGA studies were done to understand the thermal properties of the sample. Moreover, the reduction in the ratio of crystalline PVA with lithium salt concentration was noticed from XRD spectra. They also studied the influence of salt concentration on crystallinity and the Isotactic regularity of PVA with the help of Raman spectra. The electrical properties of the film were also reported.

Change in crystallinity of a polymer electrolyte due to the application of gamma irradiation was extensively studied by Nanda et al.[1]. They used $PEO(1-x)ANH_4ClO_4(x)$ samples with x = 0.18 and irradiation was done from 10 to 50 kGy. The reduction in crystallinity was reported from DSC and XRD measurements. Viscosity measurement of the aqueous solution of the sample at the same concentration depicts an ultimate chain scission due to irradiation in association with some amount of cross-linking at a higher irradiation

dose which can be also conformed from the FTIR measurement. Their experimental studies concluded that gamma irradiation results in a reduction in crystallinity and improve in ionic conductivity. Tarafder et.al[20] worked with the same above mentioned sample and studied the variation in viscosity of the aqueous solution of the sample which also provide ideas regarding the variation in molecular weight and depicts its general correlation with ionic conductivity inside the solid polymer electrolyte.

Mukhopadhyay et. al.[21] has investigated the variation in the crystalline, thermal, and structural properties of PEO due to the application of gamma irradiation. Two different states i.e. powder (P-S series) and solution (P-L series) of PEO have been taken. DSC study confirms enhancement in crystallinity up to 20kGy for P-S series post which enhancement in the amorphous region has been observed till 30kGy of irradiation. On the other hand enhancement in crystallinity for the P-L series has been noticed around 7kGy which is followed by a sharp decreasing nature up to 30kGy. FTIR study confirms the generation of a new functional group due to gamma irradiation. Moreover, the variation in microstructural distribution, viscosity, distribution of amorphous and crystalline phases, etc. are also studied. In her other work, Mukhopadhyay et. al.[22] investigated the variation in porosity and pore size distribution of the films made by PEO powder due to the application of gamma irradiation using the BET adsorption technique. The pore size of the PEO films (made by both irradiated and un-irradiated powder)are found to have the pore dimension with the range 20-500nm. They primarily studied the tailored irradiation effect within the lower dose of 1-10 kGy. The overall porosity of PEO is increased up to 3kGy post which a linear reduction has been observed till 30kGy. The effect of high-energy irradiation on the particle and pore size variation correlates with the microstructure of the sample. Their work concludes that selective irradiation is capable of tailoring the pore size within a definite regime resulting in a reduction of the multimodal trait.

Raghu et al.[23] worked with $PEO - CdCl_2$ as a polymer electrolyte sample to study the variation in different physical and chemical properties as well as the structure and surface morphology due to the application of gamma irradiation on it. DSC and TGA study confirms the significant reduction in crystallinity and thermal stability of the film due to irradiation. FTIR study confirmed the degradation by chain scission/cross-linking reaction. An optical micrograph study confirms that the size of the spherulite structure and the surface roughness were reduced with the increase of irradiation dose. Similarly, the Urbach energy and optical band gaps (Eg) were measured and found to be decreased and the number of carbon atoms in a cluster enhanced with the irradiation dose.

KILIC et al.[24] investigated the dielectric and mechanical properties of low-density polyethylene (LDPE) doped with basalt minerals. The sample (composite film prepared by hot pressing method) was irradiated with gamma-ray from Co-60 source from 6 to 24 gray. Stress-strain measurement and dielectric spectroscopy were used to estimate the mechanical and dielectric properties within the frequency range of 100 Hz –15 MHz at room temperature. It was observed that the doping of basalt eventually reduced the mechanical properties of LDPE. Application of gamma irradiation reduces the mechanical properties of the LDPE and LDPE/salt composite at the almost same rate. On the other hand, the structure of the polymer is deteriorated also.

Manjunatha et al.[25] worked with poly(ethylene oxide) PEO-based solid polymer electrolyte system doped with NaBr salt. The change in morphology was investigated by the application of low-energy ion beam irradiation. The variation in conductivity and relaxation process of the system is then studied by the complex impedance spectra and it was observed that conductivity was enhanced by one order after irradiation. The temperature-dependent study suggests more disordered/amorphous behavior than the pure system. Moreover, XRD studies support this fact, as the peak width associated with a reduction in peak intensity, is increased. The Raman spectra studies also confirm the morphological changes inside the system as the disordered-longitudinal acoustic mode band can be observed.

3.3. Basic Assumptions for The Computer Simulation

In this chapter, we are aimed for a detailed investigation of the variation in structural properties theoretically with the help of computer simulation. The computer simulation performed here is based on some basic assumptions that are mentioned below:

a. The host polymer molecules under consideration are mathematically modeled with the help of deterministic, loopless, and finitely ramified Vicsek fractals. The molecular weight of an arbitrary molecule is represented by the respective fractal stage (s) of those fractals. Here (s) is an integer. The higher the molecular weight of the polymer molecule, the higher will be the value of its fractal stage (s). The concept of a monomer is incorporated by the fundamental unit cell (seed) of a Vicsek fractal. Hence, a polymer molecule that is modeled with an arbitrary fractal stage = s contains 5^s numbers of monomer units.

b. Application of gamma irradiation introduces a significant structural change inside the host polymer sample which is incorporated into the simulation with the help of two radiation-induced processes: scission and cross-linking. Scission and cross-linking processes

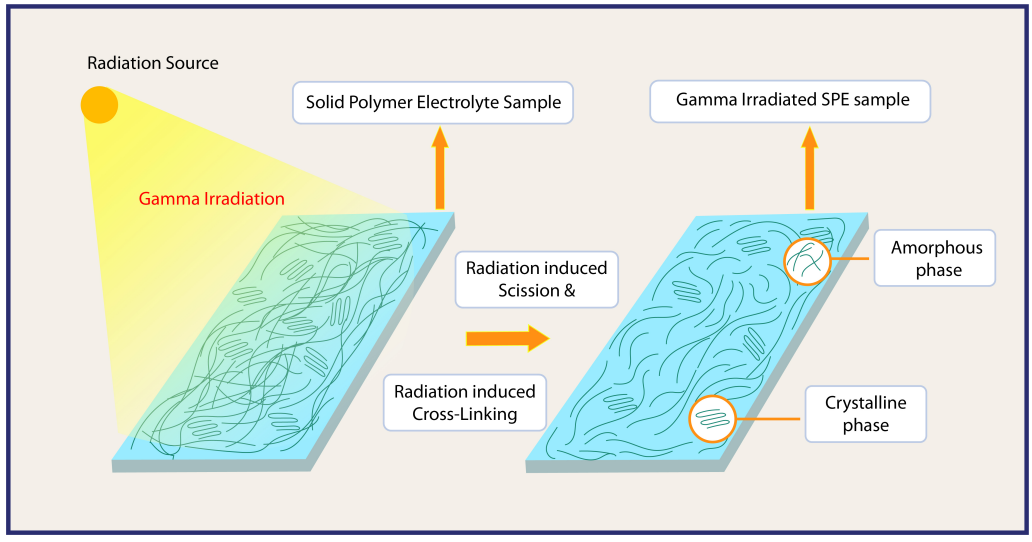

Figure 3.1: *Schematic diagram of solid polymer electrolyte (SPE) sample. The un-irradiated sample has an arbitrary arrangement of polymer chain segments. The application of gamma irradiation introduces crystalline and amorphous phases inside the sample which can be seen clearly*

are opposite by nature and they occur simultaneously inside the sample at the time of irradiation.

c. The effect of gamma irradiation on the polymer sample is assumed to be instantaneous and the molecules inside the sample absorb 100 % of the applied radiation energy which implies that there is no dissipation of applied radiation energy in the intermediate stages.

d. There exist different types of physical and chemical factors such as the addition of plasticizer, fillers, salt, ionic liquid or blending of polymer, etc.,[26–33] that introduce significant alteration in different structural properties inside the host polymer sample. In our present research study, we have not taken into account those factors to avoid any additional complexity in the simulation algorithm. Hence, the morphological changes of the host polymer sample are assumed to be solely responsible for the external irradiation only.

e. The radiation-induced intermolecular cross-linking process is assumed to take place between the polymer molecules that are modeled with Vicsek fractals with the same fractal stage (s). Thus, at least 5 molecules (Vicsek fractal) with the same arbitrary stage=s must be needed to have a successful intermolecular cross-linking process to produce a bigger size molecule with subsequent higher fractal stage=(s+1). Cross-linking between molecules

having different fractal stages has not been taken into account for the sake of the simplicity of the simulation process.

f. In the case of a practical sample, both the interchain and intra-chain cross-linking processes take place simultaneously as a consequence of gamma irradiation. But in the present case, the inclusion of intra-molecular cross-linking will make the system more complicated, thus failing to fulfill the purpose of its use. Hence, we have taken into account only the inter-molecular cross-linking process to avoid any additional complicacy in the simulation.

g. The probability of having scission and/or cross-linking processes inside an arbitrary polymer molecule is directly proportional to the area of its exposure to external irradiation. The area of exposure to the external irradiation is directly linked with the molecular weight or the fractal stage (s) of the Vicsek fractal. Molecules with higher fractal stages expose themselves more to the incident gamma irradiation. Hence, the bigger size molecules have a higher chance to involve themselves in radiation-induced scission or cross-linking process.

h. The number of molecules with a definite fractal stage (s) that responds to the radiation-induced scission and/or cross-linking process is proportional to the total number of polymer molecules with that particular fractal stage (s), present inside the sample at that irradiation time step (t).

i. The intensity of the gamma irradiation is taken as a constant factor in our simulation. Rather we vary the time of exposure (t) of the polymer molecule to the external irradiation. Hence, the variation of different morphological properties has been investigated in our present chapter with respect to the exposure time of the sample to external irradiation. We have mentioned this parameter in our entire thesis as exposure time to irradiation or time steps (t)

3.4. Novelty of Using Vicsek Fractals as a Mathematical Tool for Modelling Polymer Sample

Experimental research studies regarding the structural characterization of polymer materials confirm the fractal-like behaviour of different polymer samples[34–36] which have already been discussed in the chapter-2. Owing to this fact, many researchers construct polymer samples mathematically with the help of fractals which are stochastically self-similar[37,38]. But,

despite the resemblance of stochastic fractals with the real polymer sample, they have some limitations to be used as a mathematical tool for constructing host polymer substrate as it introduces some additional complexity into the computer simulation process. Moreover, the determination of intrinsic parameters like fractal dimension (d_f) happens to be a major point of concern in that case. In that context, the use of deterministic fractals is deemed to be an appropriate way to study different structural and dynamical properties of the polymer sample. The application of the Vicsek fractal for modeling the hyperbranched polymers by studying the Eigenvalue spectrum has been reported earlier by some researchers[39,40]. In the present work, Vicsek fractal has been used as a mathematical tool to construct the host polymer sample. The structural pattern of Vicsek fractal of the first five stages (1st stage to 5th) has been shown in the figure-3.2. The main advantages that compelled us to use Vicsek fractal as a tool in our present siumulation is mentioned below: a. Vicsek

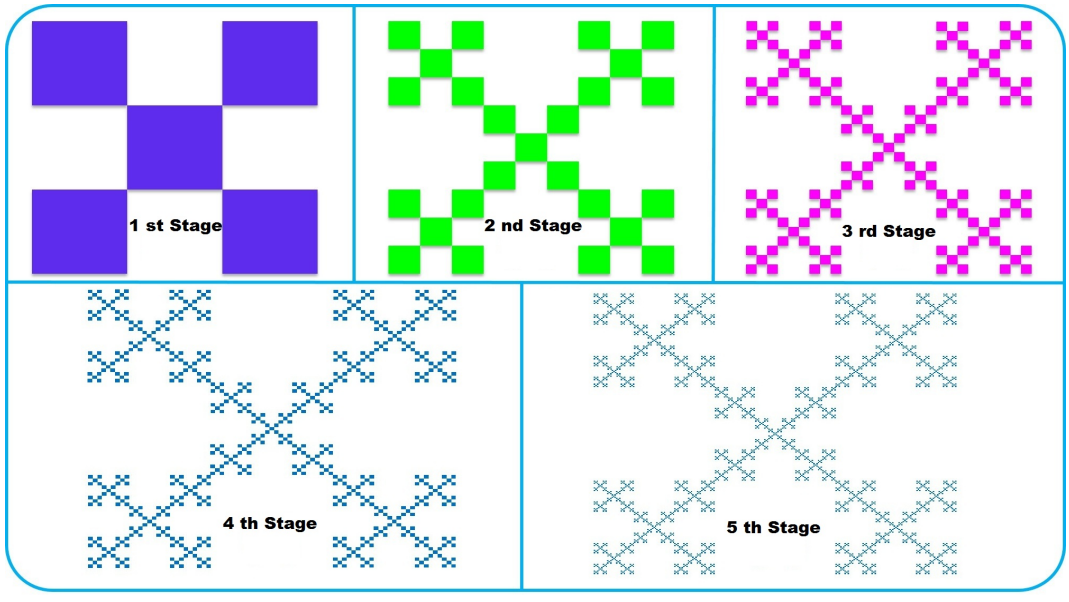

Figure 3.2: *Schematic representation of Vicsek fractal from 1st to 5th stage. It can be observed clearly that the number of monomers and the structural complexity is increased rapidly but the self-similarity behavior is maintained perfectly.*

fractal is a deterministic fractal, so the self-similarity property is maintained perfectly. Any stage of this fractal can be generated following a definite iterative rule. The actual polymer substrate contains a collection of a large number of polymer molecules with different molecular weights. Therefore, it is easier to construct the host polymer system with the help of Vicsek fractal having different fractal stages (s).

b. Fractal dimension (d_f) of deterministic fractals can be estimated using some

simple mathematical techniques[41]. Vicsek fractal is not an exception to this fact. The fractal dimension of Vicsek fractal is:

$$(d_f) = \frac{ln(5)}{ln(3)} = 1.465 \tag{3.1}$$

This numerical value remains the same for all the stages (s). On the other hand, the determination of the fractal dimension for a random fractal is not so straightforward and requires some rigorous approaches.

c. Vicsek fractal is a loopless fractal. Different structural and other properties of loopless fractal have already been discussed elaborately in the second chapter. The intrinsic loopless nature of the Vicsek fractal enables one to relate it easily with the polymer molecules having multiple branches with a defined backbone.

d. Study of different transport properties inside an fractal object requires a clear knowledge regarding the dynamic and structural exponents. In case of loopless, branched,deterministic fractals, the study of different transport properties becomes easier as there exist exact mathematical relations among the structural and transport exponents[42–44]. The diffusion exponent (d_w), spectral dimension (d_s), and the diffusion exponent in chemical space (d_w^l) can be expressed as[43,44]:

$$\begin{aligned} d_w &= d_f(1+\frac{1}{d_l}) \\ d_s &= \frac{2d_l}{(d_l+1)} \\ d_w^l &= d_l+1 \end{aligned} \tag{3.2}$$

Here d_l stands for the chemical distance exponent. In the case of Vicsek fractal, d_f and d_l can be evaluated with the help of some simple mathematical rules. Hence, the above mentioned dynamical exponents can be evaluated very easily by following the above relations.

e. The ramification happens to be one of the important parameters for the structural characterization of a fractal. A detailed discussion pertaining to ramifications has been carried out in the previous chapter. In the case of finitely ramified loopless fractals, the diffusion exponent (d_w) can be estimated in a comparatively easier process. Vicsek fractal is a finitely ramified fractal and therefore, the application of Vicsek fractal to configure polymer samples helps one to evaluate different dynamic exponents easily.

Considering all these structural advantages of the Vicsek fractals, mentioned above, one can conclude the relevance of its use for the mathematical modeling of polymer materials

in our present simulation study.

3.5. Method of Computer Simulation

The entire computer simulation has been carried out on both mono-disperse as well as poly-disperse SPE samples. We will discuss the method of the computer simulation for both cases in the preceding subsections.

3.5.1. Modelling of the Host Polymer Sample

The polymer system in general is partially crystalline[45,46]. The crystallinity part depicts a regular stack of chains while a complete disordered arrangement of those chain segments can be observed in the amorphous phase. The order of crystallinity and the type of arrangements of the polymer chain segments vary from system to system depending on various factors. On the other hand, entanglement, branching, etc. of the polymer chains introduce other degrees of complexities. In the present section, we will discuss the method of using the Vicsek fractal, corresponding to a certain stage with a definite structure and length to model the host solid polymer electrolyte sample.

Despite the artificiality in the present mathematical modeling, its application may yield the results which is highly relevent for us. The structural characteristics of a Vicsek fractal have been discussed in chapter-2. Here a linear polymer chain has been modelled by joining the Vicsek fractals with different stages diagonally side by side in a two-dimensional Euclidean plane. This particular type of arrangement represents a linear chain of a polymer molecule with branches of different lengths. In our present work, we have used the Vicsek fractal to construct two types of host polymer samples: a. mono-disperse and b. poly-disperse polymer sample.

3.5.2. Modelling of Mono-disperse SPE Sample

A host polymer sample is said to be monodisperse when all the polymer molecules inside the sample have the same molecular weight. In order to construct such kind of mono-dispersed polymer sample, one needs to use Vicsek fractals having the same fractal stage (s). The structural units (smallest square boxes of unit length) of the Vicsek fractal of any arbitrary stage have been considered as the monomer. Thus, if N numbers of Vicsek fractals of

the stage (s) are used to construct a mono-disperse linear chain, then the total number of monomers will be:

$$N_m = N.5^s \tag{3.3}$$

In our present simulation study, we have used 1000 numbers of 7th Vicsek fractals to model the mono-dispersed host polymer sample. Hence, the total number of monomers present in the sample is:

$$N_m = 1000.5^7 = 78125000 \tag{3.4}$$

It should be noted that the application of gamma irradiation may change the molecular

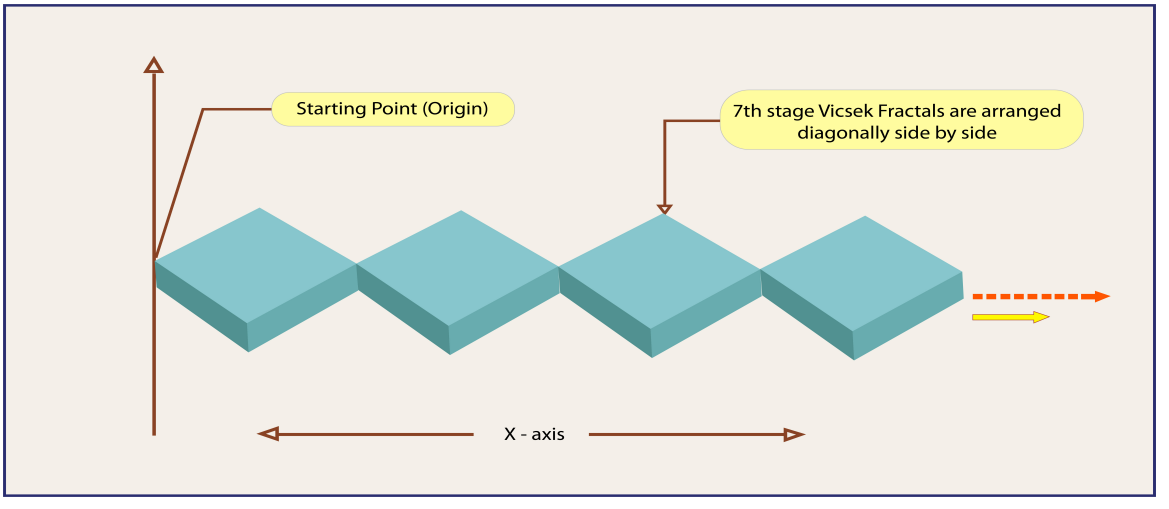

Figure 3.3: *Schematic representation of 1-dimensional mono-disperse polymer sample, modeled by 7th stage Vicsek fractals. Here Vicsek fractals are arranged linearly side by side and joined diagonally with each other along X-axis. 7th stage Vicsek fractal have a highly complicated structure that may not be observable easily in the present scaling, Therefore they are represented by the green squares in the picture.*

weight distribution pattern of the sample and make it poly-disperse, but the total number of monomers, present inside the sample, will be conserved throughout the irradiation process according to the law of conservation of mass. Thus, 78125000 monomers will always be conserved. The radiation-induced scission process breaks bigger size molecules into smaller ones and as a result, a large number of molecules, with lower values of fractal stages are generated inside the sample. With the passage of irradiation time steps(t), the number of smaller size molecules increases so rapidly that the molecular distribution curves for all the

required time steps can not be fitted in a single picture. This difficulty is eliminated by introducing a new parameter which is known as "Weight Fraction: $W_f(s,t)$". It is the ratio between the total numbers of monomers used for modelling polymer molecules with fractal stage= s at the time step = t to the net number of monomers, present in the host polymer sample. It can be expressed mathematically as:

$$W_f(s,t) = \frac{N(s,t).5^s}{\Sigma N(s,t).5^s} \tag{3.5}$$

In present case of mono-disperse sample we can write:

$$W_f(s,t) = \frac{N(s,t).5^s}{78125000} \tag{3.6}$$

Where A= $\Sigma N(s,t).5^s = 78125000$ is the total number of monomers present in the sample. $W_f(s,t)$ also signifies the probability of finding a polymer molecule with a fractal stage (s) in the host polymer sample at a certain irradiation time (time step (t)). A schematic diagram of the 1-D mono-disperse polymer sample has been shown in figure-3.3. The mono-disperse polymer sample is an idealized concept, and in real scenarios, polymer samples are poly-disperse in nature. Hence, the same investigation is carried out for a poly-disperse polymer sample to get a more realistic result.

3.5.3. Modeling of Poly-Disperse SPE Sample

The present subsection is aimed for a detailed description regarding the mathematical modelling of an arbitrary host poly-disperse polymer electrolyte sample. Unlike the mono-disperse sample, molecules don't have the same molecular weight (fractal stage). Rather Vicsek fractal with some definite stages (s) has been chosen to configure the sample mathematically. Hence their probability of existence in the linear chain has an impact on the nature of the weight fraction ($(W_f(s,t))$) distribution curve. As we have discussed, fractals are arranged randomly in a linear chain in both the mono-disperse and poly-disperse cases. In the case of a poly-disperse system, the polymer chain is not homogeneous, and its side branches are of different lengths as shown in figure-3.4.

The choice of molecular size (fractal stage (s)) depends on the objective of the simulation. In the present case, the number of molecules (N(s,t)), as well as their respective fractal stages (s), are chosen such a fashion that the parameter weight fraction ($W_f(s,t)$)

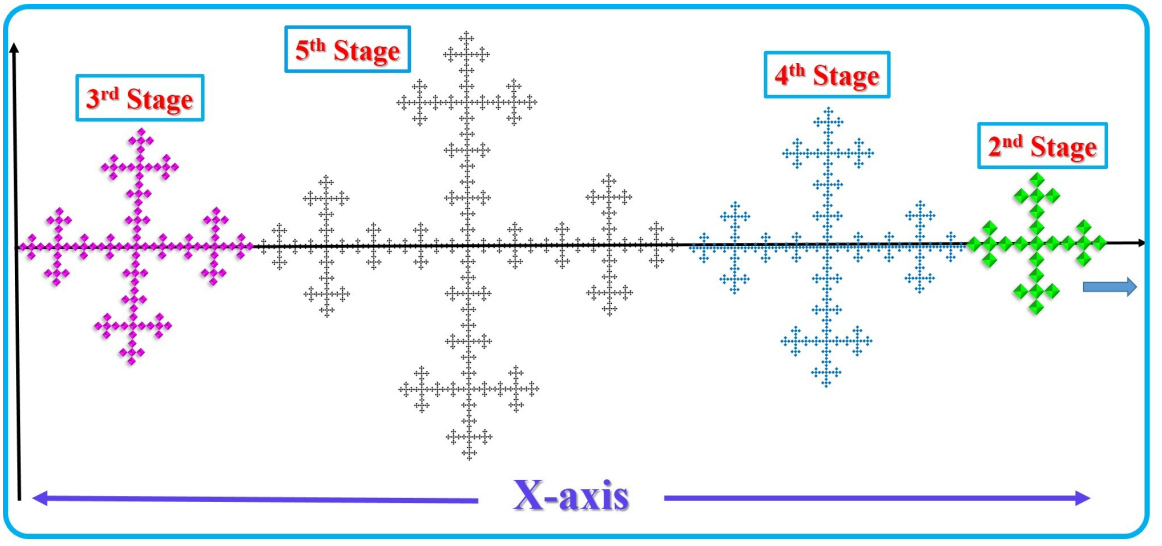

Figure 3.4: *Schematic representation of an un-irradiated poly-disperse sample, modeled by Vicsek fractals of different fractal stages. A random arrangement of* 2nd,3rd,4th,5th, *stages Vicsek fractals has been shown here. They are joined diagonally with each other along X-axis. It should be noted that the figure only shows the random alignment of the Vicsek fractals but they are not drawn as per their original scalling for better visualization.*

of the chosen molecules shows a symmetric distribution pattern for the unirradiated sample. $(W_f(s,t))$ signifies the probability of finding a molecule with the fractal stage (s) at irradiation time step (t) inside the polymer sample. As per our assumption, the impact of gamma irradiation on an arbitrary type of polymer molecule (molecules with a definite fractal stage) depends on the probability of their presence inside the sample. Therefore, the symmetric distribution behaviour of $(W_f(s,t))$ indicates symmetry in the probabilistic existence of the polymer molecules in the un-irradiated sample. Initially, we have considered a host polymer sample where 500 molecules are modelled with 5th stage Vicsek fractal, 200 molecules with 6th stage, and 20 molecules that have a fractal stage (s) = 7 . Thus, a total 720 number of polymer molecules are present inside the un-irradiated sample initially. The system is therefore considered as poly-disperse by nature. The total number of monomers present in the poly-disperse sample is:

$$\Sigma N(s,0).5^s = 500.5^5 + 200.5^6 + 20.5^7 = 6250000 \tag{3.7}$$

The weight fraction $(W_f(s,t))$ of molecules with the above mentioned fractal stages of the un-irradiated polymer sample can be calculated readily following the formula mentioned in equation-(3.5)

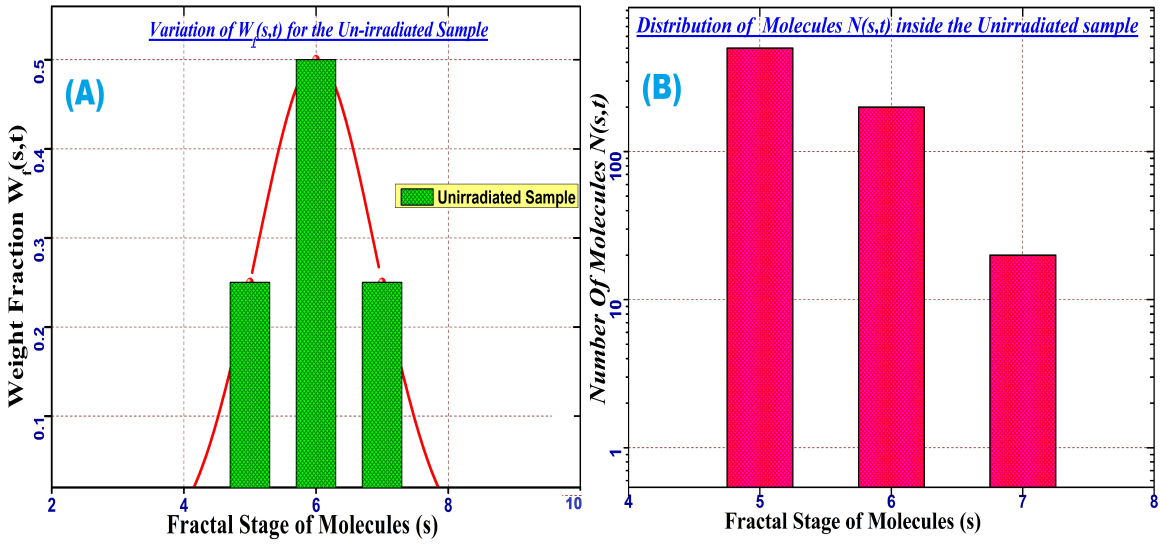

Figure 3.5: *Graphical representation of the molecular distribution among different fractal stages of an un-irradiated mono-disperse polymer sample, modeled by Vicsek fractals.(A) Symmetric distribution of weight fraction* $(W_f(s,t))$ *among* $5^{th}, 6^{th}, 7^{th}$ *stages. (B) Distribution of molecules N(s,t) among those stages. N(s,t) is plotted in log scale for better understanding.*

Thus, 500 numbers of molecules which are modeled with 5th stage fractal have the $(W_f(s,0) = W_f(5,0))$ value:

$$W_f(5,0) = \frac{N(5,0).5^5}{\Sigma_s N(s,0).5^s} = \frac{500.5^5}{6250000} = 0.25 \tag{3.8}$$

200 numbers of molecules which are modeled with 6th stages fractal have the $(W_f(s,0) = W_f(6,0))$ value:

$$W_f(6,0) = \frac{N(6,0).5^6}{\Sigma_s N(s,0).5^s} = \frac{500.5^6}{6250000} = 0.5 \tag{3.9}$$

20 numbers of molecules which are modeled with 7th stages fractal have the $(W_f(s,0) = W_f(7,0))$ value:

$$W_f(7,0) = \frac{N(6,0).5^7}{\Sigma_s N(s,0).5^s} = \frac{500.5^7}{6250000} = 0.25 \tag{3.10}$$

Thus, the weight fraction distribution $(W_f(s,0))$ of the initial un-irradiated sample shows a centrally peaked symmetric distribution which is shown in the figure-3.5.

3.5.4. Implementation of Scission and Cross-linking Process Mathematically

The linear arrangement of the polymer molecules with Vicsek fractals having the same as well as different fractal stages (s) for both mono-disperse and poly-disperse samples is shown in the figure-3.3 and figure-3.4. Experimental studies have reported that the application of external irradiation on polymer samples introduces some significant consequences such as the generation of new functional groups, rearrangement of molecular bonds, scission and/or cross-linking of polymer branches, etc.[1,2,47,48]. It was also reported that different physical and chemical factors such as radiation dose, the existence of oxygen, nature of the polymer concerned, the addition of plasticizers, etc. also affect the rate of scission and cross-linking[47,48]. In the present computer simulation, the effect of gamma irradiation has been incorporated through two simultaneous processes inside the host polymer molecule: scission and cross-linking. Scission is the disintegration of polymer molecules into smaller

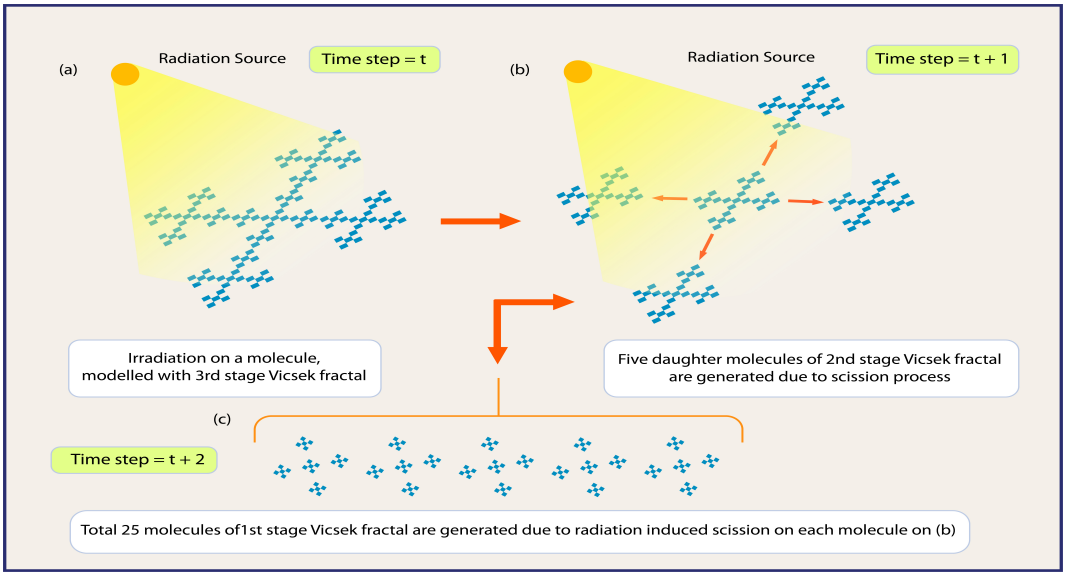

Figure 3.6: *Schematic representation of the radiation-induced intra-molecular scission process inside the SPE sample, modelled by Vicsek fractal. Here, scission process is presented in two consecutive time steps on* 3rd *and* 2nd *stage Vicsek fractal respectively.*

chain fragments. As a consequence, molecules having smaller molecular weights are produced in large numbers, while the overall average molecular weight of the sample is reduced considerably. The concept of scission, in the present computer simulation, is incorporated on Vicsek fractal of a definite fractal stage (s) which has been mentioned before. When

external gamma irradiation is applied on an arbitrary polymer molecule with a definite fractal stage (s) and molecular weight 5^s, it disintegrates into 5 daughter molecules due to the radiation-induced scission process at an arbitrary time step=t+1. The daughter molecules thus generated, are identical by nature but smaller in size whose fractal stages happen to be the immediately previous stage of the parent molecule i.e. $(s-1)^{th}$ stage. Therefore, each of the daughter molecules has a molecular weight of $5^{(s-1)}$.

In the next irradiation time step i.e. at t= t+2, each of the byproduct molecules having fractal stage s= (s-1), disintegrates through scission into 5 identical daughter molecules, smaller in size having fractal stage (s-2) and molecular weight $5^{(s-2)}$. Thus, a single molecule of sth fractal stage at an arbitrary time step=t, degrades into a total 25 number of identical molecules, smaller in size with fractal stage s=(s-2) at the irradiation time step t= t+2. This process will go on and at the nth irradiation time step (t=n), the total number of byproduct molecules will be 5^n which are identical and with fractal size (s-n) where $s > n$. The disintegration pattern due to the scission process of an arbitrary parent molecule is the same irrespective of its fractal stage so that we can apply the same iterative disintegration rule for all irradiation doses. The process of scission in a polymer molecule with a fractal stage (s) for two consecutive irradiation steps (t) is shown in the adjoining figure-3.6. Cross-

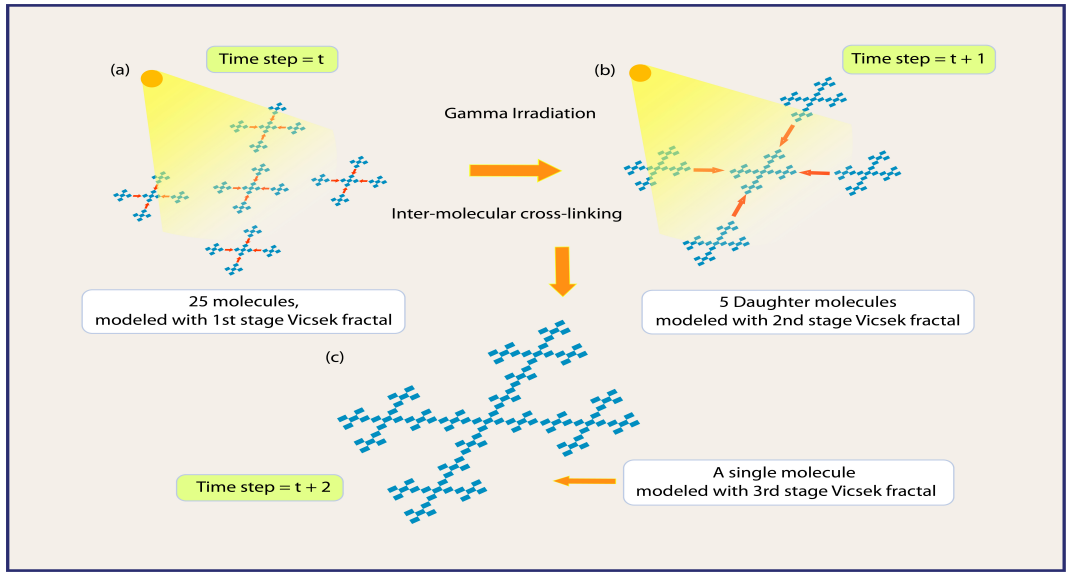

Figure 3.7: *Schematic representation of the radiation-induced inter-molecular Cross-linking process inside the SPE sample, modelled by Vicsek fractal. Here, scission process is presented in two consecutive time steps on 3rd and 2nd stage Vicsek fractal respectively.*

linking happens to be the opposite phenomenon of scission which is considered as another

radiation-induced process taking place in our simulation. Under the application of external irradiation and in presence of a suitable physical and chemical environment, polymer chain segments cross-link with each other at some definite sites by the formation of inter and/or intra-molecular chemical bonds and generate molecules with higher molecular weight. In most cases, cross-linking process generates more structural complexity inside the polymer sample and a higher probability of crystallization.

The implementation of cross-linking in our present simulation is done by joining identical Vicsek fractals having the same fractal stage (s). The cross-linking sites inside the molecules, modeled with Vicsek fractals, are definite and the possibility of intra-molecular cross-linking has not been taken into account as per our assumption. Therefore, in each case of the radiation-induced cross-linking process, molecules follow the same iterative technique to join with each other and produce bigger size molecules. To explain the implementation of the radiation-induced cross-linking process in our simulation, let us consider the situation when external irradiation is applied on the polymer molecules (Vicsek fractal) with a fractal stage (s) at the irradiation time step=t. The cross-linking process enables five identical polymer molecules having fractal stage (s) and molecular weight 5^s to join following a definite joining rule and produce a bigger size molecule with a fractal stage (s+1) and molecular weight $5^{(s+1)}$ at the irradiation time step t=(t+1). At the next irradiation time step t=(t+2), 5 molecules (Vicsek fractal) of the fractal stage (s+1) are joined by virtue of intermolecular cross-linking process following the same joining technique and produce a molecule with a fractal stage (s+2) and molecular weight $5^{(s+2)}$. This process will continue iteratively for the next higher irradiation time steps.

Thus, if we consider a host polymer system with an initial 5^n number of un-irradiated polymer molecules (Vicsek fractal) with a fractal stage (s) and molecular weight 5^s, then after n irradiation time steps i.e. t=(t+n), all these 5^n molecules with an initial stage (s) are joined iteratively and produce a single large molecule of the fractal stage (s+n) and molecular weight $5^{(s+n)}$. The process of cross-linking in Vicsek fractal for two consecutive steps has been shown in the figure-3.7. Radiation-induced scission and cross-linking processes occur simultaneously inside a real polymer sample and they cannot be measured separately at the time of irradiation. In our present simulation, the probability of scission inside the polymer sample is implemented by a variable X and the probability of cross-linking is incorporated through (1-X). The magnitude of X varies between two boundary values 0 and 1 i.e. $0 \leq |X| \leq 1$. The two boundary values represent two extreme cases which are as follows:

1. The upper limit i.e. X=1 represents 100% scission process which is an extreme case of radiation-induced scission process where all the polymer molecules with any arbitrary fractal stage disintegrate into daughter molecules. No cross-linking process is observed inside the system. 100 % scission is an idealized situation and can not be observed practically inside the sample at the time of external radiation.

2. The lower limit i.e. X=0 or (1-X) =1 stand for another extreme case where all the host polymer molecules are involved in the intermolecular cross-linking process in response to the external irradiation. In this case, the probability of the radiation-induced scission process is zero. This happens to be another idealized situation.

The value of X in between these two above-mentioned extreme cases represents the real situation where scission and cross-linking phenomena take place simultaneously. Besides these two special cases (i.e. the cases for X=0 and X=1) the entire intermediate radiation-induced process is classified into three regions depending upon the value of X for both mono-dispersive and poly-dispersive systems:

1. When the value of X is greater than 0.5 and less than 1.0, the probability of scission takes a lead over the cross-linking process. This region is named as the scission dominating region.

2. When X takes any value between 0.5 and 0, the probability of the cross-linking process is greater than that of scission. This region is known as the cross-linking dominating region.

3. The value of X=0.5 represents another special case where the radiation-induced scission and cross-linking process take place with equal probability.

3.5.5. Master Equation to Calculate the Molecular Weight Distribution

The impact of the scission and cross-linking process on the solid polymer system and the method of inclusion of these two radiation-induced processes into the simulation have already been discussed in the previous section. It is very evident that the external perturbation by gamma irradiation results in significant structural changes inside the system, keeping the total number of monomers unaltered. In our present simulation study, the number of molecules with different fractal stages (s) at an irradiation time step (t)(N(s,t)) has been evaluated from a Master Equation which will be extensively discussed here.

Let us consider the host polymer sample contains the total N(s,t) number of polymer molecules (Vicsek fractals) with a fractal stage(s) at the irradiation time step=t. N(s,t) appears as an element of the $(s \times t)$ matrix in our present simulation. According to the assumption, we have taken, the probability of sth stage molecules ($P_{VN}(s,t)$) to participate in the radiation-induced scission and the cross-linking process will depend on the total number of molecules (Vicsek fractal) with s^{th} fractal stage that is present inside the system at the irradiation time step =(t-1). The probability can be written as:

$$P_{VN}(s,t) = \frac{N(s,t-1).5^s}{\Sigma N(s,t-1).5^s} \tag{3.11}$$

Hence the total number of molecules with s^{th} fractal stage that will participate in the radiation-induced reaction at the radiation time step=t, will be:

$$\begin{aligned} N_T(s,t) &= N(s,t-1).P_{VN}(s,t) \\ &= N(s,t-1).\frac{N(s,t-1).5^s}{\Sigma N(s,t-1).5^s} \end{aligned} \tag{3.12}$$

The rest of the molecules having a fractal stage (s) will not respond to the irradiation at the irradiation time step (t). The number of molecules that will be unaffected by external irradiation will be :

$$\begin{aligned} N_U(s,t) &= N(s,t-1) - N_T(s,t) \\ &= N(s,t-1) - N(s,t-1).P_{VN}(s,t) \\ &= N(s,t-1) - N(s,t-1).\frac{N(s,t-1).5^s}{\Sigma N(s,t-1).5^s} \end{aligned} \tag{3.13}$$

$N_T(s,t)$ represents the total number of outgoing molecules from the set of sth stage molecules by both the scission and cross-linking process at any arbitrary radiation time step (t). The number of molecules that are affected by the incident radiation will either degrade due to the scission process or undergo intermolecular cross-linking. The feasibility of the scission process inside the polymer host is incorporated into the simulation with the help of a scission parameter X and the value of this parameter is assumed to be known and is provided externally. Hence the total number of molecules having fractal stage (s) that will participate in the radiation-induced scission process ($N_{sc}^{out}(s \to (s-1),t)$) can be written as:

$$\begin{aligned} N_{sc}^{out}(s \to (s-1),t) &= X.N_T(s,t) \\ &= N(s,t-1).\frac{N(s,t-1).5^s}{\Sigma N(s,t-1).5^s}.X \end{aligned} \tag{3.14}$$

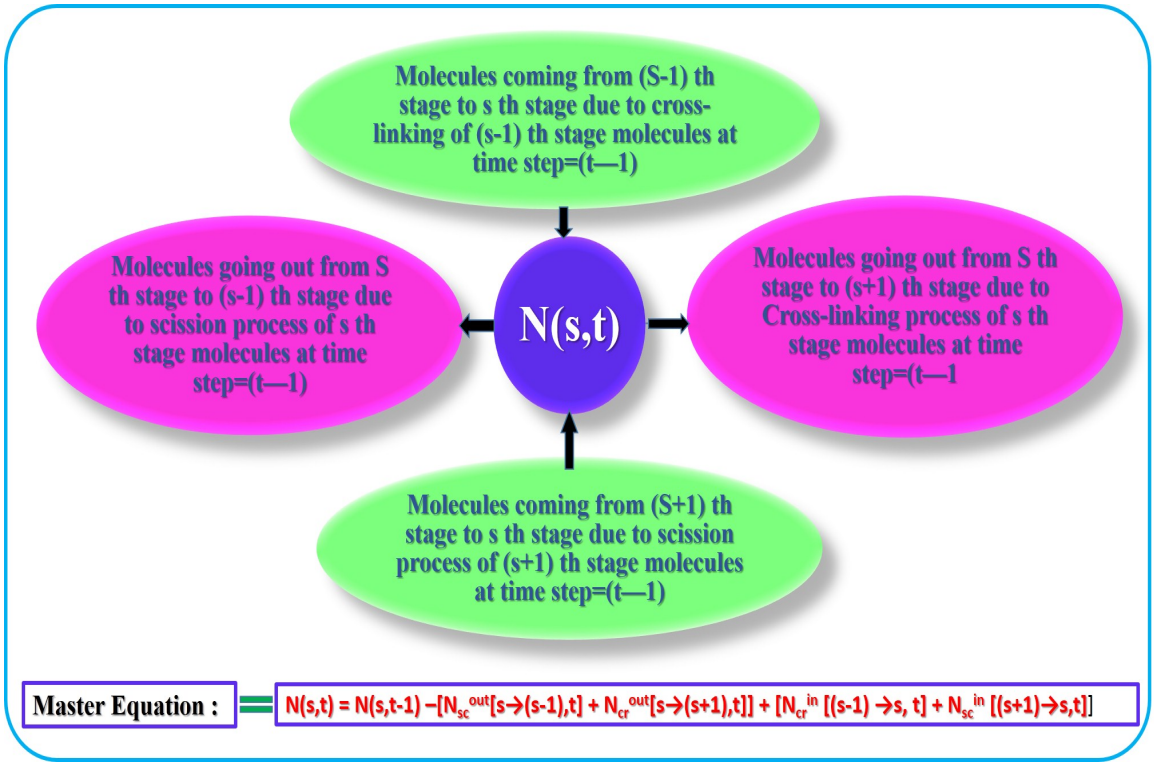

Figure 3.8: *Schematic representation of the computer simulation algorithm*

Each of these molecules with a fractal stage (s) will disintegrate into five identical molecules with a fractal stage (s-1) and therefore they are included in the set of $(s-1)^{th}$ fractal stage molecules. Thus the total number of incoming molecules $(N_{in}(s-1,t))$ into the set of $(s-1)^{th}$ stage molecules from the set of sth stage at the irradiation time step=t will be:

$$\begin{aligned} N_{in}(s-1,t) &= 5.N_{sc}^{out}(s \rightarrow (s-1),t) \\ &= 5.N(s,t-1).\frac{N(s,t-1).5^s}{\Sigma N(s,t-1).5^s}.X \end{aligned} \tag{3.15}$$

The number of molecules with s^{th} fractal stage that will respond to the radiation-induced cross-linking process at the instance of exposure time t, will be :

$$\begin{aligned} N_{cr}^{out}(s \rightarrow (s+1),t) &= (1-X).N_T(s,t) \\ &= N(s,t-1).\frac{N(s,t-1).5^s}{\Sigma N(s,t-1).5^s}.(1-X) \end{aligned} \tag{3.16}$$

As per our assumption, each set of 5 molecules with s^{th} fractal stage from $N_{cr}^{out}(s \rightarrow (s+1),t)$ will join with each other due to the cross-linking process and generate a single molecule having $(s+1)^{th}$ stage and therefore it is included into the set of molecules having fractal

stage s=(s+1). If $N_{cr}^{out}(s \rightarrow (s+1), t)$ is perfectly divisible by 5, then the total number of molecules that are joined with the set of molecules having $(s+1)^{th}$ fractal stage, will be:

$$\begin{aligned} N_{in}(s+1,t) &= \frac{1}{5}.N_{cr}^{out}[s \rightarrow (s+1), t] \\ &= \frac{1}{5}.N(s,t-1).\frac{N(s,t-1).5^s}{\Sigma N(s,t-1).5^s}.(1-X) \end{aligned} \tag{3.17}$$

If $N_{cr}^{out}[s \rightarrow (s+1), t]$ is not perfectly divisible by 5 then the nearest integer number of $N_{cr}^{out}[s \rightarrow (s+1), t]$ that is divisible by 5 will participate in the cross-linking process and the bigger size molecules, thus generated, will be included into the set of the $(s+1)^{th}$ stage molecules. The rest of the molecules will remain unaffected in s^{th} stage.

Now, the radiation-induced scission and cross-linking will also take place among those molecules having $(s-1)^{th}$ and $(s+1)^{th}$ fractal stages at the irradiation time step = t. The fraction of molecules, modeled with $(s-1)^{th}$ stage Vicsek fractals, that respond to the incident radiation, can be written as:

$$\begin{aligned} N_T(s-1,t) &= N(s-1,t-1).P_{VN}(s-1,t) \\ &= N(s-1,t-1).\frac{N(s-1,t-1).5^{(s-1)}}{\Sigma N(s,t-1).5^s} \end{aligned} \tag{3.18}$$

These $N_T(s-1,t)$ number of molecules are involved in the radiation-induced scission or cross-linking process. In our present simulation, we will focus on those molecules of $(s-1)^{th}$ fractal stage which are involved in the cross-linking process. Hence the number of molecules with $(s-1)^{th}$ fractal stage $(N_{cr}[(s-1), t])$ that are involved in the radiation-induced cross-linking process can be written as:

$$\begin{aligned} N_{cr}[(s-1),t] &= (1-X).N_T(s-1,t) \\ &= (1-X).N(s-1,t-1).\frac{N(s-1,t-1).5^{(s-1)}}{\Sigma N(s,t-1).5^s} \end{aligned} \tag{3.19}$$

According to the assumption, a set of each 5 molecules from $N_{cr}[(s-1), t]$ will join with each other and generate bigger molecules (Vicsek fractal) of fractal stage = s. Hence the number of molecules (Vicsek fractal) $(N_{cr}^{in}[(s-1) \rightarrow s, t])$ that are joining from the set of $(s-1)^{th}$ stage molecules to the set of to s^{th} stage due to radiation-induced cross-linking process in $(s-1)^{th}$ stage at the irradiation time step = t, can be written as:

$$\begin{aligned} N_{cr}^{in}[(s-1) \rightarrow s, t] &= (1-X).\frac{1}{5}.N_T(s-1,t) \\ &= (1-X).N(s-1,t-1).\frac{N(s-1,t-1).5^{(s-2)}}{\Sigma N(s,t-1).5^s} \end{aligned} \tag{3.20}$$

It should be kept in mind that we have come across two variables that play a significant role in establishing the master equation in the present section. These two variables are :

a. $N_{cr}^{in}(s-1) \rightarrow s), t)$ = the total number of molecules coming from the set of $(s-1)^{th}$ stage molecules to the set of to s^{th} stage due to cross-linking.

b. $N_{cr}^{out}(s \rightarrow (s+1), t)$ = total number of molecules that are going out at the time step t from s th stage to (s+1) th stage due to cross-linking.

A successful cross-linking must require a minimum of 5 molecules of the same fractal stage as per our assumption for the present simulation. Therefore these two variables are desirable to be perfectly divisible by 5. If they are not then the nearest integer numbers of $N_{cr}^{in}((s-1) \rightarrow s, t)$ and $N_{cr}^{out}(s \rightarrow (s+1), t)$ which are divisible by 5 perfectly, are taken for the cross-linking process and the rest of the molecules are kept un-effected with their respective fractal stages.

Similarly, the fraction of molecules that are modelled with $(s+1)^{th}$ stage Vicsek fractals will also respond to the incident radiation through radiation-induced scission and cross-linking process. The number of molecules with $(s+1)^{th}$ stage that is taking part in the radiation-induced process will be :

$$\begin{aligned} N_T(s+1,t) &= N(s+1,t-1).P_{VN}(s+1,t) \\ &= N(s+1,t-1).\frac{N(s+1,t-1).5^{(s+1)}}{\Sigma N(s,t-1).5^s} \end{aligned} \tag{3.21}$$

These molecules will involve in both scissions and cross-linking processes. In our present simulation study, we are concerned about those molecules with $(s+1)^{th}$ fractal stage, which involve radiation induces scission process and they can be expressed as:

$$\begin{aligned} N_{cr}[(s+1),t] &= X.N_T(s+1,t) \\ &= X.N(s+1,t-1).\frac{N(s+1,t-1).5^{(s+1)}}{\Sigma N(s,t-1).5^s} \end{aligned} \tag{3.22}$$

Each of these molecules disintegrates through the scission process and generates 5 smaller-sized molecules which are modeled with Vicsek fractals of fractal stage (s). Thus, the number of molecules that are coming from the set of molecules having $(s+1)^{th}$ stage to the set of molecules with s^{th} stage due to radiation-induced scission process, at the irradiation

time step = t, can be written as:

$$\begin{aligned} N_{sc}^{in}[(s+1) \rightarrow s, t] &= 5.X.N_T(s+1, t) \\ &= X.N(s+1, t-1).\frac{N(s+1, t-1).5^{(s+2)}}{\Sigma N(s, t-1).5^s} \end{aligned} \tag{3.23}$$

Hence, the total number of molecules that are found in s^{th} stage after the irradiation time step = t, can be written as:

$$\begin{aligned} N(s,t) &= N(s, t-1) - N_{sc}^{out}[s \rightarrow (s-1), t] - N_{cr}^{out}[s \rightarrow (s+1), t] + N_{cr}^{in}[(s-1) \rightarrow s, t] \\ &\quad + N_{sc}^{in}[(s+1) \rightarrow s, t] \end{aligned} \tag{3.24}$$

$$\begin{aligned} N(s,t) &= N(s, t-1) - N(s, t-1).\frac{N(s, t-1).5^s}{\Sigma N(s, t-1).5^s}.X \\ &\quad - N(s, t-1).\frac{N(s, t-1).5^s}{\Sigma N(s, t-1).5^s}.(1-X) \\ &\quad + N(s-1, t-1).\frac{N(s-1, t-1).5^{s-2}}{\Sigma N(s, t-1).5^s}.(1-X) \\ &\quad + N(s+1, t-1).\frac{N(s+1, t-1).5^{s+2}}{\Sigma N(s, t-1).5^s}.(X) \end{aligned} \tag{3.25}$$

This is considered as the master equation in our present research work and it is used to calculate the number of molecules (Vicsek fractals) i.e. N(s,t) that are present in s^{th} stage when the system is exposed to the external irradiation at the irradiation time step = t. The smallest molecule in the present case of simulation is modeled with Vicsek fractal of stage s=1. Formation of molecules with fractal stage, smaller than s=1 is not physically permissible here. Therefore, we have introduced an additional parameter (H) which restricts our master equation to be operable below the value s=1. We have defined the parameter H as follows:

$$H = \begin{cases} 0 & when \quad s = 1 \\ 1 & when \quad s = \text{any other integer value} \end{cases}$$

After incorporating this parameter (H) in the master equation, it takes the final

form which can be expressed as:

$$\begin{aligned} N(s,t) &= N(s,t-1) - H.N_{sc}^{out}[s \rightarrow (s-1),t] - N_{cr}^{out}[s \rightarrow (s+1),t] \\ &\quad + H.N_{cr}^{in}[(s-1) \rightarrow s,t] + N_{sc}^{in}[(s+1) \rightarrow s,t] \end{aligned} \tag{3.26}$$

$$\begin{aligned} N(s,t) &= N(s,t-1) - H.N(s,t-1).\frac{N(s,t-1).5^s}{\Sigma N(s,t-1).5^s}.X \\ &\quad - N(s,t-1).\frac{N(s,t-1).5^s}{\Sigma N(s,t-1).5^s}.(1-X) \\ &\quad + H.N(s-1,t-1).\frac{N(s-1,t-1).5^{s-2}}{\Sigma N(s,t-1).5^s}.(1-X) \\ &\quad + N(s+1,t-1).\frac{N(s+1,t-1).5^{s+2}}{\Sigma N(s,t-1).5^s}.(X) \end{aligned} \tag{3.27}$$

This is considered as the final form of the Master equation where all possible restrictions and conditions are incorporated mathematically. However, despite the modification, the master equation is constructed in such a fashion that the total number of monomers (unit cells of Vicsek fractal) will be conserved throughout the irradiation process.

3.6. Detailed Analysis of the Results Obtained from Computer Simulation

In this present section, we will extensively analyse the outcome of the computer simulation regarding the effect of gamma irradiation on mono-disperse as well as poly-disperse solid polymer electrolyte samples. The structural change has been analysed on the basis of the variation in molecular distribution (N(s,t)) and Weight fraction ($W_f(s,t)$) of the host polymer sample with the irradiation time steps (t) for different scission probalities.

3.6.1. Effect of Gamma Irradiation on Molecular Distribution pattern of Mono-disperse SPE

The un-irradiated mono-disperse sample is configured with 1000 numbers of Vicsek fractal of 7th stage where each of these molecules contains 5^7 numbers of structural units (seeds) i.e., monomers. Thus, the un-irradiated monodisperse sample contains 78125000 numbers of monomers as mentioned before. The effect of external gamma irradiation on molecular distribution has been discussed considering four different cases:

3.6.1.1. Variation of Weight Fraction $(W_f(s,t))$ in Case of Pure Scission and Pure Cross-linking Process.

We know that the initial un-irradiated mono-disperse sample contains 1000 numbers of the same type of molecules which are modelled by 7th stage Vicsek fractal. Hence the probability of finding the molecules in the 7th stage Vicsek fractal is unity and therefore the value of corresponding weight fraction $(W_f(7,0))$ =1. The pure scission process is an idealized situation where each parent fractal molecule breaks itself into five daughter molecules with subsequent lower stages. Hence, all molecules (Vicsek fractals) with the 7th stage break themselves and produce molecules (Vicsek fractals) of the 6th stage in the first irradiation time step (t=1). Total numbers of molecules, represented by 6th stage Vicsek fractals will be 5000 at the time step t =1 and the corresponding weight fraction will be $W_f(6,1)) = 1$ (here the weight fraction of the molecules configured with 6th stage Vicsek fractal at the irradiation time step t=1 is represented by the variable $(W_f(6,1))$. Since this is a case of 100% scission process, not a single molecule will participate in the inter-molecular cross-linking process and hence no molecule will be found at any fractal stage other than the 6th stage in the first irradiation step (t=1). This can be interpreted mathematically as:

$$\Sigma_{s\neq 6} W_f(s,1) = 0 \tag{3.28}$$

This iterative process will until the system contains the smallest size molecules having fractal stage s=1. The variation of $(W_f(s,t))$ with respect to the irradiation time step (t) has been depicted in the figure-3.9(A) . Here, the value of $(W_f(s,t))$ always remains unity . The variation in the total number of molecules N(s,t) for different time steps (t) has been shown in figure-3.9(B).

It is very evident from the figure-3.9(B) that the total number of molecules with fractal stage=s at a time step=t i.e. N(s,t) has increased rapidly with the increase of time steps (t) due to the pure scission process. The host polymer sample will contain 5000 molecules at the irradiation time step t=1 and 25000 (with fractal stage s=5 i.e. N(5,2)), 125000(with fractal stage s=4 i.e. N(4,3)), 625000(with fractal stage s=3 i.e. N(3,4)), 3125000(with fractal stage s=2i.e. N(2,5)), and 15625000(with fractal stage s=1i.e. N(1,6)) numbers of molecules at the irradiation time steps t=2, t=3, t=4, t=5, and t=6 respectively. Therefore the value of weight fraction $(W_f(s,t))$ for the respective values of N(s,t) will be $(W_f(5,20) = 1 for N(5,2) = 25000)$, $(W_f(4,3) = 1 for N(4,3) = 125000)$, $(W_f(3,4) = 1 for N(3,4) = 625000$, $(W_f(2,5) = 1 for N(2,5) = 3125000)$ and $(W_f(1,6) =$

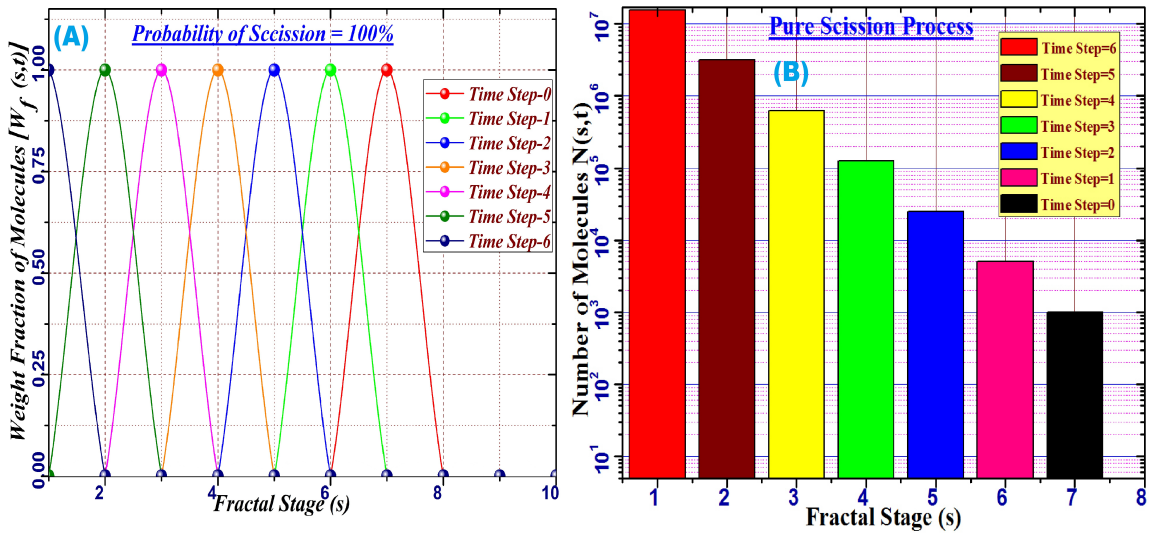

Figure 3.9: *Graphical presentation of the variation in molecular weight distribution in case of pure scission process. (A) $(W_f(s,t))$ vs fractal stage (s) curves for different irradiation time steps t. (B) N(s,t) vs s variation curve for different time step t. The continuous curves in (A) are for the "guide to the eye". Although, the respective data are in the form of discrete points.*

$1 for N(1,6) = 15625000)$. Where the irradiation time step are t=2, t=3, t=4, t=5, and t=6 respectively. It is very evident from figure-3.9(A) and (B) that the total number of molecules (Vicsek fractal) at any arbitrary time step (t) is increased by 5 times of its value in the previous time step (t-1) but the probability of finding the molecules with a certain fractal stage (s) at a certain time step (t) i.e. $(W_f(s,t))$ will always remain the unity. Variation of N(s,t) for different time steps (t) can not be plotted in linear scale in a single graph for the extremely large values of N(s,t) for the lower values of s. Therefore we have taken the N(s,t)-axis in log scale for the sake of a better understanding of the variation in N(s,t). Hence the host polymer system eventually remains mono-dispersive throughout the irradiation process.

Another idealized case is the pure cross-linking process. It happens to be a special situation where all the constituent molecules with any arbitrary fractal stage (s) of the host polymer sample will undergo an intermolecular cross-linking process. According to the assumption, five molecules (Vicsek fractal) with a definite fractal stage (s) join with each other and produce a single bigger molecule with a higher fractal stage (s+1)in this case. Thus, unlike the pure scission process, the total number of molecules inside the polymer sample at a certain irradiation time step (t) becomes one-fifth of its value as compared to

the time step (t-1) in this case. The variation in the total number of molecules with fractal stage s i.e. N(s,t) due to the external irradiation has been shown in figure-3.10(B). It also represents the variation in $(W_f(s,t))$ with respect to t in a separate graph.

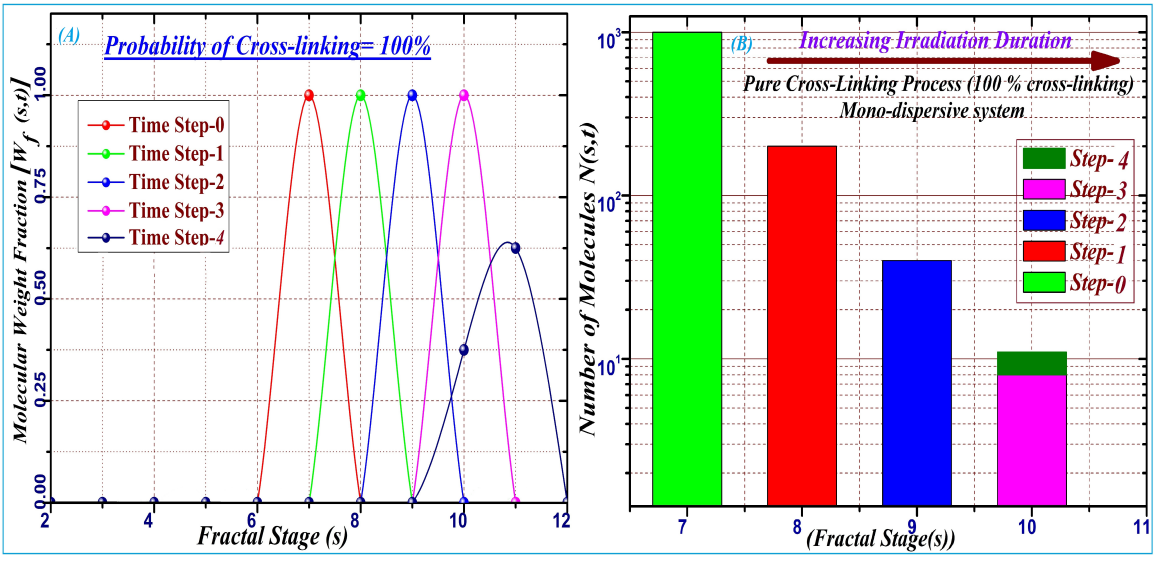

Figure 3.10: *Variation of weight fraction distribution and molecular number distribution in pure cross-linking (*100% *cross-linking)process inside a mono-disperse sample. (A)* $(W_f(s,t))$ *vs (s) curves for different time steps t. (B) N(s,t) vs s curves for different time step t. The continuous curves in (A) are for the "guide to the eye". Although, the respective data are in the form of discrete points.*

The un-irradiated (time step t= 0) sample is modeled with 1000 Vicsek fractals of the 7th stage which has been indicated with the highest column in the graph. In this case, the total number of molecules decreases rapidly with the increase of the exposure time to irradiation (t) due to the inter-molecular cross-linking process. Thus, only 200 molecules with fractal stage s=8 are found in time step s=1. In the same manner, 40 numbers of molecules with fractal stage s=9 and 8 numbers of molecules with fractal stage s=10 will be generated after the irradiation time step t= 2 and t=3 respectively as shown in the figure-3.10(B). The system remains mono-dispersive throughout the irradiation process up to this level. This trend is changed at the irradiation time step t = 4. At this step, the whole polymer matrix consists of 3 molecules with fractal stage s=10 and a single very large molecule modeled by the 11th stage Vicsek fractal. Thus, the host polymer matrix eventually turns into a poly-dispersive sample on and from the irradiation time step t=4. This situation arises because we have assumed in our simulation that at least 5 molecules of the same arbitrary fractal stage must be needed to participate in the pure cross-linking

process otherwise they will not respond to the cross-linking process.

The variation of $(W_f(s,t))$ with the irradiation time steps has been shown in figure-3.10(A). Here, the peak of the distribution curve is shifted towards the higher fractal stage with the increase in irradiation time step (t) up to the value t = 3. At the irradiation time step t = 4, the host polymer contains molecules with fractal stage s=10 and 11. Hence the PD curve changes its nature from its previous value.

3.6.1.2. Variation of Weight Fraction $(W_f(s,t))$ in Case of intermediate Scission Process Dominating region

Apart from the two extreme situations (pure scission or 100% scission process and pure crosslinking or 0 % scission probability) mentioned above, there exist numerous intermediate cases where the radiation-induced scission and cross-linking processes occur simultaneously inside the host polymer sample. In the present section, we will discuss those intermediate cases where the probability of the radiation-induced scission process is higher than that of cross-linking. This situation is implemented in the computer simulation process by incorporating the value of scission factor X within the range of $0.5 < X < 1.0$. The variation of $(W_f(s,t))$ distribution curve with respect to the irradiation time step (t) at two different scission probabilities (90 per cent and 70 per cent scission) has been shown in figure-3.11(A) andfigure-3.11(B) respectively for better understanding.

Figure-3.11(A) shows a radiation-induced process where the scission parameter has been taken as X=0.9. i.e. in this process, the radiation-induced scission i.e. breaking down of a polymer molecule of any arbitrary fractal stage (s) into five daughter molecules with its subsequent lower stage (s-1) occurs in 90 % cases which happens to be a much higher probability. The opposite process i.e. radiation-induced cross-linking process where five molecules with the same arbitrary fractal stage (s) join with each other and produce a single molecule with immediate next higher fractal stage (s+1), occurs only in 5% cases. As a result, the peaks of the $(W_f(s,t))$ distribution curve of host polymer molecules with different fractal stages (s) are shifted towards the left side i.e. towards the lower fractal stage (s) region with the passage of irradiation time steps (t) which can be observed clearly in figure-3.11(A).

Unlike the pure scission process, the host polymer system becomes poly-disperse in these cases from the beginning of the irradiation process (time step = 1) as the scission and

cross-linking process takes place simultaneously. The sharpness of the probability distribution curves of polymer molecules is decreased gradually with the increase of irradiation time steps (t) and the system becomes more poly-dispersed. After the irradiation time step t=10, the distribution curve has got flattened enough and the polymer sample contains all types of molecules with various sizes ranging from fractal stage s = 1 to stage s=8.

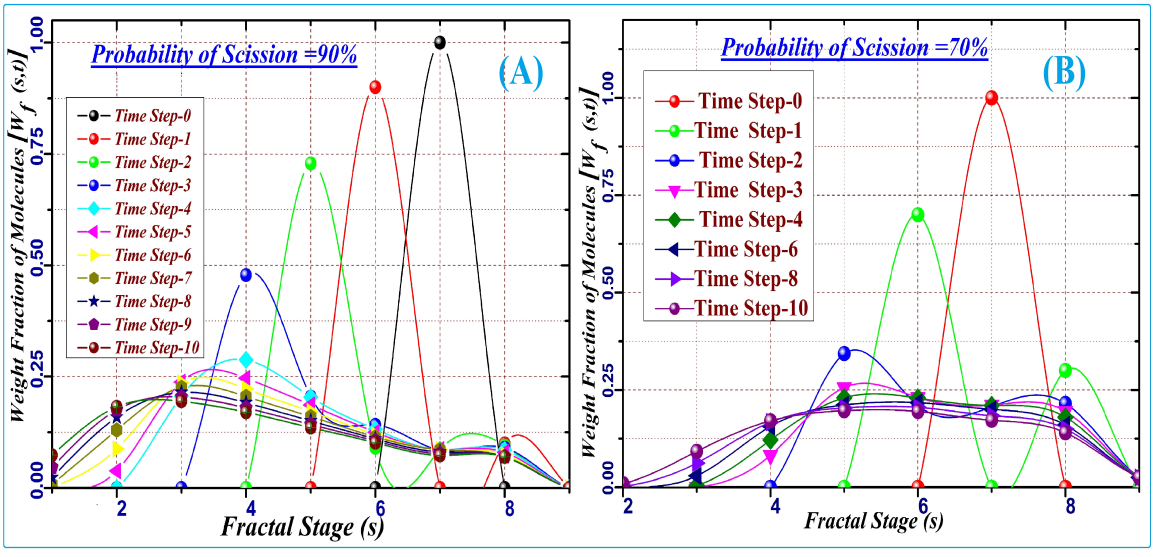

Figure 3.11: *Variation of* $(W_f(s,t))$ *distribution of a mono-disperse SPE sample for different time steps t in scission dominating region. (A)* $(W_f(s,t))$ *variation curve for different time steps t in case of 90% Scission process. (B)* $(W_f(s,t))$ *variation curve for different time steps t in case of 70% Scission process. The continuous curves in (A) and (B) are for the "guide to the eye". Though the respective data are in the form of discrete points.*

Another $(W_f(s,t))$ vs s curve for different irradiation time steps t is shown in figure-3.11(B). The rate of radiation-induced scission process occurs here in 70% cases and it is incorporated into the simulation by assuming the value of scission factor X=0.7. In this case, the breaking of a molecule with an arbitrary stage (s), into 5 daughter molecules with a stage (s-1) occurs at a comparatively slower rate than the case of the 90 % scission process. On the other hand, the rate of the cross-linking process where five molecules with the same arbitrary fractal stage (s) join with each other and produce a single molecule with the immediate next higher fractal stage (s+1) has been increased from 10 % to 30 %. Hence the distribution curve gets flattened considerably after time step t = 3 as shown in the figure-3.11(B). Moreover, the shifting of the peak of $(W_f(s,t))$ vs s curve towards the lower molecular weight region occurs at a comparatively slower rate than the case of 90 % scission process but the polymer system becomes poly-dispersive by nature from the very

beginning of the application of external irradiation.

3.6.1.3. Variation of Weight Fraction ($W_f(s,t)$) in Case of intermediate Cross-linking Dominating Processes

Another part of the radiation-induced scission and cross-linking process is the intermediate cross-linking dominating case. This is a situation where the inter-molecular cross-linking process plays a predominant role inside the host polymer matrix. This situation has been incorporated into the simulation by implementing the value of cross-linking factor (1-X) within the limit of 1.0 and 0.5 i.e. $0.5 < (1 - X) < 1.0$. The rate of the cross-linking process increases gradually with the decrease of the value of X (i.e. increase of the value of (1-X)). According to the assumption, five molecules of the same arbitrary stage (s) join with each other by cross-linking process and produce a bigger size molecule with a subsequent higher fractal stage (s+1). Hence the total number of molecules inside the sample decrease and the size and molecular weight of each molecule increases gradually with the increase of irradiation time steps (t). Since the scission and cross-linking processes occur simultaneously inside the host polymer sample, the shifting of the peak of probability distribution curve (i.e. molecular weight fraction ($W_f(s,t)$) variation curve) is not so rapid as the pure cross-linking process. ($W_f(s,t)$) vs s curves of the host polymer molecules in two different cases (i.e. in case of 90% and 70% cross-linking processes)for different irradiation time steps (t) has been shown in figure-3.12(A) and figure-3.12(B) for better understanding.

Variation of probability distribution curve (in the form of molecular weight fraction ($W_f(s,t)$) variation curve) of polymer molecules with different stages (s) for 90% cross-linking process is shown in figure-3.12(A). This is another cross-linking dominating intermediate case where the radiation-induced inter-molecular cross-linking process occurs in 90% of cases. This implies that 90% of the host polymer molecules that are responding to the external gamma irradiation, are engaged in the inter-molecular cross-linking process and each of the five molecules with an arbitrary fractal stage (s) join with each other and produce a single molecule with a fractal stage (s+1). As a result, the peaks of probability distribution curves (($W_f(s,t)$ variation curve) shift towards the right side in the higher fractal stage region comparatively faster rate than that of the 70% cross-linking case as shown in figure-3.12(B). Whereas figure-3.12(A) shows the rapid shifting of the distribution curve peak. We have also noticed that the amplitude of the distribution peaks decreases gradually with the increase of irradiation time steps (t). Thus the un-irradiated sample which happens to be mono-disperse manifests the highest ($W_f(s,t)$ vs s peak and the peak

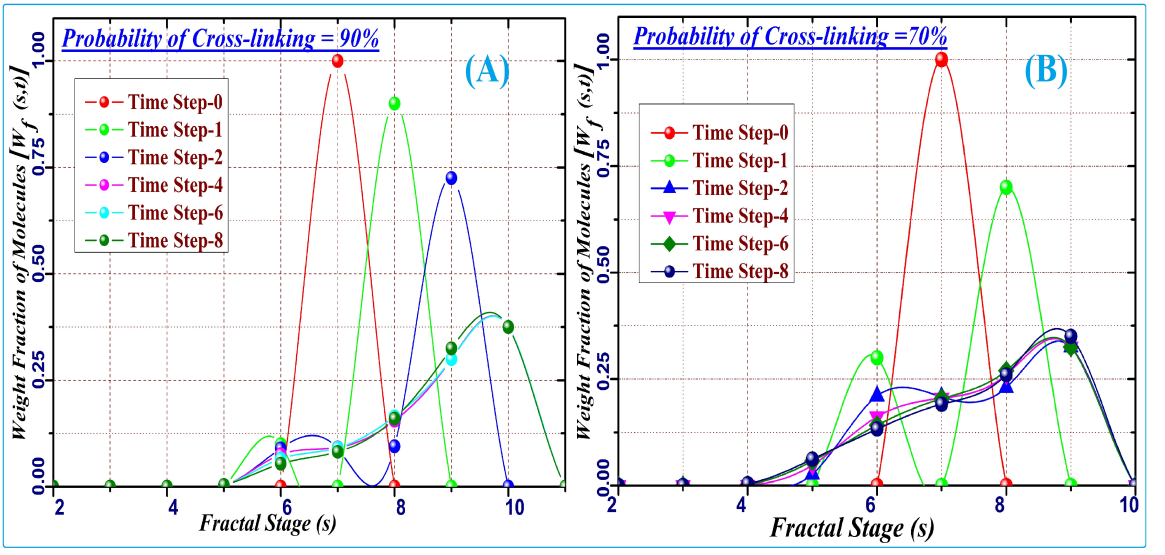

Figure 3.12: *Variation of* $(W_f(s,t))$ *distribution of a mono-disperse SPE sample for different time steps t in cross-linking dominating region. (A)* $(W_f(s,t))$ *variation curve for different time steps t in case of 90% Cross-linking process. (B)* $(W_f(s,t))$ *variation curve for different time steps t in case of 70% Cross-linking process.The continuous curves in (A) and (B) are for the "guide to the eye". Although, the respective data are in the form of discrete points.*

appears at the fractal stage s=7. The next $(W_f(s,t)$ vs s peak appears at fractal stage s=8 at the irradiation time step t=1 but the height of the peak is smaller than the previous one. This trend continues at further irradiation time steps and the lowest peak appears at the fractal stage s=10 at the irradiation time step t=8. For irradiation time steps t= 4 to t=8, the distribution curves show a similar kind of shape and nature. In the case of 90% cross-linking probability (10% scission probability), the molecules that are generated due to the gamma irradiation, are bigger but the number of molecules is reduced gradually with the increase of irradiation time steps (t). Here also the total number of monomers remain conserved throughout the radiation process which is similar like the other cases.

Figure-3.12(B) represents the variation of probability distribution curve (in the form of molecular weight fraction $(W_f(s,t))$ variation curve) of polymer molecules with different stages (s) when the radiation-induced scission process occurs inside the sample only in 30% cases.This implies that the external irradiation results in inter-molecular cross-linking inside the host polymer sample in 70% of cases. This phenomenon has been incorporated inside the simulation by assuming the value of scission factor X=0.3. As a result, molecules, bigger in size, are generated at a comparatively slow rate.

The shifting of the probability distribution curve peak ($W_f(s,t)$) vs s curve) is observed towards the right i.e. towards the region of higher fractal stages (s). This trend of shifting distribution peak is observed up to the irradiation time step t=2. Post which, no positional shifting of probability distribution peaks (($W_f(s,t)$) variation curve) has been observed. Only the height of the distribution peaks changes slowly with the increase of irradiation time steps (t). Similarly, no significant alteration in the shape of the probability distribution curve has been noticed in the case of higher irradiation time steps (($W_f(s,t)$) variation curve for t=4 to t=8). The total number of molecules inside the sample is reduced gradually with the increase of irradiation time step (t), but the molecular weight of the individual molecule is increased significantly. It should be noted that the total number of monomers (unit cell of Vicsek fractal) will be unchanged and it will be 78125000 throughout the irradiation process. The system becomes poly-disperse from the starting of the application of gamma irradiation.

3.6.1.4. ($W_f(s,t)$) vs (s) variation curves in case where Scission and Cross-linking Processes Occur with Equal probabilities

This is a special case where gamma irradiation-induced scission and cross-linking processes occur at an equal rate inside the host polymer sample. Hence the molecules of any arbitrary fractal stages (s) have the equal probability of either breaking themselves into smaller molecules with a fractal stage (s-1) or join with each other and produce a bigger size molecule with a fractal stage (s+1). The probability distribution curves (in the form of ($W_f(s,t)$) variation curve) at different irradiation time steps (t) have been shown in figure-3.13(A) and (B). After the first irradiation time step (t=1), these molecules participate in the radiation-induced scission and cross-linking process with equal probabilities and are distributed among the 6th and 8th stages.

The probability of finding polymer molecules with both fractal stages s=6 and s=8 are equal and their value is 0.5 after the irradiation time step t=1 as shown in figure-3.13(A). It indicates that the weight fraction values ($W_f(s,t)$) of the 6th and 8th stage molecules (s=6 and s=8), according to the definition of ($W_f(s,t)$), is also 0.5 after the irradiation time step t=1 i.e. we can write ($W_f(6,1)$)= ($W_f(8,1)$)=0.5 but the number of the molecules in the respective stages are different i.e. total number of molecules with fractal stage s=6 and s=8 will be 2500 and 100 respectively at t=1. In the next subsequent irradiation time steps (t=2,3,4,5 etc), the constituent molecules undergo both scission and crosslinking processes and are distributed among different fractal stages as shown in the ($W_f(s,t)$) distribution

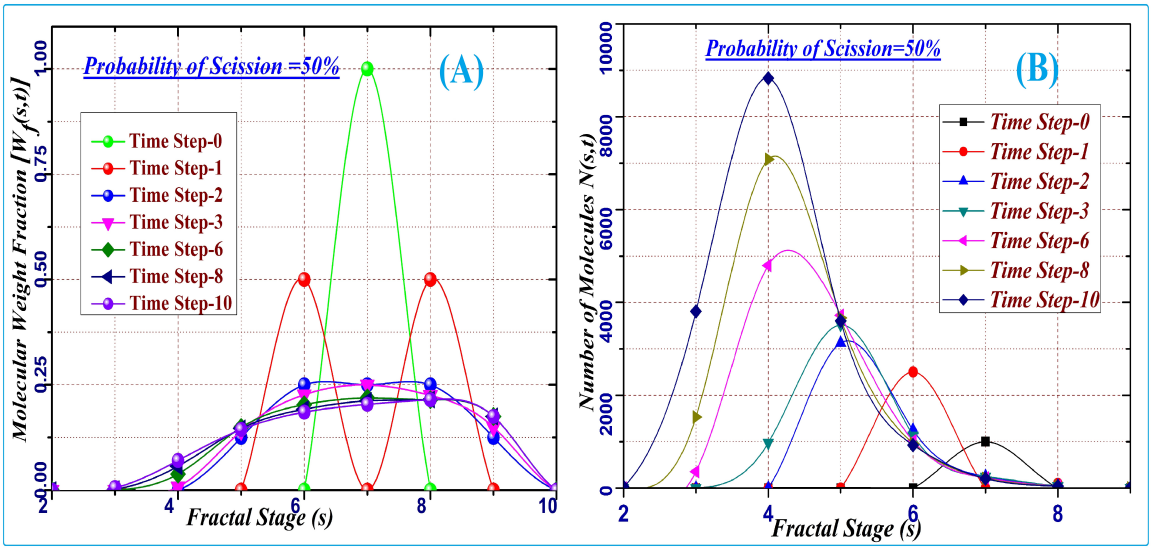

Figure 3.13: *Variation of molecular weight distribution curve for different irradiation time steps t when scission and cross-linking occurs in equal rates(50% scission). (A) ($W_f(s,t)$) vs s curves for different time steps t. (B) N(s,t) vs s curves for different time steps t. The continuous curves in (A) and (B) are for the "guide to the eye". Though, the respective data are in the form of discrete points.*

curve in figure-3.13(A). After careful observation of figure-3.13(A), we can infer that the probability distribution curve ($W_f(s,t)$ variation curve) becomes progressively flattened with no significant shift in their peaks at the higher values of irradiation time steps (t). The total number of monomers (unit cell or the seed of the Vicsek fractal) remains unchanged throughout the process and its value in our present case is 78125000. The variation in the number of molecules N(s,t) vs fractal stage s curves for different irradiation time steps t has been presented in figure-3.13(B). The peak of the N(s,t) vs s curves shifts slowly towards the left side i.e. the lower fractal stage region though the hight of those peaks are increased significantly as they shift towards the left side. This phenomenon also confirms the fact that the total monomer units inside the sample remains conserved throughout the irradiation process.

3.6.2. Effect of Gamma Irradiation on Molecular Distribution pattern of a Poly-disperse SPE Sample

In this present subsection, we will discuss the effect of gamma irradiation on the molecular distribution pattern of a poly-disperse sample. The molecular distribution as well as the

distribution of $(W_f(s,t))$ of the un-irradiated sample has been shown in figure-3.5(A) and figure-3.5(B). The variation of molecular distribution has been investigated on the basis of the variation of $(W_f(s,t))$. The complete analysis of the simulation result has been segregated into four different subsections depending on the probability of radiation-induced scission and cross-linking processes as we have already done in the mono-disperse case.

3.6.2.1. Variation of Weight Fraction ($(W_f(s,t))$ and molecular distribution in Case of Pure Scission and Pure Cross-linking Process

These two idealized cases have already been discussed for a mono-dispersive system in the previous section. The main difference in the present case is that the entire system happens to be poly-dispersive from the beginning . The total number of molecules in the un-irradiated host polymer sample is 720. Among them, 500, 200, and 20 numbers of molecules are modeled by 5th, 6th, and 7th stages Vicsek fractal respectively. The weight fractions of those molecules with their respective fractal stages are $W_f(5,0)$=0.25, $W_f(6,0)$ =0.5, and $W_f(7,0)$ = 0.25 respectibely resulting in the $(W_f(s,t))$ vs s distribution curve to be symmetric by nature which we have already seen in figure-3.5(A). Figure-3.14(A) and

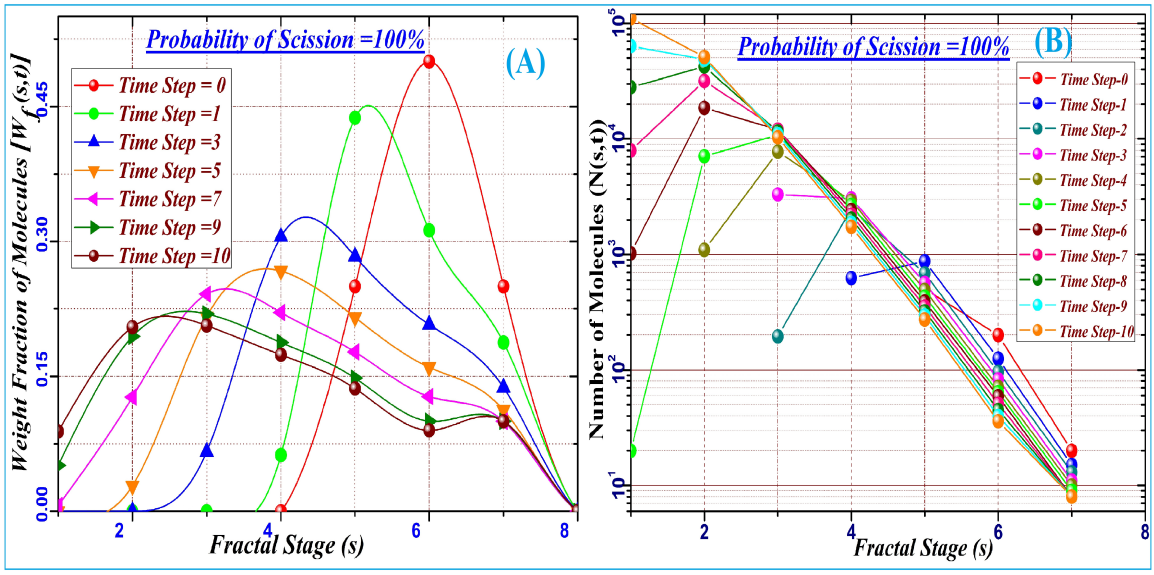

Figure 3.14: *Graphical presentation of the variation in molecular weight distribution in case of pure scission (100% scission) process for a poly-disperse SPE sample. (A) $(W_f(s,t))$ vs fractal stage (s) curves for different irradiation time steps t. (B) N(s,t) vs s variation curve for different time step t. The continuous curves in (A) and (B) are for the "guide to the eye". Although, the respective data are in the form of discrete points.*

figure-3.14(B) also represent the variation in both N(s,t) and ($W_f(s,t)$ distribution curves for different time steps (t) in case of pure scission (100% scission) process. This is the situation when only the radiation-induced scission process occurs inside the sample. As a consequence, molecules responding to the external irradiation undergoes complete scission process and generate comparatively smaller size molecules with the subsequent lower value of fractal stages.

Therefore, the number of molecules increases rapidly inside the host poly-dispersive sample with an enhancement in irradiation time steps (t). Here the molecular distributions in different fractal stages are shown in the figure-3.14(B) up to the irradiation time step t=10. Initially, the un-irradiated molecules are distributed among 5th, 6th, and 7th fractal stages. When the gamma irradiation is applied externally, smaller-sized molecules with lower values of fractal stages are generated due to the pure scission process and as a result, the system becomes more and more poly-disperseive by nature. After the irradiation time step t=5, the system consists of molecules with all possible values of fractal stages starting from s=1 up to s=7. Further increase in irradiation time steps results in the generation of a large number of molecules with lower values of fractal stages ranging from 1st stage to 3rd stage because of the radiation-induced pure scission process. On the other hand, the probability of finding bigger size molecules with higher values of fractal stage becomes increasingly small. Variation of N(s,t) among lower values of fractal stages is significantly high which creates a problem in representing all the N(s,t) variation curves in a single figure. Therefore, the N(s,t) axis in figure-3.14(B) is taken in log scale so that all the respective curves can be identified easily.

Variation of weight fraction ($W_f(s,t)$) among different fractal stages (s) in different irradiation time steps has been shown in figure-3.14(A). We have come across the fact that pure scission results in the segregation of bigger-sized molecules into smaller ones. Thus, ($W_f(s,t)$) distribution peak shifts towards the left side i.e. towards the region of lower value of fractal stages very rapidly with the increase of irradiation time steps (t). The height of the peak in ($W_f(s,t)$) vs s curve also decreases gradually and they become more flattened, which indicates the probability of finding molecules with their respective fractal stages decreases gradually with the increase in time steps. This phenomenon eventually turns the system into more poly-dispersive. We can observe this trend of the weight fraction ($W_f(s,t)$) distribution curve very evidently in figure-3.14(A). It should be noted that, unlike the mono-disperse sample, here the system is poly-disperse from the beginning of the irradiation process.

The opposite types of behavior can be observed in the case of the pure cross-linking process. Figure-3.15(A) and figure-3.15(B) show the variation in $W_f(s,t)$ distribution as well as the molecular distribution for different time steps (t) due to the pure cross-linking process. Unlike the previous host polymer system, here the initial un-irradiated sample is poly-disperse. Hence the nature of the molecular distribution is generally different from that of the mono-dispersive case. figure-3.15(B) shows the molecular distribution pattern due to external gamma irradiation up to irradiation time step t=10. The molecular distribution of the un-irradiated sample shows the highest peak at fractal stage s=5 (where the number of molecules with fractal stage s=5 is 500). When the irradiation starts, molecules with an arbitrary value of fractal stage undergo a radiation-induced pure intermolecular cross-linking process and generates bigger-sized molecules with subsequent higher values of fractal stages.

As a result, the number of molecules inside the sample decreases which reflects in the molecular distribution curves i.e. N(s,t) vs s curves in figure-3.15(B). We can observe that the height of the peak in N(s,t) vs s curve gradually decreases with the increase of irradiation time steps (t). This trend continues till time step t=10. Though the rate of decrease of distribution peak slows down considerably after the time step t=4, the peak does not shift from s=5 throughout the irradiation process. In the same way number of molecules with higher values of fractal stages like s= 7 and 8 increases with the increase in irradiation time steps (t) resulting in the sample being more poly-dispersive by nature. Since external irradiation results in 100% cross-linking, no molecules can be found with fractal stage below s=5.

The nature of weight fraction ($W_f(s,t)$ distribution pattern in 100% cross-linking process is very different from the molecular distribution pattern and is shown in figure-3.15(A). Initially (t=0) the distribution pattern is symmetric by nature, which is indicated by the black curve in figure-3.15(A). With the increase of irradiation time steps (t), this symmetric nature changes, and the peak shifts towards the right side among the higher values of s because the molecules are involved in radiation-induced pure inter-molecular cross-linking process and according to the assumptions, every 5 molecules with same fractal stage join with each other to produce a bigger sized molecule with the next higher value of fractal stage. We can observe from the molecular distribution curve in figure-3.15(A) that the number of molecules with 6th, and 7th,8th, and 9th, fractal stages are very less compared to the molecules with fractal stage s=5 at different irradiation time steps (t). But their size is much larger than the molecules with s=5. Hence, the value of ($W_f(s,t)$) for the

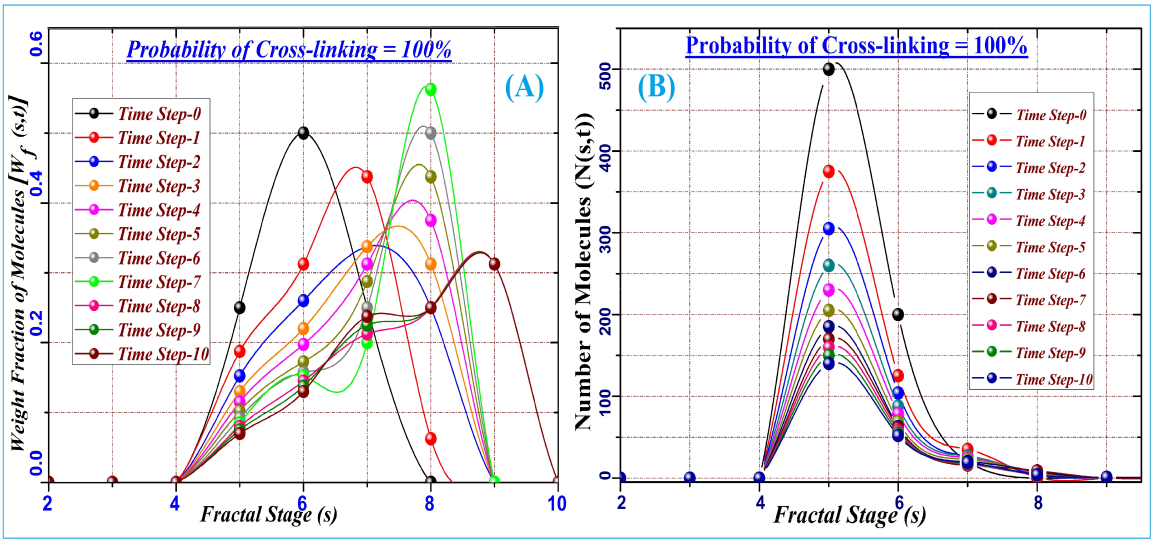

Figure 3.15: *$(W_f(s,t))$ and N(s,t) Variation curves in pure cross-linking (100% cross-linking) process inside a poly-disperse sample. (A) $(W_f(s,t))$ vs s curves for different time steps t. (B) N(s,t) vs t curves for different time steps t. The continuous curves in (A) and (B) are for the "guide to the eye". Though the respective data are in the form of discrete points.*

molecules with s= 6,7,8, and 9 are considerably high. This happens to be the prime reason that the $(W_f(s,t))$ distribution peak shifts gradually towards the right side into the higher fractal stage region with the increase of irradiation time steps (t) and after the time step t=3, the distribution peak is observed at the fractal stage s=8. This phenomenon indicates the probability of finding molecules with fractal stage s=8 becomes maximum after the irradiation time step t=3. The peaks of the next $(W_f(s,t))$ vs s distribution curves remain at the same position (at s=8) up to the irradiation time step t=9 which can be seen clearly in figure-3.15(A). At the time step t=10, a molecule with fractal stage s=9 is generated due to the cross-linking of 5 molecules having fractal stage s= 8. Hence, the distribution peak of $(W_f(s,t))$ is shifted from s=8 to s=9.

3.6.2.2. Variation of Weight Fraction $(W_f(s,t))$ in Case of intermediate Scission Process Dominating Region

The effect of intermediate scission dominating cases has already been discussed for the mono-dispersive system in the previous section. Here, we will discuss the same case for a poly-disperse sample. As we have mentioned before, the radiation-induced scission and

cross-linking have been implemented in the simulation with the help of two parameters: X and (1-X) respectively to avoid any additional complexity. In this sub-section, we will discuss the case where the probability of scission is greater than that of the cross-linking. This situation has been incorporated into the simulation by taking the value of X between 0.5 to 1.0 ($0.5 < X < 1.0$). The molecular distribution pattern changes with the variation of scission probability i.e. the value of X. We will discuss here regarding the ($W_f(s,t)$) vs s variation curves for the same scission probabilities for 70% and 90% scission processes which we have already discussed in case of mono-disperse sample and the analysis of the difference in results between the respective curves of two systems will be done thereafter.

Figure-3.16(A) represents the variation in weight fraction ($W_f(s,t)$) with the fractal stage (s) for different values of time steps t when the probability of scission inside the sample is X=0.9. This implies that 90% of the molecules that are responding to the external irradiation are involved in the scission process. The simulation has been carried out up to the irradiation time step t = 10. We have come across the fact that the initial ($W_f(s,t)$) vs t distribution curve is symmetric with a peak at s=6. In the first irradiation time step (t=1), the peak is shifted at s=5. This is a clear indication of the overall scission dominating process inside the system.

Further increase of the irradiation time steps results in a gradual shift of the weight fraction ($W_f(s,t)$) distribution peak towards the lower fractal stage region which can also be seen in figure-3.16(A). Shifting of distribution peak is also associated with a gradual reduction in the peak height and as a result, the distribution curves become more flattened. This phenomenon suggests that the host polymer sample becomes more and more poly-dispersive by nature when it is being exposed to gamma irradiation for a longer duration of time. As a result, the polymer sample contains molecules with different sizes having different values of fractal stages ranging from s=1 to s=8 at the higher values of the irradiation time steps (t = 7 to 10).

Figure-3.16(B), represents the variation in weight fraction $W_f(s,t)$) of the host polymer molecules for different time steps (t) when the probability of scission inside the sample is X=0.7 i.e. out of 100 molecules which will respond to the external irradiation, 70 will participate in intra-molecular scission process and rest of the molecules (i.e. 30) will take part in intermolecular cross-linking. As compared to the previous case, it is very evident from the figure-3.16(B) that the ($W_f(s,t)$) distribution peak moves comparatively slow towards the lower fractal stages (s) region as the irradiation time steps (t) are increased gradually. The main reason behind this phenomenon is that the probability of scission is reduced from

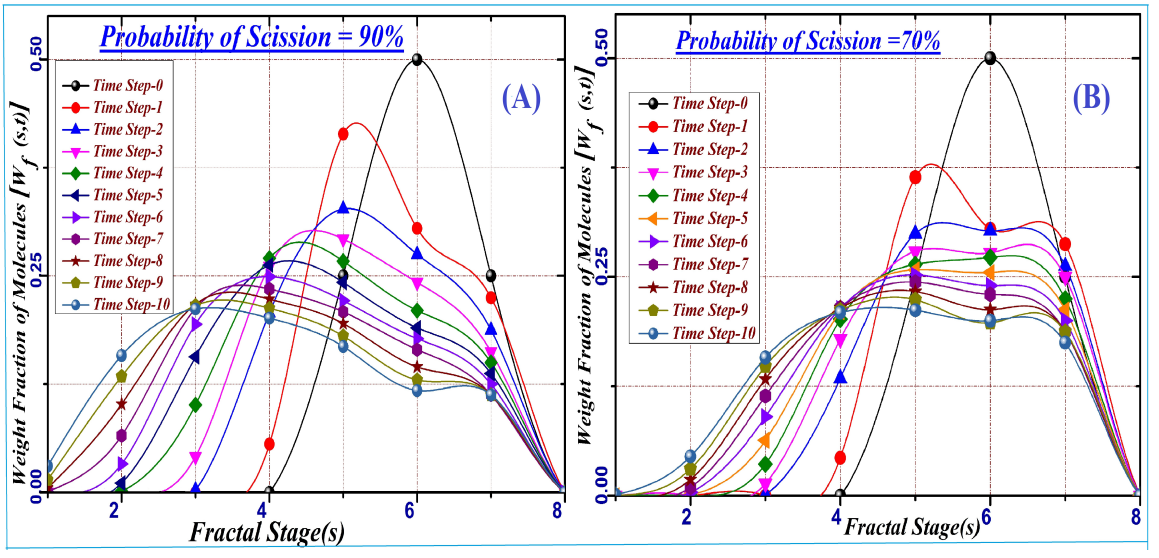

Figure 3.16: *Variation of weight fraction* $(W_f(s,t))$ *of a poly-disperse SPE sample in scission dominating region. (A)* $(W_f(s,t))$ *vs s curves for different time step t when the probability of scission is 90%. (B)The same* $(W_f(s,t))$ *vs s curves in case of 70% scission process. The continuous curves in (A)and (B) are for the "guide to the eye". Though, the respective data are in the form of discrete points*

90% to 70% and on the contrary, the probability of inter-molecular cross-linking is increased from 10% to 30%. In the case of the 70% scission process, the biggest molecule that can be found inside the sample is of fractal stage s=7 but the probability of their presence throughout the irradiation process happens to be higher than that of the 90% scission case. Also, the height of the $(W_f(s,t))$ distribution peaks decreases slowly with the increase of irradiation time steps similar to the 90% cases shown in figure-3.16(A). But one can observe a slower rate of reduction in the height of peak in $(W_f(s,t))$ vs s curve compared to the 90% scission case. This can be considered as the result of increased cross-linking probability though the system remains poly-dispersive throughout the radiation process.

3.6.2.3. Variation of Weight Fraction $(W_f(s,t))$ in Case of Intermediate Cross-linking Dominating Processes

This subsection is aimed for a detailed discussion regarding the outcome of the simulation for those cases where the radiation-induced intermolecular cross-linking process plays the predominant role inside the host polymer sample. Similar to the mono-disperse sample, the chances of scission process lies here between 0% to 50% and therefore, we have taken the

value of the parameter X between 0 to 0.5 i.e. $0.0 < X < 0.5$ and the cross-linking parameter (1-X) have the value between 1.0 to 0.5 ($0.5 < X < 1.0$). The molecular distribution pattern changes with the variation of scission probability i.e. value of X. In the present case, we have discussed the nature of the variation of weight fraction ($W_f(s,t)$) for two different cases, where the chances of the scission process are 10% and 30% i.e. the chances of the inter-molecular cross-linking process are 90% and 70% respectively. The distribution of weight

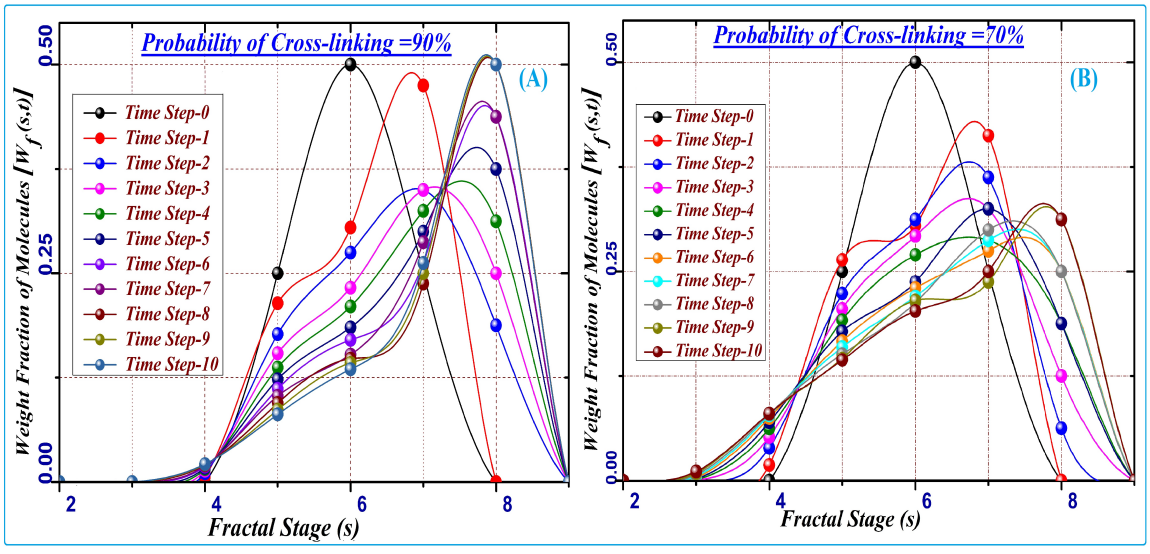

Figure 3.17: *Variation of* ($W_f(s,t)$) *distribution of a poly-disperse SPE sample for different time steps t in cross-linking dominating region. (A)* ($W_f(s,t)$) *variation curve for different time steps t in case of 90% Cross-linking process. (B)* ($W_f(s,t)$) *variation curve for different time steps t in case of 70% Cross-linking process. The continuous curves in (A) and (B) are for the "guide to the eye".Although, the respective data are in the form of discrete points.*

fraction ($W_f(s,t)$) at different irradiation time steps has been shown in figure-3.17(A) where the probability of scission is 10% i.e. the probability of cross-linking is 90%. This implies that, if 100 polymer molecules with a fractal stage (s) respond to the external irradiation then only 10 out of those 100 molecules will participate in the scission process and the rest 90 molecules will undergo the inter-molecular cross-linking process and produce 18 bigger sized molecules with a fractal stage (s+1). This phenomenon produces a significant impact on the nature of the ($W_f(s,t)$) variation curve which can be observed easily in figure-3.17(A). Here, the high cross-linking rate results in a gradual shift of the ($W_f(s,t)$) distribution peak towards the higher fractal stage region. When the external gamma irradiation is applied (at the irradiation time step t=1), the symmetric nature of the ($W_f(s,t)$) variation curve is gone and the peak shifts at s= 7. This indicates the probability of finding molecules

with fractal stage s=7 inside the sample is maximum at the irradiation time step t=1. The height of the $(W_f(s,t))$ distribution peak is reduced at the irradiation time step t=2 as new molecules with fractal stage s=8 are generated inside the sample due to the high rate of the cross-linking process.

The position of the peak of $(W_f(s,t))$ vs s variation curve remains fixed at s=7 up to the irradiation time step t=4. Post which the position of the peak shifts at s=8 from s=7, and the height of the peak increases with the increase in time step t. The $(W_f(s,t))$ distribution peak again attains its maximum value at s=8 at the time step t=8 and this value is the same as that of the $(W_f(s,t))$ distribution peak of the un-irradiated sample. This phenomenon happens to be very different from the nature of the $(W_f(s,t))$ distribution curve which is observed in the mono-disperse case. The shifting of the peak towards the right side of the graph indicates the generation of larger size polymer molecules due to cross-linking process with greater probability. The resultant gamma-irradiated sample is poly-disperse and consists of different types of molecules with fractal stages ranging from s=4 to s=8.

The variation of $(W_f(s,t))$ with fractal stage (s) for different values of time steps has been shown in figure-3.17(B). The molecules are more probable to undergo the cross-linking process than the scission one. Therefore, the probability of finding a bigger-sized molecule is greater than that of the small one. But the rate of generating bigger-sized molecules with higher values of fractal stages is not as much high as observed when the probability of cross-linking is 90%. Thus a gradual shifting of $(W_f(s,t))$ distribution peak has been observed from fractal stage s=6 to 7 and lastly at s=8 with a comparatively slower rate when the irradiation time step (t) is increased. The height of the $(W_f(s,t))$ distribution peak is reduced significantly after the starting of gamma irradiation (from irradiation time step t=1). Another observable fact is the probability of finding molecules with 7th fractal stage decreases with the increase in time step t and the opposite feature has been noticed in the case of molecules with fractal stage s=8. Here, the probability of finding molecules with fractal stage s=8 increases with the increase in irradiation time steps (t) and it attains its maximum value at t= 9 and t=10. This is the direct consequence of the radiation-induced cross-linking process in the sample. Unlike the previous case, here the resultant sample is poly-disperse having molecules with fractal stages ranging from s=3 to s=8.

3.6.2.4. Variation of Weight Fraction ($W_f(s,t)$) in The Case Where Scission and Cross-linking Processes Occur with Equal Probabilities

There exists another special case where radiation-induced scission and cross-linking occur with equal probability inside the sample. This phenomenon has been incorporated into the simulation by taking the value X=0.5. This special case has already been studied for the mono-disperse sample. In the case of the poly-disperse sample, the molecular distribution, as well as the distribution of weight fraction $W_f(s,t)$, is shown in figure-3.5(A) and figure-3.5(B). Though the scission and cross-linking occur here with equal probabilities, the number of molecules produced due to scission is much larger than that of the cross-linking, as per the assumptions taken at the beginning of the simulation. Hence, the peak of the molecular distribution curve has a general tendency to shift towards the left side at the lower fractal stage region which can be seen in figure-3.18(B). The radiation-induced final sample is poly-dispersive by nature having molecules with fractal stages ranging from s=3 to s=7.

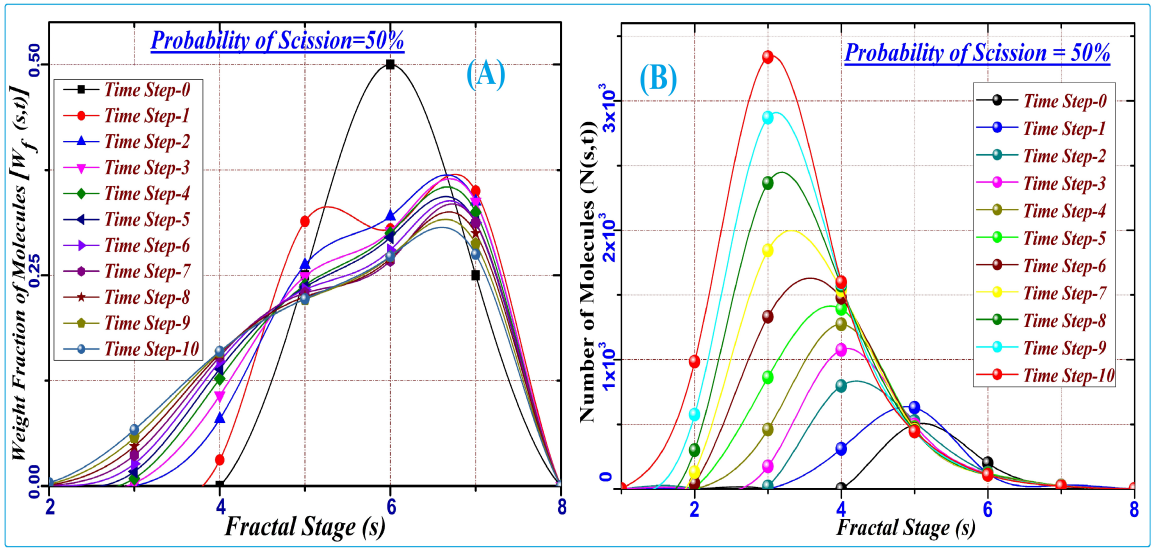

Figure 3.18: *Variation of* $(W_f(s,t))$ *and N(s,t) distribution curves for a poly-disperse SPE sample when the probability of scission is 50%. (A)* $(W_f(s,t))$ *vs s curves for different time steps t. (B) N(s,t) vs s curves for different time steps t. The continuous curves in (A) and (B) are for the "guide to the eye". Though, the respective data are in the form of discrete points*

The variation of weight fraction $(W_f(s,t))$ is depicted in figure-3.18(A). It suggests that the peak of the distribution curve shifts towards the higher fractal stage region with

the increment in irradiation time steps t. This phenomenon is in contradiction to the trend that has been observed in the molecular distribution curve in figure-3.18(B). The reason behind this nature is the generation of bigger size molecules with higher values of fractal stages that requires a large number of monomers (fractal seeds). As a result, the value of $(W_f(s,t))$ of the respective bigger size molecule becomes greater than the smaller size molecules. Hence, despite being small in number, the probability of finding bigger size molecules inside the sample with higher values of fractal stages is greater than that of the molecules having a lower value of fractal stage. With the increment of irradiation time steps, the curves become progressively flattened and spread among different fractal stages resulting in the sample being more poly-disperse in nature.

3.6.3. Discussion about the simulation results on the basis of Experimental outcomes

The effect of gamma irradiation on the molecular distribution pattern has been experimentally studied by many researchers. It has been reported that the application of gamma irradiation on PEO in presence of oxygen results in a chain scission reaction whereas scission and cross-linking occurs simultaneously in vacuum[49]. This fact eventually correlates with the assumption-(b) that we have taken for our simulation. Other experimental studies provide clear shreds of evidence about the change in molecular weight as well as crystallinity due to the application of gamma irradiation[50,51].

An experimental study has been done by Mou Saha et.al[52] which has a sufficiently good agreement with our simulation outcome up to some extent. They have taken PEO powder from BDH, England (MW 10^5). The sample was then irradiated by gamma-ray from a conventional gamma chamber with a ^{60}Co source with the irradiation dose rate of $6.4kGyh^{-1}$. The gamma irradiation dose was varied from 1 to 30kGy in air. Gel permeation chromatography (GPC) method has been used to study the variation of MWD. In addition with that Q-TOF YA263 high-resolution instruments were used for the High-resolution mass spectroscopy (HRMS) analysis. The result thus obtained from these experiments shows four different weight fraction distribution curves in four different irradiation doses (5, 10, 15, 20 kGy respectively). The peak of each curve shifts towards the left in the lower molecular weight region with the increase in the external irradiation dose and this phenomenon has a very good agreement with the overall trend of $W_f(s,t)$ variation in

our present simulation outcome in the case of scission dominating region for both mono-dispersive and poly-dispersive sample. More precisely figure-3.11(a) and (b) for the mono-disperse sample and figure-3.14(a),figure-3.16(a),figure-3.16(b) for the poly-disperse sample in case of our present simulation work are in excellent agreement with the experimentally observed graph in the said article.

Another experimental study has been reported by M. Mukhopadhyay et. al[53], where they have taken Poly [-Ethylene Oxide] as a substrate and irradiate it with gamma irradiation to study its structural modification. The experimental outcome that was presented in figure-1 of their paper shows similar types of trend which is observed in the above-mentioned figures of our simulation in scission dominating region.

Thus the novelty of the present research work lies in the fact that, despite the artificiality on the construction of polymer network, the simulation result of the variation in molecular distribution due to gamma irradiation shows a good agreement with the experimental result.

3.7. Conclusion

The detailed investigation through computer simulation concludes that in spite of some inherent artificiality, deterministic Vicsek fractal can be used successfully as a tool for the modelling of the host polymer system. Extensive study based on computer simulation reveals the fact that externally applied gamma irradiation promotes scission and intermolecular cross-linking that occurs simultaneously inside the polymer system and eventually produces a strong impact on the structural pattern of the host SPE and this phenomenon can be estimated on the basis of the variation in the rate of the aforementioned scission and cross-linking probabilities.

When the radiation-induced scission process takes place with greater probability, molecules break down at a faster rate. The peak of the molecular distribution curves shifts towards the left i.e. towards the lower molecular weight region indicating that the system mostly contains smaller-sized molecules. On the other hand, if the cross-linking process occurs inside the sample with greater probability, molecules mostly join with each other and produce bigger-sized molecules. As a result, the peak of the distribution curve shifts towards the right in the higher molecular weight region with the increase of irradiation exposure time (t). This trend can be found in both mono-dispersive and poly-dispersive samples. It

should be kept in mind that, instead of investigating the variation of different structural as well as transportational properties of the host SPE with the change in irradiation dose, we have taken an initiative to study the nature of variation of those aforementioned properties with respect to the exposure time to irradiation (t). The experimental studies show good agreement with the simulation outcome.

Bibliography

[1] Nanda, P., De, S.K., Manna, S., De, U. and Tarafdar, S., 2010. Effect of gamma irradiation on a polymer electrolyte: variation in crystallinity, viscosity and ion-conductivity with dose. Nuclear Instruments and Methods in Physics Research Section B: beam Interactions with Materials and Atoms, 268(1), pp.73-78.

[2] Perloni, P., Magistris, A., Chiodelli, G., Faucitano, A. and Buttafava, A., 1991. Effects of gamma-radiation on polymer electrolytes: PEO and PEO20-LiClO4. International Journal of Radiation Applications and Instrumentation. Part C. Radiation Physics and Chemistry, 37(4), pp.615-621.

[3] Pucić, I. and Turković, A., 2005. Radiation modification of (PEO) 8ZnCl2 polyelectrolyte and nanocomposite. Solid State Ionics, 176(19-22), pp.1797-1800.

[4] Havlin, S. and Ben-Avraham, D., 1982. Fractal dimensionality of polymer chains. Journal of Physics A: Mathematical and General, 15(6), p.L311.

[5] Kozlov, G.V., Temiraev, K.B., Shustov, G.B. and Mashukov, N.I., 2002. Modeling of solid state polymer properties at the stage of synthesis: fractal analysis. Journal of applied polymer science, 85(6), pp.1137-1140.

[6] Rahaman, M.H.A., Khandaker, M.U., Khan, Z.R., Kufian, M.Z., Noor, I.S.M. and Arof, A.K., 2014. Effect of gamma irradiation on poly (vinyledene difluoride)–lithium bis (oxalato) borate electrolyte. Physical Chemistry Chemical Physics, 16(23), pp.11527-11537.

[7] Terabe, K., Hasegawa, T., Nakayama, T. and Aono, M., 2020. Invention and Development of the Atomic Switch. In Atomic Switch (pp. 139-160). Springer, Cham.

[8] Ismail, A.M., Mohammed, M.I. and El-Metwally, E.G., 2019. Influence of Gamma irradiation on the structural and optical characteristics of Li ion-doped PVA/PVP solid polymer electrolytes. Indian Journal of Physics, 93(2), pp.175-183.

[9] Mindemark, J., Sobkowiak, A., Oltean, G., Brandell, D. and Gustafsson, T., 2017. Mechanical stabilization of solid polymer electrolytes through gamma irradiation. Electrochimica Acta, 230, pp.189-195.

[10] Moad, C.L. and Winzor, D.J., 1998. Quantitative characterization of radiation degradation in polymers by evaluation of scission and cross-linking yields. Progress in polymer science, 23(5), pp.759-813.

[11] Suarez, J.C.M., da Costa Monteiro, E.E. and Mano, E.B., 2002. Study of the effect of gamma irradiation on polyolefins—low-density polyethylene. Polymer degradation and stability, 75(1), pp.143-151.

[12] Singh, T.J. and Bhat, S.V., 2003. Morphology and conductivity studies of a new solid polymer electrolyte:(PEG) x LiClO 4. Bulletin of Materials Science, 26(7), pp.707-714.

[13] Jurjiu, A., Friedrich, C. and Blumen, A., 2002. Strange kinetics of polymeric networks modelled by finite fractals. Chemical physics, 284(1-2), pp.221-231.

[14] Jurjiu, A., Koslowski, T., von Ferber, C. and Blumen, A., 2003. Dynamics and scaling of polymer networks: Vicsek fractals and hydrodynamic interactions. Chemical physics, 294(2), pp.187-199.

[15] Pucić, I. and Jurkin, T., 2007. Crystallization of γ-irradiated poly (ethylene oxide). Radiation Physics and Chemistry, 76(8-9), pp.1318-1323.

[16] Amir, S., Mohamed, N.S. and Ali, S.H., 2007. Simulation of the Fractal Patterns in Polymer Membranes. In Proceedings of the International Conference on Electrical Engineering and Informatics, Institut Teknologi Bandung, Indonesia June 17-19.

[17] Sharma, T., Aggarwal, S., Kumar, S., Mittal, V., Kalsi, P.C. and Manchanda, V.K., 2007. Effect of gamma irradiation on the optical properties of CR-39 polymer. Journal of materials science, 42(4), pp.1127-1130.

[18] Sinha, M., Goswami, M.M., Mal, D., Middya, T.R., Tarafdar, S., De, U., Chaudhuri, S.K. and Das, D., 2008. Effect of gamma irradiation on the polymer electrolyte $PEO - NH_4ClO_4$. Ionics, 14(4), p.323.

[19] Khafagy, R.M., Madani, M. and Badr, Y.A., 2008, September. Structural, Vibrational, Thermal And Electrical Characterization Of Gamma Radiation Crosslinked Poly (Vinyl Alcohol)Based Solid Polymer Electrolytes Blended with LiOH H_2O Salt. In AIP Conference Proceedings (Vol. 1047, No. 1, pp. 292-295). American Institute of Physics.

[20] Tarafdar, S., De, S.K., Manna, S., De, U. and Nanda, P., 2010. Variation in viscosity and ion conductivity of a polymer-salt complex exposed to gamma irradiation. Pramana, 74(2), pp.271-279.

[21] Mukhopadhyay, M., Saha, M., Ray, R. and Tarafdar, S., 2014. Structural Modificationand Variation in the Kinetics of Isoconversional Phenomena: A Study on the Effect of Gamma Irradiation on Poly (Ethylene Oxide). arXiv preprint arXiv:1411.5809.

[22] Saha, M., Makhopadhyay, M., Ray, R., Ballabh, T.K. and Tarafdar, S., 2015. Impact of tailored gamma irradiation on pore size and particle size of poly (ethylene oxide) films: correlation with molecular weight distribution and microstructural study. Modeling Simul Mater Sci Eng, 49, pp.5816-5832.

[23] Raghu, S., Archana, K., Sharanappa, C., Ganesh, S. and Devendrappa, H., 2015. The physical and chemical properties of gamma ray irradiated polymer electrolyte films. Journal of Non-Crystalline Solids, 426, pp.55-62.

[24] Kilic, M., Karabul, Y., Alkan, U., Yagci, O., Okutan, M., Okutan, M. and Icelli, O., 2017. Gamma-Ray Irradiation Effect on Mechanical and Dielectric Properties of Volcanic Basalt Mineral Reinforced low density Polyethylene Films. Physicochemical Problems of Mineral Processing, 53(1), pp.578-590.

[25] Manjunatha, H., Damle, R., Pravin, K. and Kumaraswamy, G.N., 2018. Modification in the transport and morphological properties of solid polymer electrolyte system by low-energy ion irradiation. Ionics, 24(10), pp.3027-3037.

[26] Stephan, A.M. and Nahm, K.S., 2006. Review on composite polymer electrolytes for lithium batteries. Poly-mer, 47(16), pp.5952-5964.

[27] Ngai, K.S., Ramesh, S., Ramesh, K. and Juan, J.C., 2016. A review of polymer electrolytes: fundamental, approaches and applications. Ionics, 22(8), pp.1259-1279.

[28] Nan, C.W., Fan, L., Lin, Y. and Cai, Q., 2003. Enhanced Ionic Conductivity of Polymer Electrolytes Containing Nanocomposite S i O 2 Particles. Physical review letters, 91(26), p.266104.

[29] Rajendran, S., Sivakumar, P. and Babu, R.S., 2007. Studies on the salt concentration of a PVdFPVC based polymer blend electrolyte. Journal of power sources, 164(2), pp.815-821.

[30] Ahmad, A., Rahman, M.Y.A., Low, S.P. and Hamzah, H., 2011. Effect of LiBF4 salt concentration on the properties of plasticized MG49-TiO2 based nanocomposite polymer electrolyte. ISRN Materials Science, 2011.

[31] Van Schalkwijk, W. and Scrosati, B., 2002. Advances in lithium ion batteries introduction. In Advances in Lithium-Ion Batteries (pp. 1-5). Springer, Boston, MA.

[32] Rogers R.D., Seddon K.R., 2002, Ionic Liquids: Industrial Applications to Green Chemistry, American Chemical Society (Distributed by Oxford University Press): Washington, DC. 2002

[33] Utracki, L.A. and Wilkie, C.A. eds., 2002. Polymer blends handbook (Vol. 1, p. 2). Dordrecht: Kluwer academic publishers.

[34] Sun, J., Wu, G. and Geng, J., 2013. Preparation of fractal-like structures of insoluble polythiophene via solvent vapor annealing of solid thermocleavable polythiophene films and subsequent thermal curing. Polymer journal, 45(8), p.813.

[35] Shin, S., Gu, M.L., Yu, C.Y., Jeon, J., Lee, E. and Choi, T.L., 2017. Polymer self-assembly into unique fractal nanostructures in solution by a one-shot synthetic procedure.Journal of the American Chemical Society, 140(1), pp.475-482.——

[36] Domenech, T., Zouari, R., Vergnes, B. and Peuvrel-Disdier, E., 2014. ormation of fractal-like structure in organoclay-based polypropylene nanocomposites. Macromolecules,47(10),pp.3417-3427.——

[37] Havlin S, Ben-Avraham D (1982) Fractal dimensionality of polymer chains. J Phys A Math Gen 15:L311–L316

[38] Vicsek T.(1992) Fractal growth phenomena, 2nd Edn.World scientific, Singapore

[39] Jayanthi, C.S. and Wu, S.Y., 1993. Frequency spectrum of a general Vicsek fractal. Physical Review B, 48(14), p.10188.

[40] Blumen, A., Jurjiu, A., Koslowski, T. and von Ferber, C., 2003. Dynamics of Vicsek fractals, models for hyperbranched polymers. Physical Review E, 67(6), p.061103.

[41] Vicsek, T., 1992. Fractal growth phenomena. World scientific.

[42] Havlin, S., Trus, B. and Stanley, H.E., 1984. Cluster-Growth Model for Branched Polymers That Are" Chemically Linear". Physical review letters, 53(13), p.1288.

[43] Havlin, S. and Ben-Avraham, D., 1987. Diffusion in disordered media. Advances in physics, 36(6), pp.695-798.

[44] ben-Avraham, D. and Havlin, S., 2000. Diffusion and Reaction in Fractals and Disordered Media.

[45] Aziz, S.B. and Abidin, Z.H.Z., 2015. Ion transport study in nanocomposite solid polymer electrolytes based on chitosan: electrical and dielectric analysis. Journal of Applied Polymer Science, 132(15).

[46] Nicolau, A., Nucci, A.M., Martini, E.M. and Samios, D., 2007. Electrical impedance spectroscopy of epoxy systems II: Molar fraction variation, resistivity, capacitance and relaxation processes of 1, 4-butanediol diglycidylether/succinic anhydride and triethylamine as initiator. European polymer journal, 43(6), pp.2708-2717.

[47] Charlesby, A., 2016. Atomic radiation and polymers: international series of monographs on radiation effects in materials. Elsevier.

[48] Faltermeier, A., Behr, M., Reicheneder, C., Proff, P. and Römer, P., 2011. Electron-beam irradiation of polymer bracket materials. American Journal of Orthodontics and Dentofacial Orthopedics, 139(1), pp.e7-e11.

[49] Zainuddin, Albinska, J., Ulański, P. and Rosiak, J., 2002. Radiation-induced degradation and crosslinking of poly (ethylene oxide) in solid state. Journal of Radioanalytical and Nuclear Chemistry, 253(3), pp.339-344.

[50] Bittner, B., Mäder, K., Kroll, C., Borchert, H.H. and Kissel, T., 1999. Tetracycline-HCl-loaded poly (DL-lactide-co-glycolide) microspheres prepared by a spray drying technique: influence of γ-irradiation on radical formation and polymer degradation. Journal of Controlled Release, 59(1), pp.23-32.

[51] Nanda, P., De, S.K., Manna, S., De, U. and Tarafdar, S., 2010. Effect of gamma irradiation on a polymer electrolyte: Variation in crystallinity, viscosity and ion-conductivity

with dose. Nuclear Instruments and Methods in Physics Research Section B: beam Interactions with Materials and Atoms, 268(1), pp.73-78.

[52] Saha, M., Mukhopadhyay, M., Ray, R., Ballabh, T.K. and Tarafdar, S., 2014. Influence of gamma irradiation on the molecular weight distribution and related properties of a polymer: study through simulation and experiment. Modelling and Simulation in Materials Science and Engineering, 23(2), p.025003.

[53] Mukhopadhyay, M., Saha, M., Ray, R. and Tarafdar, S., 2016. A study on the effect of gamma irradiation on Poly [-Ethylene Oxide]: structural modification and variation in the kinetics of isoconversional phenomena. Indian Journal of Physics, 90(10), pp.1133-1147.

Chapter- 4

Response of Different Molar Mass Averages of a Solid Polymer Electrolyte to Gamma Irradiation: A Theoretical Analysis Based on Computer Simulation on Deterministic Fractal Model

Chapter 4

Response of Different Molar Mass Averages of a Solid Polymer Electrolyte to Gamma Irradiation: A Theoretical Analysis Based on Computer Simulation on Deterministic Fractal Model

4.1. Introduction

Polymer materials consist of macromolecules that are made of one or a group of small repetitive units, called monomers[1]. Their chemical structure and compositions happen to be identical or nearly identical, only the degree of polymerization or the molecular weight changes. The preparation of an arbitrary polymer sample is done by a suitable polymerization reaction which is controlled by different external parameters. Molecules generated by the Polymerization process have many chain segments with a variety of lengths that are distributed following a Probability Distribution Function (PDF). The PDF is controlled by the method of the polymerization process that one is adopting to manufacture it and also other necessary conditions applied to execute that process[2]. Thus the degree of polymerization introduces poly-dispersive behavior inside the sample and hence the concept of average molecular weight is turned out to be a very relevant topic of research.

We have discussed in our previous chapter the effect of gamma irradiation on the molecular distribution pattern of the host polymer sample and investigated how the radiation-induced scission and cross-linking processes influence the nature of the molecular distribution pattern of the SPE. We have noticed that the probability of finding a molecule with an arbitrary molecular weight (fractal stage) depends on the probability of occurrence of radiation-induced scission and cross-linking processes inside the sample. In our present simulation work, the concept of scission and cross-linking has been implemented following some basic assumptions that have been mentioned in chapter-3. The detailed theoretical study suggests that the exposure time of the host polymer sample to the external gamma irradiation imposes a significant impact on the nature of its molecular weight distribution inside the host polymer sample. The system appears more poly-disperse with the passage of irradiation time steps (t). This phenomenon gives a direct impact on different molar mass averages and their values change significantly with the increase of irradiation time steps (t).

In this chapter, we will investigate the variation of different types of molecular weight averages (molar mass averages) with respect to the exposure time to irradiation (time step (t)). The molecule of a definite size is represented by a Vicsek fractal with an arbitrary fractal stage (s), same as we have done in the previous chapter. The average molecular weights are calculated with the help of some mathematical equations which will be discussed in the subsequent sections of this chapter. Here we have used the molecular weight distribution data obtained from the master equation in chapter-3 to calculate the four molar mass averages namely: number average molecular weight $\langle M_n \rangle$, weight average molecular

weight $\langle M_w \rangle$, Viscosity average molecular weight $\langle M_v \rangle$, Z-average molecular weight $\langle M_z \rangle$ for an arbitrary instant of exposure time to irradiation (t). The outcome of the simulation studies for both mono-disperse and poly-disperse samples has been analyzed separately in the result and discussion section.

4.2. Literature Review

The morphological changes due to the application of gamma irradiation on SPE happens to be one of the most interesting topics to researchers. Several research works were done in this field and it is well-established facts that the structural pattern of a host polymer sample in any form has been changed significantly due to the application of the externally applied field. Researchers have studied these changes based on different parameters among which molecular distribution happens to be an important one. Now there are different types of physical and chemical properties of the host polymer samples which are characterized by different types of molar mass averages and they explicitly depend on the molecular weight of the host polymer molecules. Therefore we can easily infer a direct correlation between the variations of molecular weight with different molar mass averages due to the application of different types of external fields.

Zhang Zhaomu et.al.[3] have used an interesting method to determine the weight average molecular weight of a polymer sample having an unknown value of the Mark-Houwink coefficient. They have used an approximate relationship between the intrinsic viscosity and GPC data of the sample. This process has been passed through the reliability check by universal calibration method which needs known values of Mark-Houwink coefficients for seven samples that have various types of molecular weight distribution. The uniqueness of their method is that it is based on universal calibration theory whether it does not require the values of K and α. Hence the determination of Mw becomes very easy for those polymers which don't have a perfect value of K and α.

C.Volland et.al.[4] worked with Captopril microspheres from different biodegradable polyesters of the general structure poly (D, L-I-lactide-co-glycolide) (PLG). Spray dying technique has been used to prepare this product. They observed the effect of gamma irradiation (with different doses) on captopril microspheres with different molecular weights. Using ^{60}Co source they studied the variation in weight average molecular weight (M_w) for the gamma irradiation with doses 6.9, 15.0, 27.7 and 34.8 kGy. They have noticed that the magnitude of M_w decreases with the increase of irradiation dose and this degradation

extent has been more intense for a higher initial value of M_w.

Norzita Yacob et.al.[5] have investigated the effect of gamma irradiation on the Viscosity-average molecular weight and intrinsic viscosity of the Ubbelohde viscometer. They have used the intrinsic viscosity measurement method to measure the molecular weight to characterize chitosan. In this regard, they prepared chitosan samples with different concentrations. Intrinsic viscosity was calculated from flow time data in this regard the reduced viscosity is extrapolated to zero concentration. The magnitude of intrinsic viscosity was again recalculated using the Mark-Houwink equation. They have determined the value of the constants k and α as k=$9.66X10^{-5}$ and α=0.742 in 0.15M Ammonium Acetate and 0.2 Acetic Acid solution at 25^oC room temperature. It has been observed that the magnitude of intrinsic viscosity reduces with the increase of irradiation dose up to 35kGy. The magnitude of viscosity average molecular weight (M_v) is also varied in the same way with the increase of irradiation dose. This relevant experiment also concludes that the external irradiation promotes chain scission or degradation in the chitosan at its solid-state.

A different kind of review work has been done by the Saviour A. Umoren et.al.[6]. They have reviewed different experimental techniques to measure the various types of average molecular weights. Initially, they have discussed the mathematical approach to calculate different average molecular weights. Post which some useful techniques like Osmometry, End Group Analysis, Light Scattering, Sedimentation technique, Gel Permeation Chromatography (GPC), Viscometry, Matrix-assisted laser desorption/ionization mass spectroscopy (MALDI-MS), and lastly Diffusion-ordered NMR spectroscopy (DOSY) method have been discussed for the calculation of different average molecular weights. It is very evident from their review work that the method that should be selected depends on the type of information required, experimental conditions, operative region, costing, etc.

M. Kassai et.al. and his co-workers[7] have studied the relationship between viscosity and molecular weight of chitosan in 0.25 M acetic acid 0.25M sodium acetate. Acid hydrolysis (HCl) and oxidative fragmentation ($NaNO_2$) techniques have been followed to prepare the chitosan sample from shrimp-shell chitosan. Different average molecular weights like (M_w), (M_v), number average molecular weight (M_n), and poly-dispersity were determined from Size exclusion chromatography (SEC), and membrane osmometry and light scattering method have been used to evaluate absolute molecular weights. Using the Mark–Houwink–Sakurada equation (MHS), the viscometric constants, α, and K were determined for a poly-disperse sample with the degree of acetylation (DA) of 20 and 25%. They succeeded to determine the value of α =0.79 which indicates a flexible chain-like structure

of chitosan in the solvent.

R. Dorati et. al.[8] deal with various kinds of multiblock copolymers like PEGd,lPLA, PEG-PLGA, PLA, and PLGA and they are irradiated with ^{60}Co irradiation source for different irradiation doses like 5,15,25 and 50 kGy. Each sample was characterized before and after the irradiation with the help of nuclear magnetic resonance (NMR), infrared absorption spectrophotometry (FTIR), and gel permeation chromatography (GPC). The NMR and FTIR study confirm a radiation-induced scission reaction due to the increase in -OH and -COOH groups inside the samples. Variation of M_w has been plotted against the irradiation dose from the data obtained by GPC analysis which shows a decreasing nature of M_w value with the increase in irradiation dose. On the other hand, the % of Mw reduction was distinctly observed in those polymer samples which have high molecular weight like PEGd, lPLA, and PLA. It was also observed that PEGd, lPLA shows greater sensitivity to the applied irradiation than PLA dye to the presence of PEG in the matrix. The consequence of gamma irradiation persists for a prolonged time duration after its application on the sample.

P. Nanda et. al.[9] have worked with ammonium perchlorate i.e. $PEO_{(1-x)} - NH_4ClO_4(x)$ samples with x = 0.18. They used gamma irradiation on it varying up to 50kGy. XRD and DSC analysis revealed that the crystallinity decreases with the increase of irradiation dose. The viscosity of the sample has been measured in its aqueous solutions having the identical concentration and it confirmed radiation-induced chain scission in addition with some cross-linking at the higher dose. The relative viscosity in the aqueous solution of the un-irradiated sample and samples irradiated to 10,25,53 and 45 kGy gamma dose were plotted on the graph. The graph suggests that relative viscosity decreases with the increase of irradiation dose. The same type of sample was used by Sujata Tarafdar and her co-workers[10] to study the variation of its microstructural properties as well as viscosities in the aqueous solution due to the application of gamma irradiation. They used 60Co as a source with a dose rate 60 Gy/min or 6 krad/min and doses 10, 12, 15, 17, 20, 25, 30, 35, 40, 45, and 50 kGy respectively and DSC studies are also done for all the samples. The variation of relative viscosity has been plotted in a graph which also shows a decreasing behavior with the increase of irradiation dose.

J. U. Izunobi et. al.[11] worked with two materials R-methoxy-ω-amino polyethylene glycol ($MPEG - NH_2$) and R-methoxy-polyethylene, glycol-block-poly-ϵ-(benzyl oxy carbonyl)-L-lysine (MPEG-b-PLL(Z)) as a model homopolymer and block copolymer, respectively to calculate the number average molecular weight $< M_n >$ using 1H NMR

method. The size exclusion chromatography (GPC) and mass spectrometry (MALDI-TOF) method has been used to calculate the molecular weight of the polymer. Their work reveals the fact that 1H NMR spectroscopy happens to be a very useful technique for the determination of $< M_n >$. On the other hand, though GPC is considered a highly acceptable method for the determination of molecular weight averages its limitations have also been discussed here.

Weibin Li et. al.[12] reported for the first time the determination of $< M_w >$ for kinetic samples from the diverse living/controlled polymerization processes using diffusion-ordered NMR spectroscopy (DOSY) technique.In this regard, they used three separate controlled polymerization techniques which are:atom transfer radical polymerization (ATRP), reversible addition-fragmentation chain transfer (RAFT),and ring-opening metathesis polymerization (ROMP).An external calibration curve was generated with the help of the logarithm of molecular weight ($\log < M_w >$) and diffusion coefficient (logD) which can predict the molecular weight of the narrowly dispersed polymer. The value $< M_w >$,evaluated by Dosy method shows a satisfactory similarity with the respective GPC data. They suggested this method more efficient than different types of alternative methods due to its, low sample loading, short measurement time, and high accuracy at a low molecular range.

Mario A. Garcı´a and his co-workers[13] prepared two sets of chitosan found from a heterogeneous chemical named N-deacetylation of chitin which is collected from common lobsters. The sample was then irradiated using ^{60}Co source with doses 5, 10, 20 and 50kGy and with a dose rate of 10kGy/h. the chemical properties of these samples were measured with the help of Attenuated Total Reflection Fourier Transform Infrared Spectroscopy. The viscosimetric method and potentiometric method were used to estimate the average viscometric $< M_w >$ and deacetylation degree respectively. They observed that $< M_w >$ of chitosan decreased significantly with the increase of irradiation dose up to 50kGy.

4.3. Classification of Molar Mass Averages

The molecular weight happens to be an important parameter to characterize the macromolecular system like polymer sample and it is also useful in describing the polymer chain lengths[14]. Therefore, the estimation of average molecular weight of an arbitrary polymer sample happens to be one of the prime targets of researchers. If an arbitrary poly-disperse polymer sample consists of different types of molecules having molecular weights M_1, M_2, M_3, etc. and they appear in the sample with probabilities p_1,p_2,p_3, etc. respectively, then

the average molecular weight of the sample can be defined as[15]

$$\begin{aligned} < M > &= p_1.M_1 + p_2.M_2 + p_3.M_3 + ... \\ Or < M > &= \Sigma p_i M_i \end{aligned} \tag{4.1}$$

An arbitrary polymer sample does not have a definite type of average molecular weight. Instead, different types of average molecular weights can be defined for a single polymer sample. Therefore, a unified form of the alternative expression of $\langle M \rangle$ can be written as[15]:

$$< M >= \frac{\Sigma n_i.M_i^{\alpha}}{\Sigma n_i.M_i^{\alpha-1}} \tag{4.2}$$

Where n_i is the total number of molecules with molecular weight M_i inside the polydispersive sample at an arbitrary time of polymerization process. Equation-(4.2) suggests that the nature of $\langle M \rangle$ explicitly depends on the parameter α. Therefore α happens to be a very important index that introduces the concept of different types of average molecular weights of the sample which will be discussed later.Molecular weight (M_w) of the host polymer sample is directly linked with its various kind of physical properties such as optical property, viscosity, chemical reactivity, etc.[16,17] One can define the average molecular weight of a polymer sample in different ways[18].

It can also be inferred from the equation—(4.2) that, the variation of α eventually generates different types of average molecular weights. Among them, viscosity average molecular weight $\langle M_w \rangle$, number average molecular weight $\langle M_n \rangle$, weight average molecular weight $\langle M_w \rangle$ are very common and widely discussed. In addition to that, Z average molecular weight also plays important role in many cases. The experimental data plotting of average MWs for an arbitrary polymer sample gives a clear idea about the numerical values of $\langle M_n \rangle$, $\langle M_v \rangle$, $\langle M_w \rangle$, and from those results, we can arrange the average molecular weights in ascending order as follows: $\langle M_n \rangle < \langle M_v \rangle < \langle M_v \rangle < \langle M_z \rangle$[18].

Different types of experimental techniques have been applied so far to measure the above-mentioned average $\langle M \rangle$. Among them, osmometry, static light scattering, gel permeation chromatography (GPC),matrix-assisted laser desorption-ionization mass spectrometry, end-group analysis, viscometry, field-flow fractionation, small-angle X-ray scattering, ultracentrifugation, small-angle neutron scattering, cryoscopy, ebulliometry are significant[19–23]. The four important types of average MWs are discussed below:

4.3.1. Number Average Molecular Weight $\langle M_n \rangle$

Number average molecular weight $\langle M_n \rangle$ can be obtained by setting the value of the exponent $\alpha = 1$ in equation-(4.2). The mathematical expression of number average molecular weight $\langle M_n \rangle$ can be written as[15]:

$$\langle M_n \rangle = \frac{\Sigma n_i.(M_i)}{\Sigma n_i} \tag{4.3}$$

Since Σn_i = N = total number of polymer molecules present inside the sample, equation-(4.3) can be written as:

$$\langle M_n \rangle = \Sigma \frac{n_i}{N}.M_i = \frac{n_1}{N}.M_1 + \frac{n_2}{N}.M_2 + \frac{n_3}{N}.M_3 + ... \tag{4.4}$$

$$= p_1.M_1 + p_2.M_2 + p_3.M_3 + ... \tag{4.5}$$

Where $p_i = \frac{n_i}{N}$ and the above-mentioned equation is similar to the equation-(4.1) . Here each fractional co-efficient of M_i (i.e. $\frac{n_i}{N}$) represents the molar fraction of an arbitrary type of molecular species with MW M_i. Equation—(4.3) clearly suggests that $\langle M_n \rangle$ has a strong dependence on the number of molecules, present inside the host polymer sample. In fact, $\langle M_n \rangle$ is highly sensitive for the samples with lower molecular weight[24] because the addition or subtraction of a small amount of this types of sample results in the variation of a large number of molecules. On the contrary, variation in a small amount of mass for a sample having bigger size molecules with higher molecular weights gives comparatively lesser impact on the $\langle M_n \rangle$. Hence, the total number of molecules having an arbitrary value of molecular weights inside the polymer material plays a significant role in determining the value of $\langle M_n \rangle$.

Number average molecular weight $\langle M_n \rangle$ happens to be the arithmetic mean of the molecular weight (M_i) of all types of molecules, present in the sample. It is directly related to different types of physical properties of the polymer sample. Tensile strength of a polymer sample happens to be one of them which can be expressed as:

$$\sigma_1 = c_1 + \frac{c_2}{(< M_n >)} \tag{4.6}$$

Where σ_1 is tensile strength and c_1 and c_2 are constants[25]. Researchers across the globe have adopted various techniques so far to measure $\langle M_n \rangle$ of a polymer solution. Among them, osmometry, end group titration,[21,26] are very common and used in various cases.

End group titration happens to be a straightforward method whose efficacy depends on various factors such as it requires quantifiable end groups (through NMR spectroscopy or titration reaction), end groups should be well known and consistent, reactive end groups should have very high concentration, the molar mass of the respective molecules should be below 10^4 Dalton to prevent steric blockage of the end groups, etc.[27].

On the other hand, osmometry happens to be a method that needs a dilute solution that consists of solute and solvent with a known number of moles. This method is based on the comparison between the pressure of the solute molecules against one solvent vs another solvent to estimate the number of molecules inside the host polymer sample[27]. Some other methods are used to estimate the $\langle M_n \rangle$ of a polymer sample. Determination of $\langle M_n \rangle$ using cryoscopic (freezing point depression), ebulliometric (boiling point elevation), and osmometric (membrane osmometry) measurement of polymer in dilute solution[15] are also recommendable. Similarly, 1-D and 2-D NMR techniques are also convenient options for the determination of $\langle M_n \rangle$ as well as the microstructure and chemical composition of the host polymer sample[21] Most of these methods have some limitations as well e.g. the end group titration method is useful for sparsely branched, short-chained polymer molecule such as synthetic polyesters and polyamides which consists with monodisperse molecules of synthetic origin[21, 29].

On the other hand, the osmometric process does not provide an accurate value for those polymers having molecules with molecular weights above 10^6 Dalton, and its accuracy is restricted by the sensitivity of the osmometric pressure sensor[21, 29]. But one advantage of this process is that it does not require any calibration as it measures the absolute molecular weight of the sample. The other two methods are used for samples having low molecular weight and low resolution. Sometimes boiling point and freezing point (also known as colligative properties) are used to estimate $\langle M_n \rangle$ of the sample but their use is restricted to low molecular weight sample and a large sample volume is also needed for the determination of $\langle M_n \rangle$ of the sample[21, 29].

4.3.2. Weight Average Molecular Weight $\langle M_w \rangle$

We have mentioned before the parameter α plays a significant role in case of the classification of molecular weight averages of the host polymer sample. If we put the value $\alpha = 2$ in equation-(4.2), it will give the mathematical form of weight average molecular weight $\langle M_w \rangle$

of the said sample which can be expressed as:

$$\langle M_w \rangle = \frac{\Sigma n_i.(M_i)^2}{\Sigma n_i.M_i} \tag{4.7}$$

Therefore $\langle M_w \rangle$ consider the contribution of an arbitrary polymer molecule as per its size[11,30]. It is also known as the second moment of molar mass average. Instead of calculating the total number of molecules, weight average molecular weight of a polymer sample is estimated from the average molecular size[27] of the host polymer molecules. Equation-(4.7) can also be modified and written in the form of a summation series similar to equation-(4.1) as[15]:

$$\begin{aligned} \langle M_w \rangle &= \frac{\Sigma n_i.(M_i)}{\Sigma n_i.M_i}.(M_i) = \frac{\Sigma(w_i)}{W}.(M_i) \\ &= \frac{w_1}{W}.M_1 + \frac{w_2}{W}.M_2 + \frac{w_3}{W}.M_3 + ... \\ &= p_1^w.M_1 + p_2^w.M_2 + p_3^w.M_3 + ... \end{aligned} \tag{4.8}$$

Here p_i^w = signifies the weight fraction of an arbitrary molecular species of molecular weight M_i in the polymer solution and w_1, w_2, w_3, etc represent the net weight of various molecular species with molecular weight M_1, M_2, M_3, etc. respectively. The ratio for $\langle M_w \rangle$ to the $\langle M_n \rangle$ signifies the poly-dispersity index (PDI) of an arbitrary polymer sample and it always has a positive value[15,30]. The higher value of PDI comes from the higher value of $\langle M_w \rangle$ and it signifies the wide range of molecular weight distribution due to the presence of a large number of macromolecules having a veriety of molecular weights[15,30].

It can be explained mathematically that the value of $\langle M_n \rangle$ and $\langle M_w \rangle$ are equal (i.e. $\langle M_w \rangle = \langle M_n \rangle$) for a pure mono-disperse sample and their ratio: $\langle M_w \rangle / \langle M_n \rangle$ happens to be always unity[14]. But in the case of any poly-disperse sample $\langle M_w \rangle$ is always greater than $\langle M_n \rangle$. Hence, $\langle M_w \rangle / \langle M_n \rangle$ will always be greater than unity in a poly-disperse sample, and it is considered as the measure of poly-dispersity of the polymer material[15,30]. The importance of the $\langle M_w \rangle$ is considered in the context of different bulk properties like rheological and resistance properties, elastic modulus and elongation at break, toughness and impact resistance, softening/melting, and hot deformation, tensile and compressive strength, etc.[15,30]. In the case of studying these properties, one should consider the effect of the chemical nature of the repeat units, thermochemical as well as thermal background, degree of branching, cross-linking of the polymer sample, etc.

Light scattering method is considered as one of the most convenient ways to measure $\langle M_w \rangle$ of a polymer sample. In this method, incident light beam on any arbitrary polymer molecule gets scattered at an angle with respect to the incident ray when it passes through the target. The intensity of the scattered light is controlled by the concentration of the sample solution, polarity, and chain size[6]. Therefore considering all these conditions, $\langle M_w \rangle$ is evaluated from the intensity of Raleigh scattering (elastic light scattering) from individual polymer molecule. The mathematical relation that is used to evaluate $\langle M_w \rangle$ from the scattered light is[6,27]:

$$\Delta R_\theta = k_c . < M_w > . < P(\theta)_z > \tag{4.9}$$

Here $< P(\theta)_z >$ is the average particle scattering factor that serves the purpose of determining scattering from large molecules with relatively small wavelength. k_c is an optical constant, c being polymer concentration and ΔR_θ represents the deviation in Rayleigh scattering at a definite angle θ. The advantage of this process is that, it can be performed in a wide molecular weight range. The process is sensitive, and can yield a result with high resolution. It can also measure poly-disparsity. But the process has some drawbacks too. It is a slow process and requires costly equipment, the sample must be free from dust or any other impurities etc[6,29].

Another useful technique to measure the $\langle M_w \rangle$ of a polymer solution is known as the sedimentation method[6]. It is a classical method that can be performed by two techniques: sedimentation equilibrium and sedimentation velocity with the help of ultracentrifugation. The sedimentation equilibrium method does not involve any transport of solute. Thus, $\langle M_w \rangle$ can be determined directly[6]. This method is applicable for different aggregating and dissociating systems. On the other hand, sedimentation velocity is suitable for mainly mono-disperse systems, but it can also be applicable for poly-dispersed systems. Here the rate of displacement of particles under the influence of strong centrifugal force is measured with the help of some suitable relation and from this, the value of $\langle M_w \rangle$ can be estimated[32].

4.3.3. Viscosity Average Molecular Weight $\langle M_v \rangle$

Viscosity average molecular weight $\langle M_v \rangle$ happens to be another important parameter whose quantitative analysis is different from that of the other molar mass averages. It is related to the intrinsic viscosity (η) of the polymer sample, and is derived from the semi-empirical

equation known as the Mark–Houwink–Sakurada (MHS) equation[32,33]:

$$[\eta] = k_v.[< M_v >]^{\alpha} \tag{4.10}$$

Here $[\eta]$ represents intrinsic viscosity, and k_v and α are constants that depend on the nature of the solute-solvent system as well as the temperature and collectively known as Mark–Houwink–Sakurada (MHS) constant[34]. This equation contains two constant parameters. Researchers have proposed some experimental techniques[35] to estimate the value of k_v and α from two polymer samples with two distinct intrinsic viscosities. Evaluation of k_v and α from the $\langle M_n \rangle$ and intrinsic viscosity $[\eta]$ has also been reported[36]. Generally, one needs either several mono-disperse polymer samples whose molecular weight is known or several poly-disperse samples whose value of $\langle M_v \rangle$ is known to determine the value of k_v and α[7]. Theoretically, the value of α varies between 0 and 1 but experimental observation suggests that the value of α lies between 0.5 to 0.8 ($0.5 < \alpha < 0.8$)[15] in other literature this range is estimated between 0.5 to 0.9[32]. In some other experimental studies the value of α is estimated as 0.742[5]. α can also be estimated from the plot of $\log[\eta]$ vs $\log[k_v]$ graph.

The mathematical expression of $\langle M_v \rangle$ can be derived from the Mark–Houwink–Sakurada (MHS) equation[15]. To do so, let us consider an infinitely dilute poly-disperse polymer solution of concentration c ($c \longrightarrow 0$) where the individual constituent molecules contribute to increasing viscosity independently. Based on this consideration, we assume the specific viscosity offered by the sth size molecules is $(\eta_{sp})_s$. Hence net viscosity is[15]:

$$[\eta_{sp}] = \Sigma(\eta_{sp})_s \tag{4.11}$$

Let us consider η and η_0 happens to be the viscosity of the polymer solution and the pure solvent respectively at a definite temperature. For a very dilute solution, the polymer sample, dissolved in the pure solute at a given temperature, provide negligible effect on the density change of the solution. Under this condition, the viscosities of the solution (η) and the solvent (η_0) would be proportional to their respective flow times t and t_0 in a given capillary viscometer. Therefore the specific viscosity of a polymer solution is defined as:

$$\eta_{sp} = \frac{(\eta - \eta_0)}{\eta_0} = \frac{(t - t_0)}{t_0} \tag{4.12}$$

If c_s be the concentration of the molecular species of size (s) with molecular weight M_s then the ideal specific viscosity component will be[15,29]:

$$(\eta_{sp})_s \quad = \quad K.(M_s)^{\alpha}.c_s \tag{4.13}$$

Therefore the overall specific viscosity η_{sp} can be written as[15,29]:

$$\eta_{sp} = \Sigma(\eta_{sp})_s = K.\Sigma(M_s)^{\alpha}.c_s$$

$$\Rightarrow \frac{\eta_{sp}}{c} = [\eta] = \frac{(K.\Sigma(M_s)^{\alpha}.c_s)}{c} \tag{4.14}$$

Here c stands for the total concentration of the solution considering all types of polymer molecules. Thus $c = \Sigma c_s = \Sigma N_s.(M_s)$. Also, $[\eta]$ is called the reduced viscosity and defined by :$[\eta] = \eta_{sp}/c$[15]. Putting these values in equation-(4.14) we can write[15,29]:

$$[\eta] = \frac{(K.\Sigma(M_s)^{\alpha}.c_s)}{c} = K.\frac{\Sigma N_s.(M_s)^{(1+\alpha)}}{\Sigma N_s.M_s} \tag{4.15}$$

We have the Mark–Houwink–Sakurada (MHS) equation which has been mentioned in equation-(4.10). Therefore compairing equation-(4.10) and equation-(4.15), we can write:

$$\langle M_v \rangle = \left[\frac{\Sigma N_s.(M_s)^{(1+\alpha)}}{\Sigma N_s.M_s}\right]^{\frac{1}{\alpha}} \tag{4.16}$$

Equation-(4.16) is the mathematical expression of $\langle M_v \rangle$ which will be used later in this chapter to investigate the effect of gamma irradiation on $\langle M_v \rangle$ of the host solid polymer sample.

Different types of methods are there to measure the value of $\langle M_v \rangle$ of the polymer solution. Gel electrophoresis and capillary viscometry method happens to be the very relevant and convenient among them[15]. Basically, $\langle M_v \rangle$ is estimated from the difference in viscosity of the pure solvent and that of the polymer mixed solvent where different polymer mixed solutions of varying concentrations are prepared with the same polymer and solvent[15]. In 1930, Hermann Studinger proposed a quantitative relation between the increase in viscosity and the molecular weight of the polymer sample. Ubbelohde capillary viscometer is used most conveniently to determine the viscosity of the polymer solution[6]. Various factors control the viscosity of the polymer solution such as the solvent-solute interaction, concentration of polymer, molecular weight of polymer sample, etc[15]. Intrinsic viscosity happens to be a lucrative characterization method as the required instruments are of low cost,the process is comparatively rapid. viscometric methods is comparatively simple and overall a convenient method for many chemical companies[29,37].

4.3.4. Z-Average Molecular Weight $\langle M_z \rangle$

We know that the weighting factor α in equation-(4.2) plays a significant role in determining the nature of the average molecular weight inside the host polymer system. Considering the value of the weighting factor $\alpha = 3$, we get the mathematical form of z-average molecular weight $\langle M_z \rangle$ as[14,15,27]:

$$\langle M_z \rangle = \frac{\Sigma n_i.(M_i)^3}{\Sigma n_i.(M_i)^2} \tag{4.17}$$

It is also known as the third moment of the molar mass average. ($\langle M_z \rangle$) happens to be highly sensitive to the large size molecules present inside the polymer sample and they are relevant for the characterization of polymer samples focusing on the long polymer chains[38]. For a given molecular distribution, the molar mass averages can be arranged in a descending order as follows: ($\langle M_z \rangle$) > ($\langle M_w \rangle$)> ($\langle M_v \rangle$) > ($\langle M_n \rangle$)[14]. $\langle M_z \rangle$ is comparatively more acute to the polymer molecules having higher molecular weight. The value of $\langle M_z \rangle$ for a polymer solution is measured with the help of ultracentrifuge where one follows the sedimentation equilibrium technique[11].

In this method, a dilute solution of an arbitrary polymer sample is taken and a centrifugal force is applied to the sample for a long period of time with a very low speed of rotation avoiding the convection-related disturbance[15]. Under this condition, the probability of the polymer molecules to diffuse out is balanced by the force of sedimentation applied on them. Hence, thermodynamic equilibrium is achieved after a certain period of time. Under this equilibrium condition, the polymer fractions are arranged based on their size. With the help of this method, one can estimate the value of $\langle M_z \rangle$ for both mono-disperse, as well as poly-disperse samples, and the molecular weight as obtained from this process is known as z-average molecular weight $\langle M_z \rangle$[15].

4.4. Computer Simulation Method to Study the Variation of Molar Mass Average due to Gamma Irradiation

The concept of different types of molar mass averages, their significance, and various types of measurement techniques have already been discussed in the previous section. In this section, we will discuss the metod that we have followed for our computer simulation to study the effect of gamma irradiation on different types of average molecular weights (molar mass averages) of the host polymer system.

We recall the generalized mathematical equation which has been mentioned in equation-(4.2). We have followed this fundamental equation in our present computer simulation process to originate the mathematical formulas of different types of average molecular weights.

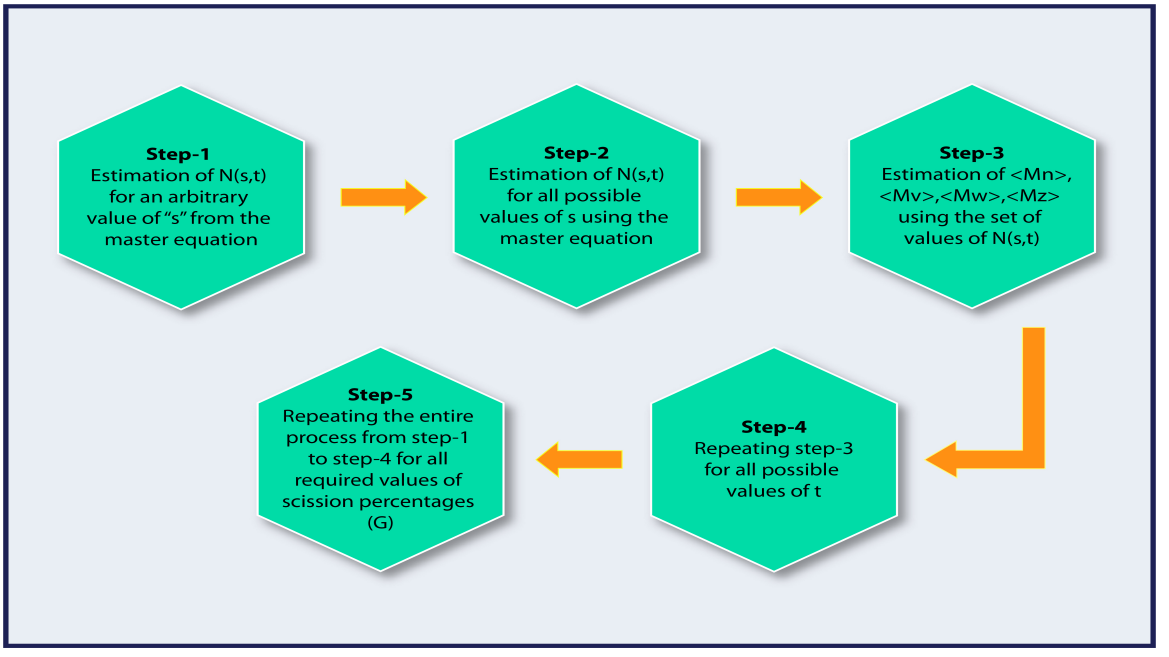

Figure 4.1: *Representation of the computer simulation process to study the radiation induced molar mass average variation with the help of a flow chart*

It is very evident from equation-(4.2) that average molecular weights extensively depend on the molecular distribution pattern (PDF) inside the host polymer sample at an arbitrary instant of irradiation time step (t). We have already discussed in chapter-3 that the host polymer molecules with different molecular weight have been modelled with Vicsek fractal with different fratal stages. We have also concluded from the detailed comutational study in chapter-3 that gamma irradiation introduces significant changes in the molecular distribution pattern (i.e. the N(s,t) and $W_f(s,t)$ vs s distribution pattern)of the host polymer sample. Therefore, it can easily be understood that the application of gamma irradiation also results in noticeable modifications in the molar mass averages. The entire simulation process in this chapter is based on some steps that are mention below:

Step-1: Initially we have considered a monodisperse polymer sample which contains 1000 molecules that are modelled with the 7th stage Vicsek fractals. Therefore the initial un-irradiated polymer sample contains 78125000 number of monomers which will be conserved throughout the irradiation process same as it was in chapter-3.

Step-2: The sample is then being exposed under the external irradiation and therefore we have estimated the number of molecules N(s,t) with fractal stage s that are present inside the host polymer sample at an arbitrary instant of exposure time to irradiation (time step t). In this case, we have used the master equation that we have established in the chapter-3.

Step-3: Following the same procedure, mentioned in step-2, we account for a set of N(s,t) for all possible values of (s) at an arbitrary time step (t). This gives us knowledge about the molecular distribution pattern (i.e. the N(s,t) vs s variation pattern) of the all polymer molecules of the sample at an arbitrary instant time step (t).

Step-4: We use four different mathematical equations (we have discussed them in the previous section) to evaluate four different molar mass averages. The number of molecules n_i having molecular weight $M_i = 5^s$ in those four mathematical equations of the molar mass averages, has been represented by the set of N(s,t)that we have estimated following the master equation in chapter-3. Thus we can get the values of four different molar mass averages at an arbitrary instance of irradiation time step (t)

Step-5: This process is repeated for all values of irradiation time steps (t) that is required to analyze the nature of variation of different types of molar mass averages of the polymer electrolyte sample. Thus we can find four different molar mass averages vs time step (t) variation curves for an arbitrary scission percentage.

Step-6: Again this entire process, mentioned from step-2 to step-5 is repeated for different values of scission percentages (which has been incorporated in our simulation with the help of the scission parameter G) for a complete analysis of the radiation-induced molar mass averages variation of the host SPE sample. In this case, we actually vary the numerical value of the parameter G as per our requirement within the limit 0.0 to 1.0, mentioned in chapter-3 .

Step-7: The entire process from step-1 to step-6 has been repeated again to study the same molar mass averages variation in case of poly-disperse sample. In this case we have taken the same poly-disperse sample which we have taken in chapter-3.

The abovementioned steps are followed to study the effect of external radiation on all types of molar mass averages. The entire simulation procedure has been explained through a flow chart in figure-4.1. The mathematical equations that have been used in our computer simulation are discussed in the preceding sub-sections.

4.4.1. Number average molecular weight $\langle M_n \rangle$

The mathematical formula required to calculate the number average molecular weight $\langle M_n \rangle$ can be established from the equation-(4.2) by taking the value of the exponent α=1. Thus the expression for $\langle M_n \rangle$ can be written as:

$$< M_n >= \frac{\Sigma n_i.(M_i)}{\Sigma n_i} \tag{4.18}$$

In the case of our present simulation, n_i is replaced by the total number of molecules N(s,t) inside the polymer sample with a fractal stage (s) at an arbitrary irradiation time step=t. We have derived the value of N(s,t) from the master equation mentioned in chapter-3. It is a function of molecular size index (s) and the exposure time to irradiation (t). According to our assumptions in chapter-3, we have modelled each polymer molecule inside the sample with Vicsek fractals with any arbitrary stage (s). Hence, the molecular weight of each of the N(s,t) number of molecules with molecular size index (s) can be written as: $M_i = M(s) = 5^s$. Thus the mathematical formula that we have used for our simulation to calculate $\langle M_n \rangle$ can be written as:

$$\langle M_n(t) \rangle = \frac{\Sigma_s N(s,t).(5^s)}{\Sigma_s N(s,t)} = \frac{\Sigma_s N(s,t).}{N(t)}.(5^s) \tag{4.19}$$

The denominator $\Sigma_s N(s,t)$ represents the total number of molecules present inside the sample at an instant (t) which can be calculated from the master equation mentioned in chhapter-3. $\frac{N(s,t)}{\Sigma_s N(s,t)}$ represents the fraction of the total number of molecules with molecular weight 5^s inside the host polymer sample at an instant (t). It is very clear that the numerator term in the equation-(4.19) also represents the total number of the monomer (A) inside the sample. Therefore it will be conserved (constant) throughout the irradiation process. Number average molecular weight $\langle M_n \rangle$ happens to be a function of irradiation exposure time (t) only.

4.4.2. Weight average molecular weight $\langle M_w \rangle$

The mathematical expression for the weight average molecular weight $\langle M_w \rangle$ can be obtained from the generalized equation-(4.2) by putting the value of α =2 in it. Therefore $\langle M_w \rangle$ can be written as:

$$\langle M_w \rangle = \frac{\Sigma n_i.(M_i)^2}{\Sigma n_i.(M_i)} \tag{4.20}$$

Where, M_i and n_i have their standard meaning, mentioned previously. Here also we have replaced n_i with N(s,t) and M_i with 5^s for the sake of our simulation study. Thus equation-(4.20) can be re-written as:

$$\begin{aligned}\langle M_w(t)\rangle &= \frac{\Sigma_s N(s,t).(5^s)^2}{\Sigma_s N(s,t).(5^s)} \\ &= \frac{\Sigma_s N(s,t).(5^s)}{W_T}.(5^s) \\ &= \frac{\Sigma_s W(s,t)}{W_T}.(5^s) \end{aligned} \tag{4.21}$$

Here, $W_T = \Sigma_s N(s,t).(5^s)$ is the net weight of the polymer sample which represents the total number of monomer present inside the system and it is conserved throughout the irradiation process. It is expressed as A in chapter-3. $W(s,t) = N(s,t).(5^s)$ is considered as the total number of monomer required to construct N(s,t) numbers of polymer molecules which have molecular weight $m(s) = (5^s)$ and the probability of finding an arbitrary molecule with fractal stage =s can be written as:

$$< P_w(s,t) > = \frac{W(s,t)}{W_T} = \frac{N(s,t).5^s}{W_T} \tag{4.22}$$

Here, $\langle M_w\rangle$ is also a function of irradiation exposure time (t) only. It is easily understandable from the equation-(4.21) that the molecular weights of the polymer molecules vary as a power of 5 (i.e. 5^s). Hence, change in the fractal stage s of the respective polymer molecules is expected to introduce a significant change in the $\langle M_w(t)\rangle$ variation.

4.4.3. Viscosity Average Molecular Weight $\langle M_v(t)\rangle$

The mathematical expression of viscosity average molecular weight $\langle M_v(t)\rangle$ that we have derived from the Mark-Houwink equation is[15]:

$$\langle M_v(t)\rangle = \left[\frac{\Sigma N_s.(M_s)^{(1+\alpha)}}{\Sigma N_s.M_s}\right]^{\frac{1}{\alpha}} \tag{4.23}$$

It can easily be understood that the abovementioned equation cannot be obtained directly from the generalized mathematical equation for the molar mass averages equation—(4.2) by just taking any integer value of x. We have replaced the M_i and n_i of equation-(4.23)

with 5^s and N(s,t) respectively in a similar way as we have done in the case of the other molar mass averages. Therefore the mathematical expression of $\langle M_v(t)\rangle$ for the simulation study can be written as:

$$\langle M_v(t)\rangle = \left[\frac{\Sigma N(s,t).(5^s)^{(1+\alpha)}}{\Sigma N(s,t).(5^s)}\right]^{\frac{1}{\alpha}} = \left[\frac{\Sigma W(s,t).(5^s)^{\alpha}}{W_T}\right]^{\frac{1}{\alpha}} \tag{4.24}$$

Where, $W_T = \Sigma N(s,t).(5^s)$ and W(s,t) have already been explained in case of $\langle M_w(t)\rangle$.

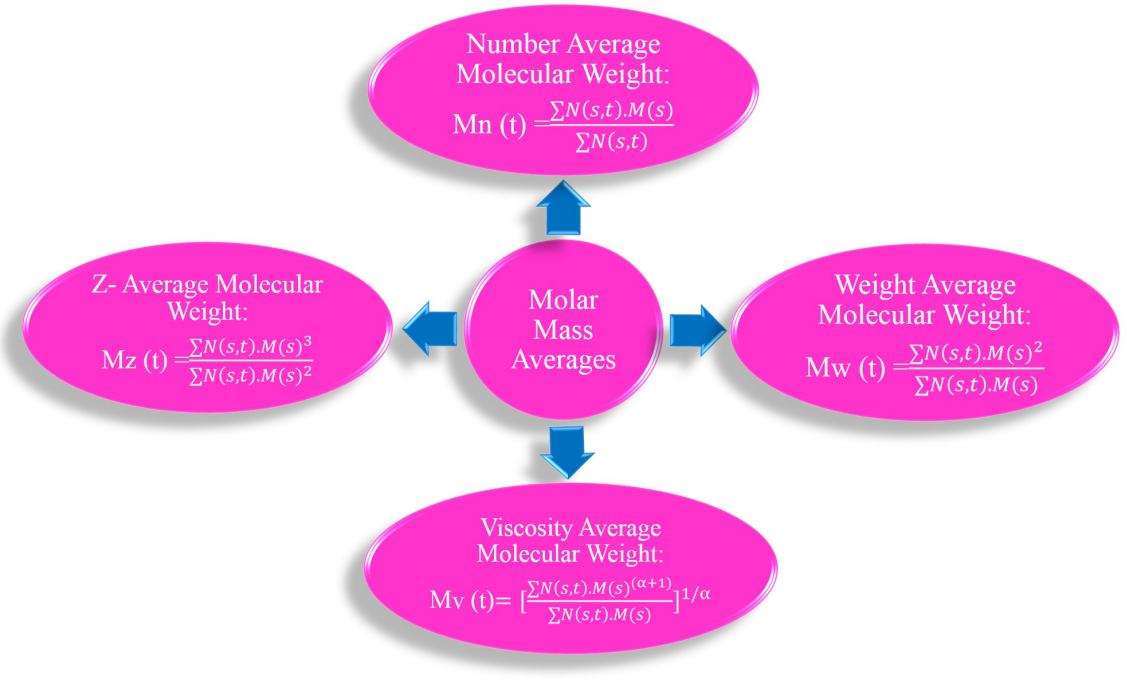

Figure 4.2: *Different types of molar mass averages and their mathematical expressions for computer simulation.*

The choice of weighting factor α in the present case is not so straightforward like the other molar mass averages, rather this selection of α plays an important role to estimate the variation $\langle M_v(t)\rangle$ with external gamma irradiation. We have alreasy mentioned in previous section that the value of the exponent α varies from 0.5 to 0.8 experimentally.[5,34] In our present simulation, we have taken two different values of α as α =0.5 and 0.7 to study the variation of $\langle M_v(t)\rangle$ under the application of gamma irradiation. The result thus obtained from these two different values of α has been analyzed, compares, and matched with respect to the experimentally observed data.

4.4.4. Z-average molecular weight $\langle M_z(t)\rangle$

Considering the value of x =3 in the generalized mathematical equation-(4.2), we get the mathematical expression for Z-average molecular weight as:

$$< M_z >= \frac{\Sigma n_i.(M_i)^3}{\Sigma n_i.(M_i)^2} \tag{4.25}$$

Same as in the case of $\langle M_v(t)\rangle$, we consider n_i= N(s,t) and $M_i = 5^s$ and get the modified expression of $\langle M_z(t)\rangle$ for our simulation purpose as:

$$\begin{aligned}\langle M_z(t)\rangle &= \frac{\Sigma N(s,t).(5^s)^3}{\Sigma N(s,t).(5^s)^2} \\ &= \frac{\Sigma N(s,t).(5^s)^2}{Z_T}.(5^s) \\ &= \frac{\Sigma Z(s,t)}{Z_T}.(5^s)\end{aligned} \tag{4.26}$$

Where $Z_T = \Sigma(s,t).(5^s)^2$ and $Z(s,t) = N(s,t).(5^s)^2.\langle M_z(t)\rangle$ is highly sensitive to polymer molecules with higher molecular weights. We will verify it in the result section. We have calculated the mathematical expression of $\langle M_z(t)\rangle$ and $\langle M_w(t)\rangle$ for our simulation study in equation-(4.26) and equation-(4.21). Therefore using these equations we can write:

$$\begin{aligned}\frac{\langle M_z(t)\rangle}{\langle M_w(t)\rangle} &= \frac{\Sigma N(s,t).(5^s)^3}{\Sigma N(s,t).(5^s)^2}.\frac{\Sigma N(s,t).(5^s)}{\Sigma N(s,t).(5^s)^2} \\ &= \frac{[\Sigma N(s,t).(5^s)^3].[\Sigma N(s,t).(5^s)]}{[\Sigma N(s,t).(5^s)^2]^2}\end{aligned} \tag{4.27}$$

The values of N(s,t) and s are always an integer and therefore we can predict from the equation-(4.27) the value of the ratio $\frac{\langle M_z(t)\rangle}{(\langle M_w(t)\rangle)}$.

4.5. Results of the computer simulation

The quantitative study from the last section, reveals tha fact that the variation of molecular weight distribution gives a direct impact on the different molar mass averages. In the present section, we will analyze the outcome of the simulation study regarding the radiation induced different molar mass averages variation of the host polymer sample. The whole simulation has been carried out on both mono-disperse as well as poly-disperse samples same as we have done in the previous chapter.

4.5.1. Effect of Gamma Irradiation on Different Average Molecular Weights (Molar Mass Averages) for Mono-disperse SPE sample

The mathematical modelling of an un-irradiated mono-disperse sample is done by 1000 molecules that are configured by 7th stage Vicsek fractals and the detailed description of this modelling technique has been presented in the previous chapter-3. In this present sub-section, we will discuss the outcome of the computer simulation which is performed to study the effect of gamma irradiation on the four molar mass averages $\langle M_n \rangle$, $\langle M_w \rangle$, $\langle M_v \rangle$,$\langle M_z \rangle$)of the mono-disperse sample.

4.5.1.1. Effect of Gamma Irradiation on Number Average Molecular Weight $\langle M_n \rangle$ for Mono-disperse SPE sample

The variation of number average molecular weight $\langle M_n \rangle$ of the host polymer sample with respect to the external gamma irradiation is shown in figure-4.3 and figure-4.4. The entire simulation is carried out following the equation-(4.19). It should be noted that the value of N(t) in the denominator of equation-(4.19) changes with the change in irradiation time step-t whereas the numerator remains unchanged as it denotes the total numbers of monomer, present inside the sample. Therefore the parameter N(t) happens to be the sole responsible for the variation in $\langle M_n \rangle$. The effect of gamma irradiation on $\langle M_n \rangle$ of a mono-disperse sample in case of pure scission and the pure cross-linking process has been presented in figure-4.3. Figure-4.3(A) represent the radiation induced $\langle M_n \rangle$ variation in case of pure scission process where each molecule of the sample (with fractal stage s) participate in scission process and break down into five daughter molecules, smaller in size (with fractal stage (s-1)).

The molecular distribution pattern has been presented in the inset of figure-4.3(A). The rapid increase of N(t) results in a fast reduction in the magnitude of $\langle M_n \rangle$ of the sample with the passage of time steps (t) as per the equation-(4.19) and it can be visible in figure-4.3(A). Here the rapid fall of the $\langle M_n \rangle$ vs t curve continues till the irradiation time step t=4. Post which the said curve attains a saturation value. The opposite types of behavior can be noticed in the case of pure cross-linking process (where the probability of cross-linking is 100%) which is shown in figure-4.3(B). In this case $\langle M_n \rangle$ vs t curve increases very fast and attains the saturation value at the time step t= 4, post which the value of $\langle M_n \rangle$ remains unaltered throughout the irradiation process. Variation of the number of molecules N(s,t) for 100% cross-linking process has been shown in the inset of figure-4.3(B).

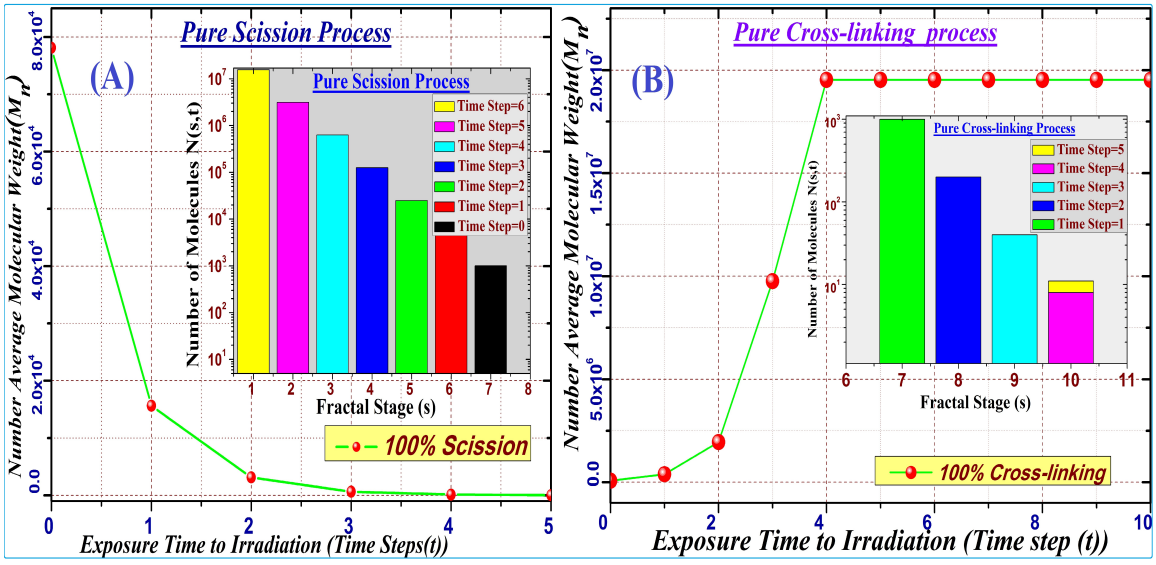

Figure 4.3: *Variation of number average molecular weight* $\langle M_n \rangle$ *with the external gamma irradiation for pure scission and pure cross-linking process. (A) Rapidly decreasing* $\langle M_n \rangle$ *variation curve in case of pure scission process. (B)* $\langle M_n \rangle$ *variation curve increases sharply in the case of pure cross-linking process. The variation of molecular distribution in the case of pure scission and cross-linking process are respectively shown in the inset of both figures.*

It is very evident from this graph that the number of molecules N(t) decreases very fast with the increase in time step (t) but on contrary, their size (fractal stage) increases gradually. This phenomenon eventually enhances the value of $\langle M_n \rangle$ over time step (t).

Except these two idealized extreme situations, there are many intermediate cases where scission and inter-molecular cross-linking processes occur simultaneously inside the sample. In figure-4.4(A), the variation of $\langle M_n \rangle$ with the exposure time to irradiation (time steps (t)) has been shown where the scission process takes the predominating role i.e. here the value of G in the master equation (derived in chapter-3) has been chosen between the range $0.5 \leq G \leq 1.0$). Hence, the degradation of molecules having higher values of the fractal stage is more likely to occur due to the higher rate of scission probability inside the sample.

As a result, the number of molecules with lower values of fractal stages are increased rapidly and their respective molecular weights are decreased simulteniously as the exposure time of the sample to gamma irradiation (time steps (t)) increases. Hence, the value of $\langle M_n \rangle$ decreases continuously with the increase of time steps (t) which is shown in figure-4.4(A). Here $\langle M_n \rangle$ variation for different scission percentages ranging from 50% to 90%

scission probabilities are presented chronologically. Each graph is showing a general trend of rapid reduction of the magnitude of $\langle M_n \rangle$. In each case, the value of $\langle M_n \rangle$ decreases very fast up to the irradiation time step t = 3. Post which, the reduction rate slows down gradually and proceeds towards the saturation value. The rapidity of fall of $\langle M_n \rangle$ vs t curves increases with the increase of scission percentage. Thus, the value of $\langle M_n \rangle$ falls at a faster rate in the case of 90% scission probability rather than that of 60% scission. The saturation values of each curve are very close to each other. The nature of $\langle M_n \rangle$ vs t curves

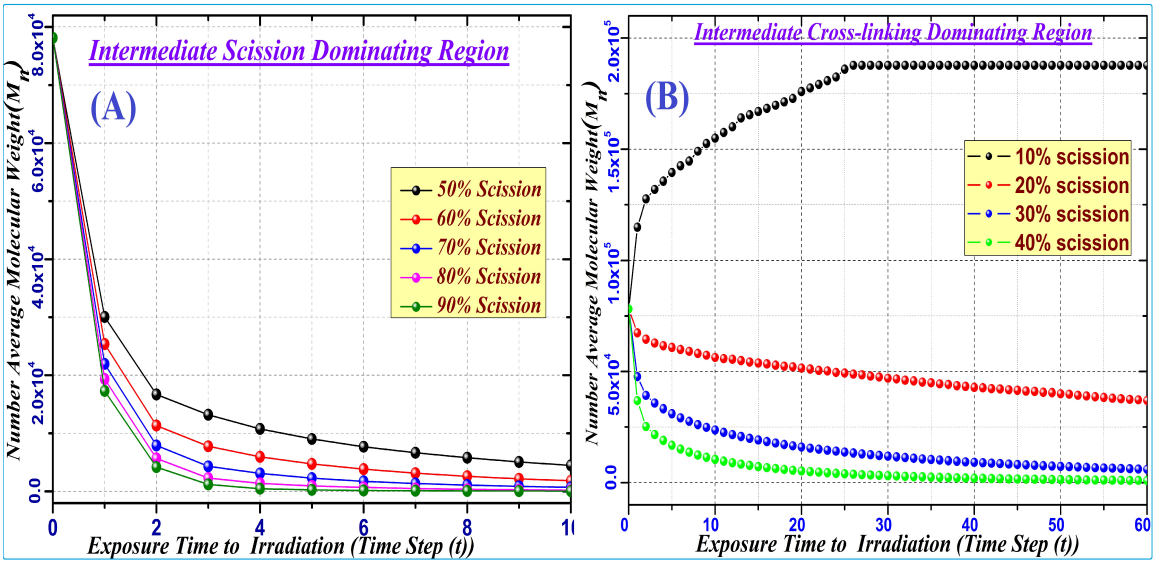

Figure 4.4: $\langle M_n \rangle$ *vs t variation curves for radiation induced intermediate cases.(A) Rapidly decreasing* $\langle M_n \rangle$ *vs time step t curves in the case of intermediate scission dominating region (50% to 90% scission process). (B)* $\langle M_n \rangle$ *vs time step t curves in the case of intermediate cross-linking dominating process (10% to 40% scission process).*

in the cross-linking dominating region has been presented in figure-4.4(B). Four different scission probabilities (ranging from 10% to 40% scission with an interval of 10%), have been thoroughly investigated. In this case, the probability of inter-molecular cross-linking plays the predominant role. The trend of gradual reduction of $\langle M_n \rangle$ vs t curves is also observed here up to 20% scission probability, which has been presented in figure-4.4(B). Post which a reverse trend has been noticed (in case of 10% scission process) where the value of $\langle M_n \rangle$ increases with the increase of time steps =t.

4.5.1.2. Effect of Gamma Irradiation on Weight Average Molecular Weight $\langle M_w \rangle$ for Mono-disperse SPE sample

The mathematical expression of weight average molecular weight $\langle M_w \rangle$ has been mentioned in the equation-(4.7) of this chapter and the formula that is used for simulation, is mentioned in equation-(4.21). It is very evident from these two equations that, the relation between $\langle M_w \rangle$ and (M_i) is different from that of the $\langle M_n \rangle$ as the numerator of the equation—(4.7) and equation—(4.21) carries the square term of (M_i) whereas the denominator contains a simple product of N(s,t) and (M_i).

Hence, $\langle M_w \rangle$ is more sensitive to the value of (M_i) rather than N(s,t). Another noticable feature is that the denominator of equation-(4.21) happens to be a constant term throughout the irradiation process as it indicates the total number of the monomer, present inside the sample. Therefore, the variation of $\langle M_w \rangle$ solely depends on the variation of the numerator of equation-(4.21). The bigger size molecules, which are configured with higher fractal stages (s ranging from 7 to 10), eventually give a significant impact on the determination of $\langle M_w \rangle$ of the host polymer sample. Thus, a strong tendency of gradual increment of $\langle M_w \rangle$ vs t curve has been predicted in most of the cases.The adjoining figure-4.5 represents the variation of $\langle M_w \rangle$ with time step (t) in case of pure scission (100% scission probability) and pure cross-linking (100% cross-linking probability) processes. The $\langle M_w \rangle$ vs (t) variation curve for the pure scission process has been shown in figure-4.5(A). Value of $\langle M_w \rangle$ falls very rapidly in this case up to the time step t=3.

The saturation value of $\langle M_w \rangle$ is achieved after the time step t=4 post which the nature of $\langle M_w \rangle$ vs t curve is unaltered and this feature can be observed clearly in figure-4.5(A). The pure scission process results in rapid degradation of the molecules with higher molecular weights and therefore the number of molecules inside the sample, is increased and their molecular weight is decreased. This phenomenon is considered as the prime reason for the rapid fall of $\langle M_w \rangle$ vs t curve. An opposite kind of behavior can be observed in the case of a pure cross-linking process which is shown in figure-4.5(B). The nature of the molecular distribution is shown in the inset of the figure-4.3(B). Molecules, in this case, join with each other due to the intermolecular cross-linking process and generates bigger-sized molecules over time steps (t). As a result, the total numbers of molecules inside the sample are reduced gradually but their respective molecular weights increases. This phenomenon gives a strong impact on the $\langle M_w \rangle$ vs t variation curve and we can observe a rapid increment of $\langle M_w \rangle$ values with the increase in (t). This increment is observed up to the time step t=4

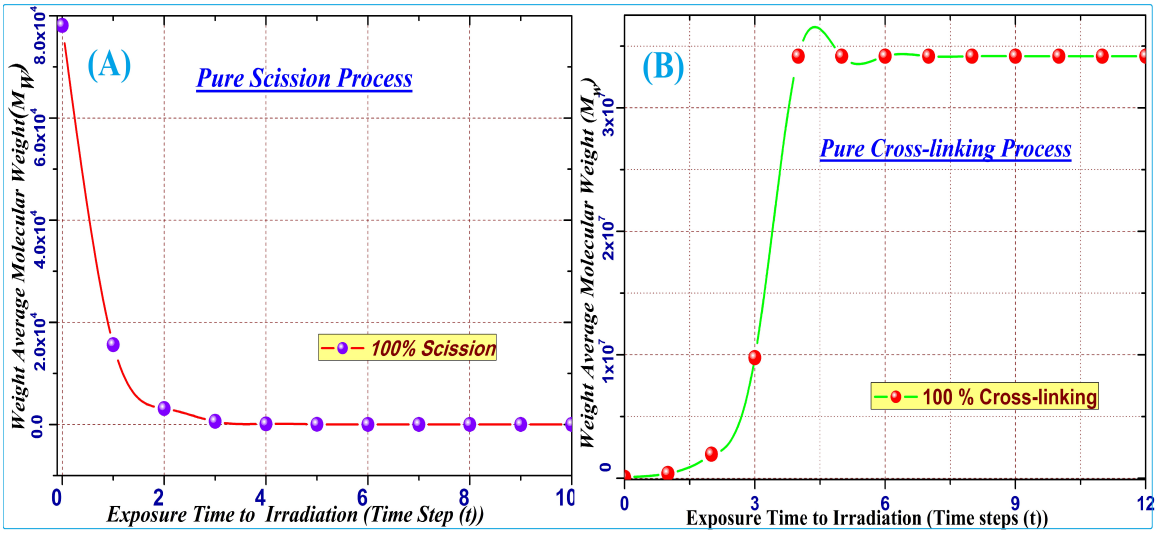

Figure 4.5: *Variation of weight average molecular weight* $\langle M_w \rangle$ *with the exposure time to irradiation (time steps (t)). (A)* $\langle M_w \rangle$ *decreases sharply with time steps (t) in case of pure scission (100% scission) process. (B) The fast increasing behavior of* $\langle M_w \rangle$ *variation curve for the pure cross-linking (100% cross-linking) process is shown here.*

post which the said curve attains its saturation stage.

The variation of $\langle M_w \rangle$ with respect to the irradiation time steps (t) for the intermediate cases where scission and cross-linking processes occur simultaneously is shown in figure-4.6. Figure-4.6(A) shows four $\langle M_w \rangle$ vs t curves representing the radiation-induced process where scission plays the predominant role (probability of scission are 90%, 80%, 70%, and 60% respectively). In the case of 90% scission probability, the $\langle M_w \rangle$ vs t curve shows a sharp descent which continues up to irradiation time steps t =10. This is because molecules with higher fractal stages, break down into a large number of smaller size molecules as mentioned before. In the case of 80% scission probability, an initial increment of $\langle M_w \rangle$ vs t curve has been noticed at the irradiation time steps t=1 post which a gradual decrease of $\langle M_w \rangle$ has also been observed. As the probability of scission decreases (i.e. in the case of 70% and 60% scission probabilities), a greater number of molecules are involved in the cross-linking process and produces bigger size molecules.

Therefore, a considerable number of polymer molecules with higher values of fractal stages (s= 7 to 9) can be found inside the polymer sample in these cases of scission probabilities. We have already mentioned that the bigger size molecules give a significant impact on the determination of the value of $\langle M_w \rangle$. Hence, an initial sharp increment has been observed in the $\langle M_w \rangle$ vs t curve up to the irradiation time steps t=3 and t=4 in case of 60% and

70% scission process respectively. After this irradiation time step, $\langle M_w \rangle$ vs t curves undergo through a gradual reduction which follows saturation stages of therespective curves. This trend remains more or less the same in all the curves and it is only their saturation values that increase with the decrease of scission probability. The variation of $\langle M_w \rangle$ with exposure

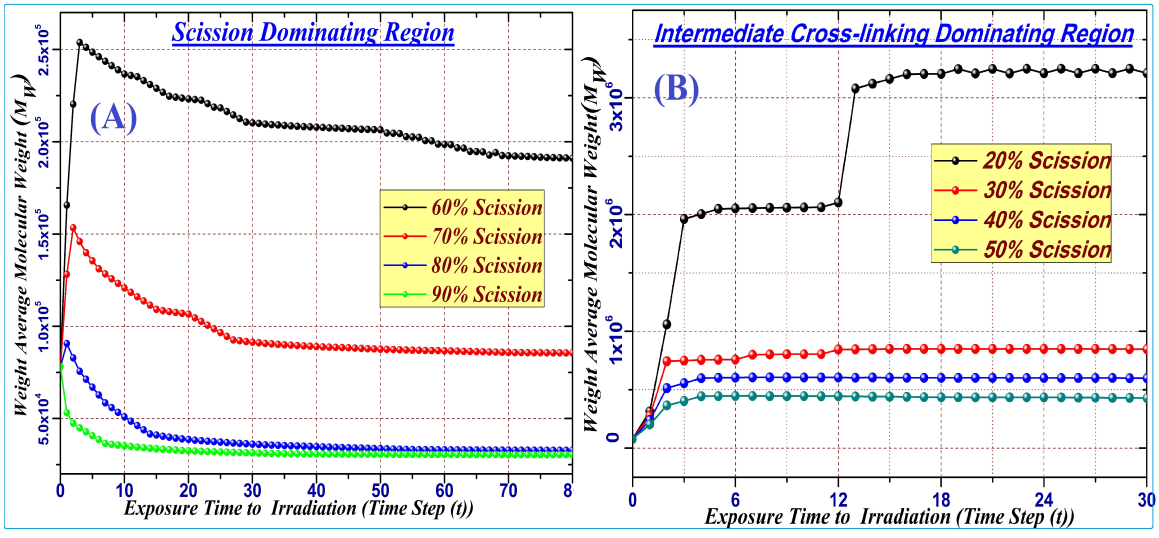

Figure 4.6: *Variation of weight average molecular weight $\langle M_w \rangle$ with the exposure time to irradiation or time steps (t) for intermediate cases where scission and cross-linking processes occur simultaneously. (A) $\langle M_w \rangle$ variation curves for different scission percentages (60% to 90% scission probability) in case of intermediate scission process dominating region. The peaks of the individual curves can be noted. (B) $\langle M_w \rangle$ variation curves in the case of the intermediate cross-linking process dominating process (20% to 50% scission probability) are presented here. The individual curves attain saturation stage very fast.*

time to irradiation (t) in those cases where the inter-molecular cross-linking process plays the predominant role, has been shown in figure—4.6(B). In these cases, molecules with arbitrary fractal stages join with each other under radiation-induced cross-linking process. Thus, bigger size molecules are produced having fractal stages ranging from s=5 to s=10. As a result, the total number of molecules that are present inside the host polymer sample is reduced and the peaks of the molecular distribution curves shift towards the right along the higher fractal stage regions, as discussed in chapter-3.

This feature has a direct impact on the $\langle M_w \rangle$ vs t curve as shown in figure—4.6(B). Here, four different $\langle M_w \rangle$ vs t curves for four different percentage of scission (i.e. 20%, 30%, 40%, and 50% scission probabilities) has been presented. The curve shows a sharp increment in $\langle M_w \rangle$ up to the irradiation step t=2 post which it attains a saturation value.

The $\langle M_w \rangle$ vs t curve for 20% scission probability shows an abrupt jump at the 12th time step (t=12). If we consider the molecular distribution pattern, we can find that the molecules with fractal stage s=9 which were constant in number so far inside the system, increase by 1 at 12th time step (t=12) post which no further increment of N(s,t) is noticed for s=12. Subsequently, the molecules of the 9th fractal stage being the largest molecule inside the system. Therefore significant impact on $\langle M_w \rangle$ can be observes which is manifested as the sudden jump at t=12 in the $\langle M_w \rangle$ vs t graph for 20% scission probability as shown in the figure-4.6(B). None of the other graphs in this figure shows similar trends.

4.5.1.3. Effect of Gamma Irradiation on Viscosity Average Molecular Weight $\langle M_v \rangle$ of a Mono-disperse Sample

The mathematical formulation, as well as different experimental techniques to evaluate the viscosity average molecular weight $\langle M_v \rangle$, have been elaborately discussed in the previous sections. It is evident from the discussion that the quantitative approach to determine the $\langle M_v \rangle$ of the host polymer sample is different from that of the other molar mass averages (i.e. $\langle M_n \rangle$, $\langle M_w \rangle$, $\langle M_z \rangle$). According to equation-(4.16) and (4.24), the parameter α plays an important role in determining the value of $\langle M_v \rangle$. There are some experimental studies[5, 15, 32] wherein the value of α is taken between 0.5 to 0.8. In our present simulation study, we have taken two arbitrary values of α as $\alpha = 0.7$ and α=0.5 and the outcome of the simulation has been analyzed here quantitatively. The entire simulation work has been carried out following the equation-(4.24).

The variation of $\langle M_v \rangle$ with respect to the time steps (t) in case of pure scission (100% sc) process considering the value of the exponent $\alpha = 0.7$ and α =0.5 has been shown in the figure-4.7. Before we analyze the result of the simulation, let us discuss the simplified form of the mathematical formula that is followed in our simulation to calculate the value of $\langle M_v \rangle$ in the case of a pure mono-disperse system. The mathematical formula that we have used to calculate the $\langle M_v \rangle$ in our simulation is:

$$\langle M_v \rangle = \left[\frac{\Sigma N_s . (M_s)^{(1+\alpha)}}{\Sigma N_s . M_s} \right]^{\frac{1}{\alpha}} \tag{4.28}$$

In case of a pure mono-disperse sample, molecules, present inside the host SPE sample have the same molecular weight. Let us address it as M. We have already seen in chapter-3 that the mono-disperse system that we have modelled for our simulation study, remains

mono-disperse throughout the irradiation in case of pure scission (100 % scission) process. Therefore, we assume the total number of molecules that are found inside the system at any arbitrary time step (t) is n(t) i.e in present case $\Sigma_s N(s,t) = n(t)$. Thus the mathematical form of $\langle M_v \rangle$ can be written as:

$$\begin{aligned} \langle M_v \rangle &= \left[\frac{n(t).(M)^{(1+\alpha)}}{n(t).M}\right]^{\frac{1}{\alpha}} \\ &= \left[\frac{(M)^{(1+\alpha)}}{M}\right]^{\frac{1}{\alpha}} = M \end{aligned} \tag{4.29}$$

It is very evident from the equation-(4.29) that the value of $\langle M_v \rangle$, in the case of pure mono-disperse sample, depends only on the molecular weight of the constituent molecules and independent of the value of the exponent α in case of pure scission process. Therefore, the $\langle M_v \rangle$ vs t curve for pure scission (100% scission probability) process will be identical for both the value of the exponents $\alpha = 0.7$ and α=0.5. Here we have presented the $\langle M_v \rangle$ vs t curve for the value of the exponent $\alpha = 0.5$ only in the figure-4.7(A).

In this case, the number of molecules inside the sample increases rapidly, but their sizes decrease step by step. Hence, a gradual fall in $\langle M_v \rangle$ can be noticed as the irradiation time steps (t) increases gradually and this phenomenon can be seen in figure-4.7(A). The rapid reduction of $\langle M_v \rangle$ is continued up to the time step t=2 post which the rate of fall slows down significantly and continues up to the time step t=6. The system contains 15625000 numbers of molecules with fractal stage s= 1 after the 6th irradiation time step (t=6) and there is no scope for further degradation of the molecules due to the scission process as per our assumption.

Hence, this molecular distribution pattern remains the same till the end of the irradiation process which leads to the saturation stage of the $\langle M_v \rangle$ vs t curve after the 6th irradiation time step. The nature of the $\langle M_v \rangle$ vs t curve for α=0.7 happens to be identical to that of the curve for α =0.5. In the case of pure cross-linking (probability of cross-linking is 100%) process, the mono-dispersive behavior of the sample is also maintained up to the irradiation time step t=3 post which the entire system contains 3 large molecules having fractal stage s=10 and one biggest molecule with fractal stage s=11. No further alteration has been observed in the molecular distribution pattern after the time step t=4. Hence the system becomes poly-dispersive after the time step t=3. This poly-dispersive nature gives a significant impact on the $\langle M_v \rangle$ vs t curve which is shown in figure-4.7(B).

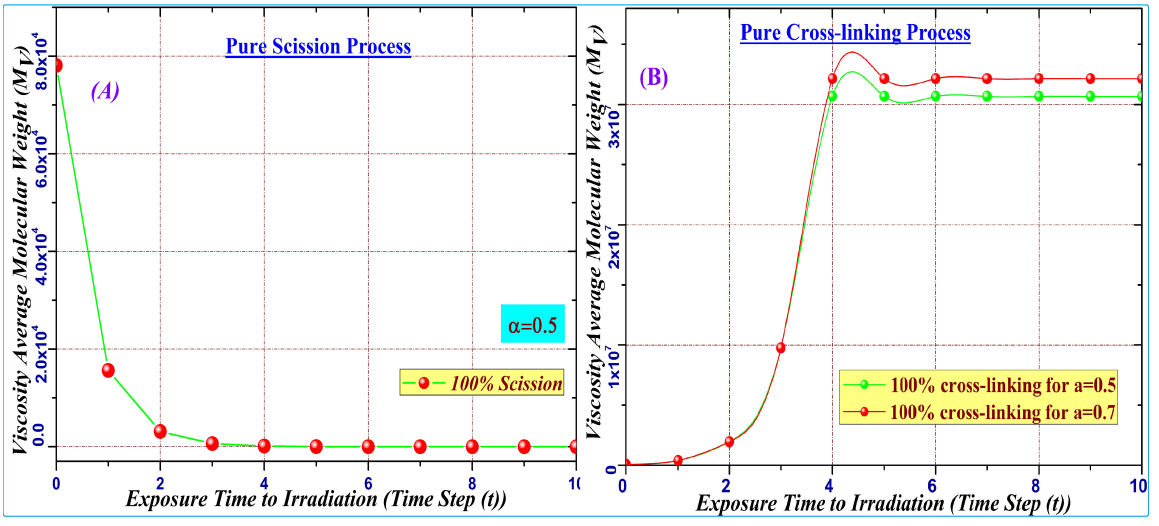

Figure 4.7: *Variation of viscosity average molecular weight* $\langle M_v \rangle$ *with the exposure time to irradiation or time steps (t). (A)* $\langle M_v \rangle$ *vs t graphs in case of pure scission process (100% scission). Value of the exponent* α *=0.5. The graph will be identical for* α *=0.7 too. (B)* $\langle M_v \rangle$ *variation curve for pure cross-linking (100% cross-linking) process. Two graphs (for* α *=0.5 and 0.7) differ from each other at the saturation region when the system becomes poly-disperse*

In this figure, we have plotted the $\langle M_v \rangle$ against time step (t) in case of pure cross-linking process considering the value of α =0.5 and α =0.7. Since the system remains mono-disperse up to the time step t=3, both curves for α=0.5 and α=0.7 are identical and merged with each other which can be observed clearly in figure-4.7(B). In this case, the $\langle M_v \rangle$ vs t curve shows a gradual increment up to the time step t=2 post which, a sharp increment is observed from time step t=2 to t=3. The $\langle M_v \rangle$ vs t curve for both α=0.5 and α=0.7 differ from each other from the 4th irradiation time step (t=4) as the system becomes poly-disperse by nature from this stage. The molecular distribution pattern, after the time step t=4, remains unchanged throughout the rest of the irradiation process which leads the said curves to their respective saturation stages after time steps t=4.

$\langle M_v \rangle$ vs time step (t) variation curves in some intermediate cases, where the radiation-induced scission process plays the significant role, has been shown in figure-4.8. Figure-4.8(A) represents the $\langle M_v \rangle$ vs t curves in scission dominating region for α = 0.5. Five graphs with different scission percentages (from 50% to 90% scission) are shown here. In the case of 80% and 90% scission, $\langle M_v \rangle$ falls very fast up to the 10th irradiation time steps (t=10) and post which those curves gradually attain their steady state values.

In case of 70%, 60%, and 50% scission process, a rapid enhancement in $\langle M_v \rangle$ can be seen at the initial stage of irradiation. The increment appears first time in the $\langle M_v \rangle$vs t curve for 70% scission process and is enhanced with the increase of cross-linking probability as shown in figure-4.8(A). As we have seen in our previous chapter, the cross-linking process at the initial stage of irradiation results in the generation of bigger size molecules with higher values of the fractal stage (s=8 and s=9) when the probability of scission is in the range of $0.5 < G < 0.7$ (i.e. within 70% to 50%). Generation of these bigger size molecules is considered as the prime reason for the enhancement in the value of $\langle M_v \rangle$ at the initial stages of irradiation. As the cross-linking probability increases, probability of generation of bigger size molecules becomes higher and consequently, the magnitude of the initial peaks increases that can be observed in the curves representing 50% and 60% scission processes in figure-4.8(A). Figure-4.8(B) represents the $\langle M_v \rangle$ variation curves in the scission dominationg

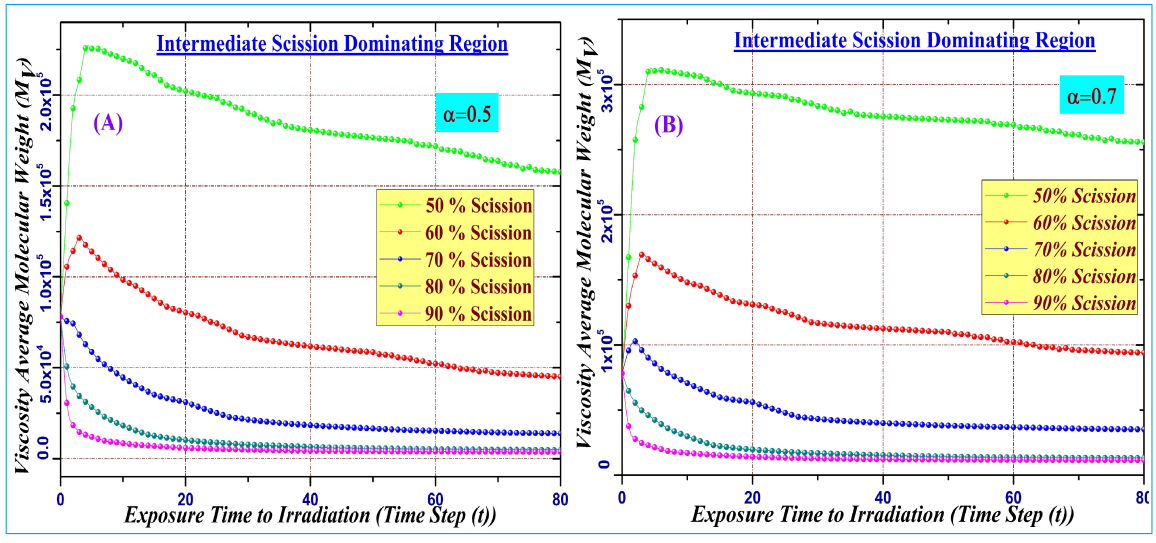

Figure 4.8: *Variation of viscosity average molecular weight $\langle M_v \rangle$ with the exposure time to irradiation or time steps (t) in case of intermediate scission dominating region (50% to 90% scission probability) for two different values of the exponent α.(A) $\langle M_v \rangle$ vs t variation curves for $\alpha = 0.5$. (B) $\langle M_v \rangle$ vs t variation curves for $\alpha = 0.7$.*

region where the value of the exponent α is taken as 0.7. Each of the $\langle M_v \rangle$ vs t curves shows considerable amount of similarities with the respective curves, shown in figure-4.8(A). The only significant difference can be noticed in the case of the magnitude of the peaks. The initial peaks of those curves (50% to 70% scission curves) in figure-4.8(B) are higher in magnitude from those in figure-4.8(A) where $\alpha = 0.5$. Moreover, we can notice a prominent peak in the case of $\langle M_v \rangle$ variation curve for 70% scission probability in case of $\alpha = 0.7$

which has not been noticed in the those curves for $\alpha = 0.5$ in figure-4.8(A)

Figure-4.9(A) represents the variation of $\langle M_v \rangle$ with the time step (t) in case of cross-linking dominating region where the value of the exponent is taken as $\alpha = 0.5$. Four $\langle M_v \rangle$ vs t curves are presented here with different scission probabilities (ranging from 10% to 40% scission). Since the cross-linking process plays the predominant role, molecules are more likely to join through the cross-linking process to produce bigger size molecules. Hence, a sharp increment in each $\langle M_v \rangle$ vs t curve has been observed at the initial stage of the irradiation process.

In case of 20% scission process, a step-like increment in $\langle M_v \rangle$ vs t curve is observed at the time step t=13. It has been observed in the previous chapter that a new large-size molecule with fractal stage s=10 is generated at this time step (at t=13). Before that i.e. at 12th time step (t=12), the total number of molecules having fractal stage s=10 is 1 i.e. N (10,12)=1 while it is 2 at t=13 (i.e. N(10,13)=2 at time step t=13). This newly generated molecule with fractal stage s=10 happens to be the largest molecules inside the system at t=13 and therefore its influence is significant which is manifested by the abrupt step-like jump in the $\langle M_v \rangle$ vs t curve at time step t=13 as shown in the figure-4.9(A) in case of 20% scission process. Another $\langle M_v \rangle$ vs t variation curve in case of cross-linking dominating region

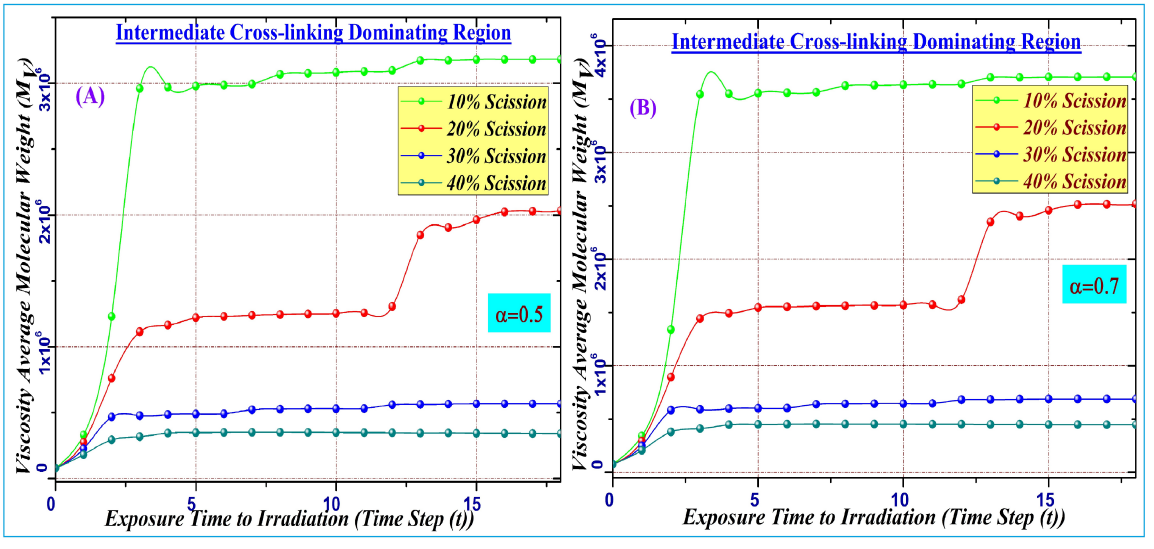

Figure 4.9: *Viscosity average molecular weight* $\langle M_v \rangle$ *variation with the exposure time to irradiation or time steps (t) in case of cross-linking process dominating region (10% to 40% scission) for two different values of* α. *(A)*$\langle M_v \rangle$ *vs t curves for* α *=0.5 (B)* $\langle M_v \rangle$ *vs t curves for* α *=0.7*

is shown in figure-4.9(B) where the value of the exponent $\alpha = 0.7$. Here also four different $\langle M_v \rangle$ vs t curves have been shown that represent the scission probabilities ranging from 10% to 40%. Each curve differs in magnitude from those curves in figure-4.9(A). The saturation stage of each curve in this case comes at comparatively higher in magnitude. Since the simulation has been carried out based on the same molecular distribution pattern, here also a step like abrupt increment in $\langle M_v \rangle$ vs t curve is noticed in case of 20% scission process which can be seen in figure-4.9(B).

4.5.1.4. Effect of Gamma Irradiation on Z-Average Molecular Weight $\langle M_z \rangle$ for Mono-disperse SPE sample

The variation z-average molecular weight $\langle M_z \rangle$ has been investigated in this subsection. $\langle M_z \rangle$ happens to be an intrinsic property of the host polymer sample whose mathematical expression has been mentioned in equation-(4.17). The more relevent mathematical form of $\langle M_z \rangle$ that we have used in our computer simulation study is mentioned in equation-(4.26). The numerator in equation—(4.26) carries the cubic term of M_i whereas the denominator contains its square term. Therefore, the value of $\langle M_z \rangle$ is highly sensitive to the molecular weight of the host polymer molecules. Bigger size molecules with higher values of fractal stages have a pronounced effect on determining nature of $\langle M_z \rangle$ variation with the time step t.

The entire result of the simulation has been segregated into two parts. First, we will discuss the result for two extreme cases i.e. variation of $\langle M_z \rangle$ with irradiation time step (t) for pure scission and pure cross-linking process. Post which we will study the $\langle M_z \rangle$ variation in the intermediate cases where the radiation-induced scission and cross-linking processes occur simultaneously. The variation of $\langle M_z \rangle$ with irradiation time step (t) for pure scission and pure cross-linking processes has been shown in figure-4.10. We have already aware of the fact that the value of $\langle M_z \rangle$ is highly sensitive to the molecular size (the fractal stage in the case of our present simulation). Therefore, pure scission process results in a rapid fall of the value of $\langle M_z \rangle$ with the passage of time step (t) which can be seen in figure-4.10(A). We can see this trend of rapid reduction of $\langle M_z \rangle$ value is continued up to the 2nd time step (t=2) post which the rapidity of fall slows down significantly.

The saturation stage has been attained by the $\langle M_z \rangle$ vs (t) curve after the time step t=4. On the other hand, the variation of $\langle M_z \rangle$ with time step (t) for the pure cross-linking process has been presented in figure-4.10(B). In this case, a slow initial increment has been

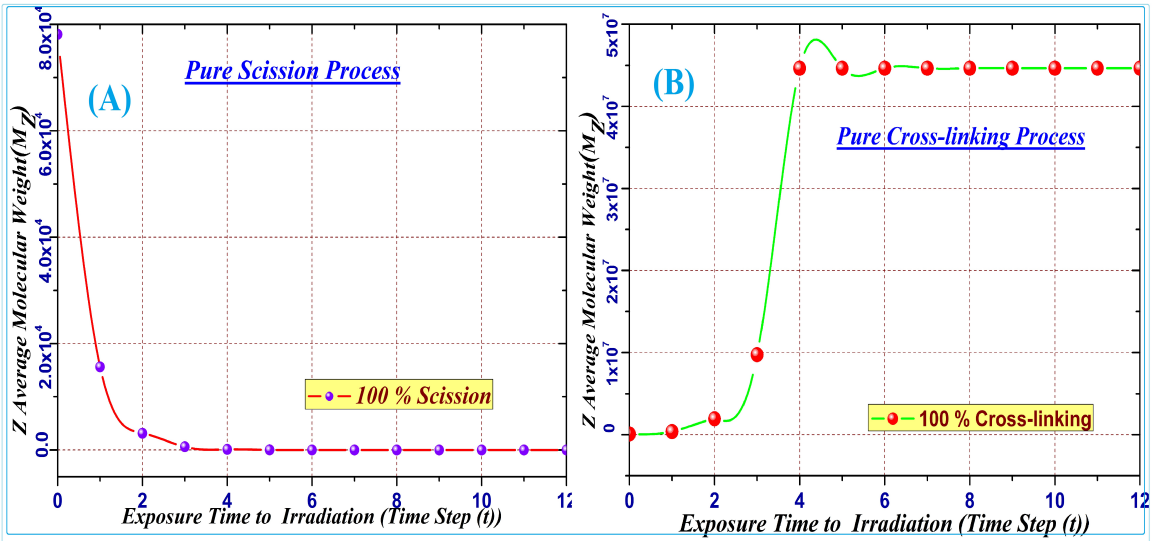

Figure 4.10: *Variation of Z- average molecular weight* $\langle M_z \rangle$ *with the exposure time to irradiation or time steps (t) in two extreme cases. (A) Rapid decrease in the behaviour of* $\langle M_z \rangle$ *vs t curve for pure scission (100% scission) process. (B)* $\langle M_z \rangle$ *increases sharply with time steps (t) in case of the pure cross-linking (100% cross-linking) process.*

noticed up to the time step t=2. Post which, the value of $\langle M_z \rangle$ shows a sharp enhancement between time steps t=2 and t=4. The saturation stage has been achieved by the $\langle M_z \rangle$ vs t curve after the time step t=4. The generation of larger size molecules due to the pure cross-linking process is considered as the main reason behind the sharp incremental behavior of $\langle M_z \rangle$ vs t curve in this case.

Except for these aforementioned two extreme situations, we have also studied the variation of $\langle M_z \rangle$ for intermediate cases where scission and cross-linking processes are taking place simultaneously. $\langle M_z \rangle$ variation in the scission dominating region has been presented in figure-4.11(A). This figure contains five $\langle M_z \rangle$ vs t curves for five different scission probabilities ranging from 50% to 90% scission. The $\langle M_z \rangle$ vs t variation curves for 50%, 60%, and 70% scission probabilities show an initial sharp increment up to the irradiation time steps t=5, 3, and 2 respectively. Post which, the rate of increase of $\langle M_z \rangle$ with time step (t) is reduced significantly in each curve.

Finally, the saturation stage for each of the $\langle M_z \rangle$ vs t curves is achieved after the irradiation time step t=30. In the case of $\langle M_z \rangle$ vs t curves representing 80% and 90% scission probabilities, the rapid growth has been observed till time step t=1, post which these curves attain their respective saturation values. Two distinguishable characteristics

can be observed here. Firstly, $\langle M_z \rangle$ vs t curves for all the scission percentages except for the pure scission (100% scission probability) process exhibit similar characteristics (a sharp increment which is followed by a saturation state). As the probability of scission increases the magnitude of the step-like increment is reduced. Secondly, the graphs for 90% and 80% scission probabilities are extremely close with each other.

If we study the nature of molecular distribution pattern N(s,t) in these two cases (80% and 90% scission probabilities), we can see that they are (i.e. molecular distribution patterns) not significantly different from each other. Only the molecules having lower fractal stages are changed in number which has less impact on $\langle M_z \rangle$ variation. But the variation in the number of higher stage molecules are very less. Therefore no significant change is observed in these two curves (i.e. in case of 80% and 90% scission process). Therefore, the respective $\langle M_z \rangle$ vs t graphs happens to be very close to each other. In figure-4.11(A) $\langle M_z \rangle$ vs t graphs are plotted within a large range of $\langle M_z \rangle$ values starting from 0 to nearly 2 X 10^6 unit. The nature of $\langle M_z \rangle$ vs t curve in those cases where the cross-linking process

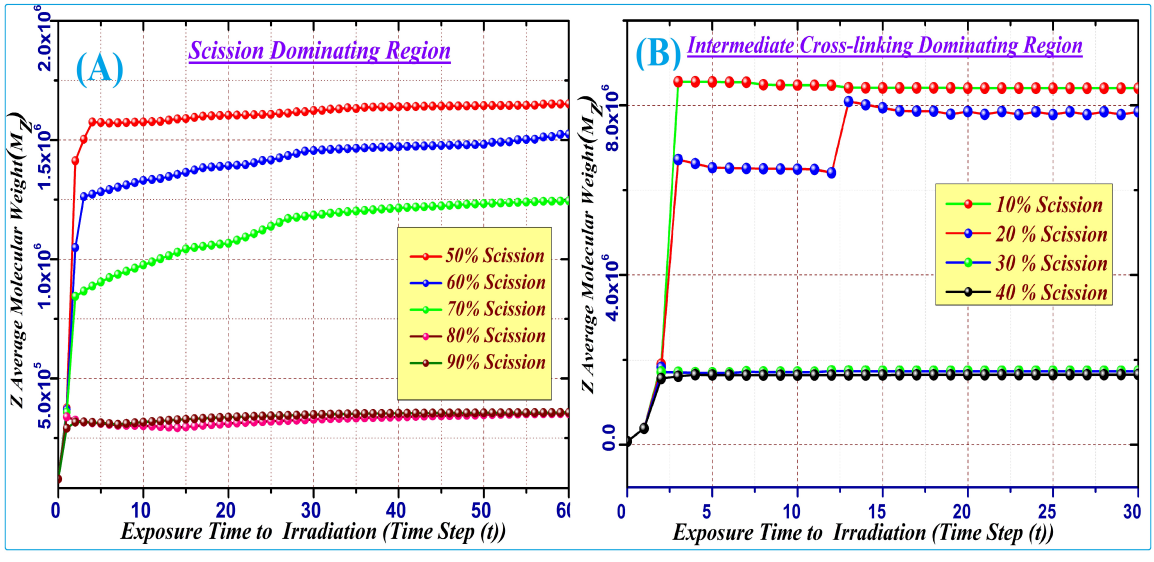

Figure 4.11: *Variation of Z-average molecular weight $\langle M_z \rangle$ with irradiation time steps (t) for intermediate cases where scission and cross-linking processes occur simultaneously. (A) $\langle M_z \rangle$ variation curves in the scission process dominating region (50% to 90% scission probabilities). (B) $\langle M_z \rangle$ variation curves in case of the intermediate cross-linking dominating region (10% to 40% scission probabilities).*

plays the predominant role i.e. in the cross-linking dominating region (10% to 40% scission probability), is shown in figure-4.11(B). Each of these curves shows a sharp step-like hike within the 3rd time step (t=3) following which, each curve attains their respective saturation

stages. In the case of 30% and 40% scission process, the molecular distribution patterns of the sample are more or less the same. Only the lower stage molecules are changed very less in number. Variation in higher stage molecules are very less in number. Therefore the respective $\langle M_z \rangle$ vs t graphs for these two cases (30% and 40% scission) are very close to each other. Their differences cannot be observed clearly like the other graphs in figure-4.11(B). In the case of 20% scission, a step-like sharp increment has been noticed $\langle M_z \rangle$ values at time step t= 13. At this irradiation time step, the number of biggest size molecules inside the sample (9th stage Vicsek fractal) increases by 1 unit which eventually has a significant impact on the value of $\langle M_z \rangle$. As a consequence, a step-like jump is observed in $\langle M_z \rangle$ values at t = 13 unit.

4.5.2. Effect of Gamma Irradiation on Different Average Molecular Weights (Molar Mass Averages) for Poly-disperse SPE Sample

We have performed our second simulation work of this chapter on a poly-disperse sample to investigate the effect of gamma irradiation on the four molar mass averages which have already been mentioned in the previous subsection. The procedure of mathematical modeling of a host poly-disperse sample has already been discussed in the previous chapter. In this section, we will discuss the result of the simulation study regarding the four molar mass averages for a poly-disperse sample.

4.5.2.1. Effect of Gamma Irradiation on Number Average Molecular Weight $\langle M_n \rangle$ for Poly-disperse SPE Sample

The variation of number average molecular weight $\langle M_n \rangle$ with exposure time to irradiation (time steps (t)) in the case of a poly-disperse sample has been shown in figure-4.12 and figure-4.13. The basic patterns of the $\langle M_n \rangle$ vs t graphs are being same but some salient dissimilarities can be observed with the mono-dispersive sample. The simulation has been done following the same equation (equation-(4.19)) which shows a linear relationship between the number of molecules $\langle M_n \rangle$ and molecular weights M_i as mentioned before. Since the host polymer sample is poly-disperse by nature, the distribution of the molecular size among different fractal stages (s) happens to be wider at the time of the irradiation process than in the case of a mono-disperse sample. This fact has been reflected in the nature of $\langle M_n \rangle$ vs t variation curves in figure-4.12.

Figure-4.12 (A) and (B) represent the variation of $\langle M_n \rangle$ with time step (t) in the

case of pure scission and pure cross-linking process respectively. Figure-4.12(A) suggests that the value of $\langle M_n \rangle$ falls very rapidly with the increase in time step (t) up to t=5. Post which the reduction rate of $\langle M_n \rangle$ slows down and after t=9, it attains its minimum value which happens to be the saturation stage of $\langle M_n \rangle$. The inset of this figure represents the distribution of molecules in different fractal stages at different irradiation time steps. The reduction rate of the $\langle M_n \rangle$ vs t curve of a poly-disperse sample happens to be slower than that of the mono-disperse case. Consequently, the steady state of $\langle M_n \rangle$ is attained at time step t=9 in this case where it is attained by a mono-disperse sample comparatively faster (at t=4). On the other hand, Figure-4.12 (B) shows the variation of $\langle M_n \rangle$ in the case of

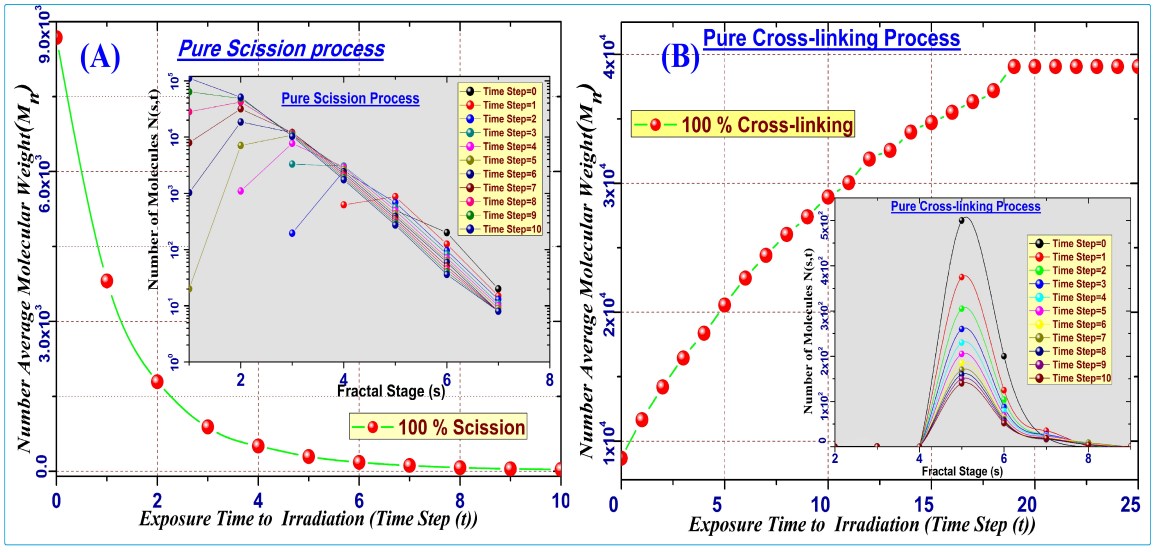

Figure 4.12: *Variation of number average molecular weight* $\langle M_n \rangle$ *with respect to the irradiation time step (t). (A) A spontaneous sharp nonlinear decrease of* $\langle M_n \rangle$ *is noticed in the pure scission (100% scission) process. (B) Gradual enhancement of* $\langle M_n \rangle$ *is observed followed by a saturation region of* $\langle M_n \rangle$ *in case of pure cross-linking (100% cross-linking) process.*

the pure cross-linking process. The inset of this figure suggests that the total number of molecules N(t) decreases with the increase of time step (t) whereas the size of the molecules is enhanced gradually. This phenomenon gives a significant impact on the nature of $\langle M_n \rangle$ variation curve that can be observed in figure-4.12(B). In this case, magnitude of $\langle M_n \rangle$ increases gradually up to the irradiation time step t=19, post which, the $\langle M_n \rangle$ curve attains its saturation value as shown in the respective figure-4.12(B).

Some noticable differences in $\langle M_n \rangle$ variation curve in case of pure cross-linking process can also be observed between mono-disperse and poly-disperse samples . A spontaneous

enhancement of $\langle M_n \rangle$ has been noticed in case of poly-disperse sample which follows a saturation stage at t=19 whereas a step-like increment of $\langle M_n \rangle$ variation curve has been noticed in case of a mono-disperse sample which is followed by the saturation stage after the time step t=4, much earlier than the present case. The highest numerical values of $\langle M_n \rangle$ for both pure scission and pure cross-linking processes are also different in both mono-disperse and poly-disperse samples.

Besides two extreme cases (100% scission and 100% cross-linking process) we have also studied the variation of $\langle M_n \rangle$ with time step (t) for the intermediate cases where the scission and the cross-linking processes occur simultaneously. Figure-4.13(A) represents the $\langle M_n \rangle$ vs t variation curves for those cases where the scission process takes the predominant role (60% to 90% scission probability). The rate of decrease in $\langle M_n \rangle$ vs t curve is slower compared to the mono-disperse case. The trend of rapid reduction of $\langle M_n \rangle$ continues up to the time step t=6 post which the reduction rate of the curves gradually slows down, and they eventually attain their saturation values after the irradiation time step t=16. It can be observed that all the $\langle M_n \rangle$ vs t curves become very close to each other at the saturation region. Moreover, the $\langle M_n \rangle$ vs t curves decrease more rapidly as the percentage of scission increases from 60% to 90%. The highest rate of fall of $\langle M_n \rangle$ can be observed at 90% scission probability which is indicated by the last curve (placed at the bottom) of figure-4.13 (A).

Figure-4.13(B) represents the variation of $\langle M_n \rangle$ vs t curve for those cases, where the probability of occurrence of the cross-linking process is either equal or greater than the scission process. The gradual decreasing nature of $\langle M_n \rangle$ vs t curves can also be observed here up to the scission probability of 20% (i.e. 80% cross-linking probability). This is because the $\langle M_n \rangle$ happens to be more dependent on the number of molecules (N(s,t)) rather than the respective molecular weights. Hence, the nonlinear decreasing behavior of $\langle M_n \rangle$ vs t curves persists up to 20% scission process. This trend is, however, changed in the case of 10% scission curve. The high cross-linking rate (90% probability) results in a fewer number of molecules with higher molecular weights. Hence, the $\langle M_n \rangle$ vs t curve shows a gradual increment up to the irradiation time step t=20, post which, it attains a saturation value.

4.5.2.2. Effect of Gamma Irradiation on Weight Average Molecular Weight $\langle M_w \rangle$ for Poly-disperse SPE Sample

Determination of weight average molecular weight $\langle M_w \rangle$ in case of a poly-disperse sample is carried out following the same procedure as in the monodisperse case. The simulation has

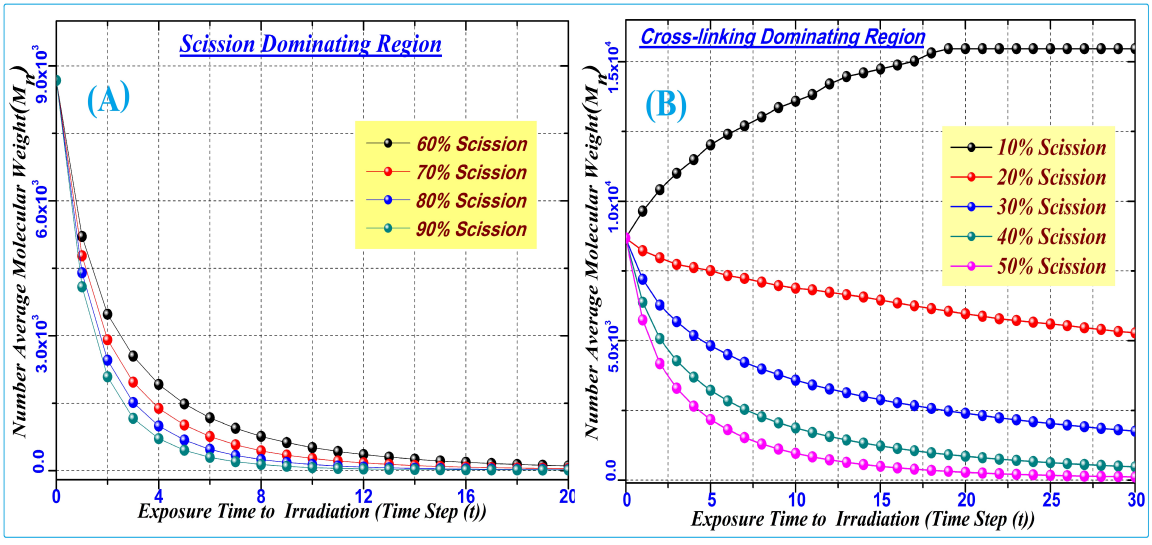

Figure 4.13: *Variation of Number Average Molecular Weight $\langle M_n \rangle$ for intermediate cases where scission and cross-linking occurs simultaneously. (A) A sharp non-linear decrease of $\langle M_n \rangle$ in case of intermediate scission process dominating region (60% to 90% scission). (B) Variation of $\langle M_n \rangle$ in case of cross-linking process dominating region (i.e. 10% to 50% scission probability). The trend of gradual decrease in behavior is changed here in the case of 10% scission probability.*

been performed based on the equation-(4.21). The molecular distribution pattern of the unirradiated sample has already been discussed in details in chapter-3. The detailed analysis of the nature of molecular distribution pattern inside the said poly-disperse sample reveals the fact that molecules, present inside the host polymer sample at any arbitrary exposure time to irradiation (t), are either small (with fractal stages s= 1 to 3) or average (with fractal stages s= 4 to 6) in size. A very small amount of molecules can be found having fractal stage s=7 or 8. But, molecules with fractal stage s=9 or 10 cannot be observed during the overall irradiation process. This is different from the distribution pattern which has been observed in case of a mono-disperse sample.

The effect of gamma irradiation on the variation of $\langle M_w \rangle$ in the case of pure scission and pure cross-linking processes has been shown in figure-4.14. A gradual fall of $\langle M_w \rangle$ with the increase of time step t can be noticed in the case of pure scission process and it is shown in figure 4.14(A). But unlike the monodisperse sample, the fall of $\langle M_w \rangle$, in this case, is not so rapid and the saturation stage comes here after the time step t=14 (in case of the mono-dispersive sample, this stage comes at time step t=4 as mentioned before). Similarly, figure-4.14(B) shows the variation of $\langle M_w \rangle$ with external irradiation in the case of pure

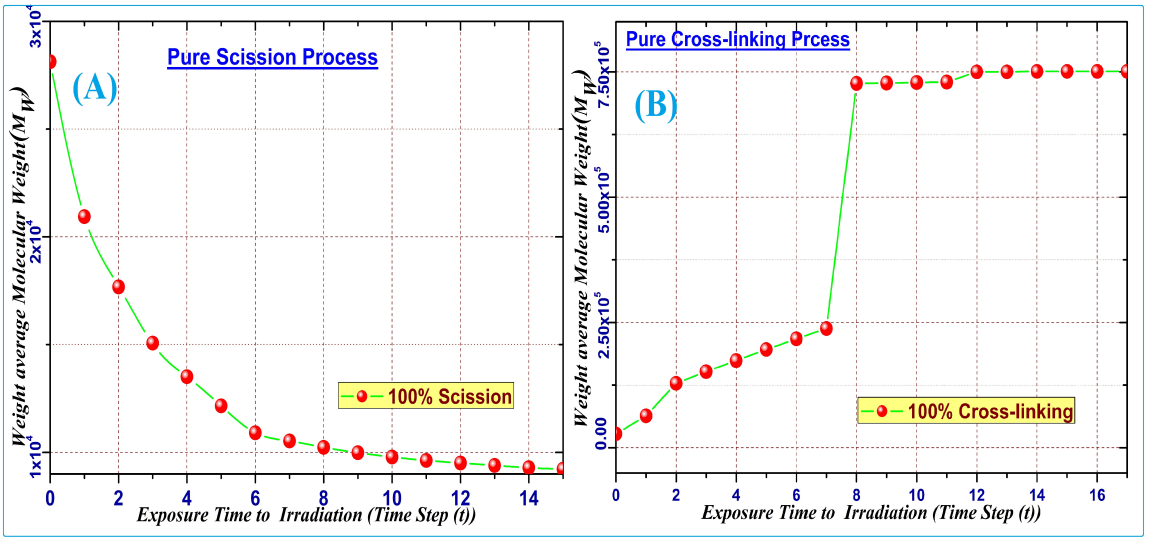

Figure 4.14: *Variation of weight average molecular weight* $\langle M_w \rangle$ *due to the application of external gamma irradiation in two extreme cases. (A)* $\langle M_w \rangle$ *decreases very fast in the case of the pure scission (100% scission) process. Later the curve attains its saturation value. (B) An abrupt step-like jump is observed in the* $\langle M_w \rangle$ *variation curve at t=7 for the pure cross-linking process.*

cross-linking process (probability of cross-linking is 100%). Here we can observe a steady and slow increment of $\langle M_w \rangle$ up to the time step t=7. Post which a sharp step-like jump in $\langle M_w \rangle$ value has been noticed at time step t=8.

As per the structural analysis performed in chapter-3, the largest molecule that can be found inside the system at the time step t=7, is modelled with fractal stage s=8. Radiation induced pure cross-linking process results in generation of a new molecules with fractal stage s=9 at the time step t=8 and further generation of new molecules with same fractal stage has not been noticed till the completion of the irradiation process. Therefore the impact of the large size molecule (s=9) formation on the magnitude of $\langle M_w \rangle$ happens to be significant and it is manifested as the sudden jump in the $\langle M_w \rangle$ vs t graph at t=8 in the figure-4.14(B). The $\langle M_w \rangle$ variation curve becomes almost steady after t=8 upto the 12th time step. A small enhancement has been noticed in the magnitude of $\langle M_w \rangle$ at t=12.Post which the curve attains its saturation stage.

The nature of $\langle M_w \rangle$ vs t curves in different scission, as well as cross-linking dominating processes, has been shown in figure-4.15. The variation of $\langle M_w \rangle$ with respect to (t) in those cases where the scission process plays a significant role is shown in figure-4.15(A)

and the trend of variation of $\langle M_w \rangle$ vs t curves happens to be different from those curves shown in figure—4.5 for mono-disperse case. Here, the variation of $\langle M_w \rangle$ in a poly-disperse sample has been investigated up to the irradiation exposure time step t = 60. In the case of 90%, and 80% scission process, a rapid decrease of $\langle M_w \rangle$ has been observed as the exposure time to irradiation is increased up to time step t=10 following which the rate of decrease of Mw slows down significantly and attains a steady value around the time step t=20.

In the case of 70%, 60%, and 50% scission process, a slight behavioral change has been noticed in $\langle M_w \rangle$ vs t variation curve. A sharp increment of $\langle M_w \rangle$ has been observed at the very begining of the irradiation process up to the irradiation to time step t=2. The rate of enhancement increases with the decrease of scission probability. Thus, the maximum increment is observed in the case of 50% scission probability. After irradiation time step t=2, the value of $\langle M_w \rangle$ decreases rapidly with the increase of time step t. This trend continues up to the 30th time step (t=30) post which, the curves attain their respective saturation values. A small amount of fluctuation has been observed between t=20 to t=30 units in case of 50% and 60% scission probability. This may be considered as the impact of the fluctuation in the number of molecules (N(s,t)) with different fractal stages (s) inside the host polymer sample in case of said scission percentages. Figure-4.15(B) represents $\langle M_w \rangle$ vs t variation curve for those cases, where radiation-induced inter-molecular cross-linking process plays the predominant role. The figure shows four different curves for four different scission probabilities (40% to 10% scission with an interval of 10%). The effect of gamma irradiation has been studied up to the irradiation exposure time step t =30. Since the probability of cross-linking is comparatively high in this case, the molecules are more likely to join with each other to produce bigger size molecules with higher values of fractal stages. Therefore, molecules with fractal stages s= 7 or 8 can be found inside the sample with greater probability. As a result, the total number of molecules inside the sample will be reduced gradually. This phenomenon directly affects the nature of $\langle M_w \rangle$ vs t curves.

A spontanious increment in the magnitude of $\langle M_w \rangle$ is observed up to time step t = 5 or 6, which is followed by a stepwise enhancement in the $\langle M_w \rangle$ variation curves when the probability of scissions are 10%, 20%, and 30% respectively. Each of the $\langle M_w \rangle$ variation curves attain its respective saturation values afterwards. The time steps of attaining the saturation stages happen to be different for different $\langle M_w \rangle$ vs t curves. The $\langle M_w \rangle$ variation curves for the 10%, 20%, 30% scission probabilities will attain their respective saturation stages at the 12th, 11th, and 10th irradiation time steps respectively. Whereas saturation stage for 40% scission probability has been achieved after time step t=5. The $\langle M_w \rangle$ vs t

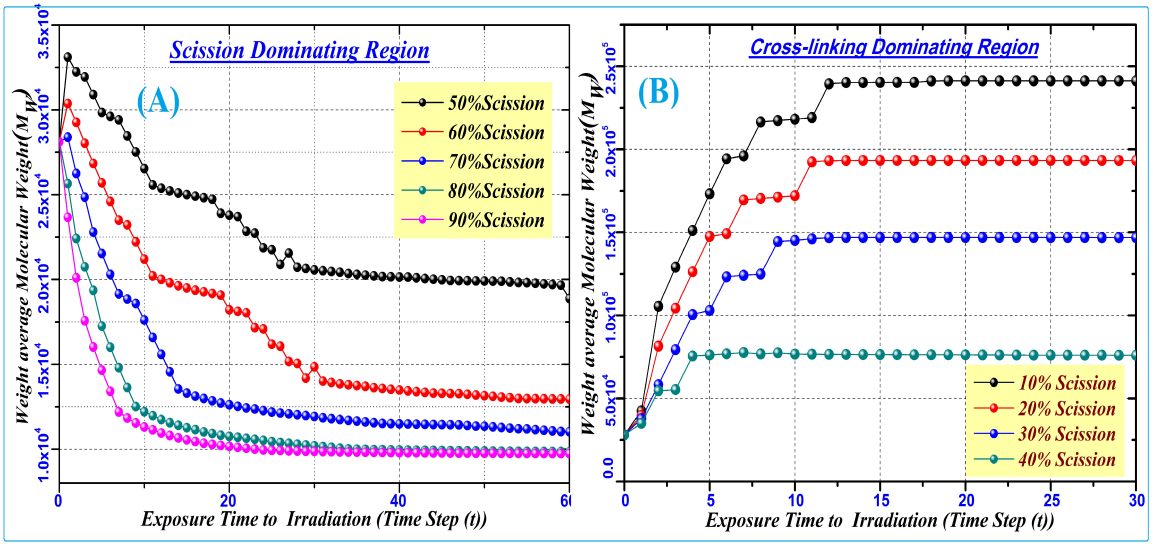

Figure 4.15: *Variation of weight average molecular weight* $\langle M_w \rangle$ *due to the application of external gamma irradiation in the intermediate cases where scision and cross-linking process occur simultaneously. (A) Gradual reduction of* $\langle M_w \rangle$ *vs t curves in case of intermediate scission (50% to 90% scission) process dominating region. (B) A gradual step-like enhancement is observed in* ($\langle M_w \rangle$) *vs t variation curve for the cross-linking process dominating(10% to 40% scission) region.*

curve for 40% scission probability is slightly different from the other three curves.

4.5.2.3. Effect of Gamma Irradiation on Viscosity Average Molecular Weight $\langle M_v \rangle$ for Poly-disperse SPE Sample

Viscosity average molecular weight of the host SPE sample and its response to external irradiation has been simulated based on equation-(4.16)and equation-(4.24) which we have already mentioned in case of the mono-disperse sample. But, since we are presently considering a poly-disperse system, the characteristic curves change to some extent. The entire simulation has been done here taking the value of the exponent as $\alpha = 0.7$ and $\alpha = 0.5$. in the same fashion as in the case of a mono-disperse sample. The $\langle M_v \rangle$ vs t curves for two extreme cases i.e. incase of 100% scission and 100% cross-linking have been shown in figure-4.16.

In case of pure scission process, the number of molecules inside the sample increases very rapidly and their respective size decreases simultaneously as the exposure time to irradiation (time step (t)) increases. Unlike the mono-disperse sample as discussed in the

previous section, the poly-disperse sample maintains its poly-dispersive nature from the begining of the irradiation process. This phenomenon of the sample results in two separate $\langle M_v \rangle$ vs t curves for two different values of α (i.e. $\alpha = 0.7$ and $\alpha = 0.5$) which have been shown in figure-4.16(A). Both the $\langle M_v \rangle$ vs t graphs show an ever decreasing nature butut the rapidity of fall of the curves is less than that in the mono-disperse case. Also, the magnitude of the variation is smaller compared to that of the monodisperse case (as shown in figure-4.16(A)). We have taken two different values of α. The $\langle M_v \rangle$ vs t curve with α=0.5 always has the smaller values of $\langle M_v \rangle$ compared to that of $\alpha = 0.7$. Therefore the rapidity of fall of the $\langle M_v \rangle$ vs t curve is higher in the case of $\alpha = 0.7$ than in the case of $\alpha = 0.5$. The variation of $\langle M_v \rangle$ with time steps (t) in the pure cross-linking process is

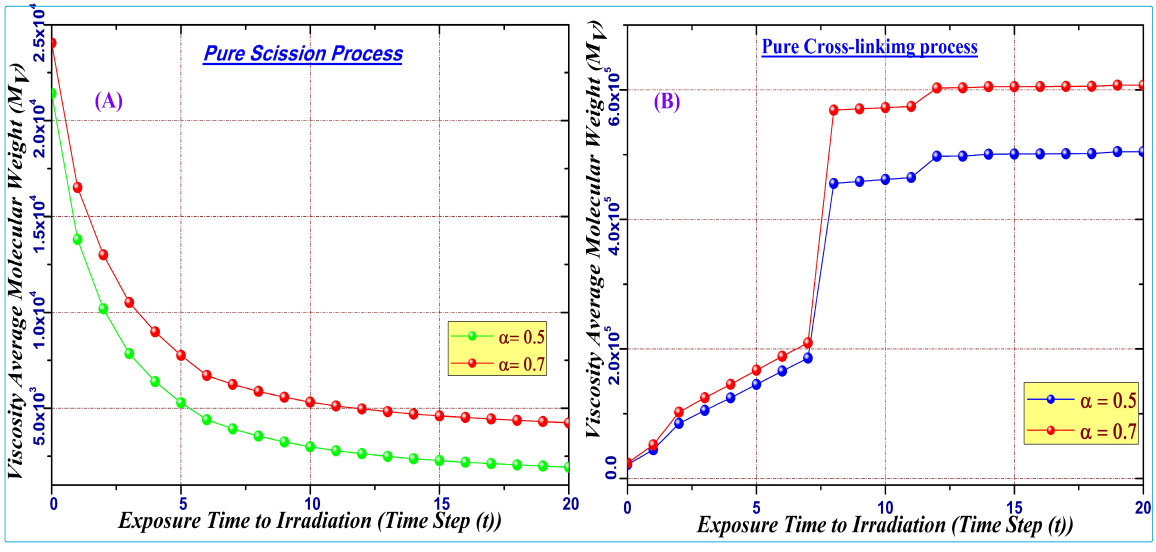

Figure 4.16: *Variation of viscosity average molecular weight ($\langle M_v \rangle$) with time steps (t) for a poly-disperse sample in case of pure scission and pure cross-linking process. (A) $\langle M_v \rangle$ vs t curve for $\alpha = 0.5$ and $\alpha = 0.7$ incase of pure scission process. (B) Variation of $\langle M_v \rangle$ in case of pure cross-linking (i.e. 100% cross-linking) process. The red curve is for $\alpha = 0.7$ and the blue one is for $\alpha = 0.5$.*

shown in figure-4.16(B). Two graphs are drawn for two different exponents which are: $\alpha = 0.7$ and $\alpha = 0.5$. Given the effect of irradiation is based on a pure cross-linking process, each molecule in this case only undergoes intermolecular cross-linking. Hence, bigger size molecules with comparatively higher values of fractal stages (s) are more likely to be present inside the host polymer sample. A significant difference in molecular distribution pattern has been observed in the case of pure cross-linking (100% cross-linking) process between mono-disperse and poly-disperse samples. This difference significantly reflects in the $\langle M_v \rangle$

vs t curves in figure-4.7(B) and 4.16(B).

In the case of the mono-dispersive sample, two curves for $\alpha = 0.7$ and $\alpha = 0.5$ superimpose with each other up to the saturation region. Post which they become separated which can be seen clearly in figure-4.7(B). This is because the system remains mono-disperse up to the saturation stage post which poly-dispersive nature is observed inside the system. But in the present case, the system is poly-disperse from the beginning of the irradiation and its poly-dispersive behavior is maintained throughout the irradiation process. Therefore the $\langle M_v \rangle$ vs t curves for $\alpha = 0.7$ and $\alpha = 0.5$ are separated from the beginning of the irradiation process. Two curves in figure-4.16(B) show an initial slow increment rate up to the 7th time steps (t=7) post which a step like jump can be observed at t=8. The saturation state has been achieved by both curves at the 12th time step (t=12). The value of $\langle M_v \rangle$ in the case of $\alpha = 0.7$ happens to be higher than that in the case of $\alpha = 0.5$ as observed in figure-4.16(B). Variation of $\langle M_v \rangle$ with respect to time steps (t) in case of intermediate scission dominating

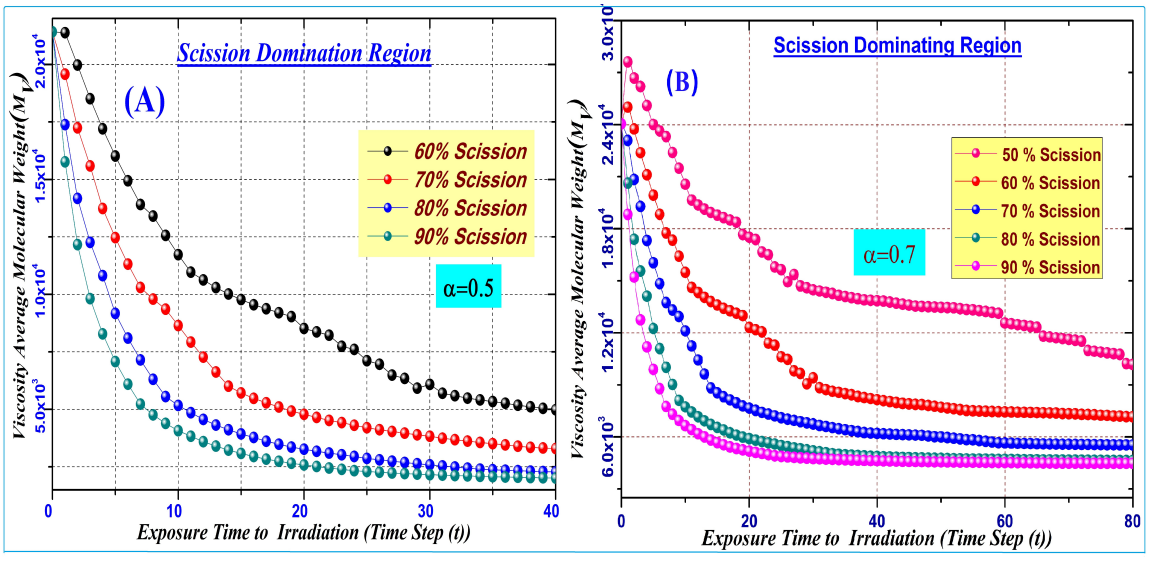

Figure 4.17: *Viscosity average molecular weight $\langle M_v \rangle$ variation curves for intermediate scission dominating region. (A) Variation of viscosity average molecular weight $\langle M_v \rangle$ in case of intermediate scission dominating region (60% to 90% scission probabilities) where the value of the exponent $\alpha = 0.5$. (B) $\langle M_v \rangle$ vs t variation curves for the same scission dominating region (50% to 90% scission probabilities) where the value of the exponent $\alpha = 0.7$.*

region has been shown in figure-4.17(A) and 4.17(B) where we have taken the value of the exponent $\alpha = 0.5$ and $\alpha = 0.7$ respectively. Unlike in the mono-disperse sample, large size molecules (e.g, molecules with fractal stage s= 9 or 10) cannot be generated here at initial

irradiation time steps (t). Therefore, initial sharp peak which we have noticed in the case of the mono-disperse sample, are absent in figure-4.17(A). In the present case, we have investigated the variation of $\langle M_v \rangle$ up to the 40th irradiation time steps (t=40) for both cases of $\alpha = 0.5$ and $\alpha = 0.7$ which is shown in figure-4.17(A) and 4.17(B).

It can be observed in both figures (for $\alpha = 0.5$ and $\alpha = 0.7$) that the magnitude of $\langle M_v \rangle$ eventually decreases very fast over time steps (t) in cases of 80% and 90% scission probabilities. Thus, a gradual decreasing curve has been observed in 80% and 90% scission processes in both cases i.e. for $\alpha = 0.5$ and $\alpha = 0.7$. The rate at which the magnitude of $\langle M_v \rangle$ falls with time steps (t) for 50%, 60%, and 70% scission processes are comparatively slower and a plateau-like region can be noticed in both figures at the intermediate stage of the irradiation process. This region is followed by the saturation stage of the said curves. In the case of $\alpha = 0.5$, this plateau-like region is continuous and smooth by nature which can be observed in figure-4.17(A). Whereas an additional step-like variation has been noticed with this plateau-like region in the case of the same $\langle M_v \rangle$ vs t curves for $\alpha = 0.7$ and they are indicated in figure-4.17(B). Besides that, an initial peak has been noticed in figure-4.17(B) for the $\langle M_v \rangle$ vs t curve of 50% scission process. The variation of $\langle M_v \rangle$ with the exposure

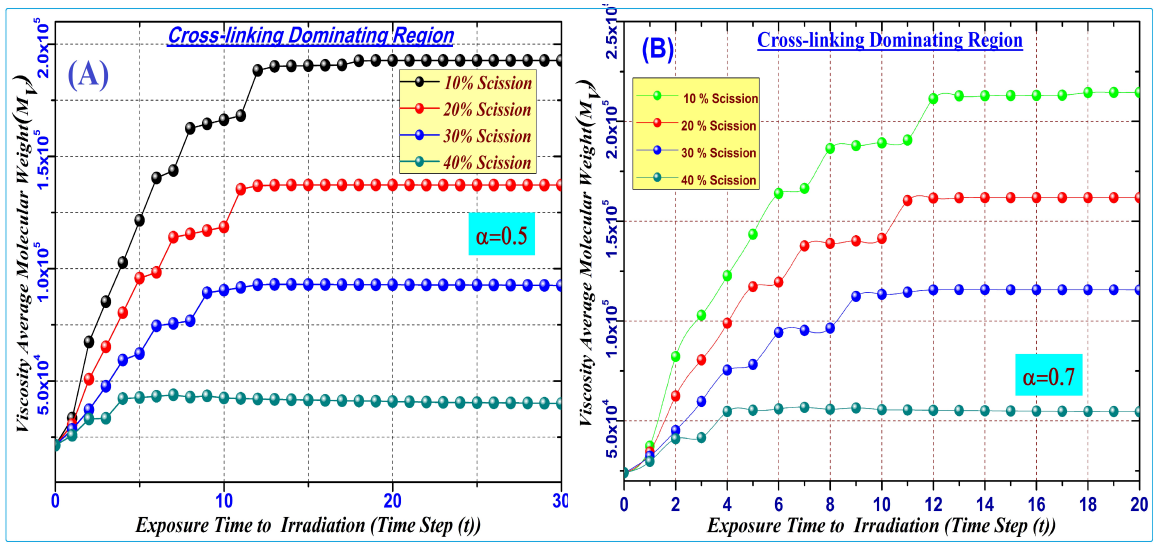

Figure 4.18: *Variation of $\langle M_v \rangle$ with respect to the irradiation time steps (t) in case of the cross-linking dominating region. (A) Four $\langle M_v \rangle$ vs t curves ranging from 10% to 40% scission process where $\alpha = 0.5$. (B) The same $\langle M_v \rangle$ vs t curves are plotted taking $\alpha = 0.7$*

time to irradiation (t) in the case of the intermediate cross-linking dominating region, is shown in figure-4.18(A) and (B). According to the assumptions that we have stated in chapter 3, a minimum of 5 molecules of an arbitrary fractal stage (s) must be required to

perform the intermolecular cross-linking process. In figure-4.18(A) and (B), four different $\langle M_v \rangle$ vs t curves are shown for four different scission percentages (10% to 40% scission i.e. 90% to 60% cross-linking) considering the value of the exponents as $\alpha = 0.5$ and $\alpha = 0.7$ respectively. One or more gradual step-like increments can be observed in each of the $\langle M_v \rangle$ vs t curves for both value of the exponents (for both $\alpha = 0.5$ and 0.7). This is due to the increase in the number of bigger size molecules (N(s,t)) having higher values of fractal stages (s) over time steps (t).

Since the probability of formation of bigger size molecules increases with the decrease of scission probability i.e. increase of cross-linking probability, the magnitude of the enhancement of $\langle M_v \rangle$ increases with the decrease of scission percentage which can be observed clearly in figure-4.18(A) and (B). Variation in the number of molecules with different fractal stages (N(s,t)) inside the host SPE sample becomes negligible after a certain irradiation time step. Therefore the value of $\langle M_v \rangle$ attains their saturation stage for any probability of scission in this cross-linking dominating region which can be observed in both cases for $\alpha = 0.5$ and $\alpha = 0.7$. It can be clearly understood from the figure-4.18(A) and (B) that the magnitude of $\langle M_v \rangle$ for each curve at the saturation region for the value of exponent $\alpha = 0.7$ is always higher than the respective $\langle M_v \rangle$ vs t curves in case of $\alpha = 0.5$.

4.5.2.4. Effect of Gamma Irradiation on Z-Average Molecular Weight $\langle M_z \rangle$ for Poly-disperse SPE Sample

We have also investigated the variation of $\langle M_z \rangle$ with irradiation time steps (t) in case of a poly-disperse sample as we have done in case of other molar mass averages. Variation of $\langle M_z \rangle$ with irradiation exposure time (t) in case of the poly-disperse sample, happens to be significantly different from that in the mono-disperse system. As mentioned before, molecules inside the sample here are initially (i.e. in case of the un-irradiated sample) modelled with $5^{th}, 6^{th}, 7^{th}$ stage Vicsek fractals. As the time step (t) is increased, sizes of the host polymer molecules are distributed among different fractal stages due to the competing effects of scission and cross-linking processes. Hence, the width of the weight fraction ($W_f(s,t)$) distribution curve increases, and the curve becomes more flattened with the increase of time step (t). This phenomenon has already been discussed in the previous chapter.

The mathematical formulae for $\langle M_z \rangle$ (equation-(4.17) and (4.26)) suggest that it is highly sensitive towards the molecular weight i.e. the fractal stage s. Therefore, broad

distribution of molecular size inside the host polymer sample provides a strong effect on the nature of $\langle M_z \rangle$ vs t graphs – a fact which has been clearly shown in figure-4.19 and figure-4.20. Variation of $\langle M_z \rangle$ with respect to external gamma irradiation in case of pure scission and pure cross-linking processes has been shown in figure-4.19. Here variation of $\langle M_z \rangle$ has been studied up to the time step t=70. Initially the curve shows a fluctuating behavior up to the time step t=7 post which a gradual nonlinear increasing behavior can be observed till the irradiation time step t=35. The increment rate of $\langle M_z \rangle$ has been slowed down after this time step and finally, it attains the saturation stage near the 70th time step as shown in figure-4.19(A). The variation of $\langle M_z \rangle$ with time step (t) for the radiation-induced

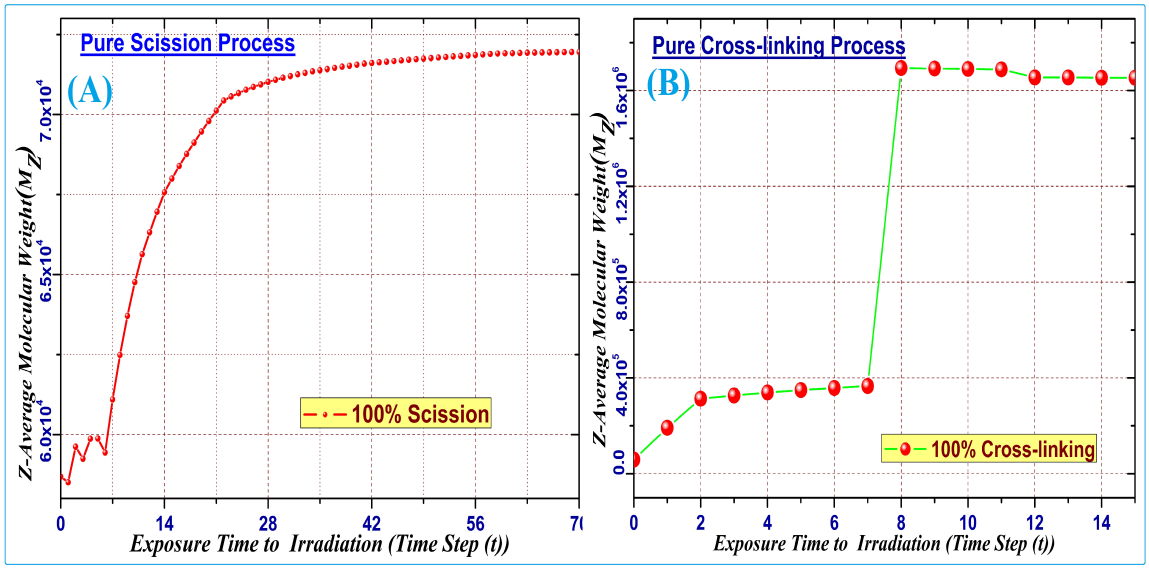

Figure 4.19: *Variation of Z-average molecular weight $\langle M_z \rangle$ with external gamma irradiation in two extreme cases. (A) $\langle M_z \rangle$ vs time step (t) curve for pure scission process. (B) $\langle M_z \rangle$ vs t variation curve in case of pure cross-linking process.*

pure cross-linking process has been shown in the figure-4.19(B). Here also we can notice an abrupt step-like increment at the 8th irradiation time step (t=8). A linear increment of $\langle M_z \rangle$ can be noticed at the initial stage of the irradiation process up to the 2nd time step (t=2) post which the rate of increment slows down significantly and this trend is continued till the time step t=7 which is followed by the abrupt hike at t=8 as mentioned before. The magnitude of $\langle M_z \rangle$ hardly varies after this time step and the saturation stage of $\langle M_z \rangle$ vs t curve has been achieved after the time step t=12. Figure-4.20(A) represent the $\langle M_z \rangle$ variation in case of intermediate scission dominating region. In this case, the $\langle M_z \rangle$ vs t graph has been plotted up to the time step t = 55 for the sake of clear understanding. We can notice the prominant fluctuating behavior of these $\langle M_z \rangle$ variation curves at the initial

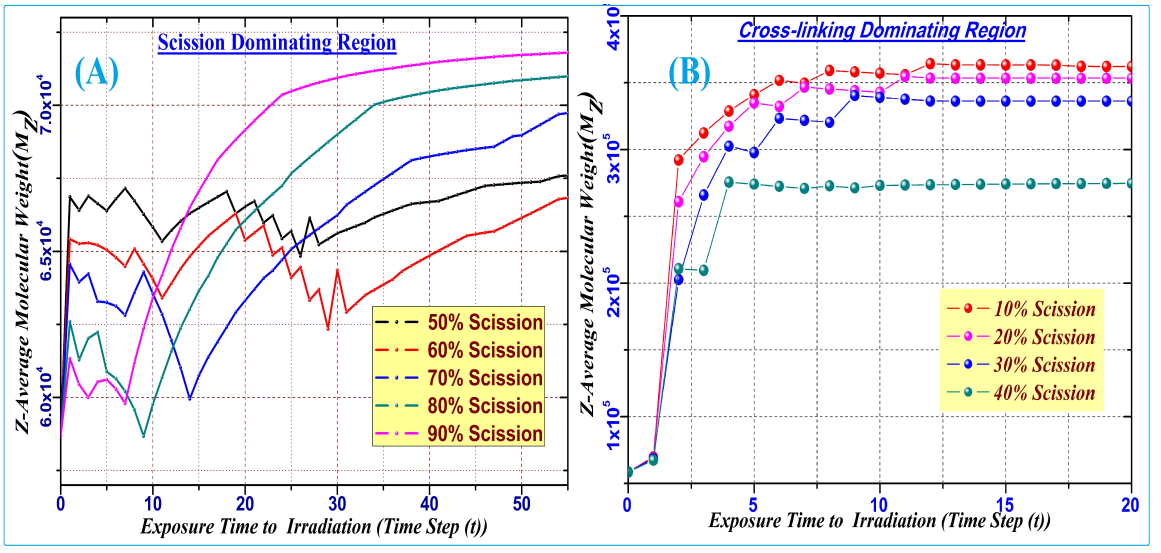

Figure 4.20: *Variation of z-average molecular weight $\langle M_z \rangle$ due to the application of external gamma irradiation in two intermediate cases where scission and cross-linkig processes occur simultaneously. (A) $\langle M_z \rangle$ vs t curves in scission process dominating region (50% to 90% scission).(B) Variation of $\langle M_z \rangle$ in case of intermediate cross-linking process dominating region (10% to 40% scission).*

stage of irradiation process and this phenomenon happens to be the most sidnificant feature of these curves.Generally this fluctuating behavior persists within the time step t=15 for the $\langle M_z \rangle$ variation curves representing 50%, 60%, and 70% scission probabilities but this trend is continued up to time step t=30 (tentative value) for those curves where probabilities of scission are 50% and 60% respectively.

The fluctuating behavior is observed most profoundly in case of 60% scission probability and it extends up to the time steps t = 32 . A steady non-linear increment of $\langle M_z \rangle$ can be noticed after the fluctuation region which is followed by a saturation stage for each of the curve. The trend of $\langle M_z \rangle$ variation for every curve in scission dominating region happens to be more or less the same, and it is only the region of fluctuation that increases with the increase of the rate of cross-linking process as shown in figure-4.20(A). The fluctuating behavior in the $\langle M_z \rangle$ vs t curves can be deemed a direct consequence of the variation in total number of molecules (N(s,t)) with different fractal stages (s) for every time step t.The variation in molecular size distribution is considerably high in case of poly-disperse samples and this phenomenon eventually leads to the abovementioned fluctuating behavior at the initial stages of $\langle M_z \rangle$ vs t curves.

Figure-4.20(B) shows the radiation induced $\langle M_z \rangle$ variation curves for those cases where the cross-linking process plays the predominant role. Four $\langle M_z \rangle$ vs t graphs for four different scission probabilities (10%, 20%, 30%, and 40% scission) are shown here. Cross-linking dominating region results in a higher chance of the generation of bigger size molecules inside the sample. This phenomenon directly bears a strong impact on the $\langle M_z \rangle$ vs t curves. Each curve shows a sharp nonlinear increment up to the time step t=3 post which the rate of increment slows down but continues up to the irradiation time t= 10. Following this, all the curves attain their respective saturation values. $\langle M_z \rangle$ vs t curves for 40% and 30% scission probability, however, display this fluctuating nature on a very small scale. The bigger size molecules present in a host polymer sample at an arbitrary time step t, play the chief role to determine the nature of the $\langle M_z \rangle$ vs t curve.

4.5.3. Discussion Regarding the Outcome of Simulation on the Basis of Various Experimentally Observed Facts

Working on different polymer samples, researchers have performed various experimental studies to illustrate the variation of $\langle M_n \rangle$ due to external gamma irradiation[8,13]. Some of these studies have used PEGd, lPLA, and PEG-PLGA Multiblock Copolymers[8] and have varied the irradiation doses ranging from 0 kGy to 40 kGy. Alternatively, the variation of gamma irradiation from 0kGy to 50kGy has also been reported by some researchers[8]. In some other cases, researchers have used chitosan or other suitable materials as samples and studied the variation of $\langle M_n \rangle$ with external irradiation up to 30 kGy[13,39]. All these experimental studies have shown a gradual decay in the value of $\langle M_n \rangle$ with the increase in irradiation dose.

Some of the researchers have concluded that the degradation of $\langle M_n \rangle$ takes place through the chain scission process[8]. These experimental results show a good agreement up to some extent with our simulation results for both mono-disperse as well as poly-disperse system mostly in case of scission dominating region which has been observed in figure-4.4(A) and figure-4.13(A). These figures clearly show the gradual reduction of $\langle M_n \rangle$ mostly in case of scission dominating region. However, there are also some cases in cross-linking dominating region where we can find the same trend of $\langle M_n \rangle$ variation which is shown in figure-4.4(B) and figure-4.13(B). There are also some theoretical studies regarding the variation of $\langle M_n \rangle$ with external gamma irradiation[40]. The variation of the factor $(1/\langle M_n \rangle)$ with external irradiation has also been reported by some researchers[13,39] which is also relevant for the present simulation result. Theoretical studies to investigate the variation

of $\langle M_n \rangle$ with external gamma irradiation (t) for poly-disperse samples have been discussed in details in an article[41] of the author of this thesis.

The variation of $\langle M_w \rangle$ with the external gamma irradiation is also studied experimentally by the same researchers who have investigated the $\langle M_n \rangle$ variation in response to the external gamma irradiation[8,13]. In this regard, they have used the same samples like PEGd, lPLA, and PEG-PLGA Multiblock Copolymers, chitosan, etc.[8,13] as we have mentioned before. The irradiation varies from 0 kGy to 30 kGy, and in some cases 40 kGy. The outcome of those experiments have an overall agreement with that of the simulation result, discussed previously. They have shown a gradual degradation of the value of $\langle M_w \rangle$ with the increase of gamma irradiation dose which shows a satisfactory similarity with the outcome of the present simulation for both mono-disperse as well as poly-disperse sample in mostly scission dominating region as is seen in figure-4.6(A) and figure-4.15(A).

The experimental study has also reported that the degradation of $\langle M_n \rangle$ happens to be faster than that of the $\langle M_w \rangle$[39] which shows some similarities with our present simulation result and can be understandable from $\langle M_w \rangle$ vs t variation curves plotted in figure-4.6(A) and figure-4.15(A). The variation in the factor $(1/\langle M_w \rangle)$ with external irradiation has also been reported by some researchers[39]. Furthermore, the simulation results discussed here regarding the variation of $\langle M_w \rangle$ with external irradiation for a poly-disperse sample have been reported in an article[41].

Experimental studies concerning the response of $\langle M_v \rangle$ to external gamma irradiation are also adequate in the literature. Different researchers have investigated the variation of $\langle M_v \rangle$ with external gamma irradiation taking different types of materials as a sample. Some of them have used Poly-(ethylene oxide) from B.D.H., England, and ammonium perchlorate to produce the desired sample $PEO(1-x) - NH_4ClO_4(x)$[9,10]. Many researchers have used chitosan as a sample[3,33]. They have used gamma rays from a ^{60}Co source as external irradiation[9,10].

In some cases, the applied gamma irradiation dose varies from 0 kGy to 40 kGy[5] whereas in some other cases, the same vary up to 30 kGy[40].The detailed experimental study regarding the variation of $\langle M_v \rangle$ concluded a gradual degradation of $\langle M_v \rangle$ as the external gamma irradiation is increased[5,9,40]. In this chapter, the outcome of our simulation work to study the variation of $\langle M_v \rangle$ with gamma irradiation for different scission percentages in both mono-disperse, as well as a poly-disperse system, has been plotted in figure-4.8 and figure-4.17 respectively. After careful observation, we can state that all the above-mentioned

experimental results are in good agreement with the simulation study up to some extent mostly for the scission-dominating region. The computer simulation study of the variation of $\langle M_v \rangle$ to the external gamma irradiation which is discussed in the present chapter has also been reported in a published journal by this author[41–43].

Some researchers have reported that different types of radiation-induced chain scission processes[8] happens to be the prime factor for the variation of different types of molar mass averages ($\langle M_n \rangle$,$\langle M_v \rangle$,$\langle M_w \rangle$, etc.) of the host polymer sample in response to the external gamma irradiation. As a consequence, each of the molar mass averages shows a gradual decreasing behavior as the radiation doses increases. This trend of variation of the respective molar mass averages is in good agreement with our simulation studies of the molar mass variation in the scission domination region. There is another part of our simulation which consists of the study of the molar mass averages variation due to the gamma irradiation in the cross-linking dominating region where we have seen a general trend of the gradual enhancement of molar mass average vs irradiation time step curves (t) followed by a saturation stage in each case. Despite the artificiality in the mathematically modeled SPE system, we can ultimately say that the overall outcome of the simulation has a good agreement with the experimentally observed fact.

4.6. Conclusion

We have investigated the nature of variation of different molar mass averages of host SPE due to the external irradiation. The extensive quantitative analysis on both mono-dispersive as well as poly-dispersive solid polymer systems reveals the fact that the probability of cross-linking and scission play significant role on determination of the molar mass averages variation. Radiation induced scission dominating process generates large number of molecules with low molecular weight. Hence the value of $\langle M_n \rangle$ decreases with the increase in irradiation time steps (t) for both mono-dispersive and poly-dispersive systems. But other molar mass averages e.g. $\langle M_v \rangle$, $\langle M_w \rangle$, $\langle M_z \rangle$ vary slightly in a different way for mono-disperse system rather than the poly-disperse one. The values of $\langle M_w \rangle$ and $\langle M_v \rangle$ in mono disperse system shows an initial sharp increase and then a gradual decrease which is followed by a saturation stage. Whereas the value of $\langle M_z \rangle$ shows a sharp increase initially and after that it attains a saturation value. This trend of variation is different in case of poly disperse sample. In this case, a very small increment in the value of $\langle M_w \rangle$ has been observed and it cannot be noticed in case of the variation $\langle M_v \rangle$. But both values decrease with the increase

of irradiation time step (t) and afterwards, they attain their respective saturation states. On the other hand, value of $\langle M_z \rangle$ in case of poly-disperse system fluctuates at the initial irradiation time steps and afterwards it is followed by a saturation state for the higher value of (t).

The discrepancies which are observed in the variation of $\langle M_v \rangle$, $\langle M_w \rangle$, $\langle M_z \rangle$ values between mono-disperse and poly-disperse systems, happens to be the direct consequence of their sole dependence on the molecular weight distribution of the respective polymer molecules. In case of mono-disperse sample one can find very large size molecules, very few in number at initial irradiation time steps. This phenomenon result in the sharp increment in case of $\langle M_v \rangle$, $\langle M_w \rangle$, $\langle M_z \rangle$ values in case of mono-disperse sample. The variation of $\langle M_v \rangle$, $\langle M_w \rangle$, $\langle M_z \rangle$ in cross-linking prone process happens to be more or less same for both mono and poly dispersive systems, as inter molecular cross-linking generates bigger sized molecules. Hence all the respective curves shows a common trend of sharp increment at some initial time steps (t) post which those graphs attain their saturation values. We thus conclude from these above mentioned properties that every molar mass averages strongly depends on the molecular weight distribution of the host polymer molecules and this simulation results match up to certain extent with the experimentally observed variation.

It should be kept in mind that our method of construction of the host polymer matrix is deterministic Vicsek fractal whose molecular weight increases in the order of 5^s with the fractal stage (s). But the actual polymer molecules shows different kind of structural properties. In spite of the artificiality of our model, the outcome of the simulation works regarding different molar mass averages shows reasonable good agreement with their experimentally observed trend of variation.

Bibliography

[1] Gad S.E.,2014,Polymers,Gad Consulting Services, Cary, NC, USA,https://doi.org/10.1016/B978-0-12-386454-3.00912-X

[2] Ghosh, P., 2007. Molecular Weights of Polymers.

[3] Zhaomu, Z.H.A.N.G. and Guojun, Y.A.N.G., 1986. A new method for estimation of weight-average molecular weight of polymer from the intrinsic viscosity and chromatogram. Chinese J. Polym. Sci, 4(2), pp.142-147.

[4] Volland, C., Wolff, M. and Kissel, T., 1994. The influence of terminal gamma-sterilization on captopril containing poly (d, l-lactide-co-glycolide) microspheres. Journal of Controlled Release, 31(3), pp.293-305.

[5] Norzita, Y., Norhashidah, T. and Maznah, M., 2011. Determination of viscosity-average molecular weight of chitosan using intrinsic viscosity measurement.

[6] Umoren, S.A. and Solomon, M.M., 2016. Polymer characterization: Polymer molecular weight determination. Polymer Science: research advances, practical applications and educational aspects, Formatex Research Center SL, 1, pp.412-419.

[7] Kasaai, M.R., Arul, J. and Charlet, G., 2000. Intrinsic viscosity–molecular weight relationship for chitosan. Journal of Polymer Science Part B: Polymer Physics, 38(19), pp.2591-2598.

[8] Dorati, R., Colonna, C., Serra, M., Genta, I., Modena, T., Pavanetto, F., Perugini, P. and Conti, B., 2008. gamma-Irradiation of PEGd, lPLA and PEG-PLGA multiblock copolymers: I. effect of irradiation doses. AAPS PharmSciTech, 9(2), pp.718-725.

[9] Nanda, P., De, S.K., Manna, S., De, U. and Tarafdar, S., 2010. Effect of gamma irradiation on a polymer electrolyte: Variation in crystallinity, viscosity and ion-conductivity

with dose. Nuclear Instruments and Methods in Physics Research Section B: beam Interactions with Materials and Atoms, 268(1), pp.73-78.

[10] Tarafdar, S., De, S.K., Manna, S., De, U. and Nanda, P., 2010. Variation in viscosity and ion conductivity of a polymer-salt complex exposed to gamma irradiation. Pramana, 74(2), pp.271-279.

[11] Izunobi, J.U. and Higginbotham, C.L., 2011. Polymer molecular weight analysis by 1H NMR spectroscopy. Journal of Chemical Education, 88(8), pp.1098-1104.

[12] Li, W., Chung, H., Daeffler, C., Johnson, J.A. and Grubbs, R.H., 2012. Application of 1H DOSY for facile measurement of polymer molecular weights. Macromolecules, 45(24), pp.9595-9603.

[13] García, M.A., de la Paz, N., Castro, C., Rodríguez, J.L., Rapado, M., Zuluaga, R., Ganán, P. and Casariego, A., 2015. Effect of molecular weight reduction by gamma irradiation on the antioxidant capacity of chitosan from lobster shells. Journal of Radiation Research and Applied Sciences, 8(2), pp.190-200.

[14] Dragostin, O. and Profire, L., 2017. Molecular weight of polymers used in biomedical applications. In Characterization of Polymeric Biomaterials (pp. 101-121). Woodhead Publishing.

[15] Ghosh, P., 2006. Polymer science: Fundamentals of polymer science. Kolkata: Polymer Study Centre.

[16] Mark, J., Ngai, K., Graessley, W., Mandelkern, L., Samulski, E., Wignall, G. and Koenig, J., 2004. Physical properties of polymers. Cambridge University Press.

[17] Flory, P.J., 1953. Principles of polymer chemistry. Cornell University Press.

[18] Cowie, J. M. G. Developments in Block Copolymers - 1; Goodman, I., Ed.; Applied Science: London, 1982; pp 1-37.

[19] Allcock, H.R., Lampe, F.W., Mark, J.E. and Allcock, H.R., 2003. In Contemporary Polymer Chemistry, 3rd ed. Pearson,Prentice Hall,Upper Saddle River, NJ, 2003; pp 393-491.

[20] Stevens, M. P. In Polymer Chemistry: 1999, An Introduction, 3rd ed. Oxford Univeristy Press: New York, pp 35-60.

[21] Young, R. J.; Lovell, P. A. 2011, In Introduction to Polymers, 3rd ed.,CRC Press: Boca Raton, FL, pp 269-341.

[22] Carraher, C. E. J. 2011, In Carraher's Polymer Chemistry, 8th ed.; CRC Press: Boca Raton, FL, pp 55-91.

[23] Cowie, J.M.G. and Arrighi, V., 2007. Polymers: chemistry and physics of modern materials. CRC press.

[24] Cazes, J., 1989. A Question of Molecular Weight. International Division, Waters Associates.

[25] Flory, P.J., 1945. Tensile strength in relation to molecular weight of high polymers. Journal of the american chemical society, 67(11), pp.2048-2050.

[26] Volkov, A.V., Moskvina, M.A., Volynskii, A.L. and Bakeev, N.F., 1993. Effect of copper ions on phase state in polymer blend based on poly (vinyl alcohol) and poly (acrylic acid). Polymer science, 35(2), pp.248-252.

[27] Li, M., 2008. A microfluidic method for determining the molecular weight of polymers of unknown concentrations. A Thesis of the School of Biomedical Engineering, Georgia Institute of Technology.

[28] Isayev, A.I. and Palsule, S. eds., 2011. Encyclopedia of polymer blends ,volume 2 processing. John Wiley and Sons.

[29] Rudin, A., 1998. Elements of Polymer Science and Engineering: An Introductory Text and Reference for Engineers and Chemists. Elsevier.

[30] Viéville, J., Tanty, M. and Delsuc, M.A., 2011. Polydispersity index of polymers revealed by DOSY NMR. Journal of magnetic resonance, 212(1), pp.169-173.

[31] Anthonsen, M.W., Vårum, K.M. and Smidsrod, O., 1993. Solution properties of chitosans: conformation and chain stiffness of chitosans with different degrees of N-acetylation. Carbohydrate Polymers, 22(3), pp.193-201.

[32] Oberlerchner, J.T., Rosenau, T. and Potthast, A., 2015. Overview of methods for the direct molar mass determination of cellulose. Molecules, 20(6), pp.10313-10341.

[33] Kasaai, M.R., Arul, J. and Charlet, G., 2000. Intrinsic viscosity–molecular weight relationship for chitosan. Journal of Polymer Science Part B: Polymer Physics, 38(19), pp.2591-2598.

[34] Ghosh P., 2002, Polymer science and technology, plastics rubbers, blends and composites, 2nd edn. McGraw-Hill India, New Delhi

[35] Weiss, A.R. and Cohn-Ginsberg, E., 1969. A note on the universal calibration curve for gel permeation chromatography. Journal of Polymer Science Part B: Polymer Letters, 7(5), pp.379-381.

[36] Mahabadi, H. and O'driscoll, K.F., 1977. A gel permeation chromatography calibration method for a broad molecular weight distribution polymer. Journal of Applied Polymer Science, 21(5), pp.1283-1287.

[37] Garg, H.G. and Hales, C.A. eds., 2004. Chemistry and biology of hyaluronan. Elsevier.

[38] Musil, J. and Zatloukal, M., 2011. Experimental investigation of flow induced molecular weight fractionation during extrusion of HDPE polymer melts. Chemical engineering science, 66(20), pp.4814-4823.

[39] Saha M, Mukhopadhyay M, Ray R, Ballabh TK, Tarafdar S (2015) Influence of gamma irradiation on the molecular weight distribution and related properties of a polymer: study through simulation and experiment. Modelling Simul Mater Sci Eng 23:19

[40] Loo, J.S.C., Ooi, C.P. and Boey, F.Y.C., 2005. Degradation of poly (lactide-co-glycolide)(PLGA) and poly (L-lactide)(PLLA) by electron beam radiation. Biomaterials, 26(12), pp.1359-1367.

[41] Ghosal, S., Ray, R., Mukhopadhyay, M. and Tarafdar, S., 2017. Fractal model of polymer electrolyte to investigate influence of high energy irradiation in molecular distribution and molar mass average. Ionics, 23(10), pp.2747-2759.

[42] Ghosal, S., Mukhopadhyay, M., Ray, R. and Tarafdar, S., 2014. Competitive scission and cross linking in a solid polymer electrolyte exposed to gamma irradiation: Simulation by a fractal model. Physica A: Statistical Mechanics and its Applications, 400, pp.139-150.

[43] Ghosal, S., Ray, R., Ballabh, T.K. and Tarafdar, S., 2013. Study of diffusion and conduction in gamma irradiated solid polymer electrolytes by fractal model structure.

Chapter- 5

Gamma Irradiation Induced Ionic Conductivity Variation on a Solid Polymer Electrolyte System: Theoretical Investigation Based on Deterministic Fractal Model.

Chapter 5

Gamma Irradiation Induced Ionic Conductivity Variation on a Solid Polymer Electrolyte System: Theoretical Investigation Based on Deterministic Fractal Model.

5.1. Introduction

We have already discussed the ion transport mechanism inside the solid polymer electrolyte (SPE) in chapter-1. Experimental studies have reported the co-existence of crystalline and amorphous phases inside the SPE[1,2]. It is very evident from different experimental research studies that ion transportation inside SPE solely occurs in its amorphous phase whereas the crystalline part of the host polymer sample act as the obstacle to the ionic motion[3–5]. Different types of external influence such as the addition of plasticizer, filler, salts, ionic liquid, etc.[6,7] or application of external irradiation[8] have already proved to be effective in improving the ion transportation properties inside SPE. It has been reported that ionic motion is controlled by the local hopping of ions as well as the localized motion of the polymer chain segments[9]. Besides different theoretical models have been proposed to characterize the ion transport mechanism. All these extensive studies infer a common fact that the ion transport mechanism inside the host polymer sample happens to be a complicated phenomenon that depends on different external influences as well as the dynamical properties of the polymer chain segments.

In chapter-3 and chapter-4 we have investigated the effect of gamma irradiation on the molecular weight distribution as well as the molar mass averages of the host polymer sample due to the application of gamma irradiation. In this chapter, we will perform a theoretical study to investigate the variation of ionic conductivity inside the SPE sample due to the application of external gamma irradiation. We have considered some basic assumptions to perform the computer simulation which will be discussed in the preceding section. The effect of segmental motions of the polymer chain segments is also taken into account. The entire simulation process has been performed for both mono-disperse and poly-disperse polymer hosts similar to the previous two chapters. Variation of ionic conductivity has been studied based on two parameters: exposure time to irradiation (t) and probability of scission process inside the host polymer sample. The results of the simulation study for both type of systems (mono-disperse and poly-disperse) are analyzed separately.

5.2. Literature Review

There are a handful of pioneer research works that have been performed by various researchers across the globe to investigate different experimental techniques to enhance the ionic conductivity inside the polymer electrolyte sample. James R. Maccallum et.al[10] have

worked with poly(ethylene oxide)$/LiCIO_4$ electrolyte sample. The sample, developed in an anhydrous environment is more prone to form an amorphous phase that shows enhanced resistance to crystallization and improved conductivity. Gamma-ray was applied externally from Co^{60} source on the amorphous sample to initiate the cross-linking process which results in an initial reduction in conductivity but, gamma irradiation restricts the crystallization process and reduce the probability of mixed-phase sample formation with reduced conductivity. Esam Kronfli et.al[11] have worked with thin film of $PEO - LiCF_3SO_3$ ($[EOunits]/[Li] = 9$) sample and performed similar kind of experiment where they applied gamma irradiation at 78° C to restrict the recrystallization process and then improve its conductivity at room temperature. A number of the above-mentioned sample were exposed to gamma irradiation for a certain interval of time and estimate the temperature dependence of ionic conductivity. The effect of gamma irradiation on four activations of energies and three overall conductivity levels on the cooling cycle. Same experiment was performed on $PEO - LiClO_4$ ($[EOunits]/[Li] = 20$) and they confirmed the enhancement in ionic conductivity due to external irradiation.

The significant experimental research studies of P. Ferloni et. al.[12] have already been mentioned in chapter-3. Their work on PEO in the form of dry powder, film, and the aqueous solution was also important to investigate the radiation-induced conductivity variation study due to the external irradiation. Though, the process of radiolytic degradation and cross-linking of solid PEO was analyzed on the basis of the ESR measurement result. One of the prime objectives of their work is to study the change in conductivity due to external irradiation. Experimental studies reveal the fact that gamma-irradiated and cross-linked $PEO_{20}LiClO_4$ shows greater conductivity than the un-irradiated sample at room temperature $LiCIO_4$.

Yangyang Wang et. al.[13] did an experimental study to investigate the relation between segmental relaxation and ionic conductivity of a set of polymer electrolytes considering the alteration of chain rigidity. They measured the ionic conductivity, ionic diffusivity, and segmental relaxation time for polymer samples and found that the decoupling of ionic conductivity from segmental dynamics was confirmed in association with the correlation between decoupling strength with the fragility index instead of the glass transition temperature (T_g). This phenomenon was explained on the basis of packing frustration in the rigid polymer. They concluded that one can prepare different types of polymer electrolyte samples with a higher value of decoupled ionic conductivity introducing a rigid polymer chain structure.

A computer simulation analysis was done by C. R. A. Catlow et. al.[14] to investigate the ionic diffusion inside ion-conducting polymers by applying molecular dynamics simulation techniques on PEO/NaI system. In addition to that, they have also studied the influence of temperature and salt concentration on the activity of ionic association inside the sample. The theoretical analysis clearly suggested the strong temperature dependence on the ionic clustering inside the sample and also confirm the main role of ionic clusters on the ion transport mechanism. Moreover, they have also estimated the diffusion co-efficient for Na^+ and I^- ions inside the material and it shows good agreement with the experimentally obtained data.

Yoshiyuki Okarnoto et.al.[15] performed experimental work to investigate the effect of irradiation on the PEO-salt complex and study the degradation procedure of the aqueous solution of poly (acrylic acid) (PAA) and poly(methacry1ic acid) (PMA) applying Tb^{+3} fluorescence techniques. Initially different types of monomers that contain $-SO_3H$ and -COOH functional groups, were grafted on the PEO with the help of an external irradiation process. Post which ionic conductivity, as well as the structural properties of the Li and Na salts inside the irradiated sample, were studied thoroughly. DSC and X-ray measurement has been performed and variation of conductivity (σ) with temperature (1/T) for different irradiation doses have been studied. The enhancement of ionic conductivity was reported due to the enhancement in the amorphous phase. Tb^{3+} fluorescence technique was used for further study and it was observed that the fluorescence intensities of PEO-Tb^{3+} were increased significantly due to the application of gamma irradiation.

A.J. Bhattacharyya et.al.[16] have performed a computer simulation to investigate the nature of ionic conductivity inside the SPE with the variation in salt concentration. Considering the semi-crystalline nature of the polymer sample, they have used the random walk method to estimate ionic conductivity on the basis of the Nernst-Einstein relation. Different waiting times were taken for the sites with different phases the phenomenon of reorganization of the various phases over time scales has also been taken into account. The simulation result of conductivity variation shows a good agreement with the experimentally observed data for $PEO - NH_4I$ and $PEO - NH_4SCN$. The mean distance of each jump shows a good agreement with the reported bond length of those polymers.

Significant experimental work has been done by Joy Kumar Singh, et.al.[17] to study the increase in ionic conductivity of [Poly(ethylene glycol)] complexed with $LiClO_4$ [$(PEG)_xLiClO_4$] due to the application of ion beam (4–8 MeV) irradiation. Different techniques like differential scanning calorimetry, matrix-assisted laser desorption/ionization,

and electron spin resonance spectroscopy have been used to characterize the sample. The maximum enhancement in ionic conductivity has been observed at the 15 kGy of irradiation and this enhancement remains invariant with time for more than 100 hours. The reduction of the amorphous phase as well as the glass transition temperature (T_g) has also been reported. The enhancement in ionic conductivity is considered as the effect of the increasing chain flexibility and the amorphous fraction inside the sample due to the application of irradiation.

N. A. Stolwijk et.al.[18] have studied the nature of ionic conduction inside the amorphous $PEO_{30}NaI$, consisting of poly (ethylene oxide) (PEO) and sodium iodide in a Na-to-O ratio of 30. They have used ^{22}Na and ^{125}I to estimate the radiotracer diffusion co-efficient between the temperature limit 67 to 180^oC and compare it with the total charge diffusivity of the sample, estimated from dc conductivity data. The difference between these two diffusivity data has been explained with the help of a model which is based on the generation of neutral ion pairs. The extensive research studies have concluded that the neutral cation-anion pairs contribute to mass transport but not in charge transport and the ion pair fraction increases with the increase in temperature. Moreover, diffusivities of both single ion and ion pairs follow VTF temperature dependence and the mobile ion pair configuration is mainly responsible for the cation transport and the cation transference number is temperature-dependent.

An effective simulation study has been performed by M. Siekierski et.al.[19] to investigate the mechanism of ionic conductivity inside the composite polymer electrolyte. They have introduced a random resistor network approach to analyze the motion of the charge carriers inside the concerned system. Two types of algorithm have been followed by them where the first one is based on finding the percolation path to simulate the electrical property of the sample and the second one gives a simulated conductivity value for composites with any kind of possible geometry. The first method shows a good agreement with the experimental data. The MultiValue Random Resistor Network approach was proved to be successful for estimating the DC conductivity of the said system.

Poly(vinyl alcohol) (PVA), a water-based polymer is widely used for its various types of advantages like excellent chemical resistance, thermal and mechanical properties, easy preparation, etc. Vladimir M. Nikolic et.al.[20] have performed an experimental study where they have performed the cross-linking of 3% and 5% PVA solution and generated a three-dimensional network with the application of gamma irradiation. The sample is then submerged into an alkaline solution for a certain time period to be used as a solid polymer

electrolyte and make them more conductive by nature. The ionic conductivity of the sample is then estimated as a function of temperature and the concentration of KOH. The thermal stability of the cross-linked PVA sample happens to be more than the sample prepared from the evaporation of the solvent. The highest ionic conductivity of the sample in 6M KOH solution was found 0.015 Scm^{-1} at room temperature and it is highly dependent on the concentration of the alkaline solution.

The mechanism of ionic transport in SPE has been characterized by P.L.Cheang et.al[21] with the help of Monte Carlo simulation. The transport mechanism of the thermally active ion (Li^{+}) has been analyzed using the hopping rate of single cation simulation where the ion hops along the polymer chain and jumps into the neighboring chains overcoming the activation energy and the applied electric field. The simulation study concludes that the velocity, as well as the energy of the ion, increases with the increase of the electric field. The activation energy is found less than 0.28 eV which enable this model appropriate for the characterization of ionic transport inside SPE.

Another simulation approach was done by R. W. Munn et. al.[22] to provide a microscopic insight study the ionic motion inside the poly(ethylene oxide) loaded with lithium perchlorate [$PEO - LiClO_4$] both as bulk material as well as with tungsten oxide (WO_3) interface. Commercial software has been used to simulate the structure of the host polymer sample. Simulation of ion transportation was done by a kinetic Monte Carlo method in the presence and absence of the electric field. They have considered a clattering ion surrounded by a local energy well that can relax on a lattice to accommodate the motion of the ion and can hop as well between the neighboring wells. In presence of an electric field, ion moves against the field direction. Moreover, accumulation of ions at the interface can be observed in presence of (WO_3) eventually decreases the ionic movement generating a repulsive potential. It has been noticed that Li^{3+} ion, in presence of the field, can travel 35 angstroms $\mathring{A}$ along with it and 3 to 7 $\mathring{A}$ across it whereas this distance is to be reduced 2-5 $\mathring{A}$ in absence of the field when there is no (WO_3) interface.

The effect of gamma irradiation on a polymer electrolyte was experimentally studied by Pradyot Nanda et.al.[23]. They have used PEO(1 – x)– $NH_4ClO_4(x)$ with x=0.18 as a sample and applied gamma irradiation on it. The ionic conductivity showed a significant enhancement due to the external gamma irradiation with a dose of 35kGy. In another experimental study[24], they have worked with the same element with the value of x=0.16 to 0.26. The dose of gamma irradiation is varied from 10 to 40 kGy. Here also the conductivity of ion is enhanced due to the gamma irradiation and attains maximum value at the dose

30kGy. The said enhancement happens to be two orders of magnitude for x=0.16 and insignificant for those molecules having x greater than 0.20. The presence of an inductive element with a higher value of x was also reported here at high frequencies. Which intimate regarding some particularities of the microscopic structure.

Abdul Rahaman et. al.[25] have worked with a poly (vinyledene difluoride)–lithium bis(oxalato)borate solid polymer electrolyte, made by the solvent casting process. After irradiating the sample with gamma-ray, a DSC study has predicted the maximum amorphous nature with 35kGy of irradiation dose. The presence of the maximum number of free ions and the minimum number of contact ions have been reported at this irradiation dose. The ionic conductivity has been enhanced at this irradiation dose with 15% enhancement relative to the un eradicated sample and the final value conductivity is $3.05X10^{-4}$ s/m at room temperature. Their extensive work concludes that the application of gamma irradiation increases ionic conductivity and mechanical stability.

The effect of ion beam irradiation (O^{7+} radiations of 80 MeV at a current of 1pnA at a fluence of 1×10^{12} ions/cm) on the conductivity nature of PVA-PEO-EC-$LiCF_3SO_3$ blends was experimentally studied by Prajakta Joge et.al.[26]. The sample was prepared by solution casting method with 5 varieties of concentration in the range 3wt% to 11wt%. Characterization by impedance spectroscopy reported a significant enhancement in ionic conductivity with the increasing value of salt concentration. In the case of both irradiated and un-irradiated samples with 9wt% salt, concentration shows optimum ionic conductivity.

S. Raghu and his co-researchers[27] have worked with PEO: $CdCl_2 = 75 : 25$ sample which was made by solution casting method. The system was then irradiated by gamma-ray from a Co^{90} source with a dose rate of 9.5kGy/hour with doses 50kGy, 100kGy, and 150kGy. The system was characterized by FTIR study, dielectric and optical absorption measurement before and after irradiation. After the experimental study, they concluded that both dielectric constant and ac conductivity was increased due to the gamma irradiation.

V.R. Sunitha et. al.[28] have performed an experimental study to find the effect of gamma irradiation on the physical and electrical properties of polyethylene oxide (PEO)-based nanocomposite polymer electrolyte sample. Gamma irradiation introduces a considerable amount of change on surface morphology which has been concluded from the microstructural studies through scanning electron microscope technique. Frequency-dependent conductivity and measurement techniques were used to study the ion dynamics behavior. The FTIR spectra as well as the X-ray diffraction analysis assure the reduction

in crystallinity of the host polymer electrolyte film pre and post-irradiation process. The highest ionic conductivity of 1.717×10^{-4} has been achieved at a 40 kGy irradiation dose. The standard impedance spectroscopic technique has been used to estimate the bulk ionic conductivity.

Xi Chelsea Chen et. al.[29] have taken the semi-crystalline polymer electrolyte consisting of poly(ethylene oxide) (PEO) and lithium triflate salt $[(PEO)_{16}LiTf]$. Also they studied the nature of crystallinity, ionic conductivity, and segmental dynamics. The quasi-elastic neutron scattering (QENS) method has been used to quantify the segmental dynamics of the PEO chain segments. In this regard, they have estimated the structural relaxation time τ_0 of the PEO chains using the Cole-Cole function at an arbitrary temperature. It has been reported that the structural relaxation time of the sample (equilibrated for 1 week) at 305K happens to be six times longer than that is cooled down to 305K. Consequently, ionic conductivity becomes three times smaller in the equilibrated situation.

5.3. Basic Assumptions for the Computer Simulation to Study the Radiation Induced Ion Conductivity Variation inside the SPE

The whole simulation of ionic motion inside the mathematically modeled polymer sample is based on some fundamental assumptions which are mentioned below:

a. The host polymer sample is mathematically modelled with the help of deterministic fractal (Vicsek fractal) to study the ionic motion and the motion of a single ion is taken into account for the sake of simplicity.

b. We have assumed an idealized theoretical process where a unidirectional biased single ionic motion has been considered. The ion starts from an initial point and moves forward along a 1-D straight path as shown in figure-5.1. c. At the time of unidirectional motion, the ion exit from one molecule and enters into the next molecule immediately . Therefore there is no time lag at the time of transition of the ion from an arbitrary molecule to the next one.

d. Ionic motion inside the host polymer sample is affected by two factors: i. Trapping of ion inside the host polymer molecules.
ii. The segmental motion of the different branches associated with the backbone of the said polymer molecules.

These two effects result in two opposite impacts on the ionic motion inside the host

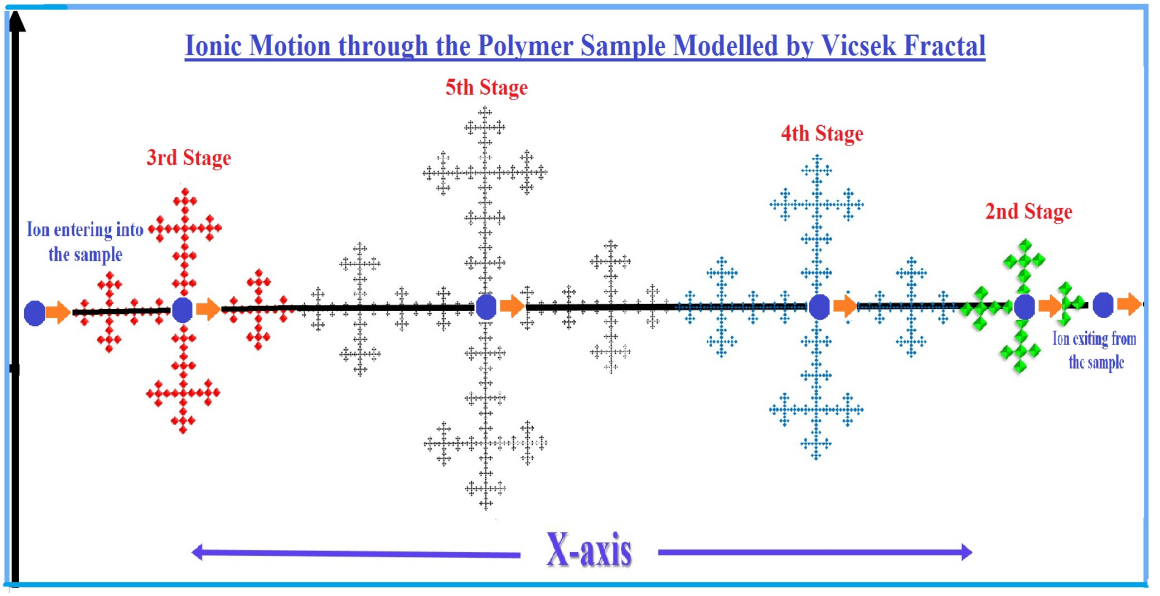

Figure 5.1: *Unidirectional ionic motion inside a SPE sample which is modelled by a 1-dimensional array of Vicsek fractals having different fractal stages. The single ion (indicated by the blue ball) moves along the positive X-axis as per our assumption.*

polymer sample. One of the prime reasons to consider the loop-less deterministic Vicsek fractal as a mathematical tool in our present simulation is to incorporate the effect of segmental motion of the polymer branches in our simulation study.

e. We have directly used the mathematical formula that has been suggested in some previous works of literature[30] to estimate the trapping time inside an arbitrary Vicsek fractal. The details of the ionic motion inside the Vicsek fractal have not been investigated separately.

f. The effect of different kinds of external influence such as the addition of plasticizer, the effect of fillers, salt concentration, behavior of the host polymer sample in the external environment, etc. have been ignored here to make the theoretical study comparatively easier.

g. The ionic motion inside the host polymer sample is assumed to be influenced by two radiation-induced factors: i. Scission of the bigger size polymer molecules into smaller ones. ii. Intermolecular cross-linking of the polymer molecules with arbitrary fractal stage and generation of bigger size daughter molecules.

We have followed the same procedure as mentioned in chapter-3 to execute the radiation-induced scission and cross-linking processes in our present simulation.

5.4. Factors Affecting the Ionic Motion inside the Host Polymer Sample

Different types of experimental as well as theoretical studies[21,22] have reported that ionic motion inside the host polymer sample is controlled by different factors such as types of ionic species, host polymer system, temperature, external perturbation, etc. As we have mentioned before, the ionic motion inside the host solid polymer sample is influenced by two factors:

A. Trapping of ion inside the host polymer molecules.
B. Segmental motion of the polymer chain segments.

5.4.1. Trapping of Ion inside the Host Polymer Molecules

Polymer samples, being a disordered medium, consist of molecules having a defined backbone and many branches with different lengths in most of the cases. When a diffusing ion enters inside this complex structure, it is trapped inside the molecule and slides through backbones and dangling ends which is shown in the figure-5.2. This happens to be one of the significant reasons for ionic diffusion being anomalous inside the SPE and the sub-diffusive behaviour of ionic motion inside the host SPE has already been reported by some researchers in their prior arts[31]. In the present case of our simulation study, the primary conditions

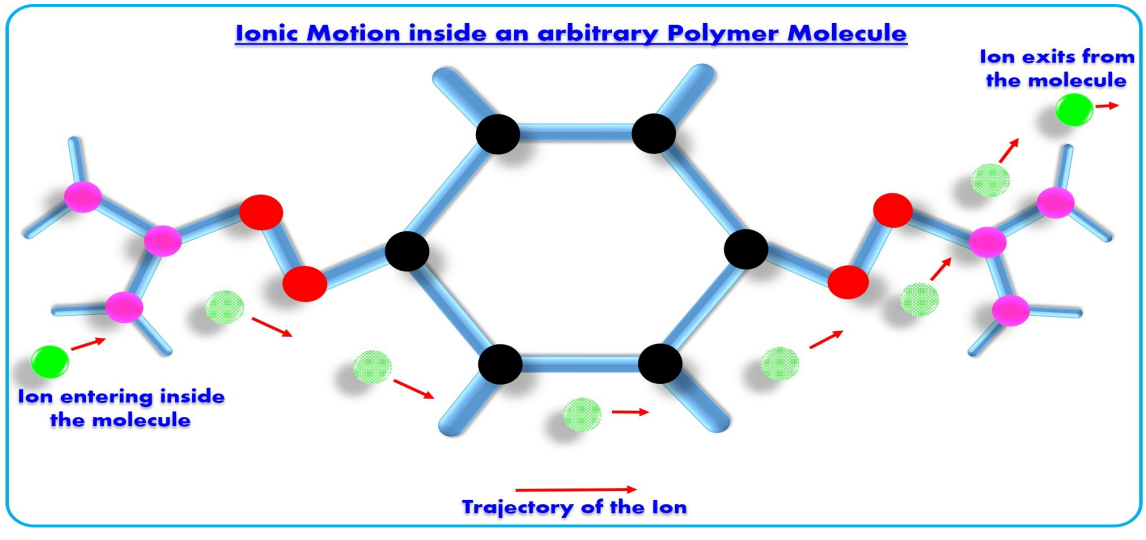

Figure 5.2: *Random hopping of ion inside a polymer chain segment. The entrance, as well as exit of the ion, is symbolized by the prominent green balls. Whereas, the faded green balls indicate the intermediate positions of the ion inside the polymer chain segment.*

imposed for the evolution of trapping time for ionic motion within the host polymer matrix are:

a.The diffusion of multiple ions and the effect of inter-ionic interaction inside the polymer molecules have been ignored as we have taken single ion motion under consideration for our simulation study.

b. Single ion enters inside an arbitrary polymer molecule and slides through its different

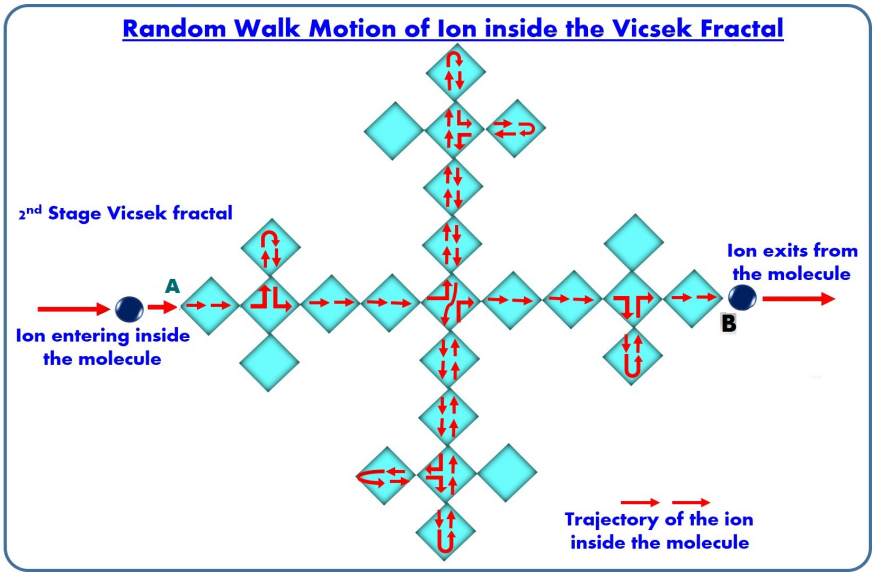

Figure 5.3: *Random walk motion of ion inside the Vicsek fractal. Ion enters from one end of diagonal (A) and exits from the opposite end (B). In the meantime, the ion moves randomly through different accessible sites inside the Vicsek fractal. The red arrows show the trajectory of the ion inside the fractal lattice. This is a schematic diagram. The trajectory can be different from that is shown in the figure*

branches. During its motion, the ion performs a random walk and visits different accessible sites randomly inside the Vicsek fractal of an arbitrary stage (s) which represents a polymer molecule.

c. The random ionic motion continues along with different accessible sites inside the fractal until it reaches the boundary, suitable for jumping to the next neighboring molecule as shown in the figure-5.3. The total time that an ion resides inside an arbitrary molecule, is known as the trapping time (τ_1) of the ion inside a molecule, which explicitly depends on the size of the corresponding molecule. The bigger the molecule, the longer will be the duration of trapping time. After spending a time τ_1 at a particular trap, the ion moves to an adjacent molecule and proceeds through the host polymer matrix.

Considering these prior conditions, polymer molecules, modelled with 2d Vicsek fractals, are arranged diagonally side by side where the fractal stages of the respective Vicsek fractals are chosen randomly as shown in figure-5.1. Therefore, the entire polymer matrix as a whole can be considered as an array of trapping sites. Each trapping site (i.e. fractal molecule) is associated with a definite value of trapping time as per the size (Vicsek fractal stage) of respective polymer molecule. We can assume a Vicsek fractal as a regular lattice with some blocked sites which are distributed in a specific pattern. When the diffusing ion performs a random walk inside the fractal, blocked sites remain inaccessible to it which causes the slowing down of the diffusing particle as shown in the adjoining figure-5.3. This phenomenon results in anomalous diffusion with diffusion exponent $d_w > 2$[32]. Therefore the process can be interpreted as the trapping of ions inside the polymer molecules. Let us consider the ion as a random walker diffusing inside the fractal molecule. If R be the total distance covered by the random walker inside a fractal lattice at a time (t) then one can write[32–34]:

$$[< R^2 > - < R >^2] \sim t^{\frac{2}{d_w}} \tag{5.1}$$

Where, d_w stands for the diffusion exponent. We have assumed here that the ionic motion inside the fractal molecules is completely random by nature. So, the walker can move in all possible directions with equal probability. Hence, $< R > = 0$. Therefore, the above equation can be transformed into:

$$[< R^2 >] \sim t^{\frac{2}{d_w}} \Longrightarrow t \sim [< R^2 >]^{(\frac{d_w}{2})} \tag{5.2}$$

In case of normal diffusion, $d_w = 2$. But, diffusion inside a fractal object has been reported as anomalous by nature[32,35]. In the present case, the total distance covered by the ion is the diagonal end-to-end length (R) of the fractal molecule. In the case of a Vicsek fractal with a stage (s), this diagonal end-to-end length is $R = 3^s$. Therefore, the total time required for a walker to cross the diagonal length can be written as:

$$\tau_1(s) \sim [\langle 3^s \rangle^2]^{\frac{d_w}{2}} = [3^s]^{d_w} \tag{5.3}$$

Where, $\tau_1(s)$ is known as the trapping time of the ion inside the Vicsek fractal with fractal stage = s. The quantitative analysis of diffusion inside the fractal has already been discussed in chapter-2. The study of diffusion process inside loopless fractals is much easier as

there exists an exact mathematical relation between their different structural and transport exponents[32,35], which we have already discussed in chapter-2. Therefore the different types of transport properties like conductivity, diffusion, etc can be determined from the structural properties of the loop-less fractals[36]. The Einstein's relation regarding the diffusion exponent d_w inside a fractal medium can be expressed as[35]:

$$d_w = \alpha + d_f = d_f[1 + \frac{1}{d_l}] \tag{5.4}$$

Where, α is the resistivity exponent as per Einstein's relation. This equation clearly shows the correlation between the exponents α and d_w. In the case of Vicsek fractal, this equation transforms into:

$$d_w = 1 + d_f \tag{5.5}$$

The value of α is unity in this case. d_w can also be evaluated from the simple mathematical

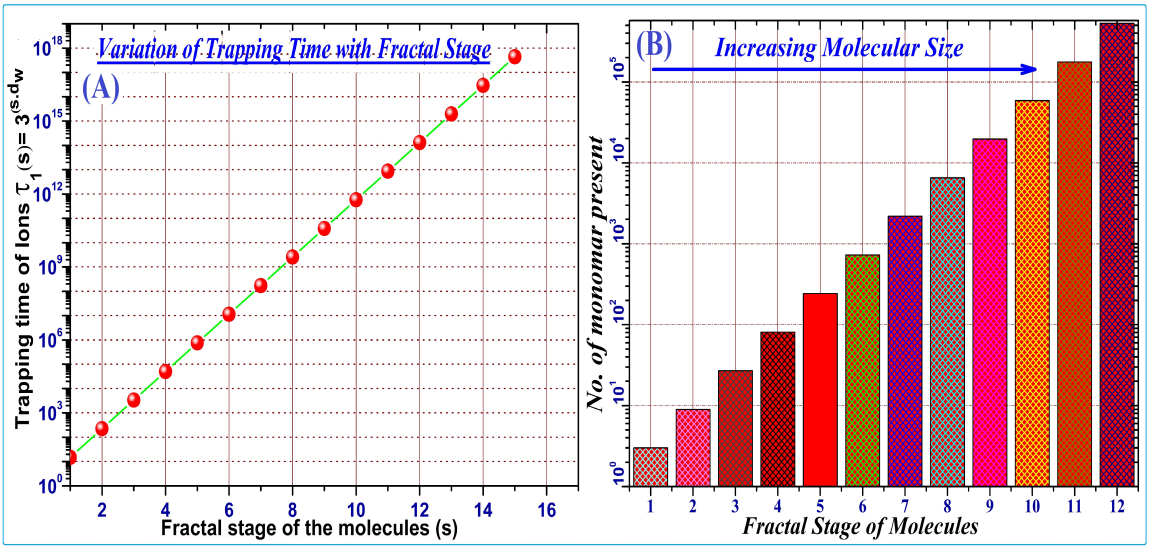

Figure 5.4: *(A) Variation of trapping time $\tau_1(s)$ of an ion with the fractal stage (s) of molecules. $\tau_1(s)$ is plotted along Y-axis in log scale as it increases very rapidly with the increase in fractal stage (s). (B) Variation of the total number of monomer M(s) in an arbitrary fractal molecule with its fractal stage (s).*

technique following the abovementioned equation. The fractal dimension of the Vicsek fractal can be obtained easily as:

$$d_w = \frac{ln(5)}{ln(3)} = 1.465 \tag{5.6}$$

Therefore, the value of d_w can be estimated as:

$$d_w = 1 + d_f = 1 + 1.465 = 2.465 \tag{5.7}$$

The final expression of the trapping time ($\tau_1(s)$) inside the Vicsek fractal can be written as:

$$\tau_1(s) = [3^s]^{d_w} = [3^{2.465}]^s \tag{5.8}$$

Estimation of the diffusion exponent d_w for Vicsek fractal has been performed previously by some researchers of our group and it was reported as d_w=2.465[37,38].The above expression clearly shows the trapping time ($\tau_1(s)$) inside the Vicsek fractal explicitly depends on the fractal stage (s) i.e. the size of the polymer molecule, modelled by Vicsek fractal. The variation of trapping time ($\tau_1(s)$) with respect to the fractal stage (s) is shown in figure—5.4(A). On the other hand, figure—5.4(B) shows the variation of total monomer units in an arbitrary Vicsek fractal with its fractal stage (s).

It is very evident from figure-5.4(B) that the number of monomer units increases very rapidly with the increase in its fractal stage. Hence, molecules that are comparatively bigger in size, can trap the diffusing ion inside them for a longer duration of time since the monomer units appear as a large number of accessible sites for the diffusing ion to perform its random-walk motion. As a result, the trapping time $\tau_1(s)$ increases with the increase in the fractal stage (s). The consequence of this phenomenon can be observed in figure-5.4(A). It can be noticed clearly that the magnitude of $\tau_1(s)$ increases very rapidly as the value of the fractal stage (s) increases. That is why the y-axis which represents the variation of trapping time $\tau_1(s)$, is plotted in log scale. This phenomenon of trapping ions by virtue of its random walk motion inside a fractal macromolecule eventually results in sub-diffusive and slow anomalous diffusion[37] inside the host polymer sample.

5.4.2. Incorporation of the effect of Segmental Motion of the Polymer Chain Segments

The ionic motion inside a polymer electrolyte sample happens to be complicated and based on some established facts[39]. One such fact is the concept of segmental motion of the free branches of polymer molecules. The state-of-art knowledge is based on the fact that ionic motion is associated with the localized motion of the polymer chain segments and this phenomenon is noticed most prominently in the case of cationic transport inside the system[40].

Significant progress has been made in the experimental field that helps us to characterize the mobility of the polymer chain segments inside the thin film[41–46]. Some of these techniques investigate polymer chain mobility that takes place in local segmental length scale and is responsible for glass transition[41–44] whereas some others have reported about the mobility of the entire chain[45,46]. A lot of attempts have also been made to investigate the dynamics of the molecular motion inside those systems that are not crystalline by nature despite slow cooling but freeze into a glassy state[47–49]. The dielectric and mechanical relaxation[50–57] method, nuclear magnetic resonance (NMR)[58,59], the rheo-dielectric method[60,61] etc. are significant among them. Theoretical studies that involve Computer simulation of these polymer films has also been reported by different researchers which provide significant information regarding the motion of the polymer chain segments of different length scales[62–66] Research studies have reported the relation between ionic diffusion

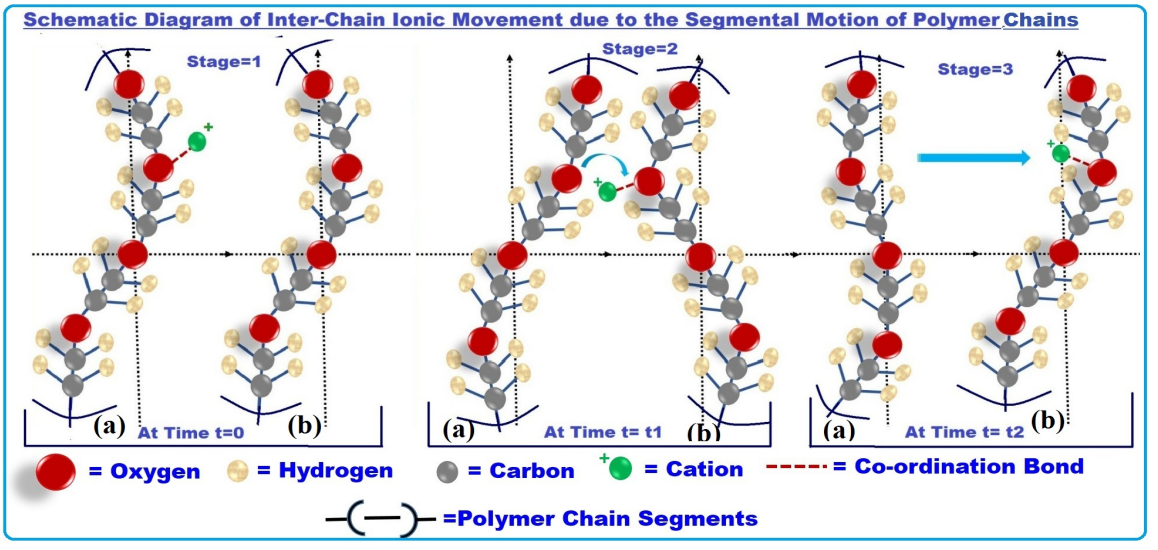

Figure 5.5: *A schematic diagram representing the segmental motion of polymer chain segments and enhancement in ionic motion associated with the respective chains. 3 consecutive stages have been used. In stage-1, chain-a and chain-b are at their initial arbitrary positions and the ion (green ball) is associated with chain-a by making a chemical bond. The arrangement of chain-b is changed in stage-2 due to its segmental motion and it eventually comes closer to the ion. As a result, the ion moved from chain-a to chain-b by making a new chemical bond with the respective atom of chain-b. The chain-b in association with that ion moves apart from chain-a in stage-3 due to its segmental motion resulting in a fast ionic transport from one position to another.*

in polymer samples and the rate of their segmental relaxation[67–69]. In our present simulation study, the concept of segmental motion of the polymer branches has been implemented with the help of a mathematical function. There are some important points that we have kept in our mind at the time of the computer simulation:

a. We know the polymer molecules having different molecular weights are modelled with Vicsek fractals having different fractal stages (s) in our present simulation. Therefore, the random segmental motion of different branches of the polymer molecules is manifested with the help of different parts of loop-less Vicsek fractal as shown in the figure-5.6

b. The prime objective of the entire simulation in this chapter is to investigate the impact of the size of host polymer molecules on the ionic motion. Therefore, the concept of the segmental motion of the polymer chain segments has been incorporated into the system in such a fashion that it will explicitly depend on the size of constituent polymer molecules.

c. The effect of temperature and other external parameters on the segmental motion has not been taken into account in our present study.

Considering the abovementioned points, the effect of segmental motion of the polymer chain segments is incorporated in our simulation mathematically. We have already come across that trapping of ions results in the slowing down of ionic motion inside the polymer molecules and its effect increases with the increase in molecular size. Therefore, incorporation of the segmental motion produces the opposite impact i.e. it facilitates ionic motion with the help of the incessant thermal waving motion of the free branches of polymer molecules keeping its center fixed which is shown in the figure-5.5 and 5.6. Polymer molecules with long branches experience waving motion up to a higher extent generating a stronger segmental motion and therefore facilitating the ion, trapped inside the molecule, to move faster. Many researchers, in their prior articles[70,71], have used exponential functions of time (t) and fractal stage (s) of host polymer molecules to characterize the segmental motion. On the other hand, temperature-dependent ionic conductivity under the variable range hopping (VRH) mechanism is also expressed with the help of an exponential function[72,73]. Considering all these research facts, this type of waving motion of polymer chain segments have been incorporated into our simulation with the help of an exponential function which is denoted as:

$$\tau_2 \sim exp[-b.s^c] \tag{5.9}$$

Where, $\tau_2(s)$ signifies the factor associated with the total time of travel and it represents the

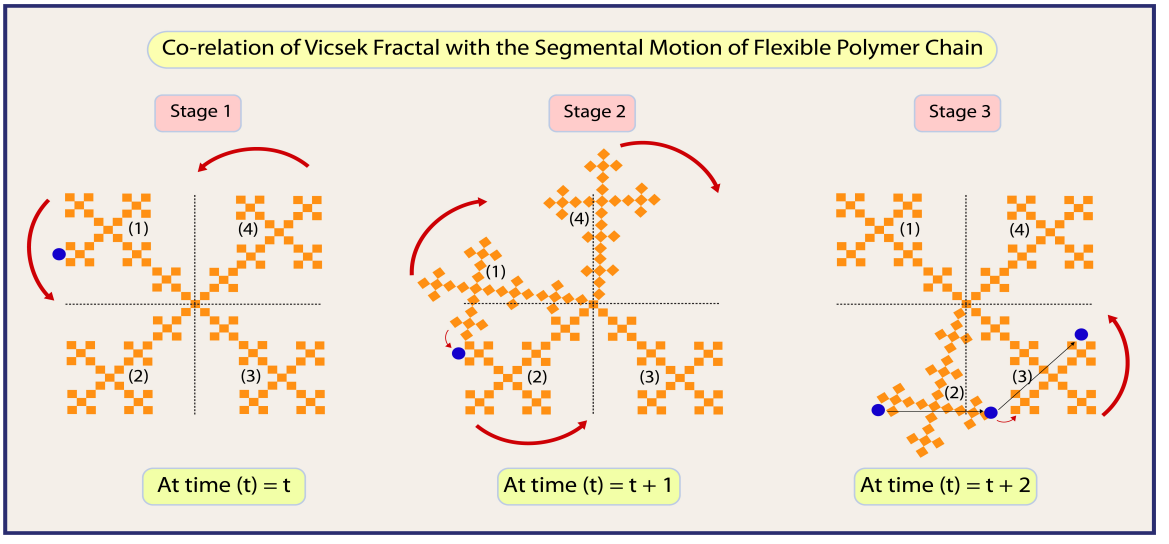

Figure 5.6: *Implementation of the concept of segmental motion on Vicsek fractal.* 3rd *stage Vicsek fractal has been taken into account and the segmental motion of the polymer chain segments are represented by the motion of four arms-(1), (2), (3), and (4) of the Vicsek fractal. Initially, the four arms are placed at their respective position at time=t as shown in stage-1. The ion (indicated by the blue ball), under consideration, is associated with the arm-(1). The arm-1 changes its position at the time=(t+1) due to the segmental motion and comes closer to the arm-2. The ion which is associated with arm-1 is eventually moved to arm-2 as shown in the stage-2. The arm-4 also changes its position in this stage. In stage-3, arm-1 and arm-4 return to their previous location whereas arm-2 comes closer to arm-3. As a result, the ion moves from arm-2 to arm-3.*

effect of segmental or waving motion of polymer chains. b and c are two fitting parameters and s corresponds to the stage of the fractal molecules. The nature of $\tau_2(s)$ happens to be highly sensitive to the two constant terms b and c. The prime objective of the present simulation study is to focus on the nature of conductivity variation due to external gamma irradiation. Therefore, a wise selection of the numerical values of b and c helps to serve our purpose. Typical values for b and c are chosen as 9.0 and 0.4 respectively for our present simulation.

The empirical formula suggests that $\tau_2(s)$ is highly sensitive towards the selection of c rather than b. A small change in c within the range of $\pm$ 0.01 keeping the value of b constant, may change both the magnitude and the nature of the conductivity curve. On the other hand, variation of b in the range $9.6 \geq b \geq 8.4$ (± 0.6) keeping c constant, does not produce any significant impact on the conductivity variation curve, only its magnitude is

shifted slightly. The variation of $\tau_2(s)$ with respect to the fractal stage (s) has been shown in

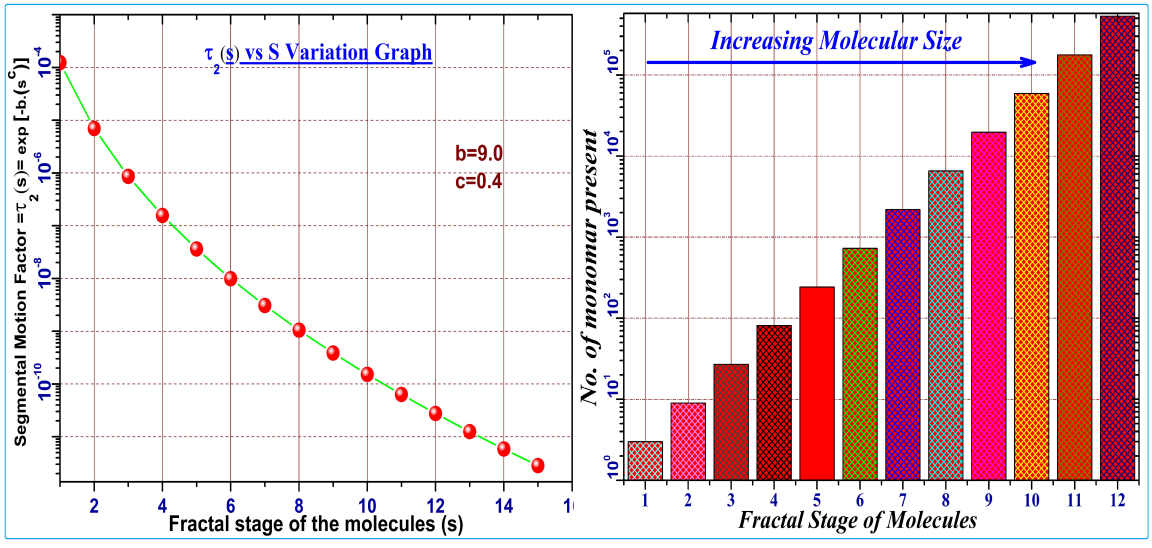

Figure 5.7: *(A)Variation $\tau_2(s)$ of the individual molecules with their respective fractal stages. $\tau_2(s)$ is plotted along Y-axis in log scale. As the size of the molecule i.e. its fractal stage (s) increases, the magnitude of $\tau_2(s)$ decreases very rapidly. The values of the fitting parameters b and c are taken as 9.0 and 0.4 respectively. (B) Variation in the number of monomers M(s) of the Vicsek fractals with their fractal stages.*

the figure-5.7. The Y-axis is taken in log scale as $\tau_2(s)$ varies within a large range. A gradual reduction of $\tau_2(s)$ can be noticed in figure-5.7 with the increase in (s) resulting in a non-linear exponentially decaying curve. This phenomenon suggests the faster-waving motion of the polymer branches with the increment in (s). It should be noted that trapping time $\tau_1(s)$ has a dimension of time whereas the segmental relaxation factor $\tau_2(s)$ is a dimensionless quantity. Hence, $\tau_2(s)$ acts as a modification factor of the total time T(s) in our simulation which will be discussed elaborately in the preceding section.

5.5. Computer Simulation Framework to Study the Ionic Motion inside the Solid Polymer Electrolyte Sample

Trapping of ions inside the polymer molecules and segmental motion of the free polymer branches are two independent phenomena that occur simultaneously inside the polymer molecules and control the nature of the ionic motion explicitly as per our assumption. In the present simulation, ions are deemed to be trapped inside a polymer molecule (Vicsek fractal) at a certain stage (s) and the effect is characterized by the trapping time $\tau_1(s)$ as

discussed earlier. In the case of trapping, the ion is assumed to hop randomly into different accessible sites of the said molecule of an arbitrary fractal stage. At the same time, ionic motion is enhanced due to the random motion of the free branches of fractal molecules. This is characterized by the segmental relaxation factor $\tau_2(s)$. The total time that an ion spends inside a polymer molecule (Vicsek fractal) of the arbitrary stage (s) is the combined effect of these two factors, and can be expressed as:

$$T(s) = \tau_1(s).\tau_2(s) \tag{5.10}$$

Whenever an ion enters a molecule with an arbitrary fractal stage (s), it must stay for the time interval T(s) inside it, and then it enters its adjacent molecule immediately.
The ion inside the sample can move from one molecule to another in different ways. In our present simulation, we construct a one-dimensional array of polymer molecules using Vicsek fractals and consider inter-molecular biased ionic motion inside the host polymer sample along an arbitrary direction which is shown in the figure-5.1. and figure-5.10.

5.5.1. An Overall Analysis of the Variation in T(s) and $\frac{R(s)}{T(s)}$ for Different Fractal Stages

According to our assumptions, polymer molecules inside the SPE are modelled with Vicsek fractals of different fractal stages (s). We have also assumed that ion enters from one diagonal endpoint of each Vicsek fractal and then visits different accessible sites of the polymer molecule in random walk process and finally exit from the opposite diagonal end as shown in the figure-5.10. The ionic motion inside the polymer molecules is influenced by two factors: i. trapping of ion inside the polymer molecule $\tau_1(s)$. ii. The segmental motion of the polymer branches $\tau_2(s)$. The mathematical form of $\tau_1(s)$ and $\tau_2(s)$ are already expressed in equation-(5.8) and (5.9).Therefore, the total time of travel inside an arbitrary host polymer sample with the fractal stage (s) can be written as:

$$T(s) \quad = \quad \tau_1(s).\tau_2(s) = [3^s]^{d_w}.exp[-b.s^c] \tag{5.11}$$

It is very evident from the above-mentioned expression that the total time (T(s)) spent by an ion inside an arbitrary polymer molecule with fractal stage s happens to be the function of the fractal stage (s) of the molecule. Variation of T(s) with the fractal stage (s) is shown in the figure-5.8. Here, the Y-axis represents the magnitude of T(s). It is plotted in log scale as the range of variation of T(s) happens to be between sufficiently large (ranging

from the order of 10^{-3} to 10^{7}) scale. Figure-5.8 shows that the magnitude of T(s) increases very rapidly with the increase in fractal stage (s). Hence, the ion takes a significantly large amount of time to travel from one end to the diagonally opposite end of a molecule as the fractal stage i.e. the size of the said molecule is increased gradually. On the other hand,

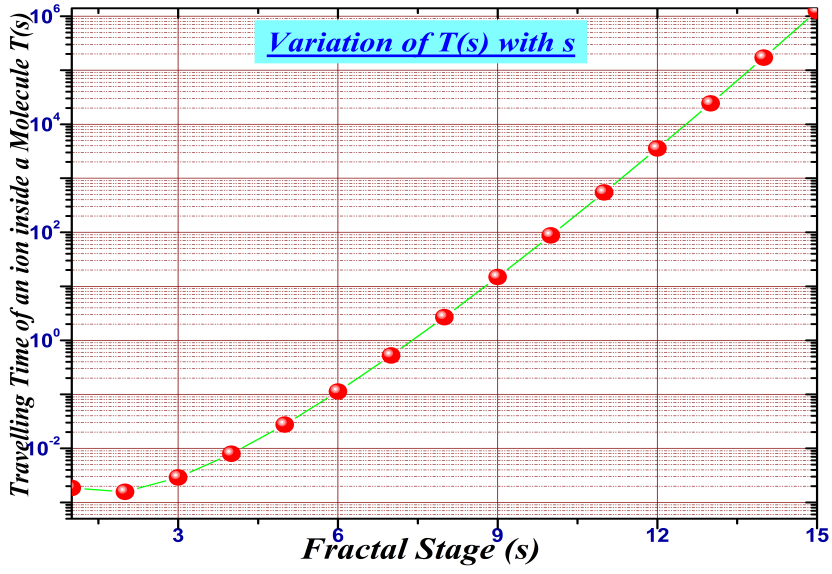

Figure 5.8: *Variation of the total traveling time T(s) of an ion inside an arbitrary fractal molecule with a fractal stage (s). The magnitude of T(s) is plotted along Y-axis and it is taken in log scale as its value increases very rapidly with the increase in fractal stage (s).*

the end-to-end diagonal distance of a molecule modelled by a Vicsek fractal with the fractal stage (s) can be expressed as:

$$R(s) = 3^s \tag{5.12}$$

Hence, the ratio between the end-to-end diagonal distance R(s) to the total time (T(s)) spent by an ion inside an arbitrary polymer molecule with the fractal stage (s) can be expressed as:

$$\begin{aligned} K(s) &= \frac{R(s)}{T(s)} \\ &= \frac{3^s}{[3^s]^{d_w}.exp[-b.s^c]} \end{aligned} \tag{5.13}$$

This expression suggests that the parameter K(s) also explicitly depends on the fractal stage of the respective molecule similar to T(s). The variations of K(s) inside individual molecules with fractal stage s are shown in the adjoining fig-5.9. The mathematical expression of K(s)

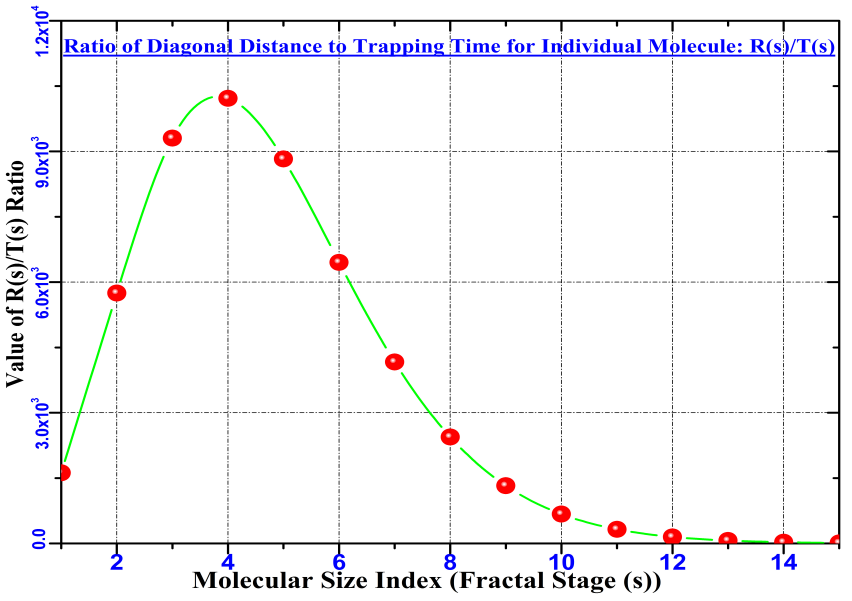

Figure 5.9: *Variation in [K(s)] i.e. the ratio of the diagonal distances R(s) of a fractal molecule to the total traveling time T(s) (* $\frac{R(s)}{T(s)}$ *) of an ion inside that polymer molecule, with its fractal stages (s). The curve shows a peak at s=4 indicating that the highest value of K(s) comes for the molecules with fractal stage s=4.*

clearly suggests that the fractal stage (s) i.e. the size of the respective molecule plays the key role to determine the magnitude of K(s) inside the individual polymer molecule as per our assumption. It is very evident from the figure-5.9 that the K(s) vs s curve attains its peak at s=4. Post which, the magnitude of K(s) decreases very fast with the increase of the value of (s). The said variation curve strongly suggests, the most significant contribution to the value of K(s) comes from the medium size polymer molecules that are modelled with 3rd, 4th and 5th stage Vicsek fractals. On the other hand, the magnitude of K(s) is reduced significantly either because the system contains a large number of molecules having a smaller value of fractal stage (s) or because it mostly contains bigger size molecules with the higher values of fractal stages (s).

5.5.2. Simulation of Inter-molecular Ionic Motion inside the Solid Polymer Electrolyte Sample

An extensive description regarding the arrangement of host polymer molecules has been given in chapter-3. Molecules are arranged side by side in a 2-dimensional plane and they are diagonally interconnected as shown in the figure-5.1 and figure-5.10. However, these

molecules are assigned randomly in the 2-D plane. This consideration provides us an independent selection of host polymer molecules but restricts their orientation along the direction of the ionic motion. As a result, we get a continuous unidirectional ionic motion through all polymer molecules that are present inside the sample at that irradiation time step (t) as shown in the figure-5.10.

Let us consider the direction of the ionic motion along the positive X-axis for our convenience. The motion of ion involves all the existing polymer molecules inside the host polymer sample at an arbitrary exposure time to irradiation. Let N(s,t) be the number of molecules (Vicsek fractals) with s^{th} fractal stage at an instant of irradiation time step= t. Hence we can write:

$$N(s,t) = P(s,t).N(t) \tag{5.14}$$

Where, P(s,t) is the probability of finding the sth stage molecule and N(t) is the total number of molecules present inside the polymer sample at the irradiation time step= (t). The ion starts from an initial position, called origin, and moves along positive X direction as shown in the figure-5.10. During its motion, the ion is assumed to enter inside a polymer molecule with an arbitrary fractal stage (s) and spend some time T(s) inside it. Post which it exits from the opposite diagonal end of the said molecule and enters into the next one. This process continues along the X-direction through all the existing molecules N(t) inside the sample at that irradiation time step=t.

Every time the ion enters inside a molecule (Vicsek fractal) of definite fractal stage = s, it spends the time T(s) inside it which is expressed in equation-(5.11). In the present simulation, the possibility of the test ion returning to the previous position has not been taken into account as per our assumption. Since the ion moves through all the molecules N(t), present inside the sample, the total traveling time of the respective ion inside the sample can be expressed as:

$$\begin{aligned} T_{total}(t) &= \Sigma_{s=1}^{s=n} P(s,t).N(t).T(s) \\ &= \Sigma_{s=1}^{n} P(s,t).N(t).[3^s]^{d_w}.exp[-b.s^c] \\ &= \Sigma_{s=1}^{n} N(s,t).[3^s]^{d_w}.exp[-b.s^c] \end{aligned} \tag{5.15}$$

This expression suggests that the total time of travel of an ion inside a polymer sample depends on the molecular distribution function=N(s,t) at that instant of time. When an ion travels through an arbitrary molecule, it has to travel the diagonal length of the said

molecule. Hence, total distance ($R_{total}(t)$) that an ion can travel through all molecules

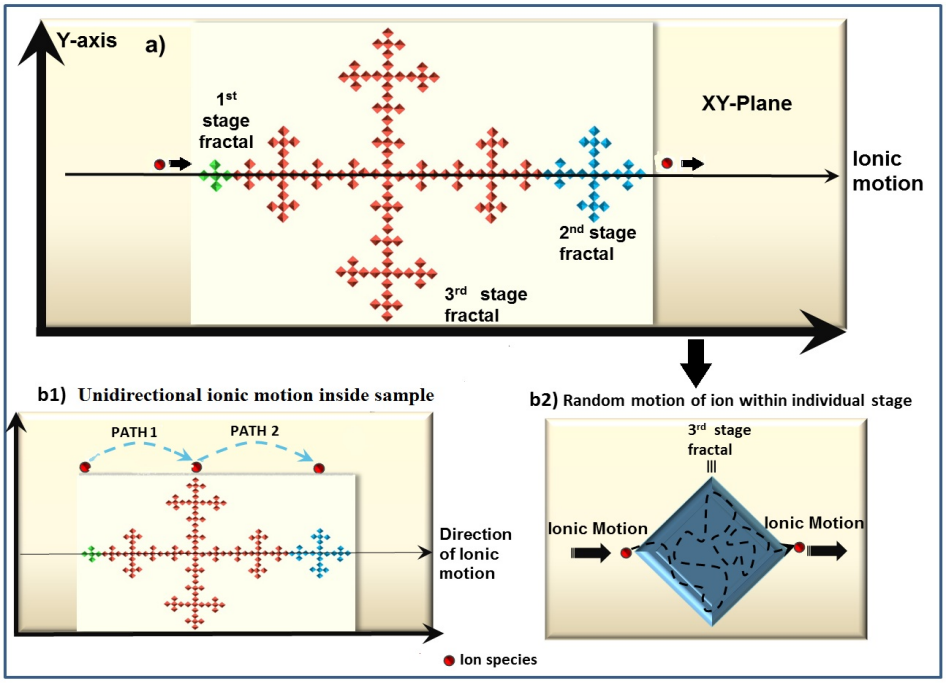

Figure 5.10: *(a) Unidirectional ionic motion through the linear array of polymer molecules modeled with Vicsek fractals of different stages. The fractals are arranged diagonally side by side in a random manner in the XY plane. (b) Unidirectional ion hopping from one molecule to another one from a macroscopic point of view. (c) Random motion of the ion inside the individual fractal molecule with arbitrary fractal stage.*

inside the polymer sample at the total time $T_{total}(t)$, will be:

$$\begin{aligned} R_{total}(t) &= \Sigma_{s=1}^{s=n} P(s,t).N(t).R(s) \\ &= \Sigma_{s=1}^{n} P(s,t).N(t).[3^s] \\ &= \Sigma_{s=1}^{n} N(s,t).[3^s] \end{aligned} \tag{5.16}$$

We consider that the ion exits from one molecule and enters into the next molecule immediately. Thus, the effective velocity of the ion can be estimated as:

$$\begin{aligned} V(t) &= \frac{R_{total}(t)}{T_{total}(t)} \\ &= \frac{\Sigma_{s=1}^{n} N(s,t).[3^s]}{\Sigma_{s=1}^{n} N(s,t).[3^s]^{d_w}.exp[-b.s^c]} \end{aligned} \tag{5.17}$$

Let us consider $\sigma(t)$ as the conductivity of the specimen ion at an instant of irradiation

dose t. Hence, we can write:

$$\sigma(t) = K_1.V(t) \tag{5.18}$$

$$= K_1.\frac{\Sigma_{s=1}^{n} N(s,t).[3^s]}{\Sigma_{s=1}^{n} N(s,t).[3^s]^{d_w}.exp[-b.s^c]} \tag{5.19}$$

It is very evident from the expression that the conductivity of the ion depends on three factors: i. The molecular distribution pattern at the instance of irradiation. ii. The resultant effect of trapping time of ion inside polymer molecules. iii. The effect of segmental motion of the polymer branches. As the time of exposure to irradiation increases, the distribution of polymer molecules inside the sample is also changed resulting in a variation in ionic conductivity which will be discussed in the preceding result section.

5.6. Result of the computer Simulation Study

The result of the computer simulation work has been segregated into two parts. In the first part, we will analyze the variation of ionic conductivity inside the mono-disperse polymer sample, and the same investigation has been performed on the poly-disperse polymer sample in the second part of this section. The change in the magnitude of ionic conductivity has been noted carefully for both the systems and a comparative analysis has been performed thereafter.

5.6.1. Variation in ionic conductivity in Case of Mono-disperse SPE Sample.

In the case of a mono-disperse polymer system, we have used an un-irradiated sample that contains 1000 molecules and each of them is modelled with 7th stage Vicsek fractal. The variation of ionic conductivity is investigated based on radiation-induced scission probability (scission percentage). The entire range of scission percentage variation has been segregated into four parts:

A. Variation in ionic conductivity in case of pure scission and pure cross-linking process.

B. Variation in ionic conductivity in scission process dominating region.

C. Variation in ionic conductivity in cross-linking process dominating region.

D. Variation in ionic conductivity in the case where scission and cross-linking processes occur with equal probabilities.

5.6.1.1. Variation in Ionic Conductivity in case of Pure Scission and Pure Cross-linking Process

As mentioned before, these two cases are completely idealized situations where all the molecules inside the system undergo either complete scission (in case of pure scission or 100 % scission) or complete cross-linking (in case of pure cross-linking or 100% cross-linking) process. We have already investigated the variation of molecular weight distribution and different types of molar mass averages due to the external gamma irradiation for pure scission and pure cross-linking processes in chapters 3 and 4 respectively. In the present subsection, we will investigate the variation in ionic conductivity $\sigma(t)$ in these two extreme cases.

Figure-5.11(A) shows the variation in ionic conductivity with respect to the irradiation time steps (t) whereas figure-5.11(B) represents the variation in N(s,t) at different time steps (t). The effect of the radiation-induced pure scission process on the molecular distribution pattern has already been discussed in the chapter-3. In the present case, we will study how this variation in molecular distribution affects the magnitude of ionic conductivity for two extreme cases (100% scission and 100% cross-linking processes). The $\sigma(t)$ vs t curve, represented by figure-5.11(A), shows a significant enhancement in ionic conductivity due to the application of external gamma irradiation. The magnitude of $\sigma(t)$ increases very fast from its un-irradiated value when the system is being exposed to the external gamma irradiation and attains a peek at the 3rd irradiation time step (t=3). Post which $\sigma(t)$ falls very rapidly as the exposure time to irradiation (t) is increased gradually.

It has been observed that the magnitude of $\sigma(t)$ is enhanced from its un-irradiated value $\sigma(t = 0) = 4166$ unit to a maximum value $\sigma(t = 3) = 10219$ unit at the 3rd time step due to the application of external irradiation. This enhancement happens to be nearly 2.5 times higher than its initial un-irradiated value. The adjoining figure-5.11(B) suggests that the system remains mono-disperse throughout the irradiation process and after the 6th time step (t=6), the whole system consists of a large number of molecules, smallest in size (fractal stage s=1). Post which the molecular distribution pattern of the system remains unaltered throughout the irradiation process. This phenomena directly influence the nature of $\sigma(t)$ vs t curve in figure-5.11(A). It can be seen clearly that the magnitude of $\sigma(t)$ attains its minimum value at 6th time step (t=6). Post which it remains invariant and becomes parallel to the time step(t) axis.

If we perform microscopic analysis regarding the ionic conductivity variation inside

the host polymer sample, we can conclude that $\sigma(t)$ variation with the external gamma irradiation is significantly influenced by the ion trapping effect and also by the effect of segmental motion of the polymer branches. The variation of trapping time ($\tau_1(s)$), segmental motion factor ($\tau_2(s)$) and the net time spent by an ion inside an arbitrary molecule T(s) with a fractal stage (s) can be estimated from figure-5.4, figure-5.7 and figure-5.8 respectively. We have already seen in equation-(5.15) that the total time of travel [$T_{total}(t)$] of an ion happens to explicitly depend on three factors:

i. Molecular distribution function (N(s,t)) at that time step (t).
ii. Trapping time ($\tau_1(s)$).
iii. Segmental motion factor ($\tau_2(s)$). We have come across the fact from figure-5.4 that

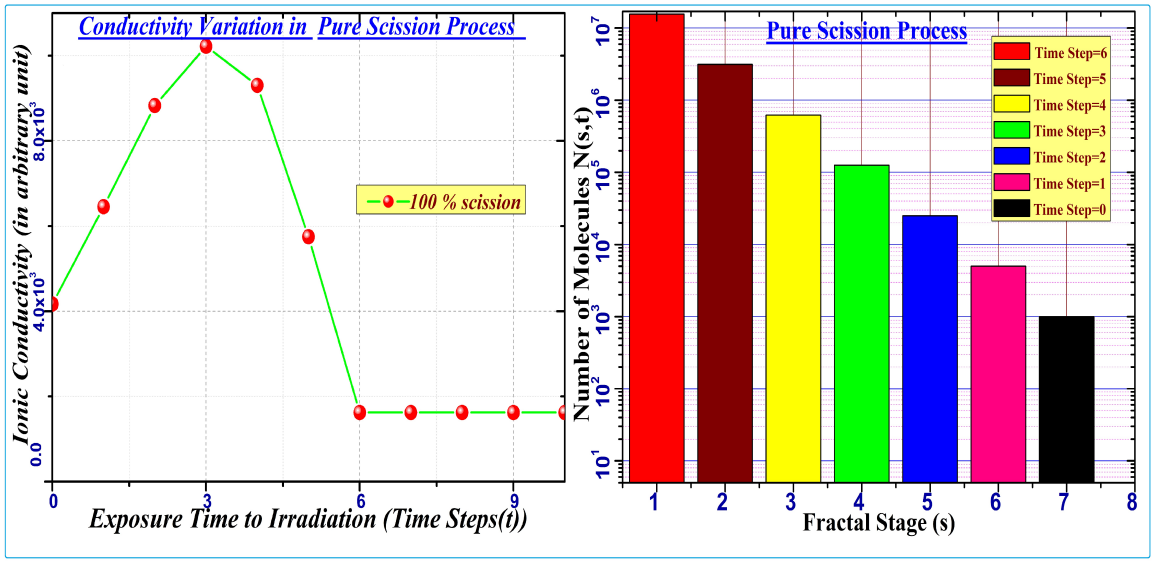

Figure 5.11: *(A) Variation in ionic conductivity $\sigma(t)$ with respect to the exposure time to irradiation or time step (t) in case of pure scission process (100% scission or 0% cross-linking). $\sigma(t)$ is plotted along Y-axis and time step (t) is along X-axis. The $\sigma(t)$ vs t curve has a peak at the 3rd time step. (B) Molecular distribution among different fractal stages (s) in different time steps (t). The system remains mono-disperse throughout the irradiation process.*

the value of ($\tau_1(s)$) decreases with the reduction of the molecular size and on the contrary, the factor ($\tau_2(s)$) increases with the decrease of the size (fractal stages (s)) of the respective molecules. Therefore, the trapping effect of ion ($\tau_1(s)$) inside a molecule has a significant impact on the ionic motion at the initial stage of irradiation where the mono-disperse system contains bigger size molecules. It has been noticed that the reduction rate

of ($\tau_1(s)$) with the fractal stage (s) happens to be higher than the rate of increase of the factor($\tau_2(s)$). Therefore, the overall effect of these two mutually opposite events which are mathematically expressed by the product of ($\tau_1(s)$) and ($\tau_2(s)$) (i.e. T(s) = ($\tau_1(s)$). ($\tau_2(s)$), is reduced gradually with the reduction of the fractal stage (s) and it can be noticed in the figure-5.8. This phenomenon is considered as the reason for the initial enhancement in ionic conductivity $\sigma(t)$ up to time step t=3 as shown in the figure-5.11(A). The molecular

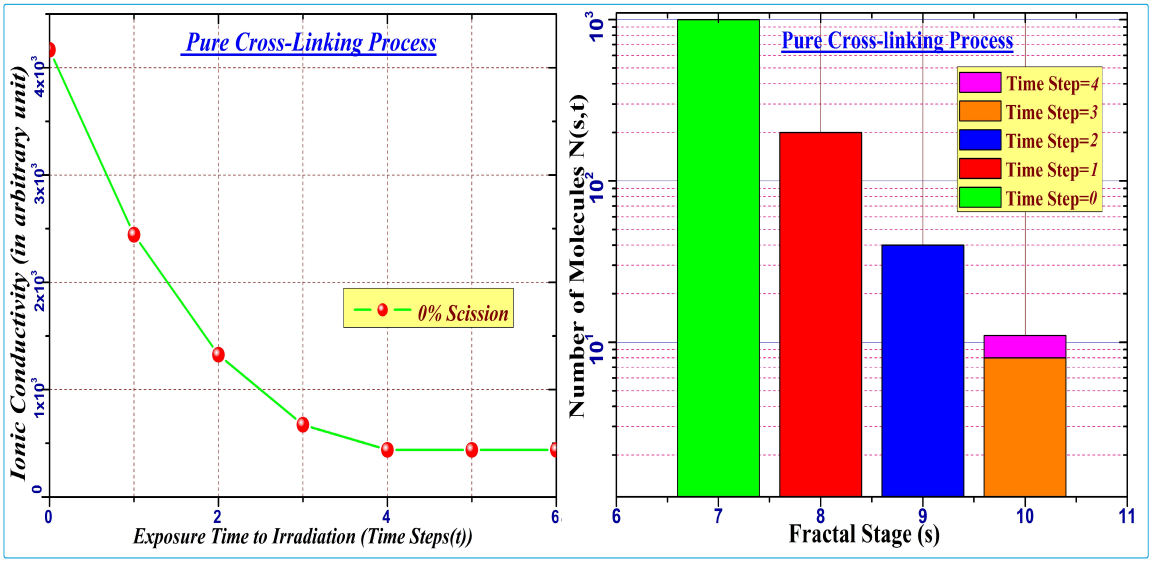

Figure 5.12: *(A) Variation in ionic conductivity ($\sigma(t)$) with the exposure time to irradiation or time step (t) in case of radiation-induced pure cross-linking (100% cross-linking or 0% scission) process. The $\sigma(t)$ vs t curve shows a gradual decrease in the rate of reduction and $\sigma(t)$ remains unchanged after time step t=4. (B) Molecular distribution in the polymer sample among different fractal stages (s) in different time steps (t).*

distribution pattern for the pure scission process in the figure-5.11(B) shows that the entire system contains molecules having fractal stage s=4 at irradiation time step t= 3. On the other hand, the K(s) vs s curve in figure-5.9 shows the maximum value of K(s) observed at s=4. Though K(s) does not have any explicit dependence on the ionic conductivity this phenomenon enables us to conclude that the highest contribution to the ionic conductivity comes from those molecules which are medium in size (especially molecules with fractal stage s=4). Therefore, the maximum ionic conductivity of the system is observed at the irradiation time step t=3 which is shown in figure-5.11(A). As the irradiation time step is increased beyond t=3, the magnitude of $\sigma(t)$ is decreased gradually and attends a minimum value at the 6th time step (t=6). In this region (i.e. where t>3), the trapping time ($\tau_1(s)$) continues to decrease, but the segmental motion factor ($\tau_1(s)$), as well as the value of N(s,t),

increases in a faster rate such a way that an overall enhancement can be seen in case of the total time of travel [$T_{total}(t)$] of the ionic species inside the sample. This phenomenon eventually decreases the magnitude of the ionic conductivity ($\sigma(t)$) of the polymer sample up to the time steps t= 6. Post which, all molecules inside the sample attain their smallest size (s=1) and do not undergo the scission process further. Hence, the conductivity attains the minimum value and remains unchanged throughout the irradiation process.

Figure-5.12(A) shows the response of ionic conductivity ($\sigma(t)$) to the external gamma irradiation in case of pure cross-linking process. Also, the variation of the molecular distribution in the case of the pure cross-linking process has also been shown in figure 5.12(B) for better understanding. We can easily notice from this figure, the system eventually contains 200 molecules at the time step t=1 having fractal stage s=8; 40 molecules at the time step t=2, each of which is represented by 9th stage Vicsek fractal, and 8 molecules at the time step t=3, with fractal stage s=10. Finally, the system contains 3 large size molecules made of 10th stage Vicsek fractal and the biggest size molecule having fractal stage s=11 at the time step t=4. The molecular distribution pattern remains invariant throughout the irradiation process after the time step t= 4. It can be observed clearly from the molecular distribution curve that pure cross-linking results in an increase in molecular size and a decrease in their numbers. This phenomenon eventually affects the overall conductivity of the host polymer system considerably.

We have already explained that the product of $\tau_1(s)$ and $\tau_2(s)$ is increased, and the net traveling time [$T_{total}(t)$] of an ion inside the host polymer sample at an arbitrary irradiation time step (t) is also enhanced due to the presence of bigger size of the molecules inside the sample at the initial stage of irradiation process. This phenomenon eventually bears a direct impact on the overall ionic conductivity and decreases its value with the passage of the exposure time to irradiation (time step=t). The rate of fall is faster at the initial stage of irradiation, and it is continued till the irradiation time step t=4. Post which, the conductivity attains its saturation value, and the $\sigma(t)$ vs t curve becomes parallel to the time step (t) axis as the molecular distribution does not change with t which can be seen in figure-5.12(A). This can reveal the fact that the bigger size molecules that are generated due to the intermolecular cross-linking process, basically hinder the ionic motion by generating a large network of long polymer chains inside the host polymer sample.

5.6.1.2. Variation in ionic conductivity in Case of Scission Process Dominating Region

In this sub-section, we will discuss the variation of ionic conductivity in those intermediate cases where the scission process plays the predominant role. Associated figure-5.13 shows four different conductivity ($\sigma(t)$) vs irradiation time step (t) curves for four different scission probabilities: 60%, 70%, 80% and 90% respectively up to the irradiation time steps t= 30. Each curve shows a peak at an arbitrary instance of irradiation time step (t). But the difference between these curves being their sharpness decreases with the reduction of their scission probabilities (an increase of cross-linking probability).

The sharpest ($\sigma(t)$) vs (t) curve is noticed in the case where the probability of scission is 90%. The magnitude of ionic conductivity $\sigma(t)$, in this case, increases from its un-irradiated value of 4166 unit to 8776 unit at the irradiation time step t= 3 resulting in a significant enhancement in $\sigma(t)$ of near about 2.1 times of its un-irradiated value. The magnitude of ($\sigma(t)$) falls very rapidly after the 3rd time step (t=3) and continues to fall up to the time step t=15. Post which, the reduction rate of $\sigma(t)$ is reduced significantly and finally it attains a minimum steady value around the irradiation time step t=25. The conductivity variation curves for other scission probabilities show similar trends provided the sharpness of those curves are reduced significantly and the position of the conductivity maxima shifted towards the region of higher irradiation time steps. We can notice from figure-5.13 that the conductivity variation curves in case of 80%, 70%, 60% scission process attain their respective peaks at the 6th, 11th, and 17th irradiation time steps respectively.

We have already discussed in the previous section that the mutual contribution of the trapping effect of ion inside the polymer molecules $\tau_1(s)$ and segmental motion of the polymer chain segments $\tau_2(s)$ produces the most significant impact on the ionic motion when the probability of finding molecules with fractal stages s=3,4,5 happens to be maximum inside the host SPE sample. In the case of 90% and 80% scission process, the rate of degradation of the bigger size molecules into smaller one happens to be very high and the system contains average-size molecules after the passage of few irradiation time steps. Thus, the conductivity $\sigma(t)$ vs time steps (t) curves attain their peaks at the value of irradiation time steps t= 3 and t=6 respectively. In the case of 60% and 70% scission process, the rate of degradation of bigger-sized molecules happens to be slower than that in case of 90% and 80% scission probabilities. Therefore, the probability of finding average-size molecules (having $3^{rd}, 4^{th}, 5^{th}$ fractal stages) is maximum at a comparatively higher value of time step

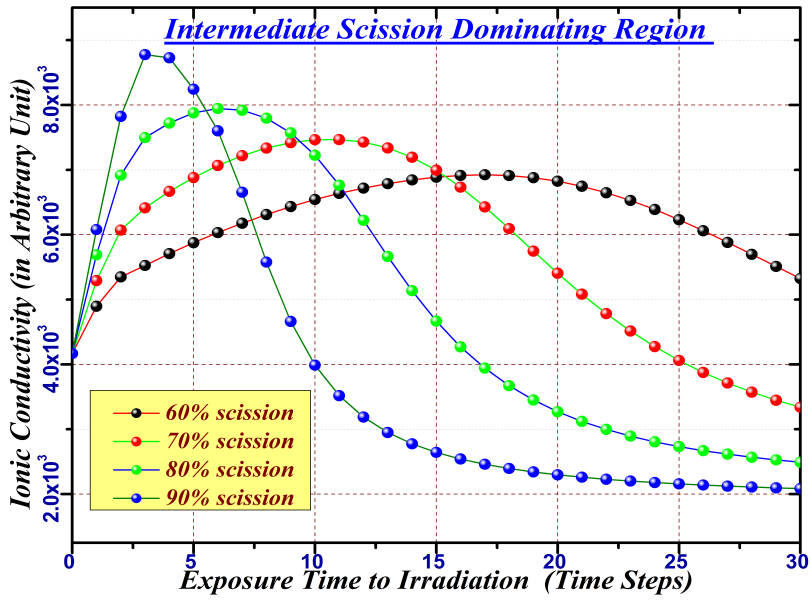

Figure 5.13: *Variation of ionic conductivity ($\sigma(t)$) with respect to the time step (t) in case of radiation-induced scission process domination region (ranging from 90% to 60% scission process). $\sigma(t)$ is plotted along Y-axis and time step (t) is along X-axis. All the $\sigma(t)$ vs t variation curves have definite peaks which indicate a significant enhancement in $\sigma(t)$. The height and sharpness of the peak in $\sigma(t)$ vs t curves reduces with the reduction in scission percentage.*

(t). As a consequence conductivity ($\sigma(t)$) vs time steps (t) curves attain their peaks at the irradiation time steps t=11 and 17 respectively which eventually justify the gradual shifting of ($\sigma(t)$) vs t curves towards the higher value of time steps (t) in case of scission dominating region. Though the rate of enhancement of $\sigma(t)$ is reduced with the decrease in the scission percentage, the occurrence of conductivity maxima could be explained by the predominance of segmental motion over the trapping effect. Further increase in irradiation time step (t) results in a significant reduction in the size of the molecules and therefore the contribution from the segmental motion becomes insignificant. This results in the gradual reduction of ionic conduction after achieving their respective maxima. Unlike in 100% scission, the conductivity maxima tends to get flatter and wider with lower magnitude in the case of 90% to 60% scission processes. In this context, it could be proposed that 90% to 60% scission involves the contribution of cross-linking in gradual increasing order which causes a reduction in the conductivity maxima but results in a higher magnitude of constant conductivity at the steady-state which is achieved at higher irradiation time steps as shown in figure-5.13.

5.6.1.3. Variation in ionic conductivity in Case of Cross-linking Process Dominating Region

In the present sub-section, we will discuss the variation in ionic conductivity in the case of the radiation-induced cross-linking dominating process. The trend of variation in ionic conductivity is significantly different from that in case of the scission dominating region. The entire discussion has been segregated into two parts. In the first part, we have investigated the trend of conductivity variation for those cases where scission probability varies from 30% to 45%. Whereas the second part deals with the conductivity variation for those cases where the probability of scission is below 30%(i.e. 10% as well as 20% scission).

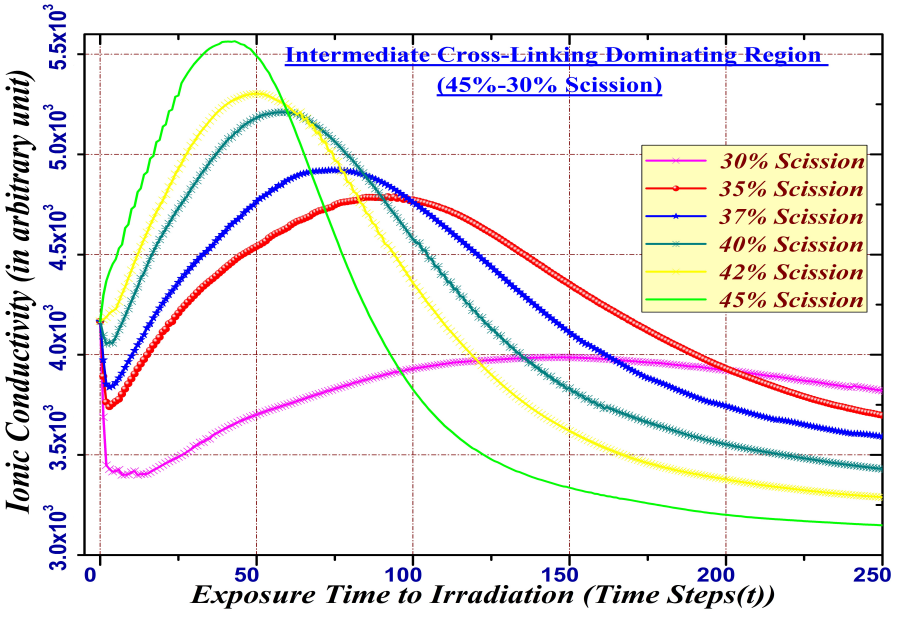

Figure 5.14: *Variation in ionic conductivity $\sigma(t)$ with the exposure time to irradiation or time step (t) in case of radiation-induced cross-linking process domination region. Total six $\sigma(t)$ vs t curves are shown indicating 30%,35%,37%,40%,42% and 45% scission probabilities respectively. $\sigma(t)$ vs t variation graphs have been plotted over a long duration of irradiation time steps (ranging from 0 to 250 units). Enhancement in $\sigma(t)$ is reduced significantly with the decrease in scission probability. An initial reduction in $\sigma(t)$ is observed in most of the curves.*

Figure-5.14 depicts the radiation-induced conductivity variation curves where scission probability varies from 30% to 45% scission processes. Unlike the scission dominating region, the variation in $\sigma(t)$ is comparatively slow in this case. The nature of ionic conductivity variation has been investigated up to the irradiation time step t=250. $\sigma(t)$ vs t

curve representing the 45% and 42% scission processes shows, a gradual enhancement in the magnitude of $\sigma(t)$ from the starting of the irradiation process and attains its peak value at a certain irradiation dose. Post which, they fall gradually and attain a steady state after the time step t=150 and t=200 respectively. The distinguishable feature that we have

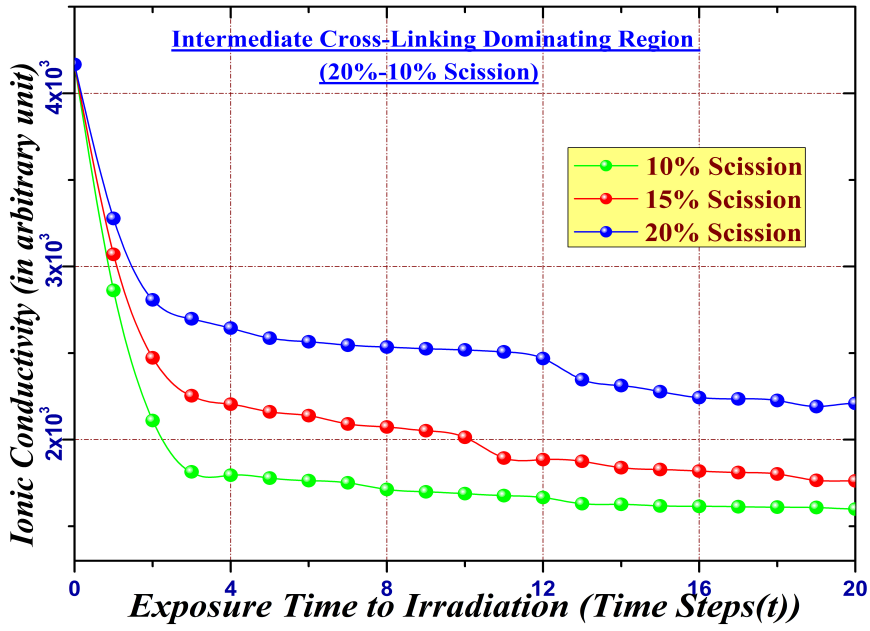

Figure 5.15: *Variation in ionic conductivity ($\sigma(t)$) to the exposure time to irradiation or time step (t) in the case of radiation-induced cross-linking process domination region. The rate of cross-linking is very high and a total of three $\sigma(t)$ vs t curves are shown here indicating 10%, 15%, and 20% scission probabilities respectively. Each $\sigma(t)$ vs t curve shows gradual decrease in behaviour and each of them achieves a steady-state value after t=20.*

noticed in the present case is that the magnitude of ionic conductivity falls very rapidly at the very beginning stage of the irradiation process. The magnitude of the conductivity minima at the initial stage of the irradiation process is enhanced gradually as the rate of the scission process is reduced which is shown in the figure-5.14. As per this trend, the initial conductivity minima has been noticed in case of the 40% scission process and the initial hinge-like shape of $\sigma(t)$ vs time step (t) curves gradually becomes more prominent in case of 37% and 35% scission processes respectively. Finally, the initial conductivity minima attain their highest magnitude in case of 30% scission process as shown in the figure-5.14.

In every case, the said conductivity minima are followed by a gradual enhancement in $\sigma(t)$ post which starts to decrease gradually. This trend can also be noticed in the same figure-5.14. The width of the $\sigma(t)$ vs time step (t) curves increases and their respective

peaks decreases with the reduction in the scission percentage. The initiation of irradiation in a monodisperse sample in a cross-linking dominating region results in the generation of bigger size molecules with higher probability.

As the scission process is reduced and the cross-linking increases, molecules bigger in size, are more likely to be found inside the sample resulting in the enhancement in the trapping effect along with the segmental motion of the polymer chains. Therefore, conductivity at the initial stage of irradiation (up to the 9th irradiation time step) gets reduced because of the simultaneous competiting effects among these two factors (i.e. trapping effect and segmental motion). This is considered as the prime reason for the generation of initial conductivity minimum in some $\sigma(t)$ vs t curves as observed in the figure-5.14. The ionic conductivity $\sigma(t)$ variation in case of 10%, 15%, and 20% scission probabilities depict a very different nature which has been shown in the figure-5.15.

In the case of the 20% scission process, the magnitude of ionic conductivity $\sigma(t)$ falls very rapidly within a few irradiation time steps (t).Post which it attains a minimum value and eventually shows a negligible variation throughout the irradiation process. Ionic conductivity $\sigma(t)$ variation in case of 10% and 15% scission process, has also been presented in figure-5.15. In these cases, a sharp fall in the magnitude of $\sigma(t)$ has been observed post which the $\sigma(t)$ attains its steady-state value. The magnitude of the initial conductivity minima in the case of 10% and 15% scission processes is much lower than that in case of 20% scission process.

We are aware from our previous discussions that the ionic conductivity increases significantly when the probability of finding the medium size molecules happens to be maximum. In the case of the 10% and 20% scission process, molecules are more likely to join with each other to produce bigger size molecules having higher values of the fractal stage. Hence there is very little possibility to find medium size molecules (with fractal stage s=3,4,5). Therefore ionic conductivity $\sigma(t)$ shows an ever decreasing behaviour at the initial stage of irradiation. The variation in molecular distribution curves are almost ceased in case of the higher value of time steps and therefore, $\sigma(t)$ attains its saturation value which is also the minimum value of $\sigma(t)$ for the corresponding scission percentage and can be observed clearly in the figure-5.15.

5.6.1.4. Variation in ionic conductivity in the Case where Scission and Cross-linking Processes Occur with Equal Probabilities

Variation of ionic conductivity $\sigma(t)$ with time step (t) for 50% scission probability is shown in this figure-5.16. In this case, the formation of bigger size molecules due to intermolecular

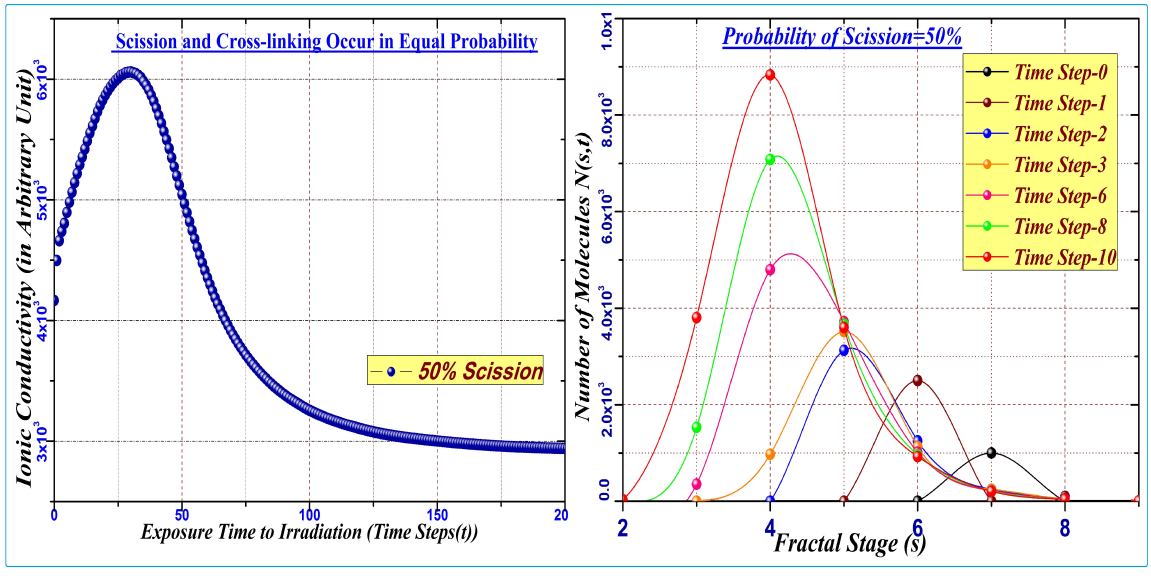

Figure 5.16: *(A) Variation of ionic conductivity $\sigma(t)$ with respect to the exposure time to irradiation or time step (t) in the case where scission and cross-linking processes occur with equal probabilities (50% scission and 50% cross-linking). $\sigma(t)$ is plotted along Y-axis and time step (t) is along X-axis. A peak curve is observed in this case and $\sigma(t)$ attains its minimum value after t= 150 units. (B) Distribution of the total number of molecules N(s,t) having fractal stage (s) at different irradiation time steps (t). The gradually diminishing peaks of the distribution curves shift towards the left side in the higher fractal stage region as the irradiation time steps increase gradually.*

cross-linking and production of smaller-sized molecules due to the scission process occur with equal probability inside the sample. The nature of molecular distribution (N(s,t) vs t variation curve) up to 10th irradiation time steps for 50% scission process has been presented in figure-5.16(B). It is very evident from this figure that the rate of the shift in distribution peak towards the lower fractal stage region is slow compared to the shift in the peaks of curves of the scission dominating region. The rate of segregation of molecules due to the radiation-induced intramolecular scission process is comparatively slower than the other cases in the scission dominating region. Therefore, the host polymer sample requires more time to be exposed to the external gamma irradiation so that the probability

of finding medium-size molecules (having fractal stage s=3, 4, 5) increases considerably and we can get the complete scenario of the ionic conductivity variation inside the host polymer sample. This happens to be the prime reason for considering the $\sigma(t)$ vs t variation curve to be investigated up to the irradiation time step t=200.

The adjoining figure-5.16 reveals the fact that the ionic conductivity inside the host polymer sample starts increasing steadily with the increase of irradiation time steps. The magnitude of $\sigma(t)$ achieves its maximum value at the 30th irradiation time step (t= 30). Post which, it starts to fall. The trend of the gradual reduction in the magnitude of $\sigma(t)$ continues up to the time step t=100. Post which this reduction rate is decreased significantly and the magnitude of $\sigma(t)$ attains its steady-state after the irradiation time step t= 150. The result of simulation ensures nearly 1.45 times enhancement in the magnitude of ionic conductivity in case of 50% scission process which happens to be smaller compared to those cases in scission dominating region and greater than those cases in cross-linking dominating region.

5.6.2. Conductivity Variation in Poly-disperse SPE Sample

We have discussed the variation in ionic conductivity inside an arbitrary mono-dispersed sample in the last subsection. In this present subsection, we will discuss the same things for a poly-disperse sample. The nature of the molecular distribution of the un-irradiated poly-disperse sample has been discussed in chapter-3. Here, we will investigate how the change in molecular distribution affects the ionic conductivity of a poly-disperse system. The entire investigation has been segregated into four subsequent parts.

A. Conductivity Variation in Case of Pure Scission and Pure Cross-linking process.
B. Conductivity Variation in Scission process Dominating Region.
C. Conductivity Variation in Cross-linking process Dominating Region.
D. Conductivity Variation in the case where Scission and Cross-linking processes occur with Equal Probability

5.6.2.1. Conductivity Variation in Case of Pure Scission and Pure Cross-linking processes

The response of ionic conductivity $\sigma(t)$ of a poly-disperse SPE sample to the external gamma irradiation in case of pure scission process (100% scission) has been shown in the figure-5.17.

In the previous case, the whole system remains mono-disperse throughout the irradiation process, only the fractal stages of the constituent molecules are decreased with the increase of the irradiation time steps (t). But in the present case (100% scission process for poly-disperse sample), the system remains poly-disperse from the beginning of the irradiation process. This phenomenon brings some significant differences in the nature of the ionic conductivity $\sigma(t)$ variation. Here, the un-irradiated sample consists of 500 molecules with fractal stage s= 5, 200 molecules with fractal stage s=6, and 20 molecules with fractal stage s=7 so that the weight fraction function ($W_f(s,t)$) values of the respective molecules shows a symmetric distribution pattern. When the poly-disperse system has been exposed to external irradiation, molecules undergo a complete scission process and produce a larger number of molecules with comparatively smaller values of the fractal stage (s). Here, the cross-linking process cannot be observed in any cases. Hence, the probability of finding molecules with the lower value of fractal stages increases very fast with the increase of irradiation time steps (t). Therefore, the range of distribution of molecules in different fractal stages is enhanced resulting in a gradual enhancement in the poly-dispersive nature of the sample and this phenomenon has been shown in the adjoining figure-5.17(B).

The weight fraction $W_f(s,t)$ vs the irradiation time steps (t) curves for pure scission process (shown in chapter-3) clearly shows the probability of finding molecules having fractal stage s=4 is significantly high at $3^{rd}, 4^{th}, and the 5^{th}$ irradiation time steps (t=3,4,5). This phenomenon provides a direct impact on the ionic conductivity $\sigma(t)$ variation curve. As per our assumption, ionic conductivity at an arbitrary irradiation time step (t) comes from the contribution of all molecules present inside the sample with all possible values of fractal stages (s). Therefore, when the external gamma irradiation is applied to the system, a gradual enhancement in ionic conductivity $\sigma(t)$ has been noticed and $\sigma(t)$ attains its maximum value at the time step t= 4. Post this, a steady and gradual decline in $\sigma(t)$ has been observed. The trend of gradual reduction of $\sigma(t)$ is continued up to the time step t=16. Post which, the magnitude of ionic conductivity of the poly-disperse system gradually attains a steady value as shown in the figure-5.17(A).

The adjoining figure-5.17(A) also suggests that the trend of conductivity variation in case of poly-disperse sample is more or less similar to that in the case of mono-disperse sample except for some significant differences in case of the conductivity enhancement, width of the $\sigma(t)$ vs t variation curve and the nature of the curve at the higher values of time steps (t), etc. In case of the pure scission process for a poly-disperse system, the magnitude of ionic conductivity is increased from 6637 units (in case of the un-irradiated sample) to 8748

units (at the 4th irradiation time step i.e. t=4) which happens to be nearly 1.32 times higher than its initial value. Whereas, this enhancement of $\sigma(t)$ is nearly 2.5 times in case of a mono-disperse sample. The variation of $\sigma(t)$, in case of a mono-disperse sample, is completed within the span of time step t=6. Post which, $\sigma(t)$ attains a constant value as shown in the fig-5.11(A). But in the present case, saturation value of $\sigma(t)$ is achieved by the system at a

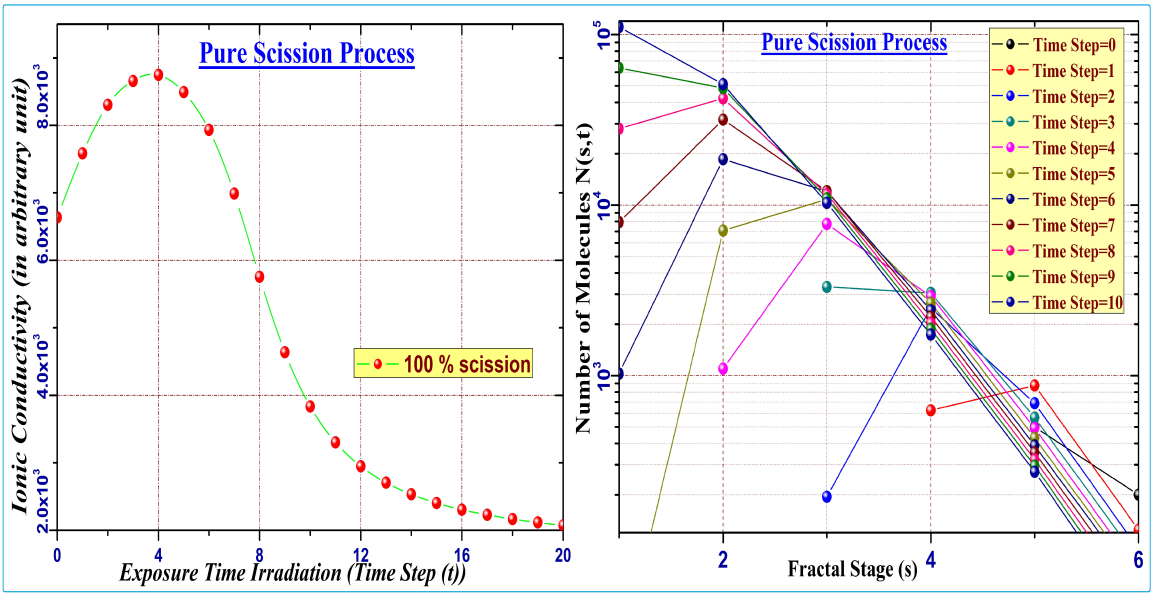

Figure 5.17: *(A) Variation of ionic conductivity ($\sigma(t)$) with respect to the exposure time to irradiation or time step (t) in case of radiation-induced pure scission process (100% scission or 0% cross-linking) for poly-disperse sample. The $\sigma(t)$ vs t curve has a peak at 4th time step. (B) Molecular distribution pattern of the polymer sample in different time steps. The number of molecules (N(s,t)) are plotted along Y-axis in log scale as N(s,t) increases very rapidly with the increase in (t).*

comparatively higher value of time steps (when the value of time step t is greater than 16) as the variation in the number of molecules (N(s,t)) with different fractal stages continues for the larger value of time steps (t). As a result, the sharpness of the conductivity variation curve is reduced considerably and the $\sigma(t)$.vs t curve stretches wider in the case of poly-disperse sample rather than the mono-disperse one which can be observed in figure-5.17(A). The magnitude of $\sigma(t)$ in the poly-disperse sample, is reduced from its initial un-irradiated value ($\sigma(0)$) after the time step t=7 and this reduction continues until $\sigma(t)$ attains a steady situation. This trend is similar to that of the mono-disperse case but in the present case, the reduction magnitude of $\sigma(t)$ is higher than that of the mono-disperse one. Moreover, the behaviour of the steady-state region of the $\sigma(t)$ vs t curve happens to be different in

both types of polymer samples which has been mentioned earlier. The opposite extreme

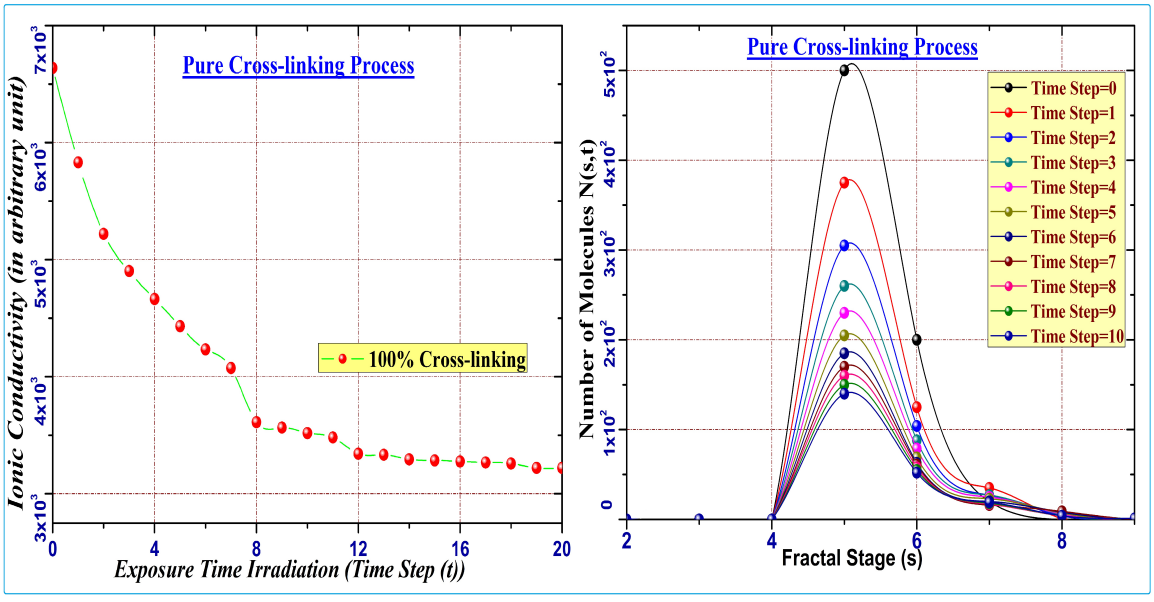

Figure 5.18: *(A) Variation of ionic conductivity ($\sigma(t)$) with respect to the exposure time to irradiation or time step (t) in case of radiation-induced pure cross-linking (100% cross-linking or 0% scission) process for poly-disperse sample. No conductivity enhancement is observed in this case. The rate of fall of $\sigma(t)$ with time step (t) is not so fast as in the case of the mono-disperse system. (B) Molecular distribution of the polymer sample in different time steps. The number of molecules (N(s,t)) are plotted along Y-axis in log scale and the fractal stages are taken along the X-axis. As the time step increases, the value of N(s,t) is reduced and the size of the molecules increases though the peak of the distribution curve remains at the same position.*

situation happens to be the pure cross-linking process where the probability of cross-linking is 100% and no scission process can be observed. Figure-5.18(A) shows the variation of ionic conductivity $\sigma(t)$ with the irradiation time steps (t) in this extreme case. Since the probability of scission is zero, all the molecules undergo the inter-molecular cross-linking process. Hence the size of the constituent molecules of the poly-disperse sample increases rapidly with the increase of irradiation time steps (t). As a result, the number of molecules (N(s,t)) with respective fractal stages (s) decreases. But eventually, the system remains poly-disperse in nature throughout the irradiation process. The variation of the number of molecules (N(s,t)) with different fractal stages (s) in different irradiation time steps have been shown in figure-5.18(B). It is very evident from the graph that the probability of finding bigger size molecules is increased very rapidly with the increase in irradiation time

steps (t). We have already mentioned in the previous section that ionic conductivity $\sigma(t)$ attains its maximum magnitude when the probability of finding medium-size molecules with intermediate fractal stages s=3,4,5 inside the SPE system happens to be maximum. Therefore, it is rarely possible in this case, to find polymer molecules with pre-mentioned fractal stages with the passage of the time steps (t). Hence, the enhancement in ionic conductivity $\sigma(t)$ cannot be expected. This phenomenon is also noticed in the adjoining conductivity variation curve, shown in figure-5.18(A).

In the present case, a rapid fall in the conductivity variation curve has been observed initially which is continued up to the time step t=8. Post which the rate of fall in ionic conductivity $\sigma(t)$ is reduced significantly and after the irradiation time step t=20, the magnitude of ionic conductivity $\sigma(t)$ attains its steady-state value. In case of the mono-disperse sample, the trend of the conductivity variation curve is familiar to the present case up to a certain limit. The reduction in $\sigma(t)$ for a mono-disperse case is spontaneous and rapid. The whole process of variation is completed within the irradiation time step t=4. Post which the magnitude of $\sigma(t)$ attains a steady-state value. But in the case of a poly-disperse sample, the same conductivity $\sigma(t)$ variation is not so fast. Moreover, the steady-state value of $\sigma(t)$ is achieved by the system around the irradiation time step t=20 and an abrupt reduction can be noticed at the time step t=7 and t=11.

5.6.2.2. Conductivity Variation in the Scission Process Dominating Region

The behaviour of ionic conductivity variation inside a mono-disperse sample in case of scission dominating region has already been discussed in the previous section. In this section, we will study the same variation for a poly-disperse SPE system. The nature of radiation-induced molecular distribution curves of a poly-disperse sample for some scission dominating cases (70% and 90% scission process) has already been analyzed in chapter-3. It is very evident from the figure-3.16(A) and figure-3.16(B), the peaks of the molecular distribution curves are shifted towards the left side with the increase in the irradiation time steps (t) which implies that bigger size molecules segregate into smaller ones and the probability of finding medium or small size molecules increases gradually with the increase in irradiation time steps.

After a few irradiation time steps (t= 5 to 10), the system is eventually equipped with molecules of intermediate sizes (s=3,4,5). Figure-3.16 also suggests that the rapidity in shifting of molecular distribution peaks towards the left side (lower fractal stage region)

increases as the probability of scission increases. But it should also be mentioned that the sharpness of molecular distribution peak is reduced and the rapidity of shifting the respective peaks becomes slower in present cases compared to those in case of the mono-disperse sample. This trend of variation in molecular distribution imposes a significant impact on the radiation-induced ionic conductivity variation curve that has been shown in figure-5.19. The magnitude of the radiation-induced ionic conductivity $\sigma(t)$ shows a

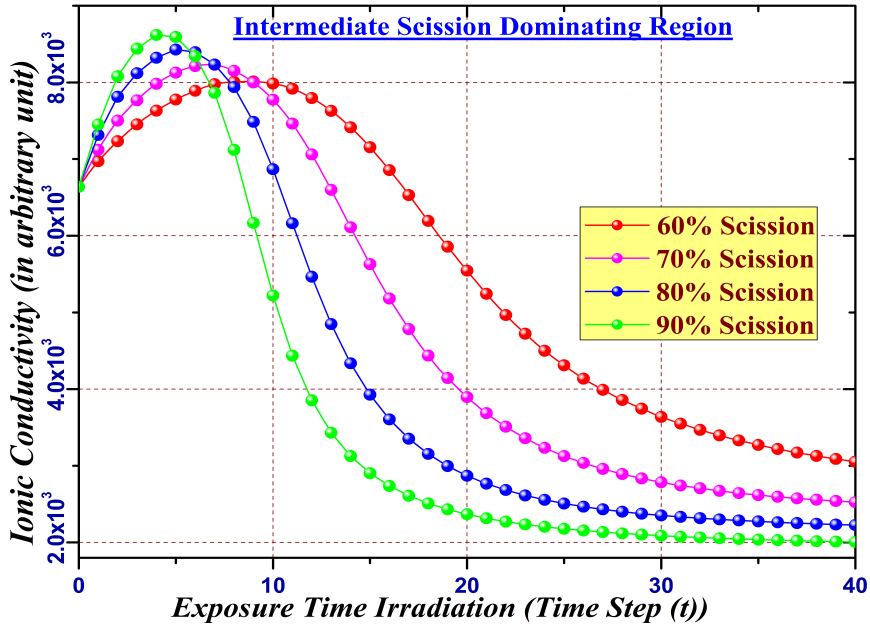

Figure 5.19: *Variation of ionic conductivity ($\sigma(t)$) with respect to the exposure time to irradiation or time step (t) in case of radiation-induced scission process dominating region ranging from 60% to 90% scission process for the poly-disperse SPE system. All the $\sigma(t)$ vs t variation curves have definite peaks showing definite enhancement in ionic conductivity $\sigma(t)$.*

spontaneous enhancement from the beginning of the irradiation process. In case of very high scission dominating region (e.g. when the probability of scission is 80% or 90%) the magnitude of $\sigma(t)$ increases very rapidly, and the maximum value is achieved around the $4^{th} and 5^{th}$ irradiation time steps respectively (t=4 and 5). Post which, it starts decreasing very fast. This trend of spontaneous fall of $\sigma(t)$ is continued up to the irradiation time step t=20 in these two cases. Post which the respective curves gradually attain their respective steady-state values. The magnitude of the peak of the $\sigma(t)$ vs t curve in case of the 90% scission process is greater than that of the 80% scission process.

It should be noted that the enhancement in ionic conductivity in case of 90% and 80%

scission processes is approximately 30% and 27% respectively compared to the conductivity observed in case of an un-irradiated sample. The sharpness of the peak also decreases with the decrease in the scission probability and eventually the curves start to become more flattened. This flattening nature can be observed more clearly in the $\sigma(t)$ vs t curves for the 70% and 60% scission processes. In the case of 70% scission probability, the magnitude of the radiation-induced ionic conductivity ($\sigma(t)$) starts increasing at a slow rate compared to the 80% and 90% scission processes. The $\sigma(t)$ vs t curve attains the maximum value around the 7th irradiation time step (t=7). Post which the curve shows a continuous reduction in magnitude and gradually attains its steady-state value after the irradiation time step t=30.

In case of the curve representing 60% scission process, the peak value takes place at the 9th irradiation time step (t=9) post which the magnitude of $\sigma(t)$ is reduced very slowly and gradually attains its saturation value after t=50. Figure-5.19 suggests that $\sigma(t)$ vs t curve for 60% scission probability happens to be the most flattened among the four curves. Moreover, its sharpness is also reduced compared to the other three curves (i.e. $\sigma(t)$ vs t curves for 70%, 80%, 90% cases). It should also be mentioned here that the enhancement of ionic conductivity in the case of 70% and 60% scission processes are approximately 24% and 21% respectively. The magnitude of the peak values of each $\sigma(t)$ vs t curve can be arranged according to the descending order as follows: $\sigma_{max}(90\%) > \sigma_{max}(80\%) > \sigma_{max}(70\%) > \sigma_{max}(60\%)$ which justifies the fact that the maximum value of $\sigma(t)$ decreases with the increase in scission probability.

The microscopic explanation of the ionic motion inside the host poly-disperse sample is similar to that of the mono-disperse sample. Here also, the segmental motion of the free polymer branches plays the predominant role compared to the trapping effect of ion when the value of $\sigma(t)$ increases with the enhancement in the time steps. The opposite phenomena occur i.e. the trapping effect plays the leading role when the $\sigma(t)$ vs t curve starts falling from its peak value. The major difference between the mono-disperse as well as poly-disperse sample is noticed in case of their molecular distribution pattern which acts as the prime factor to introduce the difference in the $\sigma(t)$ vs t curves between these two types of samples. Conductivity variation curves for intermediate scission dominating region in case of the mono-disperse sample show more or less similar kind of trend but the magnitude of the peak values of the respective curves are higher than that in case of the poly-disperse sample as shown in figure-5.19.

5.6.2.3. Conductivity Variation in Cross-linking Process Dominating Region

The present sub-section is aimed for a detailed analysis of the variation of ionic conductivity with external irradiation inside a poly-disperse sample for those cases where cross-linking process plays the major role (cross-linking dominating region). The entire study has been segregated into two parts same as we have done in case of a mono-disperse sample. The first part consists of the study of conductivity variation for certain cases of irradiation ranging from 30% to 45% scission process. In the second part, we have focused on discussion on the $\sigma(t)$ variation in case below 30% scission process (10% as well as 20% scission). It is very evident that the variation of $\sigma(t)$ in the present case happens to be very slow. Therefore, the entire simulation has been carried out for a long duration of irradiation time step of t=150 to understand the complete scenario of the $\sigma(t)$ vs t variation in this cross-linking dominating region. Ionic conductivity variation within the range of 30% to 45% scission

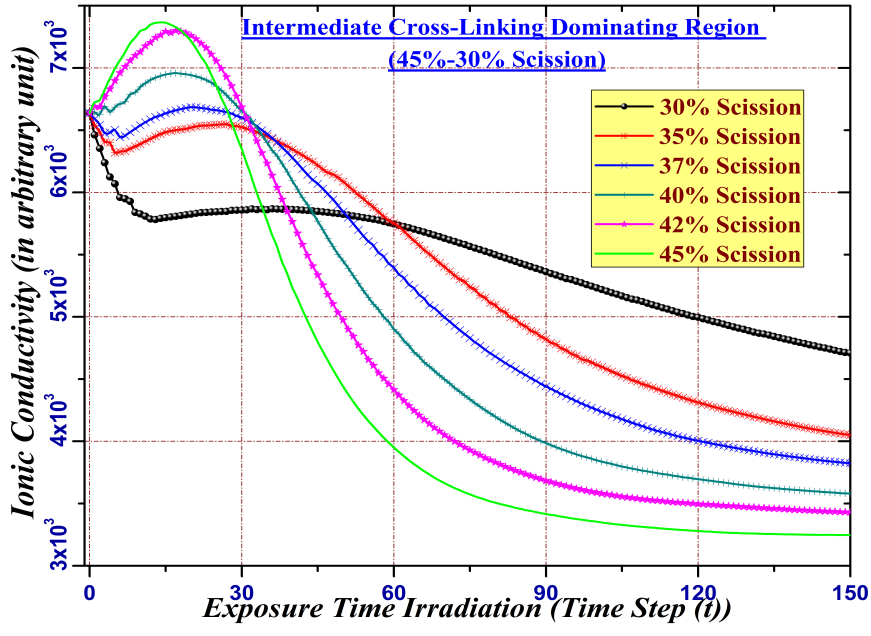

Figure 5.20: *Variation of ionic conductivity ($\sigma(t)$) with respect to the exposure time to irradiation or time step (t) in case of radiation-induced cross-linking process dominating region for the poly-disperse SPE system. Six $\sigma(t)$ vs t curves are shown here indicating 30%, 35%, 37%, 40%, 42% and 45% scission probabilities respectively. Enhancement in $\sigma(t)$ is reduced gradually with the decrease in scission percentage. The initial reduction in $\sigma(t)$ is not so intense as observed in the case of mono-disperse samples.*

process has been shown separately in figure-5.20. The figure contains six separate graphs

representing the variation of $\sigma(t)$ with time step (t) for different scission processes which are 45%, 42%, 40%, 37%, 35% and 30% respectively. The prime objective to study the $\sigma(t)$ variation curves within this region (30% to 45% scission) separately is to verify whether the initial conductivity minima which were noticed in the case of the mono-disperse sample, have also been observed here or not. We start our discussion with the analysis of the $\sigma(t)$ vs t curve for the 45% scission process. It shows a similar kind of trend as in the case of 60% scission, the only difference is that its peak value is reduced considerably and the width of the distribution curve is wide enough compared to that of 60% scission. The ionic conductivity of the sample starts increasing with the increase in irradiation time step (t) and attains its maximum value at time step t=17. Post which, a spontaneous fall in the magnitude of ionic conductivity $\sigma(t)$ has been observed up to the irradiation time steps t=100 which follow a steady state. No initial fall in the magnitude of $\sigma(t)$ has been noticed. This trend of initial conductivity minima has just appeared in the $\sigma(t)$ vs t curve for the 42% scission process.

After careful observation, one can notice a small tilting at the beginning of irradiation process. The rest part of the $\sigma(t)$ vs t curve depicts a similar kind of trend to the curve for the 45% scission process. The trend of formation initial conductivity minima is continued in the rest of the $\sigma(t)$ vs t curves. It can be observed clearly that the magnitude of the initial conductivity minima increases with the decrease in scission probability. Therefore, the highest initial conductivity minima are noticed in case of the 30% scission process at the 13th irradiation time step (t=13). The said conductivity minima are followed by a gradual enhancement in $\sigma(t)$ until it attains a maximum value at the irradiation time step t=34. Post which it falls slowly and gradually attains a steady-state value. The conductivity peaks of $\sigma(t)$ vs t curves show a general trend to shift towards the right at the higher time step region as the probability of scission decreases. This phenomenon can be observed in figure-5.20.

As the probability of scission decreases (percentage of crosslinking increases), the peak values of $\sigma(t)$ vs t curves are reduced gradually. Therefore, an overall reduction in the magnitude of ionic conductivity is observed in the case of $\sigma(t)$ vs t curves representing 45%, 42%, and 40% scission process. The rest of the curves (i.e. $\sigma(t)$ vs t curves for 37%, 35%, and 30% scission process) show gradually diminishing conductivity peaks but the magnitude of each peak is less than that of their respective un-irradiated values. It can also be noticed that the steady-state magnitudes of ionic conductivity of all these six $\sigma(t)$ vs t curves increase gradually with the decrease in scission percentage. Thus, the steady-state

value of $\sigma(t)$ for 45% scission is minimum and it is maximum in the case of the 30% scission process.

The nature of $\sigma(t)$ vs t curves for 20%,15%, and 10% scission process have been shown in figure-5.21 which depicts dfferent types of nature from that we have seen in figure-5.20. In case of $\sigma(t)$ variation for 20% scission probability, a gradual fall of $\sigma(t)$ is observed up to time step t=11. Post which, the magnitude of $\sigma(t)$ gradually attains a steady state value. Finally, $\sigma(t)$ vs t curve for 15% and 10% scission probability shows a rapid decrease in the magnitude of $\sigma(t)$ up to the time step t=15. Post which, the value of $\sigma(t)$ attains their respective steady states. The radiation-induced cross-linking process plays

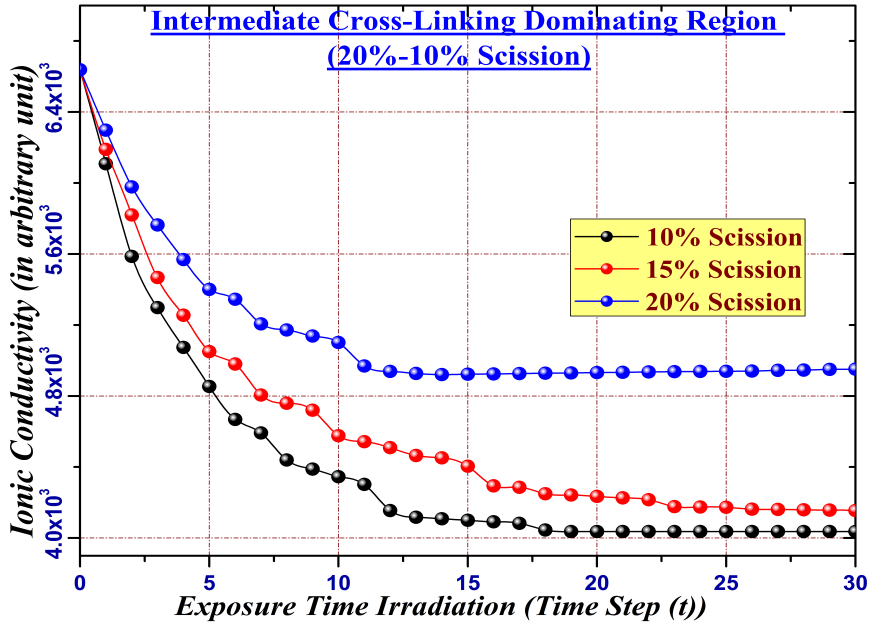

Figure 5.21: *Variation in ionic conductivity ($\sigma(t)$) with respect to the exposure time to irradiation or time step (t) for radiation-induced cross-linking process dominating region in case of a poly-disperse sample. A total of three $\sigma(t)$ vs t curves are shown indicating 10%, 15%, and 20% scission probabilities respectively. $\sigma(t)$ variation shows gradually decreasing curves and therefore no conductivity enhancement has been observed.*

the predominant role in case of the cross-linking dominating region. Therefore, the system is more likely equipped with bigger size molecules, where the trapping of ions inside the host polymer molecules gives a strong impact on the ionic conductivity $\sigma(t)$. Moreover, the probability of the presence of medium-sized molecules having fractal stages s=3,4,5 is either quite less or can be noticed after a long irradiation time step. As a result, in most cases, we can observe a gradual reduction in ionic conductivity $\sigma(t)$ which is shown in figure-5.21.

5.6.2.4. Conductivity Variation in the Case where Scission and Cross-linking Occur with Equal Probabilities

The ionic conductivity variation in the case of 50% scission process for a mono-disperse sample has already been discussed in the previous section. In this present sub-section, we will investigate the same thing for a poly-disperse sample. The variation in probability distribution function (PDF) of the molecules ($W_f(s,t)$ vs t curve) for different intervals of irradiation time steps (t) has been shown in the figure-5.22(B). It is very evident from the figure-5.22(B) that the probability of finding molecules with 3rd, 4th, and 5th fractal stages is gradually increased very slowly with the passage of irradiation time steps (t). Whereas, the probability of finding bigger size molecules having fractal stages 5th, 6th, and 7th are decreased with the increase of irradiation time step (t). We know, molecules which are

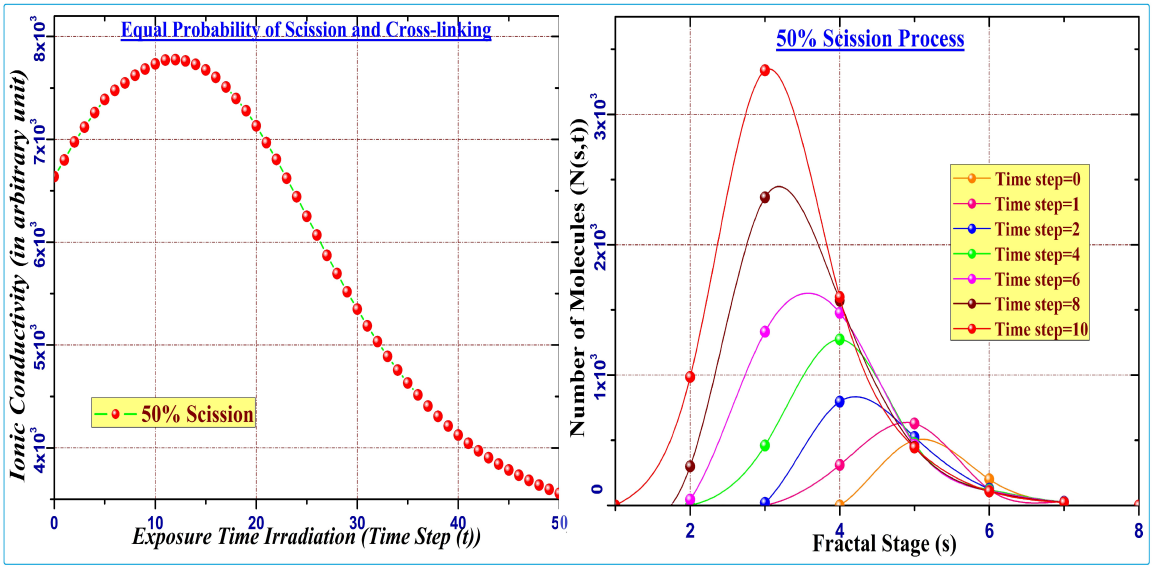

Figure 5.22: *Ionic conductivity ($\sigma(t)$) variation with irradiation time step (t) for the poly-disperse system in case where scission and the cross-linking processes occur with equal probabilities (50% scission and 50% cross-linking). $\sigma(t)$ vs t curve attains the peak at t=12 and this curve attains a steady-state value after t= 50 units which is much earlier than as compared to mono-disperse system. (B) The variation of the total number of molecules N(s,t) having different fractal stages with the irradiation time steps (t). The peak of the distribution curve shifts towards the left side in the higher fractal stage region as the irradiation time steps increase gradually.*

medium in size, (e.g. having fractal stages s=3, 4, and 5) provide a significant impact on the magnitude of ionic conductivity of the host polymer sample. Therefore, this trend of

variation in molecular distribution as shown in figure-5.22(B) eventually plays an important role in characterizing the ionic conductivity variation curve for 50% scission probability. The variation of ionic conductivity with the irradiation time steps (t) has been shown in figure-5.22(A) and it can be explained perfectly with the help of the radiation-induced molecular distribution variation of the host polymer sample. The magnitude of $\sigma(t)$ starts increasing from the beginning of the irradiation process and with the increase in time step (t), it eventually attains its maximum value at t=12. Post which, $\sigma(t)$ decreases spontaneously with the further increase of time step (t) up to t= 40. Finally, it attains its steady-state value after t=50.

Here, the trend of variation of $\sigma(t)$ with the irradiation time step (t) has some similarities with that in case of 60% and 40% scission probabilities. But in this case the maximum value of $\sigma(t)$ is greater than that of the 40% scission process and less than that of 60% scission process. Some additional differences can also be observed here, in comparison to the case for the mono-dispersive sample. In present case, the ionic conductivity enhances 1.17 times (approximately 17% enhancement of $\sigma(t)$) compared to its un-irradiated value which is smaller than the enhancement observed in the mono-disperse case. On the other hand, the steady-state value of $\sigma(t)$ is achieved in present case around t=50 as mentioned before and it is far earlier than in case of the mono-disperse sample where this steady-state value of $\sigma(t)$ can be observed around t= 150. Moreover, $\sigma(t)$ of the poly-disperse sample is reduced far below its un-irradiated value when it attains its steady-state and this phenomenon can be noticed clearly in figure-5.22(A). The steady-state magnitude of $\sigma(t)$ is reduced approximately 2.60 times from its maximum value. The sharpness of this peak is higher than that of the mono-disperse case.

5.6.3. Corroboration of Enhancement in Ionic Conductivity as an Effect of Radiation Induced Scission Process inside the SPE System.

So far we have investigated the variation of ionic conductivity with irradiation time steps for different scission percentages ranging from 0% to 100% scission process. It is very evident from our theoretical study that the trend of $\sigma(t)$ variation with t has some significant dissimilarities between the case of mono-disperse and poly-disperse sample. Despite many dissimilarities, the $\sigma(t)$ vs t variation curves for these two SPE systems manifests a common trend within the realm of 0% to 100% scission process: both of them show a conductivity peak (except those curves representing 0% to 20% scission) and these peaks shift towards the right side of higher irradiation time step region as the % of scission decreases. Another

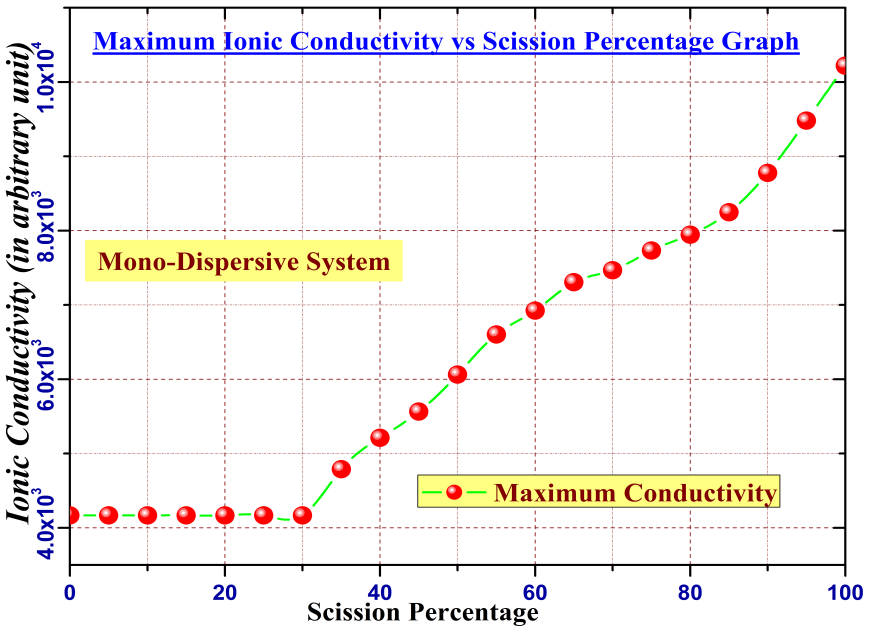

Figure 5.23: *Variation in maximum ionic conductivity $\sigma_{max}(G)$ as a function of scission probabilities (i.e. G) for the mono-disperse system. Maximum ionic conductivity $\sigma_{max}(G)$ is reduced with the reduction in scission probabilities and attains a steady-state value after the 30% scission process.*

significant characteristic that can be observed in both of the samples is that the magnitude of the ionic conductivity maxima ($\sigma_{max}(t)$) decreases gradually as the respective scission probability decreases inside the system. In this present section, we will study the variation of $\sigma_{max}(t)$ as a function of scission percentage. The said variation of $\sigma_{max}(t)$ for a mono-disperse system has been shown in the figure-5.23. The entire range of the scission process (ranging from 0% to 100% scission) has been segregated equally into 20 separate divisions having an interval of 5%. The magnitude of the maximum ionic conductivity $\sigma_{max}(t)$ has been evaluated for each scission percentage from the simulation process. Therefore, we get 20 different $\sigma_{max}(t)$ values for 20 separate scission percentages like 0%,5%,10%,15%,20% and so on up to 100% scission. These values of $\sigma_{max}(t)$ are plotted against the scission percentage which is shown in figure-5.23. The $\sigma_{max}(t)$ vs scission percentage curve remains constant and parallel to the x-axis starting from 0% to 30% scission. The magnitude of $\sigma_{max}(t)$ increases almost linearly with the further enhancement in scission percentage and this trend is continued up to the 60% scission process. This trend of linear enhancement of $\sigma_{max}(t)$ is broken after 60% scission and a gradual non-linear enhancement is noticed up to the 80% scission process post which the enhancement rate of $\sigma_{max}(t)$ becomes very high until scission percentage attains its maximum value i.e. 100%.

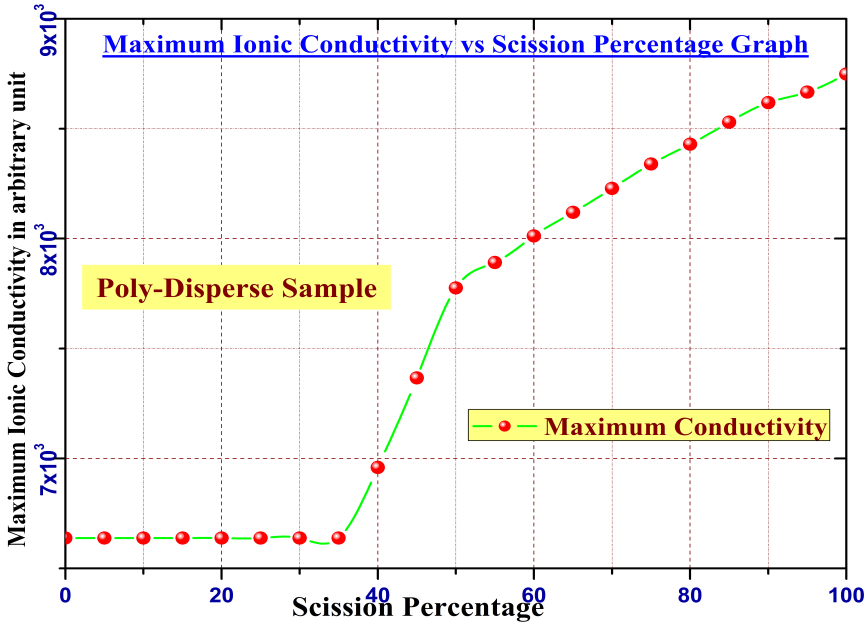

Figure 5.24: *Variation in maximum ionic conductivity i.e.* $\sigma_{max}(G)$ *as a function of scission probabilities for the poly-disperse system. Here also maximum ionic conductivity* $\sigma_{max}(G)$ *is reduced with the reduction in scission probabilities and attains a steady-state value after the 35% scission probability.*

The variation of $\sigma_{max}(t)$ with scission percentage in case of a poly-disperse SPE sample has been shown in figure-5.24. We can observe a similar trend of the $\sigma_{max}(t)$ enhancement with the increase in scission percentage. The entire $\sigma_{max}(t)$ variation curve can be segregated into three regions. The magnitude of $\sigma_{max}(t)$ remains constant in the first region which is continued up to the 35% scission process. No effective enhancement in $\sigma(t)$ can be noticed here because of the high rate of the cross-linking process. Therefore, $\sigma_{max}(t)$ happens to be the magnitude of $\sigma(t)$ of the un-irradiated sample. The magnitude of $\sigma_{max}(t)$ shows a fast linear enhancement after the 35% scission process and this trend is continued up to the 50% scission process. Post which the enhancement rate of $\sigma_{max}(t)$ is reduced considerably and the linear behavior of the $\sigma_{max}(t)$ variation has been maintained unlike the mono-disperse sample and this trend is continued until the highest limit of the scission percentage (100% scission) is achieved. The entire $\sigma_{max}(t)$ vs scission percentage curve, as shown in the figure-5.23 and figure-5.24, depicts the significant contribution of scission process on ionic conductivity of the SPE system.

5.7. Discussion Regarding the Outcome of the Simulation on the Basis of Different Experimentally Observed Facts

The prime objective of the simulation study in our present chapter is to investigate the response of ionic conductivity to externally applied gamma irradiation. The general observable trend in our simulation result happens to be the enhancement in ionic conductivity due to the application of external irradiation. The highest conductivity enhancement is observed in case of the pure scission process where the conductivity enhancement is nearly 2.5 times (from 4166 to 10219 unit) of its initial un-irradiated value in case of pure scission process for a mono-disperse sample and 1.32 times (from 6637 unit to 8748 unit) in case of a polydisperse sample. This phenomenon intimate that the radiation-induced scission process introduces some ambient morphological changes inside the host polymer sample that enhances the ionic conductivity σ. The simulation outcome has a satisfactory agreement with different experimental investigation works, performed by different researchers.[74–76]. Some experimental works were also performed previously by some of our group members that shows the application of gamma irradiation initiates an overall chain scission process with a very high probability that results in a considerable amount of enhancement in ionic conductivity and this phenomenon is in good agreement with our present simulation study[77,78].

The effect of segmental motion on ionic conductivity has been incorporated into the simulation with the help of a mathematical function termed as $\tau_2(s)$. It contains two fitting parameters named b and c. The numerical values of these parameters are chosen in such a way that it provides the optimum impact on the conductivity enhancement. It has been noticed that ionic conductivity happens to be highly sensitive to the values of b and c. A small change in the value of b and c results in a significant change in the ionic conductivity variation and in some cases this alteration may completely change the nature of the $\sigma(t)$ vs t variation curve in some cases.

Enhancement in ionic conductivity is observed due to the existence of an amorphous phase inside the polymer sample[79]. Researchers across the globe have adopted various physical (e.g. application of external irradiation)[74,77,78,80,81] as well as chemical (addition of salts, plasticizers, fillers etc.) techniques[82–88] that enhances the amorphous phase inside the sample by introducing polymer chain scission process. The present simulation study shows a general trend of enhancement in ionic conductivity with the increase in the radiation-induced scission process in both mono-disperse as well as poly-disperse samples.

Therefore, the observable trend in the present simulation outcome is in agreement with the experimentally observed results especially in those cases where the radiation-induced scission process plays the predominant role.

The conductivity variation curve for 30% and 40% scission processes in the cross-linking dominating region shows an initial sharp fall in case of both mono-disperse as well as poly-disperse samples. This trend of rapid reduction in ionic conductivity is followed by its gradual enhancement which has been shown in figure-5.14 and figure-5.20. An experimentally observed phenomenon that has been performed by our group previously[89] has also reported a similar kind of trend regarding the conductivity variation curve. Thus the present theoretical study validates well with such reported observation.

The present simulation study also involves some extreme cases where the probability of radiation-induced cross-linking process is significantly high (i.e. in the range of 100% to 80%). In other words, one can say the probability of the radiation-induced scission process happens to be very less (i.e. in between the range 0% to 20% scission). Ionic conductivity variation in these regions shows a sharp fall from the beginning of the irradiation process post which it attains saturation stage. This trend has been observed in both cases of mono-disperse as well as poly-disperse samples.

5.8. Conclusion

Application external gamma irradiation not only changes the structural properties of the host SPE, but also modifies the ion transportation properties inside the sample. In chapter-5 we have tried to estimate the variation in ionic conductivity due to external irradiation through computer simulation. The simulation studies were carried out for both mono-dispersive as well as poly-dispersive SPE samples. In each case, the outcome of the computer simulation is discussed in four different regions similar to other chapters.

In the present chapter, we have incorporated the effect of ion trapping inside the polymer molecules and the segmental motion of the polymer branches mathematically in the form of two functions τ_1 and τ_2 respectively. Our main objective was to study the effect of radiation-induced structural changes on the ionic motion. Thus, external gamma irradiation incorporates intramolecular scission and intermolecular cross-linking inside the host SPE and results in variation in the molecular size. As a result, ionic conductivity varies significantly. The entire simulation is formulated in such a way that the ionic conductivity

eventually turns out to be an explicit function of molecular size index (s).

We have noticed in chapter-5 that conductivity variation curves eventually attain their peak value when the probability of finding the medium size molecules inside the host SPE is maximum. Hence, we can say the fastest ionic movement can be observed inside those molecules which are medium in size. It is also evident from the simulation study that the enhancement in ionic conductivity is observed significantly in those cases where the radiation-induced scission process occurs inside the host SPE with greater probability. Therefore, one can conclude that enhancement in ionic conductivity is increased with the increase in probability of the intra-molecular scission process.

Maximum conductivity is observed in case of 100% scission process whereas, conductivity attains its minimum value at the pure cross-linking process (0% scission process). This trend is more or less the same for both mono-disperse and poly-disperse samples only the magnitude and width of the peaks of the respective curves changes depending on the system. Considering the strong analogy between the simulation outcome and different experimentally observed fact regatding the conductivity variation , we may infer that radiation-induced scission turns the system more ambient for ion conduction whereas cross-linking process eventually generates a large network of polymer chain segments and makes the environment adverse for ions to travel through the system that leads to a reduction in ionic conductivity.

Bibliography

[1] Aziz, S.B. and Abidin, Z.H.Z., 2015. Ion-transport study in nanocomposite solid polymer electrolytes based on chitosan: electrical and dielectric analysis. Journal of Applied Polymer Science, 132(15).

[2] Karmakar, A. and Ghosh, A., 2010. A comparison of ion transport in different polyethylene oxide–lithium salt composite electrolytes. Journal of Applied Physics, 107(10), p.104113.

[3] Croce, F., Curini, R., Martinelli, A., Persi, L., Ronci, F., Scrosati, B. and Caminiti, R., 1999. Physical and chemical properties of nanocomposite polymer electrolytes. The Journal of Physical Chemistry B, 103(48), pp.10632-10638.

[4] Berthier, C., Gorecki, W., Minier, M., Armand, M.B., Chabagno, J.M. and Rigaud, P., 1983. Microscopic investigation of ionic conductivity in alkali metal salts-poly (ethylene oxide) adducts. Solid State Ionics, 11(1), pp.91-95.

[5] Xi, J. and Tang, X., 2004. Nanocomposite polymer electrolyte based on Poly (ethylene oxide) and solid super acid for lithium polymer battery. Chemical Physics Letters, 393(1-3), pp.271-276.

[6] Ferloni P, Magistris A, Chilodelli G, Faucitano A, Buttafava A (1991) Effects of gammaradiation on polymer electrolytes: PEO and PEO20-LiC104. Radiat Phys Chem 37:615–621.

[7] Biswas A, Avasthi DK, Fink D, Kanzow J, Schürmann U, Ding SJ, Aktas OC, Saeed U, Zaporojtchenko V, Faupel F, Gupta R, Kumar N (2004) Nanoparticle architecture in carbonaceous matrix upon swift heavy ion irradiation of polymer-metal nanocomposites. Nucl Instrum Methods Phys Res Sect B 217(1):39–50

[8] Raghu S, Archana K, Sharanappa C, Ganesh S, Devendrappa H (2015) The physical and chemical properties of gamma ray irradiated polymer electrolyte films. J Non-Crystalline Solids 426:55–62.

[9] Costa, L.T., Sun, B., Jeschull, F. and Brandell, D., 2015. Polymer-ionic liquid ternary systems for Li-battery electrolytes: Molecular dynamics studies of LiTFSI in a EMIm-TFSI and PEO blend. The Journal of chemical physics, 143(2), p.024904.

[10] Maccallum, J.R., Smith, M.J. and Vincent, C.A., 1984. The effects of radiation-induced crosslinking on the conductance of LiClO4· PEO electrolytes. Solid State Ionics, 11(4), pp.307-312.

[11] Kronfli, E., Lovell, K.V., Hooper, A. and Neat, R.J., 1988. The conductivity behaviour of gamma-irradiated PEO-LiX electrolytes. I. British polymer journal, 20(3), pp.275-280.

[12] Perloni, P., Magistris, A., Chiodelli, G., Faucitano, A. and Buttafava, A., 1991. Effects of gamma-radiation on polymer electrolytes: PEO and PEO20-LiClO4. International Journal of Radiation Applications and Instrumentation. Part C. Radiation Physics and Chemistry, 37(4), pp.615-621.

[13] Wang, Y., Agapov, A.L., Fan, F., Hong, K., Yu, X., Mays, J. and Sokolov, A.P., 2012. Decoupling of ionic transport from segmental relaxation in polymer electrolytes. Physical review letters, 108(8), p.088303.

[14] Catlow, C.R.A. and Mills, G.E., 1995. Computer simulation of ionically conducting polymers. Electrochimica acta, 40(13-14), pp.2057-2062.

[15] Okamoto, Y. and Cho, M.D., 1996, March. Effects of gamma and electron beam irradiation on polymer electrolytes. In Macromolecular Symposia (Vol. 105, No. 1, pp. 75-83). Basel: Hüthig & Wepf Verlag.

[16] Bhattacharyya, A.J., Middya, T.R. and Tarafdar, S., 1998. A computer simulation study of ionic conductivity in polymer electrolytes. Pramana, 50(3), pp.205-212.

[17] Singh, T.J., Siddappa, K. and Bhat, S.V., 2004. Large enhancement of the ionic conductivity in an electron-beam-irradiated [poly (ethylene glycol)] xLiClO4 solid polymer electrolyte. Journal of Polymer Science Part B: Polymer Physics, 42(7), pp.1299-1311.

[18] Stolwijk, N.A. and Obeidi, S., 2004. Radiotracer diffusion and ionic conduction in a PEO-NaI polymer electrolyte. Physical review letters, 93(12), p.125901.

[19] Siekierski, M., Nadara, K. and Rzeszotarski, P., 2006. Conductivity simulation in composite polymeric electrolytes. Journal of New Materials for Electrochemical Systems, 9(4), p.375.

[20] Nikolic, V.M., Krkljes, A., Popovic, Z.K., Lausevic, Z.V. and Miljanic, S.S., 2007. On the use of gamma irradiation crosslinked PVA membranes in hydrogen fuel cells. Electrochemistry Communications, 9(11), pp.2661-2665.

[21] Cheang, P.L., Teo, L.L. and Lim, T.L., 2010, May. Modeling of ionic transport in solid polymer electrolytes. In IOP Conference Series: Materials Science and Engineering (Vol. 11, No. 1, p. 012003). IOP Publishing.

[22] Munn, R.W., Eilmes, A., Scarle, S. and Sterzel, M., 2009. Simulation of ion transport through poly (ethylene oxide) loaded with lithium perchlorate. Materials Science Poland, 27(3).

[23] Nanda, P., De, S.K., Manna, S., De, U. and Tarafdar, S., 2010. Effect of gamma irradiation on a polymer electrolyte: Variation in crystallinity, viscosity and ion-conductivity with dose. Nuclear Instruments and Methods in Physics Research Section B: beam Interactions with Materials and Atoms, 268(1), pp.73-78.

[24] Nanda, P., Maity, S., Pandey, N., Ray, R., Thakur, A.K. and Tarafdar, S., 2011. Conductivity enhancement in polymer electrolytes on gamma irradiation. Radiation Physics and Chemistry, 80(1), pp.22-27.

[25] Rahaman, M.H.A., Khandaker, M.U., Khan, Z.R., Kufian, M.Z., Noor, I.S.M. and Arof, A.K., 2014. Effect of gamma irradiation on poly (vinyledene difluoride)–lithium bis (oxalato) borate electrolyte. Physical Chemistry Chemical Physics, 16(23), pp.11527-11537.

[26] Joge, P., Kanchan, D.K., Sharma, P., Jayswal, M. and Awasthi, D.K., 2014, April. Conductivity enhancement in PVA-PEO-EC-$LiCF_3$ SO_3 blends upon swift heavy O^{7+} ion irradiation. In AIP Conference Proceedings (Vol. 1591, No. 1, pp. 756-758). American Institute of Physics.

[27] Raghu, S., Subramanya, K., Sharanappa, C., Mini, V., Archana, K., Sanjeev, G. and Devendrappa, H., 2014, April. The change in dielectric constant, AC conductivity and optical band gaps of polymer electrolyte film: Gamma irradiation. In AIP Conference Proceedings (Vol. 1591, No. 1, pp. 1272-1274). American Institute of Physics.

[28] Sunitha, V.R. and Radhakrishnan, S., 2020. Gamma irradiation effects on conductivity and dielectric behaviour of PEO-based nano-composite polymer electrolyte systems. Polymer Bulletin, 77(2), pp.655-670.

[29] Chen, X.C., Sacci, R.L., Osti, N.C., Tyagi, M., Wang, Y., Keum, J.K. and Dudney, N.J., 2020. Study of the segmental dynamics and ion transport of solid polymer electrolytes in the semi-crystalline state. Frontiers in Chemistry, 8.

[30] Dasgupta, R., Ballabh, T.K. and Tarafdar, S., 1994. Study of diffusion on a deterministic fractal. physica status solidi (b), 181(2), pp.313-320.

[31] Borodin, O. and Smith, G.D., 2006. Mechanism of ion transport in amorphous poly (ethylene oxide)/LiTFSI from molecular dynamics simulations. Macromolecules, 39(4), pp.1620-1629.

[32] Havlin, S. and Ben-Avraham, D., 1987. Diffusion in disordered media. Advances in physics, 36(6), pp.695-798.

[33] Havlin, S. and Ben-Avraham, D., 1983. Diffusion and fracton dimensionality on fractals and on percolation clusters. Journal of Physics A: Mathematical and General, 16(13), p.L483.

[34] Gefen, Y., Aharony, A. and Alexander, S., 1983. Anomalous diffusion on percolating clusters. Physical Review Letters, 50(1), p.77.

[35] Ben-Avraham, D. and Havlin, S., 2000. Diffusion and reactions in fractals and disordered systems. Cambridge university press.

[36] Havlin, S., 1984. Comment on the Aharony-Stauer conjecture. Physical Review Letters,53(17), p.1705.

[37] Dasgupta, R., Ballabh, T.K. and Tarafdar, S., 1994. Study of diffusion on a deterministic fractal. physica status solidi (b), 181(2), pp.313-320.

[38] Ghosal, S., Mukhopadhyay, M., Ray, R. and Tarafdar, S., 2014. Competitive scission and cross linking in a solid polymer electrolyte exposed to gamma irradiation: Simulation by a fractal model. Physica A: Statistical Mechanics and its Applications, 400, pp.139-150.

[39] MacCallum, J.R. and Vincent, C.A. eds., 1989. Polymer electrolyte reviews (Vol. 2). Springer Science and Business Media.

[40] Forsyth, M., Payne, V.A., Ratner, M.A., De Leeuw, S.W. and Shriver, D.F., 1992. Molecular dynamics simulations of highly concentrated salt solutions: Structural and transport effects in polymer electrolytes. Solid State Ionics, 53, pp.1011-1026.

[41] Anastasiadis, S.H., Karatasos, K., Vlachos, G., Manias, E. and Giannelis, E.P., 2000. Nanoscopic-confinement effects on local dynamics. Physical review letters, 84(5), p.915.

[42] Tanaka, K., Takahara, A. and Kajiyama, T., 2000. Rheological analysis of surface relaxation process of monodisperse polystyrene films. Macromolecules, 33(20), pp.7588-7593.

[43] Fukao, K. and Miyamoto, Y., 2000. Glass transitions and dynamics in thin polymer films: dielectric relaxation of thin films of polystyrene. Physical Review E, 61(2), p.1743.

[44] Dalnoki-Veress, K., Forrest, J.A., Murray, C., Gigault, C. and Dutcher, J.R., 2001. Molecular weight dependence of reductions in the glass transition temperature of thin, freely standing polymer films. Physical Review E, 63(3), p.031801.

[45] Kraus, J., Müller-Buschbaum, P., Kuhlmann, T., Schubert, D.W. and Stamm, M., 2000. Confinement effects on the chain conformation in thin polymer films. EPL (Europhysics Letters), 49(2), p.210.

[46] Murray, C.,Dutcher J.R.,McKenna G.B., Abstract in the 4th International Discussion Meeting on Relaxation in Complex Systems, June 17th-23rd 2001, Hersonissos,Crete, Greece.

[47] Prevosto, D., Capaccioli, S., Lucchesi, M., Rolla, P.A. and Ngai, K.L., 2009. Does the entropy and volume dependence of the structural α-relaxation originate from the Johari-Goldstein β-relaxation. Journal of non-crystalline solids, 355(10-12), pp.705-711.

[48] Jiang, B., Kasapis, S. and Kontogiorgos, V., 2011. Combined use of the free volume and coupling theories in the glass transition of polysaccharide ⁄ co-solute systems. Carbohydrate polymers, 83(2), pp.926-933.

[49] Colmenero, J., Arbe, A. and Alegria, A., 1993. Crossover from Debye to non-Debye dynamical behavior of the α relaxation observed by quasielastic neutron scattering in a glass-forming polymer. Physical review letters, 71(16), p.2603.

[50] Becker, O., Simon, G.P., Rieckmann, T., Forsythe, J., Rosu, R., Völker, S. and O shea, M., 2001. Dielectric relaxation spectroscopy of reactively blended amorphous poly

(ethylene terephthalate)-poly (ethylene naphthalate) films. Polymer, 42(5), pp.1921-1929.

[51] Ghosh, A., Naskar, A.K., Khastgir, D. and De, S.K., 2001. Dielectric properties of blends of silicone rubber and tetraflouroethylene ⁄ propylene ⁄ vinylidene fluoride terpolymer. Polymer, 42(24), pp.9849-9853.

[52] El Mohajir, B.E. and Heymans, N., 2001. Changes in structural and mechanical behaviour of PVDF with processing and thermomechanical treatments. 1. Change in structure. Polymer, 42(13), pp.5661-5667.

[53] Hilczer, B., Kułek, J., Markiewicz, E., Kosec, M. and Malic, B., 2002. Dielectric relaxation in ferroelectric PZT-PVDF nanocomposites. Journal of Non-Crystalline Solids, 305(1-3), pp.167-173.

[54] Mierzwa, M., Floudas, G., Dorgan, J., Knauss, D. and Wegner, J., 2002. Local and global dynamics of polylactides.: A dielectric spectroscopy study. Journal of non-crystalline solids, 307, pp.296-303.

[55] Roland, C.M. and Casalini, R., 2003. Temperature and volume effects on local segmental relaxation in poly (vinyl acetate). Macromolecules, 36(4), pp.1361-1367.

[56] Mano, J.F., Sencadas, V., Costa, A.M. and Lanceros-Méndez, S., 2004. Dynamic mechanical analysis and creep behaviour of β-PVDF films. Materials Science and Engineering: A, 370(1-2), pp.336-340.

[57] Casalini, R. and Roland, C.M., 2010. Effect of crosslinking on the secondary relaxation in polyvinylethylene. Journal of Polymer Science Part B: Polymer Physics, 48(5), pp.582-587.

[58] Moe, E., Qiu, X. and Ediger, M.D., 2000. 13C NMR study of segmental dynamics of atactic polypropylene melts. Macromolecules, 33(6), pp.2145-2152.

[59] Forte, C., Geppi, M., Malvaldi, M. and Mattoli, V., 2004. Dynamics of an amorphous polymer by an improved NMR approach based on the simultaneous analysis of 1H and 13C relaxation times. The Journal of Physical Chemistry B, 108(30), pp.10832-10837.

[60] Watanabe, H., Matsumiya, Y. and Inoue, T., 2003. Rheo-dielectrics in oligomeric and polymeric fluids: a review of recent findings. Journal of Physics: Condensed Matter, 15(11), p.S909.

[61] Capaccioli S, Prevosto D, Best A, Hanewald A, Pakula T (2007) Application of the rheo-dielectric technique. J Non-Cryst Solids 353:4267-4272.

[62] Mansfield, K.F. and Theodorou, D.N., 1991. Atomistic simulation of a glassy polymer/graphite interface. Macromolecules, 24(15), pp.4295-4309.

[63] Baschnagel, J. and Binder, K., 1995. On the influence of hard walls on structural properties in polymer glass simulation. Macromolecules, 28(20), pp.6808-6818.

[64] Baschnagel, J., Mischler, C. and Binder, K., 2000. Dynamics of confined polymer melts: Recent Monte Carlo simulation results. Le Journal de Physique IV, 10(PR7), pp.Pr7-9.

[65] Doruker, P. and Mattice, W.L., 1999. Mobility of the surface and interior of thin films composed of amorphous polyethylene. Macromolecules, 32(1), pp.194-198.

[66] Mischler, C., Baschnagel, J. and Binder, K., 2001. Polymer films in the normal-liquid and supercooled state: a review of recent Monte Carlo simulation results. Advances in Colloid and Interface Science, 94(1-3), pp.197-227.

[67] Mindemark, J., Lacey, M.J., Bowden, T. and Brandell, D., 2018. Beyond PEO—Alternative host materials for Li^+-conducting solid polymer electrolytes. Progress in Polymer Science, 81, pp.114-143.

[68] Ngai, K.S., Ramesh, S., Ramesh, K. and Juan, J.C., 2016. A review of polymer electrolytes: fundamental, approaches and applications. Ionics, 22(8), pp.1259-1279.

[69] Hallinan Jr, D.T. and Balsara, N.P., 2013. Polymer electrolytes. Annual review of materials research, 43, pp.503-525.

[70] Vogel, M., Herbers, C. and Koch, B., 2008. Effects of salt and nanoparticles on the segmental motion of poly (ethylene oxide) in its crystalline and amorphous phases: ^2H and ^7Li NMR studies. The Journal of Physical Chemistry B, 112(36), pp.11217-11226.

[71] Bahar, I., Erman, B., Fytas, G. and Steffen, W., 1994. Intramolecular contributions to stretched-exponential relaxation behavior in polymers. Macromolecules, 27(18), pp.5200-5205.

[72] Mott, N.F. and Davis, E.A., 2012. Electronic processes in non-crystalline materials. Oxford university press.

[73] Shklovskii I.and Efros A. L.,1979, Electronic Processes in Noncrystalline Materials Clarendon, Oxford,

[74] Damle, R., Kulkarni, P.N. and Bhat, S.V., 2009. The effect of composition, electron irradiation and quenching on ionic conductivity in a new solid polymer electrolyte:$(PEG)_xNH_4I$. Pramana, 72(3), pp.555-568.

[75] Maitra M., Verma KC, Sinha M., Kumar R., Middya TR, Tarafdar S, Sen P. Bandyopadhyay SK, De Udayan (2006) DSC characterization of ion beam modifications in ion conducting PEO–salt polymers. Nucl Instrum Methods Phys Res B 244:239–242.

[76] Sinha M, Goswami MM, Mal D, Middya TR, Tarafdar S, De U, Chaudhuri SK, Das D (2008) Effect of gamma irradiation on the polymer electrolyte $PEO - NH_4ClO_4$. Ionics 14:323–327.

[77] Nanda, P., De, S.K., Manna, S., De, U. and Tarafdar, S., 2010. Effect of gamma irradiation on a polymer electrolyte: Variation in crystallinity, viscosity and ion-conductivity with dose. Nuclear Instruments and Methods in Physics Research Section B: beam Interactions with Materials and Atoms, 268(1), pp.73-78.

[78] Nanda, P., Maity, S., Pandey, N., Ray, R., Thakur, A.K. and Tarafdar, S., 2011. Conductivity enhancement in polymer electrolytes on gamma irradiation. Radiation Physics and Chemistry, 80(1), pp.22-27.

[79] Ferry, A., Edman, L., Forsyth, M., MacFarlane, D.R. and Sun, J., 1999. Connectivity, ionic interactions, and migration in a fast-ion-conducting polymer-in-salt electrolyte based on poly (acrylonitrile) and $LiCF_3SO_3$. Journal of applied physics, 86(4), pp.2346-2348.

[80] Akhtar MS, Choi D-J, Lee S-K, Yang O-B (2010) Effect of electron beam irradiation on the electrochemical properties of heteropolyacid-polyethylene oxide composite electrolyte for dye-sensitized solar cell. Curr Appl Phys 10:S161–S164

[81] Raghu, S., Archana, K., Sharanappa, C., Ganesh, S. and Devendrappa, H., 2015. The physical and chemical properties of gamma ray irradiated polymer electrolyte films. Journal of Non-Crystalline Solids, 426, pp.55-62.

[82] Chung, S.H., Wang, Y., Persi, L., Croce, F., Greenbaum, S.G., Scrosati, B. and Plichta, E., 2001. Enhancement of ion transport in polymer electrolytes by addition of nanoscale inorganic oxides. Journal of power sources, 97, pp.644-648.

[83] Jiang, G., Maeda, S., Yang, H., Saito, Y., Tanase, S. and Sakai, T., 2005. All solid-state lithium-polymer battery using poly (urethane acrylate)/nano-SiO2 composite electrolytes. Journal of power sources, 141(1), pp.143-148.

[84] Rajendran, S., Sivakumar, P. and Babu, R.S., 2007. Studies on the salt concentration of a PVdFPVC based polymer blend electrolyte. Journal of power sources, 164(2), pp.815-821.

[85] Seanor, D.A. ed., 2013. Electrical properties of polymers. Elsevier.

[86] Zhao, B., Lu, X., Wang, Q., Yang, J., Zhao, J. and Zhou, H., 2020. Enhancing the ionic conductivity in a composite polymer electrolyte with ceramic nanoparticles anchored to charged polymer brushes. Chinese Chemical Letters, 31(3), pp.831-835.

[87] Sathyanathan, T. and Pugazhendhi Sugumaran, C., 2020. Enhancement of Ionic Conductivity and Dielectric Permittivity for PMMA-Based Polymer Electrolyte with BaTiO3 NanoFiller. International Journal of Nanoscience, 19(05), p.1950035.

[88] Arunkumar, R., Babu, R.S., Rani, M.U. and Rajendran, S., 2017. Influence of plasticizer on ionic conductivity of PVC-PBMA polymer electrolytes. Ionics, 23(11), pp.3097-3109.

[89] Nanda, P., De, S.K., Manna, S., De, U. and Tarafdar, S., 2010. Effect of gamma irradiation on a polymer electrolyte: Variation in crystallinity, viscosity and ion-conductivity with dose. Nuclear Instruments and Methods in Physics Research Section B: beam Interactions with Materials and Atoms, 268(1), pp.73-78.

Summary and Future Direction of Research Work

Summary and Future Direction of Research Work

5.8. Summary

We have investigated the effect of external gamma irradiation on both mono-disperse and poly-disperse solid polymer electrolyte (SPE) sample theoretically with the help of computer simulation. The deterministic Vicsek fractal has been used as a mathematical tool to model the host polymer sample. Effect of gamma irradiation on the SPE has been investigated focusing on the two radiation induced simultaneous and mutually opposite processes: scission and cross-linking. The incorporation of these two process into our simulation has been done with the help of the external parameters G and (1-G) respectively where G varies from 0.0 to 1.0. The sample was considered as the 1-D array of vicsek fractal which is configured by joining those fractals diagonally side by side. The un-irradiated mono-disperse sample was constructed with the help of 7th stage Vicsek fractal whereas 5th , 6th and 7th stage fractals has been used to configure the poly-disperse sample. In spite of some inherent artificiality, deterministic Vicsek fractal can be used successfully as a mathematical tool for the modelling of the host polymer system. The variation in molecular distribution pattern has been investigated with the help of a new parameter called weight fraction $W_f(s,t)$. It has been observed that the radiation induced scission dominating process results in the degradation of bigger size molecules into large number of smaller one which results in shifting of the $W_f(s,t)$ distribution peak towards the lower molecular weight region. On the other hand, crosslinking dominating process generate bigger size molecules which eventually shifts the $W_f(s,t)$ distribution peak towards the higher molecular weight region.

The radiation induced structural change also introduce significant variation in different molar mass averages. Four types of molar mass averages have been taken into account:

Viscosity average molecular weight $\langle M_v \rangle$, number average molecular weight $\langle M_n \rangle$, weight average molecular weight $\langle M_w \rangle$, Z- average molecular weight $\langle M_z \rangle$. Variation in these molar mass averages as a result of external gamma irradiation have been investigated in both scission and cross-linking dominating region for mono-disperse and poly-disperse samples.

The change in molecular distribution due to gamma irradiation has also provide a significant impact on the ionic motion which has also been discussed in the present thesis. The ionic motion has been characterized by two structural effects: trapping of ion inside the polymer molecules and segmental motion of the polymer chain segments. These two effects has been incorporated into the simulation with the help of two mathematical functions $\tau_1(s)$ and $\tau_2(s)$. Conductivity $\sigma(t)$ variation due to gamma irradiation has been studied in both scission and cross-linking dominating region for different scission probabilities for mono-disperse and poly-disperse systems. A substantial increment in ionic conductivity has been noticed in mainly scission dominating region for both the samples and the magnitude of the maximum conductivity $\sigma_{max}(t)$ of each $\sigma(t)$ vs t curves increases with the increase of the scission probability.

Finally the variation of the abovementioned measurable parameters (i.e. molecular distribution, different molar mass averages, ionic conductivity) are discussed on the basis of the experimentally observed facts which are reported by different researchers. We have noticed that our simulation outcomes are in good agreement with the experimentally observed results.

5.8. Future direction of the research work

As we have mentioned before that the present research work is aimed for a detailed theoretical understanding about the effect of gamma irradiation on the structural as well as transportation properties of solid polymer electrolyte through computer simulation. But the assumptions that we have taken at the time of simulation are based on some idealized concept which requires some necessary modifications as per the real polymer samples. Therefore, the tentative future plans in continuation of the work presented in this dissertation are as follows:

1. To incorporate the concept of the two fold random ionic motion into the simulation process. Instead of considering the unidirectional ionic motion inside the 1-D polymer system. The ionic species will jump on the either side of its present position with equal

probability and enter into, either the next or the previous molecule. Thus an ionic species can revisit an arbitrary molecule many times during its whole diffusion process.

2. To Study the ionic diffusion process with the above mentioned two fold random walk algorithm for both 2-D as well as 3-D system which are more realistic in nature rather than the 1-D system.

3. The future research works regarding ionic diffusion process will be carried out considering multiple ion motion inside the host polymer matrix.

4. We have assumed in the present dissertation that the applied radiation is absorbed completely by the host polymer system. But in reality, there is some wastage of the external irradiation. In our future work we will try to incorporate the concept of the dissipation of external irradiation quantitatively in our simulation study.

5. In case of the study of ionic conduction we have consider only two structural factors: intra-molecular scission and inter-molecular cross-linking. But in actual case many other factors like salt concentration, addition of fillers and plasticizer etc. also play significant role in the determination of ionic conductivity. In our future investigation all these factors will be taken under consideration at the time of simulation study.

6. To study the effect of gamma irradiation with computer simulation where a more realistic random fractal will be used as a mathematical tool to configure the host SPE sample.

Subhasish Ghosal
20.01.2022

Publications and Seminar Attended

5.8. List of Publications

1. Study of diffusion and conduction in gamma irradiated solid polymer electrolytes by fractal model structure,
S. Ghosal, R. Ray, T.K. Ballabh and S. Tarafdar, 2013, Indian Journal of Pure and Applied Physics, ISSN 0019-5596, Vol-51,324-327

2. Competitive scission and cross linking in a solid polymer electrolyte exposed to gamma irradiation: Simulation by a fractal model.
S. Ghosal, M. Mukhopadhyay, R. Ray, and S. Tarafdar, 2014, Physica A: Statistical Mechanics and Its Applications: Statistical, 400, pp.139-150. DOI: 10.1016/j.physa.2014.01.010

3. Fractal model of polymer electrolyte to investigate influence of high energy irradiation in molecular distribution and molar mass average.
S. Ghosal, R. Ray, M. Mukhopadhyay and S. Tarafdar, 2017. Ionics: International Journal of Ionics The Science and Technology of Ionic Motion,Vol-23(10), pp.2747-2759. DOI 10.1007/s11581-017-2133-7

5.8. Book Chapter

1. ENERGY STORAGE AND CONVERSION: Materials and Devices.
R. Ray, M. Mukhopadhyay, **S. Ghosal**, M. Saha, S. Tarafdar, 2016, ,Publisher: Narosa, Editor: Ashok Kumar, Shyamal Kumar Das, ISBN: 978-81-8487-578-2 (2016)

5.8. Conference Attended

1. Study of diffusion and conduction in gamma irradiated solid polymer electrolytes by fractal model structure
S. Ghosal, R. Ray, T.K. Ballabh and S. Tarafdar,2011,9^{th} National Conference of Solid State Ionics,JIIT, Noida.

2. Competitive scission and cross linking in a Solid Polymer Electrolyte Exposed to Gamma Irradiation: Simulation by a Fractal Model.
S. Ghosal, R. Ray, T.K Ballabh and S. Tarafdar, 2013, 10th National Conference of Solid State Ionics,NCSSI-10,Physics Department, IIT Kharagpur.

3. Fractal model of polymer electrolyte to investigate influence of high energy irradiation in molecular distribution and molar mass average.
S. Ghosal, R. Ray, M. Mukhopadhyay and S. Tarafdar, 2017, Asian Conference of Solid State Physics, IIT Patna, India.

4. Effect of High Energy Irradiation and Segmental Motion on Ion Transportation of Polymer Electrolyte: A Simulation Study Through Random Walk Approach With Deterministic Fractal Model.
S. Ghosal,2017,Fourth International Symposium on Semiconductor Materials and Devices (ISSMD-4), Department of Physics, Jadavpur University,Kolkata, India.

Author's personal copy

Ionics
DOI 10.1007/s11581-017-2133-7

ORIGINAL PAPER

Fractal model of polymer electrolyte to investigate influence of high energy irradiation in molecular distribution and molar mass average

Subhasish Ghosal[1] · **Ruma Ray**[2] · **Madhumita Mukhopadhyay**[1,3] · **Sujata Tarafdar**[1]

Received: 6 September 2016 / Revised: 20 April 2017 / Accepted: 28 April 2017
© Springer-Verlag Berlin Heidelberg 2017

Abstract The present work is completely based on the theoretical investigation i.e. computer simulated study of the effect of gamma irradiation on the molecular weight distribution and the molar mass averages of solid polymer electrolytes which is relevant with the present trends of experimental works in this field. We propose a fractal model corresponding to polymer molecules by deterministic loop-less fractal (Vicsek). An initial un irradiated symmetrical molecular weight distribution has been considered. Application of high energy perturbation, for example gamma irradiation, affects the molecules mainly by two processes-scission and cross-linking of molecules which results morphological changes inside the system. A new parameter named as weight fraction, has been introduced to compare the structural modification of the sample with the experimental results. The four basic parameters representing the molar mass averages have been introduced in this context to analyze various structural properties such as intrinsic viscosity, number, weight and Z-average molecular weight etc. The results of our simulation work enables us an easy understanding about the nature of the response of solid polymer electrolyte to the external perturbation.

Keywords Gaussian distribution · Fractal · Gamma irradiation · Polymer electrolyte, intrinsic viscosity, molar mass average

✉ Subhasish Ghosal
gjoy1986@gmail.com

[1] Physics Department, CMPRC, Jadavpur University, Kolkata, WB 700032, India

[2] Gurudas College, Physics Department, Kolkata, WB 700054, India

[3] Department of Chemistry, Amity Institute of Applied Sciences (AIAS), Amity University, Kolkata, India

Introduction

Polymer electrolyte is basically a solid solution of a salt in polymer substrate. The salient features like various solvating ability, unique ionic motion, rheological flexibility, results a significant application of such system in digital batteries [1–3]. Besides this, one significant feature of polymer electrolytes is the co-existence of both the crystalline and amorphous phase at the same time inside the system [4]. Researchers have studied that the ionic motion occurs in the amorphous phase where the crystalline state acts as a perfectly non-conducting state [4, 5]. It has been proved that there are different techniques [6, 7] such as, plasticization, addition of insulation particles, application of different chemical components, irradiation by high energy beam to enhance the ionic conductivity of the polymer electrolyte sample. These techniques, in general produce the morphological changes inside the system [5–10]. As a result, the rheological properties like viscosity etc. have been changed [8–11]. In case of application of external irradiation polymer molecules undergoes through a process of scission which results the.

fragmentation of larger molecules into smaller one. Otherwise they experience cross-linking effect which results the inter or/and intra molecular linkage inside the system [6, 12]. These two processes occur simultaneously inside the sample resulting a significant change in rheological properties of the sample [12, 13]. Our intention is to study the effect of gamma irradiation on Solid Polymer Electrolyte (SPE). The advantages of radiation modifications are its temperature, independent homogeneous, clean and controlled reactions resulting in sterile products without any chemical residue**.** Several attempts have been made so far to modify the properties of polymer electrolytes using gamma irradiation [6, 12, 13]. Irradiation, as a whole, affects the polymer crystallization since pure polymers are known to crosslink as well as degrade

Published online: 19 May 2017

Author's personal copy

Physica A 400 (2014) 139–150

Contents lists available at ScienceDirect

Physica A

journal homepage: www.elsevier.com/locate/physa

Competitive scission and cross linking in a solid polymer electrolyte exposed to gamma irradiation: Simulation by a fractal model

Subhasish Ghosal [a,b], Madhumita Mukhopadhyay [a,*], Ruma Ray [b], Sujata Tarafdar [a]

[a] Condensed Matter Physics Research Centre, Physics Department, Jadavpur University, Kolkata 700032, India
[b] Physics Department, Gurudas College, Kolkata 700054, India

HIGHLIGHTS

- The polymer system is modelled as deterministic Vicsek fractal.
- Theoretical simulation carried out on the polymer system perturbed by gamma irradiation.
- Simultaneous scission & cross-linking are considered as an effect of irradiation.
- Ionic motion is controlled by trapping phenomena & polymer segmental motion.
- Variations in conductivity & viscosity are simulated as a function of radiation dose.

ARTICLE INFO

Article history:
Received 11 June 2013
Received in revised form 6 November 2013
Available online 15 January 2014

Keywords:
Fractals
Polymer electrolyte
Gamma irradiation
Ionic conductivity
Segmental motion
Trapping

ABSTRACT

Gamma irradiation influences the microstructure of polymers that significantly affects the correlated properties of solid polymer electrolytes (SPEs). The present paper introduces a deterministic fractal model of polymer molecules and investigates the morphological changes due to gamma irradiation in SPE. The computer aided simulation is primarily based on radiation induced scission and/or cross linking of polymer molecules. The drift *velocity* of conducting ion which is proportional to conductivity, is calculated considering two competing effects, viz. trapping effect of ions diffusing inside a branched fractal molecule and the motion assisted by segmental motion of the polymer itself. Variations in ionic conductivity, molecular weight distribution, intrinsic viscosity etc., as a function of probability of scission and/or cross linking show significant correlation with microstructural change induced by gamma radiation of variable dose. The present theoretical study enables easy understanding for correlation of associated properties exhibited upon experimental system perturbation through gamma irradiation.

© 2014 Elsevier B.V. All rights reserved.

1. Introduction

The development of solid polymer electrolytes (SPEs) consisting of a polymer–salt complex is considered to be a breakthrough in the field of electrochemical devices. The prime peculiarity of polymer species is the co-existence of crystalline and amorphous phases. Researchers have shown that, majority of the ion dynamics occurs in the amorphous phase, where the transport properties viz. ionic conductivity, mechanical relaxations, diffusion, spin relaxation etc. are primarily associated

* Corresponding author. Tel.: +91 3324146666x2760, +91 9433882877; fax: +91 3324148917.
E-mail address: madhubanerji@gmail.com (M. Mukhopadhyay).

0378-4371/$ – see front matter © 2014 Elsevier B.V. All rights reserved.
http://dx.doi.org/10.1016/j.physa.2014.01.010

Indian Journal of Pure & Applied Physics
Vol. 51, May 2013, pp. 324-327

Study of diffusion and conduction in gamma irradiated solid polymer electrolytes by fractal model structure

Subhasish Ghosal[a], Ruma Ray*[b], T K Ballabh[a] & S Tarafdar[a]

[a]Physics Department, Jadavpur University, Kolkata 700 032

[b]Physics Department, Gurudas College, Kolkata 700 054

*E-mail: rumaray @yahoo.co.in; me.rumaray@gmail.com

Received 10 January 2013; revised 28 February 2013; accepted 18 March 2013

Gamma irradiation changes the polymer microstructure and improves the ionic conductivity of Solid Polymer Electrolytes (SPE). The present paper introduces a deterministic fractal model of polymer molecules to study the effect of gamma irradiation on it. The effect of irradiation is implemented by repeated scission of molecules resulting in variation in polymer morphology. The ionic conductivity is assumed to be proportional to the effective velocity of ions. The velocity is calculated considering the trapping effect due to the random movement of ions through the large fractal polymer molecules and the segmental motion of the branches. Calculated conductivity is compared with the experimental curves which show a qualitative agreement.

Keywords: Solid polymer electrolytes, Ionic conductivity, Gamma irradiation, Fractals

1 Introduction

Solid Polymer Electrolytes (SPE) have wide applications in modern science and technology. Usually, SPE substances show poor conductivity at room temperature. The amorphous regions contribute to the ion conduction in SPE. Hence, the conductivity may be improved by increasing the proportion of amorphous fraction by suitable techniques like plasticization, inclusion of insulating particles, addition of different chemical components, irradiation by high energy beam[1-5]. These techniques, in general, produce morphological changes in the polymer microstructure. In case of irradiation, absorption of high energy releases free radicals, which react to stabilize them either by cross-linking and/or by scission of polymer chains. Usually, these two processes occur simultaneously; one dominating the other. Experimental evidences[6,7] reveal that gamma irradiation on SPE samples in the presence of air is a scission dominated reaction. This paper presents an analytical study of the effect of irradiation on a model fractal polymer structure by scission and the resulting changes in ionic conductivity. The effect of segmental motion of free polymer branches is also taken into account.

2 Fractal Model and Scission Phenomena

The structures of polymer molecules in experimentally prepared SPE samples (PEO-NH_4ClO_4 films, prepared by solution casting technique) are found to be fractal like[8]. These real samples are stochastically self-similar and can be described by random fractals. But deterministic fractals[9] may be used to model polymer molecules because they are constructed by definite mathematical rules and exact results can be obtained from it. Here the Vicsek fractal, corresponding to a certain stage with a definite structure and length, is considered as a model polymer molecule. This particular fractal is chosen for its inherent loop-less, branched morphology, similar to polymer molecules obtained from experiments[8]. The 1st stage pattern of Vicsek structure is supposed to be the monomer unit, comprising of 5 basic units. Higher stage structures may be generated by the iterative rule of this fractal of dimension $d_f = 1.465$. The 1st and 2nd stage patterns are shown in Figs 1 and 2, respectively. The molecular weight of the basic monomer structure is assumed to be 5 and the molecular weight increases as 5^S with the increase in stage (s).

We assume that a single scission operation on a single s^{th} stage molecule (of molecular weight 5^S) produces 5 molecules of $(s-1)^{th}$ stage (corresponding molecular weight being $5^{(S-1)}$). For example, as the polymer system is exposed to radiation, scission generates five 9th stage molecules from each 10th stage molecule. On irradiation, these 9th stage molecules further break down and produces 8th stage molecules in 5:1 ratio and the process continues till the